DISS. ETH NO. 19346

ATMOSPHERIC ABUNDANCE AND ANTHROPOGENIC SOURCES OF MOLECULAR HYDROGEN: STATUS AND OUTLOOK TOWARDS A H_2-INTENSIVE ECONOMY

A dissertation submitted to

ETH ZURICH

for the degree of

Doctor of Sciences

presented by

STEVEN WALLACE BOND

BSc, The University of British Columbia – Okanagan, Canada
MSc, The University of Stirling, Scotland, United Kingdom

born 30.11.1975

citizen of Canada

accepted on the recommendation of

Professor Dr. A. Wokaun, examiner

Dr. S. Reimann, co-examiner

Professor Dr. J. Stähelin, co-examiner

2010

ACKNOWLEDGEMENTS

This project has prospered through the input and support of many people.

I would first like to extend my sincere gratitude to my PhD supervisor from the ETH and Paul Scherrer Institute, Professor Dr. Alexander Wokaun, for accepting me to take on this great challenge. His guidance and interesting and thought-provoking discussions helped develop this study into a very useful and rewarding experience.

I extend many thanks to my immediate supervisor at Empa, Dr. Stefan Reimann, for believing me to be the right person for the job and welcoming me into the Climate Gases group at Empa. His leadership and ability to challenge my capabilities were integral factors in the development of this project throughout.

I am indebted to Dr. Martin K. Vollmer and Dr. Martin Steinbacher from the Climate Gases group at Empa for their assistance and advice on countless occasions along the way. Without their invaluable input, this project would not have developed the way it did. Thank you very much to both of them.

Thank you to our department head, Dr. Brigitte Buchmann, for her class leadership of the department and for taking the time to provide valuable input at various points over the course of the project.

Thank you also to:

Matthias Hill from the Climate Gases group at Empa for his assistance and input regarding the technical aspects of the project; Dr. Stephan Henne and Dr. Dominik Brunner for the helpful discussions and assistance regarding the trajectory analysis and certain modelling aspects of the project; Dr. Christoph Zellweger for kindly giving up part of his lab for the RGA-3 instrument, and for assistance with quality control aspects of the project; Christoph Keller and Matthias Gianini for the camaraderie at Empa; Angelina Wenger for being a pleasant person with whom to share an office (even when I had the window open a lot of the time); Dr. Jörg Klausen for being a good jogging partner over many lunch hours; everyone in our department at Empa (Air Pollution/Environmental Technology (Abteilung 134)) for providing a relaxed and friendly working environment; Robert Alvarez from the Laboratory for

Internal Combustion Engines at Empa for his input and assistance at various points throughout the project; Erik Wilhelm at the Paul Scherrer Institute for the interesting and useful discussions, along with his important and intensive administrative role for our book; everyone involved with our book for the rewarding collaboration; the Laboratory for Internal Combustion Engines at Empa for allowing me to work alongside them during the chassis dynamometer measurements aspect of the project, in particular to Christian Bach for his administrative assistance and the valuable discussions, Dr. Martin Weilenmann, Dr. Patrik Soltic, Jan Stilli, Simon Tischhauser, and Mathias Huber for their assistance and helpful discussions regarding the technical automotive aspects of this project; Dr. Hal Turton from the Energy Economics Group at the Paul Scherrer Institute for valuable comments and input regarding certain modelling aspects of the project; Dr. Philipp Dietrich at the Paul Scherrer Institute for the interesting and valuable discussions; the custodians at Jungfraujoch — the families Fischer, Seiler, and Hemund — for their assistance at the research station; both the EuroHydros community and Professor John Heywood and his group at the Sloan Automotive Laboratory at MIT for the interesting collaborations; and Professor Dr. Johannes Stähelin for reviewing my work and agreeing to be co-examiner of my thesis.

I extend a heartfelt thank you to my family in Switzerland, Canada, and Taiwan, for staying close even when I was off in my own world. To my wife Vera, for without her support and understanding, this experience would not have been possible. I dedicate this work to her.

STEVEN W. BOND

TABLE OF CONTENTS

ACKNOWLEDGEMENTS iii

TABLE OF CONTENTS v

LIST OF FIGURES ix

LIST OF TABLES xi

LIST OF ABBREVIATIONS xiii

LIST OF UNITS xvi

ABSTRACT xviii

ZUSAMMENFASSUNG xxii

1 INTRODUCTION 1

1.1 Background 1

1.2 Structure of thesis 4

1.3 Characteristics of atmospheric H_2 5

1.3.1 Atmospheric seasonal cycles 7

1.3.2 Atmospheric trend analysis 8

1.4 Sources of atmospheric H_2 9

1.4.1 Anthropogenic H_2 emissions from fossil fuels 9

1.4.1.1 H_2 emissions in internal combustion engine exhaust – the role of air-fuel ratios and lambda 10

1.4.1.2 Three-way catalytic converters 11

1.4.1.3 H_2 emissions from test-bench, dynamometer, and real-world studies involving internal combustion engine vehicles 12

1.4.1.4 Non-transport-based anthropogenic H_2 emissions 14

1.4.2 Major natural sources of H_2 16

1.5 Sinks of atmospheric H_2 17

1.6 Motivation and Scope 21

2 METHODS 23

2.1 Direct exhaust gas H_2 measurements 23

2.1.1 Vehicle selection 23

2.1.2 Experimental setup of chassis dynamometer 25

2.1.3 Driving cycles and sub-cycles 27

2.1.4 Derivation of H_2 emissions factors 30

2.1.5 Derivation of cumulative H_2/CO ratios 32

2.1.6 Experimental setup of engine test bench 32

2.2 Quantitative scenarios of global anthropogenic H_2 emissions to the atmosphere throughout the 21st century 34

2.2.1 Global Multi-regional MARKAL model 34

2.2.2 Vehicle fleet scenarios 35

2.2.3 Key assumptions associated with global H_2 upscaling 36

2.2.4 Calculation and derivation of H_2 emissions factors for global upscaling 38

2.2.5 H_2 production and consumption scenarios 43

2.3 Continuous free tropospheric H_2 observations 45

2.3.1 Gas chromatographic separation and detection of H_2 45

2.3.2 Quality assurance and quality control 47

2.3.2.1 Calibration, standards, and scales 47

2.3.2.2 Target tanks 49

2.3.2.3 Independent external quality assurance and quality control 49

2.3.2.4 Non-linearity corrections of the RGA-3 50

2.3.3 Baseline estimation 54

3 MEASUREMENTS OF H_2 FROM FOSSIL FUEL-BASED INTERNAL COMBUSTION ENGINES 56

3.1 Qualitative overview of H_2 emissions from fossil fuel-powered vehicles ... 56

3.1.1 Presence/Absence of TWC 57

3.1.2 Vehicle type 59

3.1.2.1 Engine state 60

3.1.2.2 Quality of lambda control 61

3.1.3 Fuel type 63

3.1.4 Engine and catalyst temperature at start up 66

3.2 Quantified H_2 emissions from fossil fuel-powered vehicles 69

3.2.1 H_2 emission factors from 4-wheeled vehicles 69

3.2.1.1 Gasoline-powered vehicles 69

3.2.1.2 Natural gas-powered vehicles 71

3.2.2 H_2 emission factors from 2-wheeled vehicles 72

3.2.3 H_2 vs. CO 73

3.2.3.1 4-wheeled vehicles 73

3.2.3.2 2-wheeled vehicles 82

3.3 Summary 86

4 SCENARIOS FOR CURRENT AND FUTURE GLOBAL ANTHROPOGENIC H_2 EMISSIONS FROM TECHNOLOGICAL PROCESSES 88

4.1 Individual vehicle H_2 emission factors and global upscaling of H_2 emissions from road-based transportation 88

4.2 Global projections of H_2 production and consumption 108

4.2.1 Direct energy-based end-uses 108

4.2.2 Industrial end-uses 109

4.2.2.1 Petroleum refining 109

4.2.2.2 Other industrial end-uses 110

4.3 Current and future H_2 emissions from hydrogen production, distribution, storage, and non-transportation-based end-uses 114

4.3.1 State-of-the-art knowledge of non-transport-based

well-to-use leakage rates of H_2 114

4.3.2 Scenarios for non-transportation-based H_2 emissions to the atmosphere 115

4.4 Global upscaling scenarios for overall anthropogenic H_2 emissions to the atmosphere between 2010 and 2100 118

4.5 Summary 123

5 CONTINUOUS H_2 OBSERVATIONS IN THE ATMOSPHERE 128

5.1 Time series, seasonal cycles, trends 129

5.2 Case studies 134

5.3 H_2 pollution events and ratios of excess H_2 to excess CO 137

5.4 Soil uptake assessment 141

5.5 Summary 142

6 GENERAL CONCLUSIONS AND OUTLOOK 144

REFERENCES 151

CURRICULUM VITAE 161

PUBLICATIONS 163

LIST OF FIGURES

Figure 1. Global tropospheric H_2 budget 7

Figure 2. Simplified H_2 life cycle 15

Figure 3. Experimental setup of chassis dynamometer 25

Figure 4. Motorcycle on chassis dynamometer 26

Figure 5. Driving cycles conducted by 4-wheeled vehicles 28

Figure 6. Driving cycles conducted by 2-wheeled vehicles 30

Figure 7. Experimental setup for engine test bench measurements 33

Figure 8. RGA-3 instrument setup at Jungfraujoch 46

Figure 9. Chromatogram of H_2 and CO 47

Figure 10. Plot of normalized heights for working standards 49

Figure 11. Scheme of non-linearity experiment conducted at Empa 51

Figure 12. Experimental setup of non-linearity experiment 52

Figure 13. Non-linearity functions for the RGA-3 at Jungfraujoch 53

Figure 14. H_2 mixing ratios in raw gasoline exhaust gas 58

Figure 15. H_2 mixing ratios for pre- and post-catalytic converter measurements from a gasoline-powered engine 59

Figure 16. H_2 emissions from a gasoline Euro-4 automobile and a gasoline Euro-3 motorcycle 61

Figure 17. Cumulative H_2 emissions and lambda settings of 2 gasoline automobiles and a diesel delivery vehicle 63

Figure 18. Cumulative H_2 emissions for diesel vehicles, gasoline automobiles, natural gas automobiles, and 2-wheelers 64

Figure 19. H_2 emissions in gasoline and natural gas exhaust 65

Figure 20. Cumulative H_2 emissions from a cold-start cycle 66

Figure 21. Cumulative H_2 emissions from a warm-start cycle 68

Figure 22. Cumulative cold-start cycle H_2 and CO mixing ratios and cumulative molar H_2/CO ratios for gasoline-powered Euro-4 automobiles 74

Figure 23. Cumulative warm-start cycle H_2 and CO mixing ratios and cumulative molar H_2/CO ratios for gasoline-powered Euro-4 automobiles 75

Figure 24. H_2, CO, lambda, cumulative H_2/CO, and speed profile for a gasoline automobile. 76

Figure 25. Scatterplot of mean E_{H2} vs. mean E_{CO} for each sub-cycle of the gasoline automobiles 79

Figure 26. Scatterplot of mean mixing ratios of H_2 vs. CO for each sub-cycle of each gasoline automobile 81

Figure 27. H_2 emissions from each vehicle technology in 2010 96

Figure 28. H_2 emissions from each vehicle technology in 2010 separated by the absolute contribution from each world region 97

Figure 29. H_2 emissions from each vehicle technology in 2020 98

Figure 30. H_2 emissions from each vehicle technology in 2020 separated by the absolute contribution from each world region 99

Figure 31. H_2 emissions from each vehicle technology in 2050 based on an FCV E_{H2} of 26.5 mg km^{-1} and an FCV E_{H2} of 265 mg km^{-1}. 102

Figure 32. H_2 emissions from each vehicle technology in 2100 based on an FCV E_{H2} of 26.5 mg km^{-1} and an FCV E_{H2} of 265 mg km^{-1}. 104

Figure 33. Global road-based H_2 emissions 106

Figure 34. H_2 and CO datasets at Jungfraujoch 130

Figure 35. Seasonal monthly mean baseline H_2 and CO at Jungfraujoch 131

Figure 36. H_2 seasonal amplitudes vs. altitude 133

Figure 37. H_2 and CO mixing ratios illustrating a pollution event on January 12, 2008 135

Figure 38. H_2 and CO mixing ratios illustrating a CO pollution event on October 24–26, 2007 136

Figure 39. H_2, CO, CH_4, and $CHCl_3$ mixing ratios illustrating a depletion event for the latter gases with simultaneous enhancement in ambient H_2 137

Figure 40. Monthly mean atmospheric boundary layer residence times 138

Figure 41. Excess H_2 and CO at Jungfraujoch 140

LIST OF TABLES

Table 1. Main attributes of gasoline Euro-4 automobiles 24

Table 2. Main attributes of gasoline Euro-3 motorcycles and scooters 24

Table 3. Main attributes of diesel Euro-4 automobile 24

Table 4. Main attributes of diesel Euro-4 delivery vehicles 24

Table 5. Main attributes of natural gas Euro-4 automobiles 25

Table 6. Main characteristics of driving cycles conducted by 4-wheeled vehicles 28

Table 7. Cycles performed by individual gasoline automobiles 29

Table 8. Cycles performed by individual diesel vehicles 29

Table 9. Cycles performed by individual natural gas automobiles 29

Table 10. Main characteristics of driving cycles conducted by 2-wheeled vehicles ... 30

Table 11. Cycles performed by individual 2-wheelers 30

Table 12. Major settings for each engine operating point 33

Table 13. Selection criteria and derivation of E_{H2} for all vehicle technologies 42

Table 14. Primary direct energy end-uses and industrial end-uses 43

Table 15. H_2 emission factors of 4-wheeled vehicles and H_2/CO ratios of gasoline automobiles 84

Table 16. H_2 emission factors and H_2/CO ratios of 2-wheeled vehicles 85

Table 17. H_2 emission factors for all vehicle technologies and world regions 90

Table 18. Global vehicle kilometres travelled according to vehicle technology 93

Table 19. Globally projected H_2 emissions from road-based transportation 95

Table 20. H_2 production based on global oil supply 110

Table 21. H_2 production and consumption for the major industrial processes (excluding oil refining) 112

Table 22. H_2 production scenarios for industrial and direct energy-based end-uses . 113

Table 23. Global projections of non-transport-based H_2 losses under a range of loss rates 116

Table 24. Projections of overall global anthropogenic H_2 emissions to the atmosphere from technological processes..... 122

Table 25. Mean monthly H_2 mixing ratios at Jungfraujoch..... 130

LIST OF ABBREVIATIONS

ΔCO	Excess CO, CO mixing ratio minus the corresponding baseline value
ΔH_2	Excess H_2, H_2 mixing ratio minus the corresponding baseline value
$\Delta H_2/\Delta CO$	Molar ratio of excess hydrogen to excess carbon monoxide
2D-REBS	2-Dimensional Robust Extraction of Baseline Signal
ABL	Atmospheric boundary layer
AGAGE	Advanced Global Atmospheric Gases Experiment
BAB	Bundesautobahn (German real-world highway sub-cycle)
CADC	Warm-start driving cycle (Common Artemis Driving Cycle) (simulates urban, rural, and highway conditions)
CCS	Carbon capture and storage
CH	Switzerland
CH_3OH	Methanol
CH_4	Methane
CO	Carbon monoxide
CO_2	Carbon dioxide
DPF	Diesel particle filter
EC	European Commission
ECMWF	European Centre for Medium-Range Weather Forecasts
E_{CO}	Carbon monoxide emission factor
ECU	Engine control unit
E_{H2}	Hydrogen emission factor
EIMS	Electron Ionization Mass Spectrometry
Empa	Swiss Federal Laboratories for Materials Science and Technology
Euro-	European emission standard designation for vehicles

FCV	Fuel cell vehicle
FLEXTRA	Atmospheric trajectory model
GAW	Global Atmospheric Watch (program)
GC	Gas chromatograph
GH_2	Compressed gaseous hydrogen
GMM	Global Multi-regional MARKAL (MARKet ALlocation) model
GWP	Global warming potential
H_2	Molecular hydrogen
H_2/CO	Molar ratio of hydrogen to carbon monoxide
H_2ICEV	Hydrogen internal combustion engine vehicle
H_2O	Water
HCHO	Formaldehyde
HEV	Hybrid-electric vehicle
ICEV	Internal combustion engine vehicle
IFA	International Fertilizer Industry Association
IPCC	Intergovernmental Panel on Climate Change
IUFC	Cold-start driving cycle (simulates urban conditions)
L2	Cold-start driving cycle (simulates urban, rural, and highway conditions)
LA	Cold-start driving cycle (simulates urban and rural conditions)
LDV	Light-duty vehicle
LH_2	Cryogenic liquid hydrogen
$Mg(ClO_4)_2$	Magnesium perchlorate
MPI	Max Planck Institute
MS	Mass spectrometer

N_2	Nitrogen
NABEL	Swiss National Air Pollution Monitoring Network
NH_3	Ammonia
NMHC	Non-methane hydrocarbons
NO	Nitric oxide
NO_2	Nitrogen dioxide
NOAA/ ESRL-GMD	National Oceanic and Atmospheric Administration's Earth System Research Laboratory – Global Monitoring Division
NO_x	Nitrogen oxides
O_2	Oxygen
O_3	Ozone
OECD	Organisation for Economic Co-operation and Development
OH	Hydroxyl radical
OP	Engine operating point
PM	Particulate matter
Ra	Warm-start driving cycle (simulates rural and highway conditions)
Rb	Warm-start driving cycle (simulates urban and rural conditions)
RGA	Reduction Gas Analyzer
SMP	Sustainable Mobility Project transport model
SMR	Steam methane reforming
TWC	Three-way catalytic converter
UF	Ultrasonic exhaust volume flow measuring system
VOC	Volatile organic compound
WMO	World Meteorological Organization
λ	Lambda, a measure of air-fuel ratio

LIST OF UNITS

% a^{-1}	Percent per year
cm^3	Cubic centimetre(s)
EJ	Exajoule(s)
g km^{-1}	Grams per kilometre
g mol^{-1}	Grams per mole
Hz	Hertz
kg	Kilogram(s)
km	Kilometre(s)
km a.s.l.	Kilometres above sea level
km h^{-1}	Kilometres per hour
kW	Kilowatt(s)
L	Litre(s)
m	Metre(s)
m a.s.l.	Metres above sea level
m s^{-1}	Metres per second
mg	Milligram(s)
mg km^{-1}	Milligrams per kilometre
mg s^{-1}	Milligrams per second
mL	Millilitre(s)
nm	Nanometre(s)
Nm	Newton metre(s)
^oC	Degrees Celsius
PJ	Petajoule(s)

ppb	Parts per billion
ppb a^{-1}	Parts per billion per year
ppm	Parts per million
s	Second(s)
Tg	Teragram(s)
Tg a^{-1}	Teragrams per year
Tg H_2 PJ^{-1} oil	Teragrams hydrogen per petajoule oil
μm	Micrometre(s)
σ	Standard deviation of fit residuals

ABSTRACT

The role of molecular hydrogen (H_2) as a future sustainable alternative energy solution for mobile and stationary applications has generated widespread interest as the predominance of non-renewable energy has started to decrease. H_2 has the potential to take on this role and to compete with hydrocarbons as a fuel source for transportation. However, as H_2 production and the fraction of energy-based H_2 applications would increase, a potential accumulation of H_2 in the atmosphere from direct emissions, losses and leakage, and changes in chemical processes in the atmosphere could result. A significant increase in future H_2 emissions has been associated with possible impacts on the environment and various atmospheric processes. Until recently, H_2 emissions to the atmosphere from technological anthropogenic sources have been largely disregarded and viewed in large part as a product of incomplete fossil fuel combustion. Vehicle exhaust gas is currently an important source of anthropogenic H_2 to the atmosphere, and losses of H_2 from production, distribution, storage, and other end-use systems could become increasingly significant contributors. With changing vehicle fleet composition (including H_2 fuel cell vehicles (FCVs)) and increasing H_2 production, an assessment of well-to-wheel H_2 emissions, including H_2 emissions from current and emerging vehicle technologies, will help assess the magnitude of future anthropogenic H_2 emissions to the atmosphere from technological processes.

This study evaluates H_2 emissions from the most significant technological anthropogenic sources and applies quantitative scenarios of H_2 emissions throughout the 21st century based on changing vehicle fleet compositions and H_2 production strategies for industrial and direct energy-based end-uses. Additionally, atmospheric H_2 observations at a remote free tropospheric site are analysed to assess temporal variations and identify important current source regions. In the future, such observations could act as a validation tool to identify trends in background atmospheric H_2 levels as the fraction of H_2-based mobile and stationary applications increase. Such trends will help confirm whether H_2 emissions to the atmosphere are increasing or decreasing during the transition to more H_2-intensive economy.

For the first step, H_2 emissions were characterized, both qualitatively and quantitatively, through direct exhaust gas measurements of individual vehicles tested

on a chassis dynamometer. Qualitatively, these measurements showed that H_2 emissions from conventional internal combustion engine vehicles are influenced by a number of factors, including the presence/absence of a three-way catalytic converter (TWC), the engine state, the quality of lambda control, vehicle and fuel type, and engine and catalyst temperature at start-up. Quantitatively, absolute H_2 emissions were found to be highest for motorcycles and scooters, approximately 5 times higher than for gasoline-powered automobiles. All diesel-powered vehicles emitted marginal amounts of H_2. For automobiles, the highest emission factors were observed for sub-cycles subject to a cold-start. High speeds also caused elevated H_2 emission factors. Molar H_2/CO ratios from gasoline-powered vehicles were variable and typically higher than previous atmospheric ratios reported in tunnel studies and other studies characteristic of traffic-influenced measurements. The lowest mean individual sub-cycle ratios, which corresponded to high absolute emissions of both H_2 and CO, were observed during cold starts and at high vehicle speeds. This finding illustrates the importance of these conditions to observed H_2/CO ratios in ambient air. Overall, 2-wheelers displayed lower H_2/CO ratios than those from gasoline-powered automobiles. This observation, along with the lower H_2/CO ratios observed through studies without catalytic converters, suggests that less developed (e.g. 2-wheelers) and older vehicle technologies are largely responsible for the atmospheric H_2/CO ratios reported in past literature. The quantitative aspect of H_2 emission factors and H_2/CO ratios took on a significant role in the second major step of this project.

For the second step, current and future anthropogenic H_2 emissions from technological sources were assessed. The main objective of this aspect of the project was to estimate future global emissions based on changing vehicle fleet composition and global H_2 production. This was approached through scenarios on different temporal scales under the assumption that H_2-based mobile applications and H_2 production will increase throughout the 21st century. Currently, large uncertainty is associated with the contribution of H_2 from technological processes in the global H_2 budget, primarily from fossil fuels. The detailed analysis of well-to-wheel H_2 emissions, including H_2 emissions from current and emerging vehicle technologies, helped assess the current and future magnitude of such emissions to the atmosphere. Current emissions are dominated by the direct exhaust gas of road-based motor vehicles and losses during the industrial production of H_2 from fossil fuels. In 2020,

emissions from transportation were estimated at approximately 50% of those in 2010. Future emissions will occur as losses along the entire production, distribution, and end-use chain, including emissions from FCVs. Under 2050 scenarios, overall anthropogenic H_2 emissions (taken as the sum of emissions from transportation and non-transport-based well-to-use losses) only approached current levels at high-end loss rates; direct emissions from transportation are expected to be significantly lower than current levels. In 2100, a mean loss rate of 0.5% from production, distribution, storage, and utilization would result in overall H_2 emissions exceeding current levels even with no net H_2 emissions from FCVs. However, based on an average loss rate of 0.1%, H_2 emission factors from FCVs on the order to 120–170 mg km^{-1} were projected to result in overall anthropogenic H_2 emissions similar to 2010 levels. Measurements of background H_2 at remote sites in the free troposphere could act as a future validation tool through trend analysis during the potential transition to a more H_2-intensive economy.

For the third step, measurements of H_2 at the high-altitude site of Jungfraujoch, Switzerland were evaluated. Due to its high-altitude location, year-round accessibility, and terrific infrastructure, the Jungfraujoch research station is perfectly suited as an observatory to monitor background concentrations of H_2 in the free troposphere (the lowest atmospheric layer that is no longer directly influenced by the surface). Additionally, due to the periodic influence of anthropogenic pollution from source regions, Jungfraujoch is well situated as an observatory to assess regional source allocations during pollution events. Results were analysed for the period of August, 2005 – November, 2009. The time series consists of measurements that are primarily representative of free tropospheric, background conditions. Pollution events and background conditions could be distinguished using a statistical filter. Highest background H_2 mixing ratios were observed in May, while the lowest were observed in November. The mean seasonal H_2 peak-to-trough amplitude at Jungfraujoch was considerably less than at other stations of similar latitude, and the seasonal minimum in November was comparatively delayed. These differences were primarily attributed to a dampening and delay of the surface soil sink signal during its vertical propagation to the free troposphere. Compared with direct exhaust gas measurements and measurements at locations in close proximity to the source, the relationship between excess (mixing ratio minus corresponding baseline value) H_2 and excess CO for the

entire dataset displayed an atypical correlation. The low ratio was attributed to H_2 removal by soil during transport to Jungfraujoch. Although the length of the dataset in this study (~4 years) is too short to draw any concrete conclusions about recent trends in background H_2 levels, such measurements will become increasingly valuable for future trend analysis as the fraction of H_2-based mobile and stationary applications continues to increase.

ZUSAMMENFASSUNG

Vor dem Hintergrund der sich abzeichnenden Knappheit der nicht erneuerbaren Energiequellen wie Erdöl und Erdgas, wird der Einsatz von molekularem Wasserstoff (H_2) als zukünftiger Energieträger und als nachhaltige alternative Energielösung für mobile und stationäre Anwendungen derzeit weitreichend diskutiert. Speziell im Transportsektor werden H_2-basierten Anwendungen das Potential bescheinigt, eine emissionsfreie Alternative zu fossilen Antrieben darzustellen. Als Folge von direkten Emissionen und Verlusten während Produktion, Transport, Lagerung und Nutzung, könnte eine Zunahme der Wasserstoffwirtschaft (einhergehend mit einer intensiven Produktion von H_2 und verstärkten H_2-Anwendungen) jedoch zu einem Anstieg der H_2-Konzentration in der Atmosphäre führen und dadurch die chemischen und biologischen Prozesse im Umweltsystem beeinflussen. In der Vergangenheit wurde den anthropogenen Quellen des atmosphärischen H_2 nur wenig Bedeutung beigemessen und H_2-Emissionen wurden vor allem der unvollständigen Verbrennung von fossilen Brennstoffen zugeordnet, wobei insbesondere Fahrzeugabgase eine wichtige Rolle spielen. Im Falle einer Implementierung alternativer Fahrzeugantriebe (unter anderem H_2-Antriebe) könnte es somit zu einer wesentlichen Veränderung der anthropogenen H_2-Emissionen kommen, und eine sorgfältige Evaluation der H_2-Emissionen von gegenwärtigen und zukünftigen Fahrzeugtechnologien ist unablässig um Projektionen zukünftiger H_2-Emissionen zu erstellen und deren Auswirkungen auf die Umwelt abzuschätzen.

Diese Studie evaluiert die anthropogenen H_2-Emissionen der wichtigsten technologischen Quellen und erarbeitet — basierend auf veränderten globalen zukünftigen Fahrzeugtechnologien sowie Strategien für die Produktion von industriellen und direkten Energieendnutzeranwendungen — quantitative Szenarien von H_2-Emissionen für das gesamte 21. Jahrhundert. Zusätzlich werden langjährige atmosphärische H_2-Messungen an einer Hintergrundstation analysiert, um die atmosphärische H_2-Konzentration zu quantifizieren, mögliche Trends abzuschätzen, und momentane wichtige Quellregionen zu lokalisieren. Diese Resultate bilden die Grundlage für zukünftige Analysen von atmosphärischen H_2-Konzentrationen und werden es ermöglichen, langfristige Veränderungen der Hintergrundkonzentration zu identifizieren. Solche Trends erlauben eine unabhängige Validierung der Zunahme

bzw. Abnahme der atmosphärischen H_2-Emissionen während des Übergangs zu einer H_2-intensivierenden Wirtschaft.

In einem ersten Schritt wurden die H_2-Emissionen von einzelnen Fahrzeugen verschiedener Motorentechnologien durch direkte Abgasmessungen auf einem Rollenprüfstand charakterisiert. Diese Messungen zeigten, dass H_2-Emissionen von konventionellen Fahrzeugen (d.h. solchen mit Verbrennungsmotoren) von mehreren Faktoren beeinflusst werden, wie zum Beispiel dem Dreiwegkatalysator, dem Zustand des Motors, der Qualität der Lambdasonden-Kontrolle, der Art des Fahrzeuges und des Treibstoffes, sowie der Temperatur des Motors und des Katalysators beim Start des Fahrzeuges. Die grössten H_2-Emissionen wurden dabei von Motorrädern und Motorrollern beobachtet, welche etwa fünf Mal höher waren als diejenigen von Personenwagen mit Benzinantrieb, während Dieselfahrzeuge nur unbedeutende Mengen an H_2 emittierten. Für Autos wurden die höchsten H_2-Emissionen während dem Kaltstart gemessen, und grosse Mengen H_2 wurden zudem bei hohen Fahrgeschwindigkeiten emittiert. Die molaren H_2/CO-Verhältnisse im Abgas von Benzinfahrzeugen waren sehr variabel und oft höher als bisher berichtete atmosphärische Verhältnisse in Tunnelstudien und an verkehrsnahen Standorten. Die niedrigsten H_2/CO Verhältnisse wurden dabei während dem Kaltstart und bei hohen Fahrzeuggeschwindigkeiten festgestellt. Da während diesen Bedingungen die höchsten absoluten Konzentrationen sowohl von CO als auch von H_2 gemessen werden, leisten diese Situationen den grössten Beitrag zu den beobachteten atmosphärischen H_2/CO Verhältnissen. Allgemein waren die H_2/CO Verhältnisse von Zweirädern tiefer als bei den Benzinautos. Dieses Ergebnis — zusammen mit den tieferen H_2/CO Verhältnissen die bei Studien ohne Dreiwegkatalysatoren festgestellt wurden — deutet darauf hin, dass die weniger entwickelten (z.B. Zweiräder) und älteren Fahrzeugtechnologien für die in der Literatur berichteten atmosphärischen H_2/CO Verhältnisse verantwortlich sind.

In einem zweiten Schritt wurden gegenwärtige und künftige Szenarien der atmosphärischen H_2-Emissionen erstellt, basierend auf Annahmen der zukünftigen globalen Fahrzeugtechnologiezusammensetzung und einer globalen H_2-Produktionskapazität. Der Ansatz zur Abschätzung der künftigen globalen anthropogenen H_2-Emissionen bestand aus verschiedenen Szenarien unterschiedlicher

Zeitskalen unter der Annahme, dass der Anteil mobiler H_2-Anwendungen sowie die Produktion von H_2 während des 21. Jahrhunderts zunehmen werden. Gegenwärtig besteht eine grosse Unsicherheit über den Beitrag von technologischen Prozessen zum globalen H_2 Budget, wobei insbesondere der Anteil der Emissionen durch die Verbrennung von fossilen Brennstoffen nicht hinlänglich bekannt ist. Die hier durchgeführte Bewertung der Gesamtbilanz der H_2-Emissionen, einschliesslich der Emissionen von gegenwärtigen und zukünftigen Fahrzeugtechnologien, ermöglicht eine bessere Abschätzung von künftigen anthropogenen H_2-Emissionen in die Atmosphäre. Eine detaillierte Analyse der Emissionen der wichtigsten anthropogenen Prozesse, welche zum gegenwärtigen und künftigen H_2 Budget beitragen, quantifiziert dabei den Beitrag dieses Sektors. So konnte gezeigt werden, dass die gegenwärtigen Emissionen vom direkten Abgas des Strassenverkehrs und den Verlusten während der industriellen H_2-Produktion dominiert werden. Für das Jahr 2020 zeigen die Projektionen eine Reduktion der Strassenverkehrsemissionen um etwa 50% im Vergleich zu 2010, und die Analyse zeigt dass in Zukunft Emissionen über die gesamte Produktions-, Lieferungs-, und Endnutzeranwendungenskette verursacht werden (inklusive Emissionen von Brennstoffzellenfahrzeugen). Aufgrund der vorhergesagten stark abnehmenden H_2-Emissionen des Strassenverkehrs wird für das Jahr 2050 nur dann der gegenwärtige Stand der gesamten H_2-Emissionen erreicht, wenn hohe Verlustraten während Herstellung, Transport, Lagerung und Nutzung angenommen werden. Unter der Annahme einer mittleren Verlustrate von 0.5% für das Jahr 2100 werden die gesamten H_2-Emissionen zu diesem Zeitpunkt höher sein als diejenigen von 2010, selbst wenn keine Emissionen von Brennstoffzellenfahrzeugen auftreten. Für eine durchschnittliche Verlustrate von 0.1% hingegen wurde hochgerechnet, dass bei H_2-Emissionsfaktoren für Brennstoffzellenfahrzeugen zwischen 120–170 mg km^{-1}, die gesamten anthropogenen Emissionen einen ähnlichen Stand wie heute erreichen können.

Um künftige Änderungen der globalen H_2-Emissionen während dem eventuellen Übergang zu einer H_2-intensiveren Wirtschaft zu quantifizieren, sind langfristige Messungen der atmosphärischen H_2-Konzentrationen an Hintergrundstationen unablässig. Im dritten Teil dieser Studie wurden deshalb H_2-Messungen an der hochalpinen Forschungsstation Jungfraujoch in den Berner Alpen durchgeführt und für den Zeitraum von August 2005 bis November 2009 analysiert. Wegen seiner

exponierten Lage, der ganzjährigen Zugänglichkeit und der exzellenten Infrastruktur, ist die Messstation Jungfraujoch als Observatorium für die Überwachung der H_2-Konzentration in der freien Troposphäre (d.h. der nicht mehr unmittelbar durch Prozesse am Boden beeinflusste Atmosphärenschicht) sehr gut geeignet. Aufgrund seiner Lage in Zentraleuropa und dem sporadischen Einfluss anthropogener Verschmutzung von tiefer gelegenen Quellregionen, ist es zudem möglich, verschiedene charakteristische Quellregionen zu identifizieren. Dazu wurden Verschmutzungsereignisse und Episoden mit Hintergrundbedingungen mit einem statistischen Filter unterschieden. Der überwiegende Anteil der Messreihe repräsentiert dabei Hintergrundsbedingungen, mit den tiefsten beobachteten Konzentrationen im November, während die höchsten H_2-Hintergrundkonzentrationen im Mai festgestellt wurden. Die durchschnittliche saisonale Minimum-Maximum Amplitude am Jungfraujoch ist deutlich geringer als bei anderen Stationen ähnlicher nördlicher Breite, und der Zeitpunkt des saisonalen Minimums ist im Vergleich verzögert. Diese Unterschiede konnten auf die geringere Bodendeposition von H_2 und die zeitliche Verzögerung dieses Signal während dem vertikalen Transport in die freie Troposphäre zurückgeführt werden. Im Unterschied zu quellnäheren Standorten und zu direkten Abgasmessungen wurde eine sehr untypische Korrelation zwischen Exzess H_2 (Konzentration minus Hintergrund) und Exzess CO beobachtet. Das tiefe Verhältnis wurde auf die Aufnahme des H_2 durch den Boden während des Transports auf das Jungfraujoch zurückgeführt. Aufgrund der Kürze der Zeitreihe in dieser Studie (~4 Jahre) konnten keine konkreten Schlussfolgerungen über einen aktuellen Trend der H_2-Hintergrundkonzentration gezogen werden. Die hier vorgestellten Messungen werden jedoch für zukünftige Trendanalysen von grossem Wert sein und könnten es ermöglichen, den Einfluss einer intensivieren Nutzung von H_2-basierten Anwendungen auf die atmosphärische Zusammensetzung zu untersuchen.

1 INTRODUCTION

1.1 Background

Until recently, anthropogenic emissions of molecular hydrogen (H_2) to the atmosphere from technological sources, such as incomplete fossil fuel combustion, have not been given much attention as H_2 was believed to have no discernable influence on air pollution or climate. However, H_2 has received increased attention recently due to its potential as a sustainable future energy carrier and fuel source for transportation, along with the possible environmental consequences that may accompany its large-scale adoption. With volatile oil prices and the international insecurities that accompany them, many governments, companies, and individuals are considering alternative energy options. In reality, the search for renewable energy options is rampant in many areas. Hydrogen has the capacity to take on this role as a sustainable energy carrier of the future and to compete with fossil fuels as a fuel for transportation. However, increasing H_2 production, coupled with more widespread H_2-based transportation, could result in an accumulation of H_2 in the atmosphere from emissions along the entire production, distribution, and utilization chain.

At times, H_2 has been labelled “the” future energy solution and coupled with visions of a full-fledged hydrogen economy. More recently, H_2 has settled into the role of one viable option among several competing or complementing energy alternatives [1]. H_2 is ubiquitously distributed and not limited by the geopolitical constraints and uncertainties surrounding hydrocarbons. Despite being the lightest element known to man, the energy content of H_2 is the highest of any fuel, almost 3 times that of gasoline on a weight basis [2]. Currently, the most common method of producing H_2 is through steam methane reforming (SMR), with approximately 80% of global H_2 production occurring through this method [3]. Although SMR is presently the most cost-effective means of producing H_2, the use of methane (CH_4) as a non-renewable feedstock, coupled with the accompanying carbon dioxide (CO_2) emissions, make this process an unsustainable method of producing H_2 over the long-term.

The generation of H_2 from renewable resources, such as the electrolysis of water with electricity generated by wind or solar energy would provide a sustainable H_2

production system [4]. In fact, model scenarios aimed at stabilizing future atmospheric CO_2 mixing ratios predict predominant future H_2 production methods for energy services being coal gasification with carbon capture and storage (CCS), natural gas with CCS, wind energy coupled with electrolysis, and nuclear H_2 production [1, 5]. The production of H_2 through renewable resources would thus inevitably avoid, or at least substantially reduce, emissions of CO_2 along the entire production, distribution, and utilization chain. Furthermore, should H_2-powered vehicles (e.g. fuel cell vehicles (FCVs)) or H_2 internal combustion engine vehicles (H_2ICEVs)) significantly penetrate the market and replace their fossil fuel-powered counterparts, CO_2 emissions could be reduced even further. Moreover, improvements in local and regional air quality through reductions in other major vehicle exhaust pollutants, such as nitrogen oxides (NO_x, nitric oxide (NO) + nitrogen dioxide (NO_2)), carbon monoxide (CO), particulate matter (PM), and volatile organic compounds (VOCs), would inevitably result.

Through all of the advantages that H_2 would provide as a sustainable energy option, questions have been posed regarding potential disadvantages or unknown consequences accompanying its large-scale adoption. For example, with the possibility of increasing H_2 emissions that may accompany a more H_2-intensive economy, can we confidently conclude that the implications for the atmosphere and climate are insignificant? Such questions have only been previously addressed in a handful of cases, primarily through atmospheric modelling studies. Although H_2 is typically considered an ecologically benign substance, possible atmospheric and ecological consequences of increasing H_2 emissions to the atmosphere have been the subject of discussion [6-12].

After CH_4, H_2 is the second most abundant trace gas in the atmosphere. An increase in tropospheric H_2 could lead to a reduction of the atmosphere's oxidizing capacity, primarily through the reduction of the hydroxyl radical (OH), which is the primary atmospheric "cleansing" agent. The consequence would be an increase in the atmospheric lifetime and radiative forcing of CH_4 (OH initiates the removal of both H_2 and CH_4 from the atmosphere) [7, 12] — a greenhouse gas significantly more potent than CO_2. An increase in the atmospheric H_2 burden could also favour the production of tropospheric ozone (O_3) due to changes in tropospheric OH radical

concentrations [6, 13]. Through its indirect radiative effects and relationship with other direct greenhouse gases, climate implications have thus been associated with tropospheric H_2 [14], and such interactions on a large scale could ultimately upset the current chemical balance in the atmosphere. Derwent et al. [11] found that through these interactions with CH_4 and O_3, H_2 can be considered an indirect greenhouse gas with an indirect global warming potential (GWP) of 5.8 over a 100-year time horizon. In other words, on a unit mass-unit mass basis, H_2 has an indirect greenhouse effect 5.8 times stronger than CO_2. This indirect GWP is based on the time-integrated radiative forcing of both CH_4 and O_3 that would result from a specific pulse of H_2 to the atmosphere.

In addition to tropospheric effects, increasing H_2 emissions at the surface have been implicated in the impact on stratospheric chemistry. For example, an increase in stratospheric H_2 could lead to rising water vapour (H_2O) mixing ratios in the stratosphere, with the ultimate result of stratospheric cooling and enhanced O_3 destruction [9], although the extent to which this ozone destruction may occur has been the subject of debate [7, 10, 12, 15]. Ehhalt and Rohrer [16] have also pointed out that the weak vertical gradient between upper tropospheric and lower stratospheric H_2 mixing ratios means that virtually no export of H_2 into the stratosphere should occur, while Rohs et al. [17] have reported that the contribution of stratospheric H_2 to the water vapour trend is minor. Any losses of H_2 to the stratosphere would, however, likely occur as convective injections in the tropical regions.

The level of H_2 in the atmosphere has remained essentially constant over the past several decades (see section 1.3.2). Thus in reality, the actual climatic and atmospheric influence of a potentially large fluctuation in the abundance of atmospheric H_2 has likely not been experienced. Any perturbations in the source strength of anthropogenic H_2 emissions to the atmosphere should therefore be treated with caution.

1.2 Structure of thesis

In the current introductory chapter (Chapter 1), an overview of the major characteristics of atmospheric molecular H_2 is provided (section 1.3). This includes details of seasonal cycles and past trend analyses. Section 1.4 covers the major sources of tropospheric H_2, particularly as they relate to technological anthropogenic processes, primarily from fossil fuels. In this section, specific technical aspects of emissions in vehicle exhaust are covered, including the role of the air-fuel ratio in the generation of H_2 in internal combustion engine vehicles, followed by the role of three-way catalytic converters in the removal and generation of H_2. H_2 emissions from specific chassis dynamometer, test bench, and real-world studies are then covered briefly, along with H_2 emissions from non-transport-based anthropogenic processes. As natural sources of atmospheric H_2 contribute roughly half of the total source strength to the global tropospheric H_2 budget, these sources are briefly covered in section 1.4.2. The major tropospheric sinks of H_2 are then covered in section 1.5. The motivation and scope of the thesis (section 1.6), which includes a detailed overview of the major tasks associated with the experimental part of this project, concludes the chapter.

Chapter 2 provides a comprehensive account of the methods that were applied in this study. The detailed tasks, which are summarized in section 1.6, form the experimental part of this project. These tasks are then covered in full detail in the following Chapters 3–5.

Chapter 3 deals with engine-specific aspects of direct H_2 emissions from gasoline-, diesel-, and natural gas-powered internal combustion engine vehicles. Included in this chapter are qualitative aspects found to influence H_2 emissions from such vehicles, along with the quantitative aspects of H_2/CO ratios and H_2 emissions factors, both of which are applied in Chapter 4.

Chapter 4 provides an in-depth analysis of globally upscaled anthropogenic H_2 emissions through a variety of scenarios and temporal scales through 2100. This includes global upscaling from road-based transportation emissions (section 4.1) and emissions from non-transport-based end-uses (section 4.3). In order estimate current

and future H_2 emissions from non-transport-based end-uses, scenarios for global H_2 production are required. Such scenarios are developed in section 4.2. Along with H_2 production figures, leakage and loss rates from H_2 production, distribution, storage, and non-transport-based end-uses must be known. Section 4.3.1 briefly covers the state-of-the-art knowledge of such leakage and loss rates. The results from the global production scenarios and leakage and loss rates are applied in section 4.3.2 to develop scenarios for global H_2 emissions from non-transport-based end-uses. Results from transportation- and non-transportation H_2 emissions are then combined in section 4.4 to develop scenarios for overall anthropogenic H_2 emissions from technological sources.

Chapter 5 covers H_2 observations at the remote high-altitude site Jungfraujoch, which is a site typically characteristic of free tropospheric conditions. The goal of these observations is to characterize temporal variations, along with identifying major source regions of present-day tropospheric H_2. However, one of the key features of measurements at remote sites is the ability to identify trends in background measurements. Although the dataset at Jungfraujoch is currently too short to draw any concrete conclusions about trends in background free tropospheric measurements, such H_2 observations will become increasingly valuable for assessing the influence of a potentially increasingly H_2-intensive economy as the dataset lengthens. These measurements will therefore act as a starting baseline condition, to which future observations can be compared as the fraction of H_2-based mobile and stationary applications increases.

Chapter 6 provides general conclusions and a summary of the research and analyses conducted over the course of this study, and thus the major findings of this thesis. An outlook is also provided, which includes suggestions and recommendations for areas of further research.

1.3 Characteristics of atmospheric H_2

Molecular H_2 is one of the most abundant atmospheric trace gases with a globally averaged tropospheric mixing ratio of approximately 530 parts per billion (ppb) [18]. This estimation is based on the most comprehensive set of global data to date, from

several stations located throughout both the Northern and Southern Hemispheres, and is thus regarded by many as the benchmark for current overall conditions. Some of the earliest estimations of atmospheric H_2 mixing ratios do not contrast significantly from the more recent figures. For example, citing correspondence with Dr. P.M. Schuftan during the first half of the 20th century in London, Paneth [19] estimated that the mixing ratio of H_2 in 1923 was approximately 0.5 parts per million (ppm, ≈ 500 ppb). This estimation is remarkably similar to today's much more detailed and accurate global estimate of ~530 ppb, and would suggest that the overall abundance of atmospheric H_2 has not changed significantly over the past century. This being the case, it would appear that until now the sources of H_2 have largely balanced out with the sinks, and that any increases in the source strength have been offset by sinks, despite global increases in motor vehicles with inefficient emission control systems compared with today's standards, for example.

Individual studies influenced by local sources and sinks display distinctly different results from those representative of average conditions. From earlier measurements taken in 1972 in Mainz, Germany for example, Schmidt [20] reported a mean mixing ratio of 0.800±0.168 ppm, a value representative of regularly polluted air masses in an urban setting, thus illustrating the important contribution of vehicle exhaust to observed tropospheric H_2 levels at the traffic source. Through a recent study in a suburban setting involving H_2 measurements influenced by the soil sink and local traffic patterns, Steinbacher et al. [21] reported a mean value of 576±94 ppb, with maximum values reaching almost 1600 ppb. The monitoring station was located in close proximity to a main road influenced heavily by rush hour patterns, thereby also illustrating the important contribution of vehicle exhaust to observed atmospheric H_2 mixing ratios.

The global budget of molecular H_2 in the atmosphere is determined by chemical transformations, sinks, and sources from natural and anthropogenic emissions (Fig. 1). The atmospheric lifetime of H_2 in the atmosphere is ~2 years [13, 18, 22]. In recent years, many studies have provided estimates for the source and sink terms in the global H_2 budget. In the following two sections (sections 1.4 and 1.5), a range of source and sink estimates is provided. Most terms are subject to considerable

uncertainty, which is reflected by the large ranges. Anthropogenic emissions (primarily from fossil fuel-based processes) are the focus of this thesis.

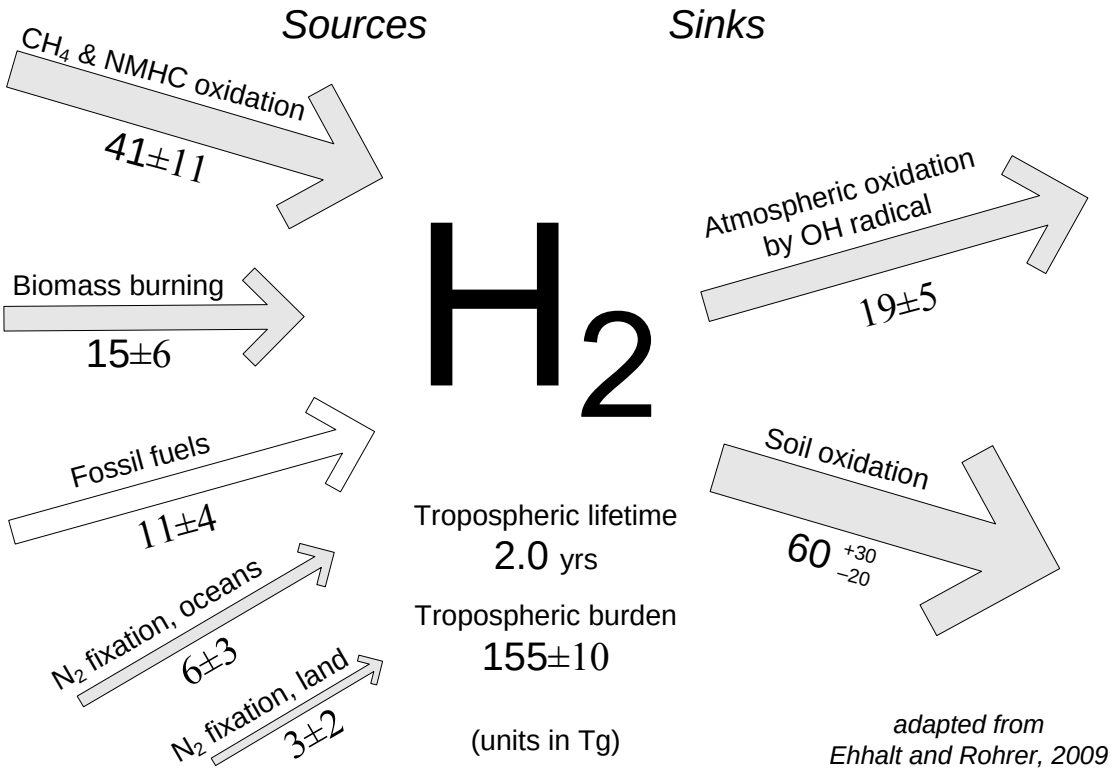

Figure 1. Global tropospheric H_2 budget. Sources are on the left, sinks on the right. Anthropogenic emissions from fossil fuels (white arrow) are the focus of this thesis. The figure has been adapted from [16].

1.3.1 Atmospheric seasonal cycles

Atmospheric seasonal cycles can provide useful information regarding the significance and influence of the major sources and sinks of a trace gas. Steinbacher et al. [21] reported traffic-influenced seasonal cycles exhibiting a minimum in summer and autumn and maximum in winter, which is likely due in part to the enhanced soil uptake of H_2 during the warmer months, but also likely due in part to higher cold start emissions from traffic under lower ambient temperatures [23]. In another local scale study above a polluted forest canopy in Harvard Forest, Massachusetts, Barnes et al. [24] reported a broad maximum from February to June, and a short, distinct minimum in September and October, which is also a pattern that is consistent with maximum H_2 oxidation by soils during the warmer and drier months. Simmonds et al. [25] also reported highest mixing ratios during spring and lowest mixing ratios in late autumn

in their study of continuous H_2 measurements at Mace Head. Grant et al. [26], in an extension of the study by [25], observed a baseline maximum in spring (April–May) and a minimum in autumn (October). Similarly, Novelli et al. [18] observed seasonal maxima and minima in the Northern Hemisphere in late winter/early spring and in autumn, respectively. Each of the above-referenced studies cites the dominant soil sink as a driving force behind the observed seasonal cycles in the Northern Hemisphere. It remains unclear as to how the seasonal H_2 cycles would change should the anthropogenic source of H_2 either fluctuate or reach an entirely new equilibrium.

1.3.2 Atmospheric trend analysis

One area that has received comparatively little attention, and one that would provide useful additional information, particularly as we progress towards a more H_2-intensive economy, is the observation of long-term trends in background atmospheric H_2 measurements. Studies addressing the topic do not cite significant large-scale trends. The longest available record, and therefore perhaps the most reliable and robust, is reported by [26], who revealed the absence of a trend in their study of continuous H_2 measurements at Mace Head over the 15-year period of 1994–2008. Other past estimates were possibly limited by the length of the available datasets, thereby leading to partly contrasting results, likely influenced by inter-annual variability. For example, in their 5-year study from 1994–1999 at Mace Head, Ireland, Simmonds et al. [25] reported a slight upward trend of 1.2±0.8 ppb a^{-1} for the Northern Hemisphere. Novelli et al. [18] reported a slight decreasing northern hemispheric trend of 2.2±0.2 ppb a^{-1} in the global marine boundary layer for the period 1991–1996. Langenfelds et al. [27] modelled a mean global H_2 increase of 1.4 ppb a^{-1}, which is based on measurements for the period of 1992–1999. In their 5-year study from 1985–1989 covering latitudes ranging from 71.5 ^{o}N to 71.4 ^{o}S, Khalil and Rasmussen [28] observed an increasing trend in global H_2 mixing ratios of 3.2±0.5 ppb a^{-1}, which was attributed to increasing anthropogenic sources. The lack of a long-term trend in background tropospheric H_2 in the last decades in Europe [26] supports the presumption that atmospheric H_2 levels have remained relatively constant over the past decades. Thus, measurements at remote free tropospheric sites should function as an effective tool to monitor the behaviour of background H_2 during the transition to

more H_2-intensive applications (e.g. long-term trend monitoring), through which anthropogenic H_2 emissions could plausibly increase.

1.4 Sources of atmospheric H_2

The overall source strength of tropospheric H_2 has been reported at 70–107 Tg a^{-1} [13, 16, 18, 29-32]. From this overall source term, 15–26 Tg a^{-1} originate from CH_4 oxidation in the atmosphere, 10–18 Tg a^{-1} from the oxidation of non-methane hydrocarbons (NMHC) in the atmosphere, 11–20 Tg a^{-1} from fossil fuel-based processes, 10–20 Tg a^{-1} from biomass burning, and 0–6 Tg a^{-1} from each of oceanic and terrestrial nitrogen (N_2) fixation processes.

1.4.1 Anthropogenic H_2 emissions from fossil fuels

The current global source strength of H_2 from anthropogenic fossil fuel-based processes represents ~14–26% of the total source term in the global atmospheric H_2 budget (see [16] for a recent review of the global H_2 budget). The contribution from vehicle exhaust represents the major source of H_2 from fossil fuel-based processes [16, 18, 20, 24]. Novelli et al. [18] reported a range of H_2 emissions strictly from transportation at 5–20 Tg a^{-1}, while Vollmer et al. [33] and Ehhalt and Rohrer [16] reported estimates towards the lower end of that range at 5.4±3.2 and 9±3 Tg a^{-1}, respectively. Stationary sources, such as fossil fuel combustion for industrial and residential heating systems, have been shown to emit marginal amounts of H_2 (M.K. Vollmer, Empa, pers. comm.). Other less well documented H_2 sources, such as leakage and losses during the reformation of hydrocarbons (e.g. SMR), currently represent a comparatively minor fossil fuel-based source [16], but could very well become a more significant contributor in the future as H_2 production for direct energy-based applications increases.

Vehicle exhaust gas from road-based transportation is currently the most significant source of anthropogenic H_2 to the atmosphere from technological processes [16, 20], but losses of H_2 from production, distribution, storage, and other end-use systems could become increasingly significant future contributors as H_2 production increases for both industrial and direct energy-based applications. It is these two sources — the exhaust gas of motorized road-based vehicles and leakage and losses from large-scale

industrial processes — that are considered to make up the majority of current global anthropogenic H_2 emissions to the atmosphere from fossil fuels [16, 18].

In many developed countries, automobiles are the dominant form of personal transportation [34]. Motorcycles are considered more leisurely vehicles in the most developed countries (e.g. Switzerland, see [35]), but are the vehicle of choice in many developing countries. In Switzerland, for example, despite the fact that passenger cars travelled almost 5 times as many kilometres as 2-wheelers under urban driving conditions in 2001, total CO emissions were still approximately 2.7 times higher for the 2-wheelers [36]. This figure is likely to be significantly higher in less developed, more populated countries reliant on compact, affordable transportation. For example in China at the end of 2008, motorcycles made up 53% of the entire vehicle fleet [37]. In Taiwan, this figure was 67% for 2007 [38]. Since the major anthropogenic source of both H_2 and CO is exhaust gas [20], it is likely that relative equivalent projections also hold true for H_2.

In the future, with changing vehicle fleet composition (including an increased fraction of fuel cell vehicles (FCVs)) and increasing H_2 production, it is possible that anthropogenic H_2 emissions to the atmosphere will not only fluctuate or reach a new equilibrium, but that these may be complemented with an overall increase in the abundance of atmospheric H_2.

1.4.1.1 H_2 emissions in internal combustion engine exhaust – the role of air-fuel ratios and lambda

H_2 emissions in vehicle exhaust result from incomplete fuel combustion in the absence of oxygen (O_2). CO emissions evolve under these same conditions, which creates a strong positive correlation between H_2 and CO in direct vehicle exhaust measurements. The air-fuel ratio — the ratio of the mass of air supplied to the engine to the mass of fuel supplied to the engine over the same time period — plays an important role. Lambda (λ) is a measure of the extent of the excursion from the air-fuel ratio relative to stoichiometry. The stoichiometric air-fuel ratio for a particular fuel type is the air-fuel ratio that ensures complete combustion of all carbon and hydrogen without any remaining oxygen. A λ value of 1 is at stoichiometry, whereas a value above 1 indicates an excess of air (lean-burn (oxidizing) conditions), and a

value below 1 indicates the opposite (rich-burn (reducing) conditions). Modern engines control λ at 1 using lambda sensors mounted both up- and downstream of the catalyst. With current technologies, gasoline engines for passenger vehicles are typically operated under stoichiometric conditions whenever possible, during which the air-fuel ratio is optimal to ensure complete fuel combustion. Exceptions are situations requiring extended periods of high power, during which rich stoichiometry is selected to cool the engine and the catalyst, short periods where the engine control unit (ECU) can not perfectly maintain lambda at 1, or when rich conditions are chosen to clear out O_2 from the catalyst after fuel cut-off phases (P. Soltic, Empa, pers. comm.). Diesel vehicles always operate under "fuel-lean" oxidizing conditions, where air-fuel ratios are consistently above stoichiometric conditions, leading to much lower mixing ratios (and often untraceable levels) of H_2 in exchange for higher levels of NO_x.

1.4.1.2 Three-way catalytic converters

Increasingly stringent legislation on emissions of CO, NO_x, and hydrocarbons in response to air pollution and the rising awareness of adverse effects on human health, man-made infrastructure, and biota, has led to the advent of three-way catalytic converters (TWCs), which simultaneously promote the oxidation of CO and hydrocarbons, along with the reduction of NO_x. Although TWCs are not always mandated by legislation, it has become impossible to reduce emissions below legislated limits without them.

Overall, TWCs deplete H_2 from raw vehicle exhaust. H_2 emissions from vehicles without TWCs are much higher than from those equipped with exhaust after-treatment systems [39]. Important to note is that not only do TWCs remove H_2 and other substances from vehicle exhaust, but current vehicle technologies also often have more sophisticated and precise onboard computer systems that consistently regulate the air-fuel ratio at the stoichiometric point. The result is much lower emissions compared with older vehicle technologies (or vehicles without a TWC). Today's TWCs are also designed to promote water-gas shift and steam reforming reactions [40], which ultimately results in the production of some H_2 through the destruction of hydrocarbons, CO, and H_2O. In steam reforming reactions, hydrocarbons are oxidized

by H_2O to produce CO and H_2. The general equation for the steam reforming of hydrocarbons is:

$$C_nH_{2n+2} + nH_2O + \text{heat} \rightarrow nCO + (2n+1)H_2$$

Steam reforming reactions are endothermic (i.e. require the input of heat and proceed at high temperatures). The water-gas shift reaction is exothermic (i.e. gives off heat and proceeds at lower temperatures), consuming CO and producing H_2 in the process:

$$CO + H_2O \rightarrow CO_2 + H_2 + \text{heat}$$

Ageing of a catalytic converter can have a significant effect on the level of H_2 emissions over the lifetime of a TWC, as for example Auckenthaler [40] observed much higher water-gas shift and steam reforming activity with a fresh TWC than with an aged device. H_2 evolution within a TWC is not solely dependent on the air-fuel ratio, but also on the O_2 storage capacity of the TWC. Ageing of a catalytic converter can significantly reduce its storage capacity for O_2 [41].

The O_2 storage capacity has been established as a key parameter for the appropriate catalytic performance of commercial TWCs, and involves storage of excess O_2 in the catalyst substrate (washcoat material containing ceria) during fuel lean conditions, and its release under fuel-rich conditions [42]. Ceria also promotes the water-gas shift reaction [43]. In the absence of O_2 (or once the O_2 has been depleted by oxidizing CO and hydrocarbons under fuel rich conditions), H_2O will take the place of O_2 on the ceria, promoting steam reforming and water-gas shift reactions. According to Auckenthaler [40], water adsorption on the ceria is required in order for the water-gas shift reaction to proceed.

1.4.1.3 H_2 emissions from test-bench, dynamometer, and real-world studies involving internal combustion engine vehicles

The majority of efforts to quantify the contribution of H_2 from technological anthropogenic processes to date have stemmed from studies scaling H_2 against CO emissions, for which reliable inventories exist [13, 18, 21, 31, 33]. Based on the strong positive correlation in the exhaust gas of fossil fuel-powered internal combustion engine vehicles, most studies base their estimations on the slope of the

regression line between simultaneously measured H_2 and CO [16]. In a 2004 highway tunnel study in Switzerland, Vollmer et al. [33] calculated a mean $\Delta H_2/\Delta CO$ molar ratio of 0.48±0.12. This ratio increased to ~0.6 during periods of rush hour traffic, which the authors attributed to a dominance of H_2 production over CO under fuel-rich conditions, likely due to increased water-gas shift activity (i.e. $CO + H_2O \rightarrow H_2 + CO_2$). In a test-bench study involving emission measurements from a light-duty vehicle (LDV) engine [39], pre-TWC measurements displayed predictable mixing ratios of both H_2 and CO in the exhaust gas under variable air-fuel ratios (see Fig. 14). Because of this correlation, and the much more well constrained CO contribution from vehicle exhaust, the molar ratio of H_2/CO has been considered a central topic in previous studies involving older vehicle technologies for establishing the H_2 contribution from fossil fuel combustion processes, primarily transportation [18, 20, 21, 24, 33, 44-46].

Studies that calculate H_2 emission factors from measurements taken directly at the tailpipe are less common, as the processes of H_2 production and emission involving vehicles simulating real-world driving conditions have only been assessed in a limited number of cases. In a study involving direct H_2 emissions and calculations of H_2 emission factors from a chassis dynamometer study, Heeb et al. [47] observed a wide range of H_2 emission factors for a series of gasoline-powered Euro-3 automobiles. The range was largely attributed to the various driving conditions characteristic of the different cycles and sub-cycles (i.e. urban, rural, and highway driving conditions). H_2 emission factors were found to be highly dependent on speed and acceleration patterns, with the highest H_2 emission factors reported for vehicles conducting cycles subject to both cold-start emissions and high speeds. The highest H_2 emission factors were found when vehicles exceeded 130 km h^{-1}, particularly during acceleration events when travelling such speeds. The lowest H_2 emission factors resulted from a speed range of 70–90 km h^{-1}, which the authors likened to a typical velocity regime found in highway tunnels. The mean H_2 emission factor across the range of sub-cycles was calculated at 59.4 mg km^{-1}. The mean H_2 emission factor for strictly highway driving conditions was calculated at 48.8 mg km^{-1}, which is consistent with the mean H_2 emission factor of 49.7±16.5 mg km^{-1} from a highway tunnel study [33].

Tunnel studies eliminate the influence from other local source and sink factors, and can thus provide robust information about H_2 emissions from real-world vehicle fleets. In a tunnel study in Switzerland, Vollmer et al. [33] reported an H_2 emission factor of 67 mg km^{-1} for a strictly gasoline-based traffic fleet comprising a wide range of emission standard technologies. A much smaller H_2 emission factor was found for heavy-duty vehicles than for LDVs, a trait pinned to the much lower H_2 emissions from diesel compared with gasoline technologies.

1.4.1.4 Non-transport-based anthropogenic H_2 emissions

Direct emissions of H_2 to the atmosphere from non-transport-based end-use systems also contribute to the overall source from anthropogenic processes. Currently, the majority of these losses are derived from fossil fuels during the production of H_2 for industrial processes (e.g. fossil fuel reforming). Approximately 96% of current global H_2 production is generated through fossil fuels [48], and the vast majority of this production is allocated for captive uses [49]. Captive uses are those involved in on-site H_2 production and direct consumption, primarily large-scale industrial processes, such as the petroleum refining, ammonia (NH_3) production, and methanol (CH_3OH) production industries, which combined account for ~92% of current global H_2 production [48].

Merchant H_2 is sold on the market, primarily by industrial gas companies [50], and includes H_2 for direct energy-based end-uses, such as fuel for transportation and industrial, commercial, and residential power. At present, however, less than 1% of global H_2 production is allocated for primary energy consumption, although this figure is expected to increase considerably throughout the 21st century [5]. Future anthropogenic H_2 emissions to the atmosphere from technological processes will therefore depend not only on the generation of H_2 from fossil fuels, but also on H_2 production strategies for both industrial processes and direct energy services, leakage and loss rates, and global vehicle numbers and fleet compositions. Figure 2 depicts a simplified version of the H_2 life cycle for current (2010) and near-term (2020) conditions, along with envisaged future (2050 and 2100) conditions (adapted from [5]).

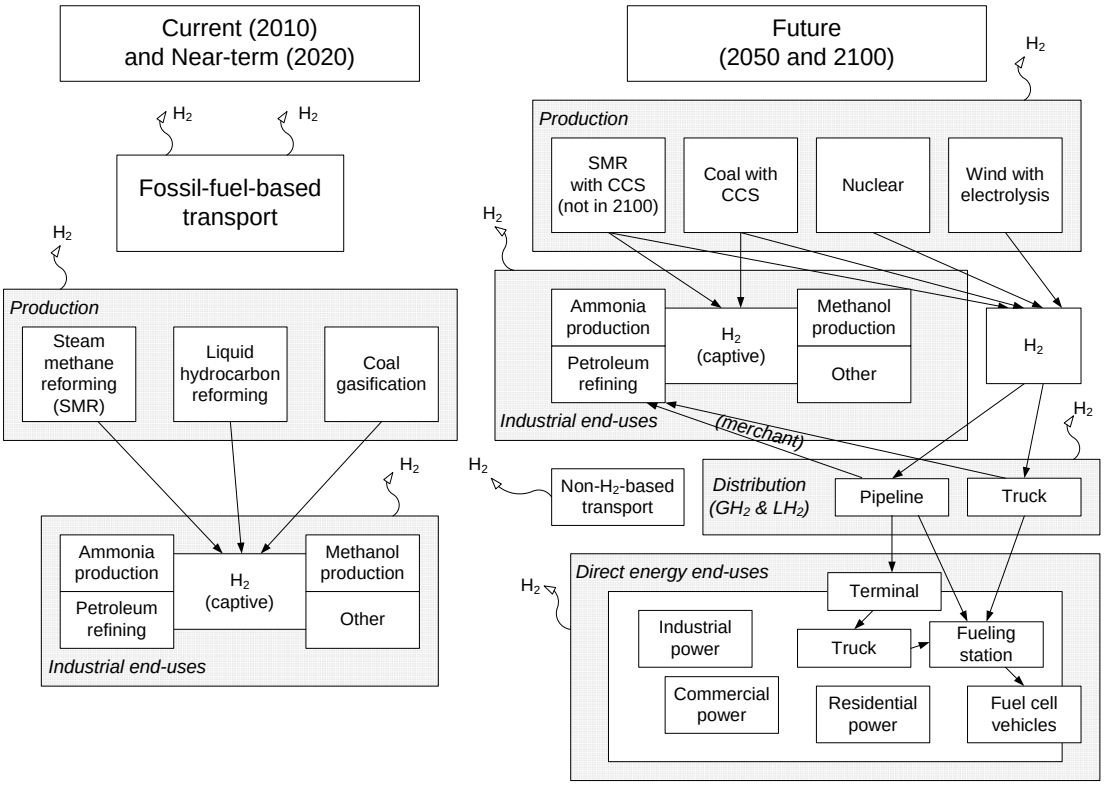

Figure 2. Simplified H_2 life cycle for the most significant processes envisaged for current (2010) and near-term (2020), along with future (2050 and 2100) conditions. Curved arrows represent vehicle exhaust H_2 emissions and losses and leakage along the H_2 production, distribution, and utilization chain. The major production sources in 2050 and 2100 are based on [5].

Generally, under identical conditions, it is widely accepted that emissions from cryogenic liquid H_2 (LH_2) dominate those of the gaseous form (GH_2). An estimated range of H_2 loss rates due to "boil off" or evaporation from LH_2 would be on the order of 0.1–10% over the entire production, distribution, and end-use chain [7, 51-56]. This range is based on leakage from mature delivery and end-use systems, including pipelines, storage systems, compressors, pumps, and vehicles. Losses associated with high-pressure GH_2 are lower than those associated with LH_2. An estimated range associated with the loss of compressed GH_2 from mature systems is marginal up to approximately 4% over the entire production, distribution, and end-use chain [7, 15, 53, 56]. Other anthropogenic processes, such as industrial and residential heating systems, have been found to expel marginal H_2 (M.K. Vollmer, Empa, pers. comm.).

Although a large-scale H_2-intensive economy would involve significantly greater H_2 production for direct energy services, losses of H_2 to the atmosphere are not

unanimously expected to increase considerably, despite the diffusive nature of H_2. Instead, it could be anticipated that losses actually decline as the maturity of the hydrogen chain develops (see section 4.3.2). Loss rates estimated by industrial sources tend to be lower, which may indeed be based on more realistic and reliable information from those involved in the industry, where safety, ecological, and monetary concerns highlight the agenda. The higher-end loss rates are often based on results from modelling studies [9]. The high-end loss rate scenarios, on the one hand, provide important reminders about the proper diligence required during the transition towards an increasingly H_2-intensive economy, while on the other hand are perhaps overestimated in today's technology-driven society. See section 4.3.1 for an account of the state-of-the-art of loss rates of H_2 to the atmosphere from various production, distribution, storage, and end-use systems.

1.4.2 Major natural sources of H_2

The primary natural sources of H_2 are the atmospheric oxidation of both CH_4 and NMHC. Together, these two pathways represent slightly more than half of the total H_2 burden of the global H_2 budget (see Fig. 1). The oxidation of CH_4 in the atmosphere is initiated by the OH radical through the following reaction:

$$CH_4 + OH \rightarrow CH_3 + H_2O$$

Through a series of intermediate steps, formaldehyde (HCHO) is formed, which is itself then photolytically degraded into H_2 (for a detailed description of the steps involved, see [18]):

$$HCHO + h\nu \rightarrow H_2 + CO$$

The rate at which H_2 is photolytically produced through the photodissociation of formaldehyde increases with elevation due to the decrease in atmospheric pressure and a corresponding growth in the quantum yield for the process [22]. Even though only a small fraction of HCHO is photolytically degraded to H_2, the ubiquitous distribution of OH, along with the widespread distribution of atmospheric O_3, H_2O, and CH_4 make tropospheric H_2 production through the oxidation of CH_4 the single largest source term in the global H_2 budget. As the production of H_2 is reliant on the

photodissociation of HCHO, the most H_2 through this reaction will be produced under high sunlight condition, i.e. during the summer months with the highest incidence of incoming solar radiation.

H_2 production through the oxidation of NMHCs is the second largest single source term in the global H_2 budget. Similarly to CH_4 oxidation, a series of chain reactions leads to HCHO as an intermediate product, which is then photolytically dissociated to H_2. Globally, biogenic VOC emissions far exceed those from anthropogenic sources [57], indicating that the oxidation of biogenic VOCs, e.g. isoprene [22, 29, 58], a VOC emitted particularly by deciduous vegetation [59], are responsible for the largest fraction of this source term. Isoprene is expected to yield much more H_2 through oxidation than is terpene, for example, as isoprene is known to produce 3 molecules of HCHO per oxidized molecule, which does not occur to the same extent with the terpene molecule [22]. Biogenic VOC emissions are highly seasonal, and Seinfeld and Pandis [57] confirm that biogenic VOC emissions are generally highest on hot summer days. This would suggest too that H_2 emissions from this source are highest under warmer conditions with greater actinic flux, as these are also the conditions that favour OH radical production in the atmosphere.

1.5 Sinks of atmospheric H_2

Two known major sinks of atmospheric H_2 exist:

1. oxidation of H_2 through enzymatic and microbial processes within soil; and
2. oxidation of H_2 through the chemical reaction with the OH radical in the atmosphere.

Microbial and enzymatic processes in soil represent the predominant sink in the global H_2 budget [60-64]. Soil uptake accounts for approximately three quarters (55–88 Tg a^{-1}) of the global sink strength, while oxidation through reaction with the OH radical accounts for the remainder (15–19 Tg a^{-1}) [13, 16, 18, 29-32].

It is not the soil in itself that acts as the primary sink for atmospheric H_2. Instead, specific microorganisms, along with enzymes within the soil — hydrogenases — are responsible for catalyzing the oxidation of H_2 through the following reaction [65-67]:

$$H_2 \leftrightarrow 2H^+ + 2e^-$$

The oxidation of H_2 is an essential role in the metabolism of certain bacteria, and these organisms are capable of oxidising H_2 and living off the liberated energy [68]. Atmospheric H_2 appears to be oxidized by abiontic soil hydrogenases [61]. These enzymes include not only free extracellular enzymes and those bound to inert soil components, but also active enzymes within dead or non-proliferating cells and others associated with the dead cell fragments [65, 69, 70].

Schmidt [20] and Conrad and Seiler [65] describe the soil uptake mechanism of H_2 as a first order reaction at the soil surface, meaning that the uptake rate is proportional to the abundance of H_2. It is therefore likely that a modest increase in atmospheric H_2 would be offset by enhanced H_2 uptake by soils. Thus, it would be difficult to accurately predict past atmospheric H_2 mixing ratios based solely on the changing source strength (e.g. increased fuel consumption [20] and atmospheric CH_4 mixing ratios [28]). Whether or not the first order reaction kinetics hold true for potentially much larger increases of H_2 at the surface on a much larger scale remains to be seen, since such a potential threshold remains unsubstantiated to date. An upper-end threshold boundary beyond which this assumption may not hold true is equally plausible.

Soil temperature is a very important characteristic influencing soil uptake of H_2 [63]. Studies evaluating temperature-dependent soil H_2 oxidation have reported an optimal uptake temperature range of 20 to 40 ^oC [62, 71, 72]. However, the presence of an inactive layer — the upper layer of soil that inhibits H_2 uptake due to the absence of microbiological activity — has been shown to limit soil uptake of H_2 due to water stress under dry conditions [63]. This observation suggests that a certain degree of moisture is indeed required to initiate the processes necessary for the oxidation of H_2. Conrad and Seiler [65] found that the H_2 decomposition activity was dependent on the soil moisture, with the maximum uptake ranging from 6–11% water content. However, excessive soil moisture content appears to inhibit uptake of H_2 by soils. Yonemura et al. [69] observed decreasing H_2 deposition velocities with increasing soil moisture content, which corresponded to decreasing gas-filled porosity in the soil.

The atmospheric oxidation of H_2 in the atmosphere is carried out through the reaction:

$$H_2 + OH \rightarrow H_2O + H$$

The loss rate of H_2 through OH oxidation in the atmosphere is proportional to the abundances of both H_2 an OH, with a reaction rate constant of H_2 + OH at 277 K of $4.0\pm0.2 \times 10^{-15}$ cm^3 $molecule^{-1}$ s^{-1} [18]. The oxidation of H_2 by the OH radical is latitudinally and seasonally dependent. OH radicals are formed in the troposphere through the following series of reactions:

$$O_3 + h\nu \rightarrow O_2 + O(^1D) \ (\lambda < 320 \text{ nm})$$
$$O(^1D) + H_2O \rightarrow 2OH$$

Hydroxyl radicals are generated at the greatest rate under high sunlight conditions, when the actinic flux is at its highest to break down the O_3 molecule to O_2 and $O(^1D)$, and when ample air humidity is present to react with the excited oxygen atom ($O(^1D)$), such as in summer when there is a significant amount of evaporation from waterbodies and evapotranspiration from vegetation. Price et al. [29] reported an approximate bell-shaped curve with OH oxidation of H_2 at a minimum at the poles and increasing to a maximum at the equator. This further illustrates the temperature and humidity dependence of H_2 oxidation by OH, indicating that this process is also most prominent during the warmer months (see also Chapter 5 for the influence of this process on measurements from this study). Although it could be assumed that the seasonal cycle of OH (i.e. highest mixing ratios in warmer months, lowest in cooler months) would noticeably influence the seasonal cycle of H_2, we will see in Chapter 5 that the complex interplay of atmospheric sources and sinks, the soil sink, and interaction with the atmospheric boundary layer all play a role in the observed atmospheric levels of H_2.

Atmospheric H_2 is not uniformly distributed across the globe. Average mixing ratios tend to vary north and south of the equator, which has been attributed to the hemispheric asymmetry of land mass area and soil sink capacity. For example, Novelli et al. [18] reported a ratio of 0.97 for the Northern Hemisphere/Southern Hemisphere burden, i.e. H_2 levels that are 3% higher in the Southern Hemisphere.

This is attributed to the hemispheric asymmetry of land masses and the dominant soil sink capacity, with the Northern Hemisphere comprising 60–70% of the global land area.

1.6 Motivation and Scope

The motivation for this project stems from the responsibility to characterize — both qualitatively and quantitatively — the major sources of current and future technological anthropogenic H_2 emissions to the atmosphere during the potential transition to an increasingly H_2-intensive economy.

The scope of the project consists of 3 major tasks.

The first major task is to qualitatively and quantitatively assess direct H_2 emissions in the exhaust gas of current technology vehicles tested on a chassis dynamometer. The second task builds on the first task and involves upscaling quantified H_2 emissions across various temporal scales. This will allow for the formulation of descriptive scenarios as the major sources of anthropogenic H_2 either diversify or change in their relative contribution to the atmospheric H_2 burden. The final task is to analyze atmospheric H_2 emissions at a remote Alpine site. Currently, these measurements are performed to evaluate temporal variations in background free tropospheric conditions and to identify important source regions H_2. Importantly, these measurements also act as an indicator of current baseline atmospheric conditions. Under mid- to longer-term conditions, trend analysis of these measurements should provide a robust tool to assess patterns or trends in background H_2 mixing ratios as H_2-based mobile and stationary applications increase their global abundance.

The major tasks are detailed sequentially below:

Task 1 – Characterize and quantify H_2 emissions from the most common current technology vehicles based on measurements taken directly at the exhaust source.

The accurate quantification of H_2 emissions from motor vehicles is essential to narrow the uncertainty associated with this term in the global H_2 budget. In Chapter 3, this task was approached through the direct online measurements of H_2 and CO in the exhaust gas of current technology vehicles tested on a chassis dynamometer in the Laboratory for Internal Combustion Engines at Empa (Swiss Federal Laboratories for Materials Science and Technology). Based on these measurements, H_2 emission factors (E_{H2}) and H_2/CO ratios were calculated — both of which were applied in the

global upscaling of H_2 in Task 2. For reference, CO emission factors (E_{CO}) are also covered in some detail.

Qualitatively, such measurements help map the processes involved in H_2 evolution from current technology vehicles. Quantitatively, E_{H2} and H_2/CO ratios help quantify the contribution of H_2 to the atmosphere from direct emissions and assist in formulating global H_2 scenarios from transportation based on variable vehicle technologies, emission standards, and spatial and temporal scales.

Task 2 – Apply E_{H2} to globally upscale direct H_2 emissions from the most significant current and future transportation and non-transport-based sources; estimate global H_2 production and consumption scenarios; establish realistic well-to-wheel leakage and loss rates of H_2; and provide quantitative scenarios of global technological anthropogenic H_2 emissions to the atmosphere throughout the 21st century.

In Chapter 4, a detailed analysis of H_2 emissions from the major technological anthropogenic processes that contribute to the present and future global H_2 budget has been performed in this work and serves to quantify the contribution from this sector.

The main objective of this task is to estimate future global anthropogenic H_2 emissions based on changing vehicle fleet composition and global H_2 production for industrial and direct energy consumption. This was approached through scenarios on different temporal scales (2010, 2020, 2050, and 2100) under the assumption that H_2-based mobile applications and H_2 production will increase throughout the 21st century.

Task 3 – Evaluate temporal variations in background free tropospheric H_2 conditions in the Northern Hemisphere and identify important European source regions.

In Chapter 5, continuous observations of H_2 at the high-altitude site Jungfraujoch, Switzerland, are analysed in order to improve our understanding of H_2 in the free troposphere, along with the effect of its various sources and sinks. Until now, the behaviour of atmospheric H_2 has not been reported upon in the free troposphere. Through these observations, temporal variations are evaluated and European source regions are identified. These current observations act as a baseline condition to which future observations can be compared.

2 METHODS

2.1 Direct exhaust gas H_2 measurements

The following section details the methodology associated with Task 1 outlined in section 1.6. This involves both direct online measurements of H_2 in the exhaust gas of fossil fuel powered vehicles and separate measurements of a stationary engine capable of combusting both gasoline and natural gas (section 2.1.6). All measurements were conducted in the Laboratory for Internal Combustion Engines at Empa.

2.1.1 Vehicle selection

For this task, an assessment of H_2 emissions from Euro-4 automobiles, Euro-4 delivery vehicles, Euro-3 motorcycles, and Euro-3 scooters was conducted. The Euro-designation represents European emission standards. All vehicles were selected from the Swiss vehicle fleet, and were not serviced prior to testing. Measurements are representative of current technology vehicles consistent with a real-world modern European vehicle fleet.

The vehicles tested in this study, along with their main attributes, are specified in Tables 1–5. The Euro-4, four-wheeled vehicles comprised 5 gasoline-powered automobiles, a diesel-powered automobile, 5 diesel-powered delivery vehicles, and 8 natural gas-powered automobiles. The Euro-3, two-wheeled vehicles comprised 8 gasoline-powered motorcycles/scooters. All gasoline-powered vehicles in this study were equipped with TWCs. All diesel-powered vehicles were equipped with oxidation catalysts and three had diesel particle filters (DPF) (see Tables 3 and 4). Emissions from an FCV have also been measured and evaluated in detail at Empa, but due to the private contract-nature of the measurements, only qualitative information is provided in this study.

Table 1. Main attributes of gasoline Euro-4 automobiles.

Make	Model	Empty mass (kg)	Displacement (cm^3)	Power (kW)	Gearbox	GDI[a]	Mileage (km)
Volkswagen	Touran	1575	1390	103	DSG6	yes	16 048
Honda	Civic	1265	1799	103	m6	no	45 050
Renault	Megane	1320	1598	83	m5	no	77 710
Renault	Scenic	1565	1998	99	a5	no	61 115
Mini	Cooper	1150	1598	85	m5	no	68 831

[a]GDI – Gasoline Direct Injection system

Table 2. Main attributes of gasoline Euro-3 motorcycles and scooters.

Make	Model	Empty mass (kg)	Displacement (cm^3)	Power (kW)	Gearbox	Class[a]	Mileage (km)
Suzuki	GSX R 1000	283	999	136.1	m6	3-2	2064
Honda	SH 125	134	125	10.1	aut	2-1	17 615
Kawasaki	ER-6N	277	649	53	m6	3-2	15 133
Honda	CBR 600 RR	259	599	88	m6	3-2	10 947
Yamaha	FZ1	289	998	110	m6	3-2	26 225
Piaggio	X8	249	244	16	aut	2-2	9447
Harley Davidson	FXDC	385	1584	56	m6	3-2	6448
Piaggio	VESPA LX 125	190	124	7.65	aut	2-1	3306

[a]Class 2-1 refers to engine displacement < 150 cm^3 and maximum speed < 115 km h^{-1}
[a]Class 2-2 refers to 115 km h^{-1} < maximum speed < 130 km h^{-1}
[a]Class 3-2 refers to maximum speed > 140 km h^{-1}

Table 3. Main attributes of diesel Euro-4 automobile.

Make	Model	Empty Mass (kg)	Displacement (cm^3)	Power (kW)	Gearbox	DPF[a]	Mileage (km)
Audi	A4	1620	1968	103	m6	Yes	25 806

[a]DPF – Diesel Particle Filter

Table 4. Main attributes of diesel Euro-4 delivery vehicles.

Make	Model	Empty Mass (kg)	Displacement (cm^3)	Power (kW)	Gearbox	DPF[a]	Mileage (km)
Fiat	Ducato	2000	2287	88	m5	No	24 867
Renault	Trafic T29	1930	2464	107	m6	Yes	38 158
Citroen	Jumper	2650	2198	88	m6	No	13 482
Volkswagen	T5	2089	2461	96	m6	Yes	32 203
Ford	Transit	1735	2198	63	m5	No	23 485

[a]DPF – Diesel Particle Filter

Table 5. Main attributes of natural gas Euro-4 automobiles.

Make	Model	Empty Mass (kg)	Displacement (cm^3)	Power (kW)	Gearbox	Mileage (km)
Volkswagen	Caddy	1642	1984	80	m5	32 429
Volvo	V70 CNG	1591	2435	103	aut	47 709
Fiat	Punto 1.2 Bipower	1025	1242	38 / 44	m5	23 426
Opel	Combo C16CNG	1395	1598	71	m5	39 459
Volkswagen	Golf Variant Bifuel	1434	1984	75 / 85	m5	93 344
Citroën	C3 1.4i	1014	1360	54	m5	11 300
Mercedes Benz	E 200 NGT	1690	1796	120	aut	44 192
Fiat	Multipla 1.6 Bipower	1470	1596	65	m5	46 401

2.1.2 Experimental setup of chassis dynamometer

All tests were conducted on a chassis dynamometer, which enabled emission measurements of simulated real-world driving scenarios under controlled stationary conditions. Figure 3 depicts the experimental setup of the chassis dynamometer.

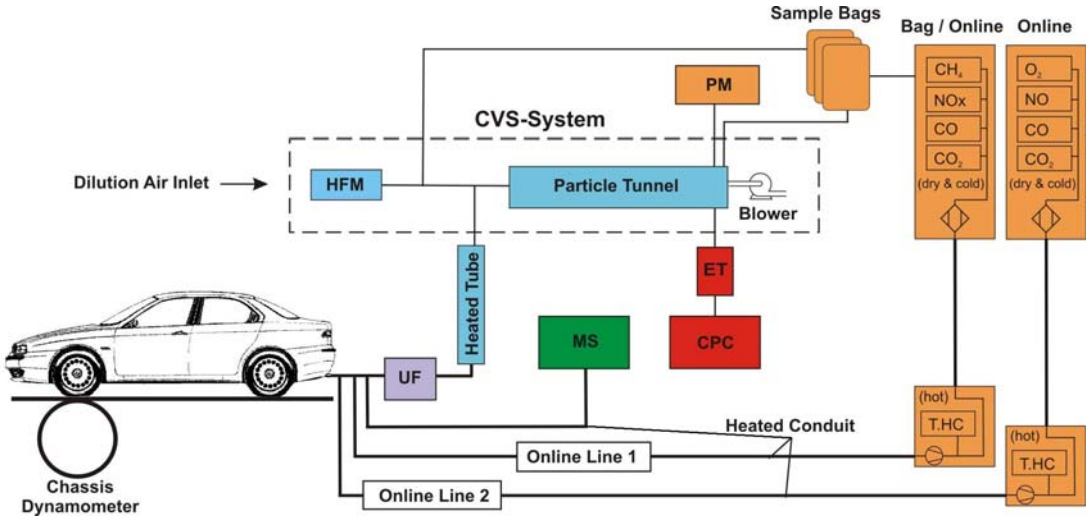

Figure 3. Experimental setup of chassis dynamometer and associated measurement systems.

All H_2 measurements were conducted using the online sampling technique. For online measurements, exhaust gas is measured directly at the tailpipe, which allows for a detailed analysis of the relationship between the characteristics of the individual cycles/sub-cycles and the resulting emissions. Measurements from 4-wheeled vehicles involved analysis of undiluted exhaust directly at the tailpipe. As 2-wheelers produce

considerably less exhaust flow, a dilution system was implemented for the motorcycles and scooters, which allowed direct online measurements similar to those for the 4-wheelers (see [35] for details of this setup). Figure 4 depicts one of the motorcycles on the chassis dynamometer.

Figure 4. Motorcycle on chassis dynamometer. A = ventilator.

All vehicles were subject to similar experimental conditions on the chassis dynamometer. Air temperature and relative humidity were approximately 23 ^{o}C and 50%, respectively, and a large ventilator (A in Fig. 4) was utilized to simultaneously cool the engine and simulate real-world driving conditions based on vehicle speed.

Dry H_2 mixing ratios were measured using an H-Sense process mass spectrometer (V&F Analyse- und Messtechnik GmbH, Austria). The H-Sense (MS, Fig. 3) measurement principle is based on Electron Ionization Mass Spectrometry (EIMS). Through electron impact ionization, the gas sample ions are energized, focused, and separated further on a magnetic field in order to detect only hydrogen (and helium). The gas inlet system automatically compensates for any pressure fluctuations between 0.5–3 bar. The sample line delivering exhaust gas to the MS was heated to 190 ^{o}C to prevent condensation within the line. The sample air was dried with a gas cooler (5

^{o}C) and filtered with a 2 μm particulate filter. Emissions were registered according to volume mixing ratio at the ppm level. Through previous measurements, the stability of the instrument was found to be constant over a period of several days. Nevertheless, the instrument was calibrated either for each cycle, or between two cycles, if both cycles were performed within a time span of a few hours. The standards used were synthetic air free of H_2 (zero gas) and a 1000 ppm H_2 standard (span gas). A second 30 ppm H_2 standard was used with some of the earlier measurements. However, this standard was later replaced by the 2-point calibration system as the instrument had been previously experimentally found to be linear over the mixing ratio range up to ~20 000 ppm [73], which is the range in which the majority of engine exhaust is found. Precision as measured at the 30 ppm (secondary standard) and 1000 ppm levels was 0.1% and 0.03%, respectively. The accuracy of the overall measurements was dominated by the uncertainty of the standards and estimated at ~2%. The detection limit of the instrument was determined empirically to be in the low ppb range. However, mixing ratios below 500 ppb were considered to be unreliable due to interferences and possible matrix effects. The signal-response time from exhaust pipe to analyzer was empirically determined to be 6–7 seconds. This delay required shifting the data in order to ensure the most accurate characterization of emissions vs. speed possible, based on the response time limitations of the system. CO was also measured online with a Horiba Mexa 7100 AIA-721A and AIA-722 (Horiba, Ltd., Japan). These instruments are based on the non-dispersive infrared detection measurement principle. The exhaust gas was dried prior to analysis. All H_2 and CO data is reported with a frequency of 1 Hz.

In order to accurately quantify H_2 emissions and derive emission factors from the measured molar mixing ratios, an ultrasonic flow measuring system (Flowsic 150 Carflow, Sick Maihak, Inc.) was used to directly monitor the exhaust volume flow at the tail pipe (UF, Fig. 3).

2.1.3 Driving cycles and sub-cycles

In this study, a driving cycle is defined as the overall speed profile driven by a vehicle from start to finish. Measurements for entire driving cycles commenced approximately 25 seconds before the vehicle accelerated and terminated

approximately 20 seconds after the vehicle came to rest. Sub-cycles are the individual parts of each cycle represented by distinct driving conditions. Sub-cycles represent urban, rural, or highway driving conditions. Table 6 lists the major characteristics of the cycles for 4-wheeled vehicles and Fig. 5 depicts their speed profiles. For 4-wheeled vehicles, a total of 6 cycles were conducted, 3 of which involved vehicles starting with cold engines, while the other 3 cycles involved starts with a previously warmed-up engine (in this study, the criterion for a warm-start cycle is vehicle engine oil of at least 80 ^{o}C). Some cycles represent real-world conditions in order to derive information about vehicle emission behaviour under specific driving conditions; other cycles are legislative for certification purposes.

Table 6. Main characteristics of driving cycles conducted by 4-wheeled vehicles. EC = European Commission, CH = Switzerland, and BAB = Bundesautobahn (a German real-world highway cycle).

Cycle	Sub-cycle			Cold Start	Description
	1	2	3		
IUFC15	urban	urban	urban	yes	real-world Europe
L2	urban	rural	highway	yes	legislative EC & CH + BAB
LA	rural	urban	rural	yes	legislative USA
CADC	urban	rural	highway	no	real-world Europe
Ra	highway	highway	rural	no	real-world CH
Rb	rural	urban	urban	no	real-world CH

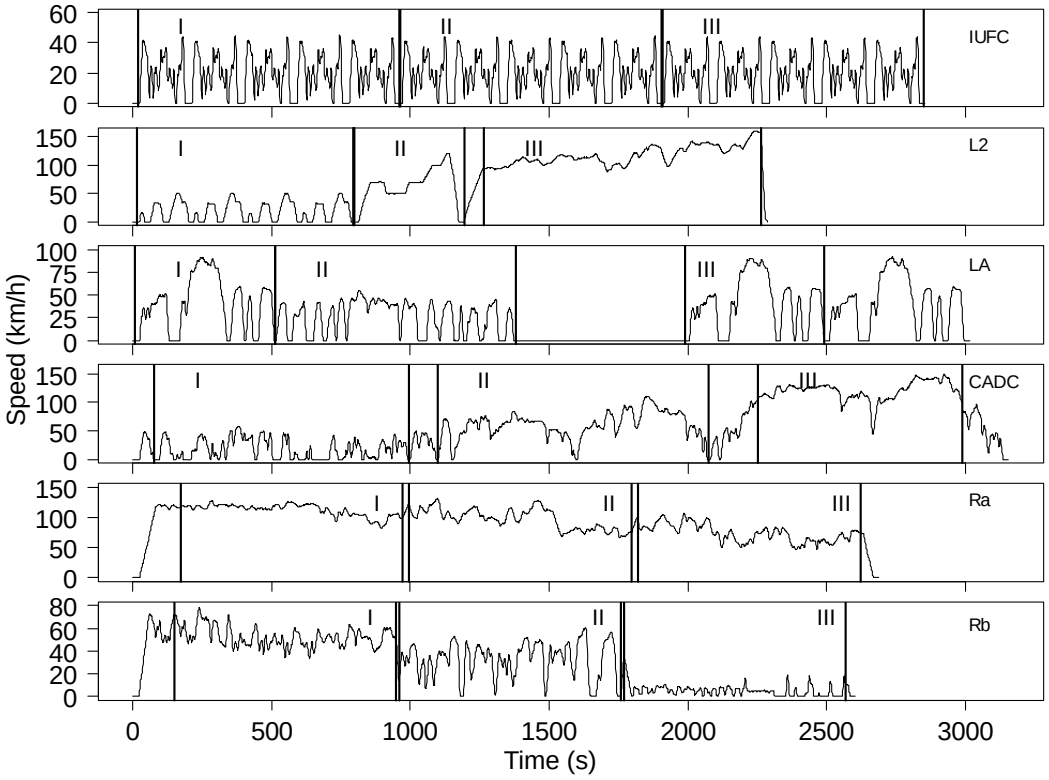

Figure 5. Driving cycles conducted by 4-wheeled vehicles.

Tables 7–9 lists the cycles performed by each of the 4-wheeled vehicles.

Table 7. Cycles performed by individual gasoline automobiles.

Make	Model	Driving Cycle					
		IUFC15	L2	LA	CADC	Ra	Rb
Volkswagen	Touran	X	X	X	X	X	X
Honda	Civic		X	X	X	X	X
Renault	Megane	X	X	X	X	X	X
Renault	Scenic	X	X	X	X	X	X
Mini	Cooper	X		X			

Table 8. Cycles performed by individual diesel vehicles.

Make	Model	Driving Cycle					
		IUFC15	L2	LA	CADC	Ra	Rb
Audi	A4	X		X	X	X	X
Fiat	Ducato	X	X	X	X	X	X
Renault	Trafic T29	X	X	X	X	X	X
Citroen	Jumper	X	X	X	X	X	X
Volkswagen	T5	X	X	X		X	X
Ford	Transit	X	X	X	X	X	X

Table 9. Cycles performed by individual natural gas automobiles.

Make	Model	Driving Cycle					
		IUFC15	L2	LA	CADC	Ra	Rb
Volkswagen	Caddy	X	X	X	X	X	X
Volvo	V70 CNG	X		X	X	X	X
Fiat	Punto 1.2 Bipower	X		X	X	X	X
Opel	Combo C16CNG	X	X	X	X	X	X
Volkswagen	Golf Variant Bifuel	X	X	X	X	X	X
Citroën	C3 1.4i	X	X	X	X	X	X
Mercedes Benz	E 200 NGT		X	X			
Fiat	Multipla 1.6 Bipower	X	X	X	X	X	X

For the motorcycles and scooters, a total of 4 cycles were conducted. Table 10 outlines the details of each of the cycles for the 2-wheelers and Fig. 6 depicts their speed profiles. Similarly to the 4-wheeled vehicles, both real-world and legislative cycles are relevant for the 2-wheelers. As with the automobiles, the same Common Artemis Driving Cycle (CADC, a real-world European cycle representing urban, rural, and highway conditions) involved the vehicle starting with a warm engine; the other 3, which are different from the cycles for 4-wheeled vehicles, involved cold engine starts. The speed profiles of certain 2-wheeler cycles were modified slightly depending on vehicle class, a reflection of the vehicle's displacement and maximum speed. This was only the case for scooters in this study.

Table 10. Main characteristics of driving cycles conducted by 2-wheeled vehicles. EC = European Commission and CH = Switzerland.

Cycle	Sub-cycle			Cold Start	Description
	1	2	3		
LM	urban	rural	-	yes	legislative EC & CH
WMTC	urban	rural	highway	yes	real-world motorcycles
CC	urban	urban	urban	yes	real-world motorcycles
CADC	urban	rural	highway	no	real-world Europe (cars)

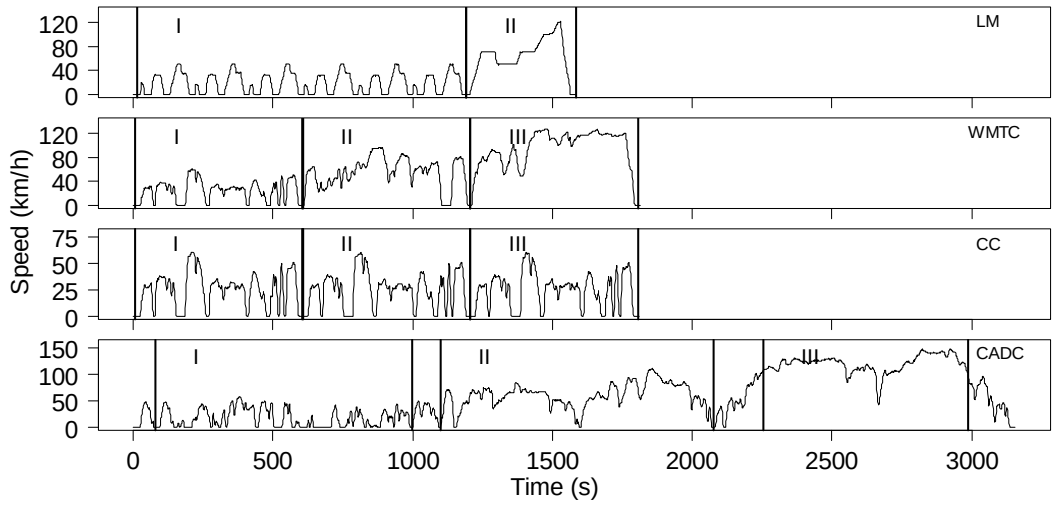

Figure 6. Driving cycles conducted by 2-wheeled vehicles.

Table 11 lists the cycles performed by each of the 2-wheeled vehicles.

Table 11. Cycles performed by individual 2-wheelers.

Make	Model	Driving Cycle			
		LM	WMTC	CC	CADC
Suzuki	GSX R 1000	X	X	X	X
Honda	SH 125	X	X		X
Kawasaki	ER-6N	X	X	X	X
Honda	CBR 600 RR	X	X	X	X
Yamaha	FZ1	X	X	X	X
Piaggio	X8	X	X		X
Harley Davidson	FXDC	X	X	X	X
Piaggio	VESPA LX 125	X		X	X

2.1.4 Derivation of H_2 emissions factors

Emission factors are widely used to quantify vehicle emissions and are often expressed as the mass of a pollutant per unit time or vehicle distance travelled. The calculation of vehicle emission factors is not only useful legislatively for monitoring regulated and other pollutants of interest in vehicle exhaust, but also serves as a tool for quantifying and upscaling the burden of specific pollutants to the atmosphere. E_{H2}

were calculated through the combination of molar H_2 mixing ratios in the exhaust gas and the exhaust mass flow.

Several steps were applied to derive emission factors from molar mixing ratio data of raw exhaust gas measurements. Background (ambient/laboratory) H_2 mixing ratios were determined through measurements representing ambient air and were routinely subtracted from overall measurements (~0.6–1.0 ppm). The dry air total exhaust mass flow ($E_{massfld}$, mg s^{-1}) is defined through the following equation:

$$E_{massfld} = E_{massfl} \cdot \left(1 - C_{H_2O}\right)$$

where, E_{massfl} is the wet exhaust mass flow (mg s^{-1}), and C_{H2O} is the water mole fraction in the vehicle exhaust. The mass flow of H_2 (mg s^{-1}) in the vehicle exhaust was then calculated through the following equation:

$$H_{2massfl} = E_{massfld} \cdot C_{H_2} \cdot \left(MW_{H_2} / MW_{ex}\right)$$

where, $H_{2massfl}$ is the mass flow of H_2 in the exhaust gas (mg s^{-1}), C_{H2} is the above-ambient dry air mole fraction of H_2 in the vehicle exhaust (ppm), MW_{H2} is the molecular mass of H_2 (2.02 g mol^{-1}), and MW_{ex} is the molecular mass of the exhaust gas (taken to be 28.8 g mol^{-1}). H_2 emission factors (E_{H2} in mg km^{-1}) can then be calculated through the following equation:

$$E_{H_2} = \overline{H_{2massfl}} \cdot \Delta T / \Delta D$$

where, $\overline{H_{2massfl}}$ is the mean mass flow of H_2 (in mg s^{-1}) in the exhaust for the time period ΔT, (in s) and distance ΔD (in km) of interest.

E_{CO} were computed through the same above-outlined method as for E_{H2}. Since 2-wheelers were measured with an open dilution system, a correction factor calculated from the measured diluted CO_2 mixing ratios was applied in the initial stages to convert the diluted molar mixing ratio of H_2 to an undiluted equivalent [35].

2.1.5 Derivation of cumulative H_2/CO ratios

Because of their importance in an atmospheric context, and relevance for the derivation of E_{H2} for vehicles not directly measured on a chassis dynamometer, mean H_2/CO ratios for specific cycles and sub-cycles were also calculated. Such cumulative ratios, which are essentially weighted mean ratios (weighted by the total emissions), are better representations of the H_2/CO emission ratios, despite some potential bias introduced by variable cycle lengths and individual experiments. For individual vehicles conducting specific cycles and sub-cycles, the cumulative ratio was calculated by dividing the sum of the measured H_2 mixing ratios by the sum of the measured CO mixing ratios. For H_2/CO ratios derived from multiple experiments, e.g. for the composite of multiple vehicles over the same cycle, the same methodology was pursued and the ratios of the summed mixing ratios of all measurements were taken.

2.1.6 Experimental setup of engine test bench

In order to map H_2 emissions from a stationary engine capable of combusting both gasoline and natural gas, an experiment was carried out under static stationary conditions. One aspect of the study focused on direct H_2 emissions from each fuel type under variable conditions, including:

- λ range (from 0.9 – 1.02);
- engine operating point; and
- pre- and post-catalytic converter measurements.

Figure 7 illustrates the experimental setup for these measurements and Table 12 outlines the details of the major engine settings for each engine operating point.

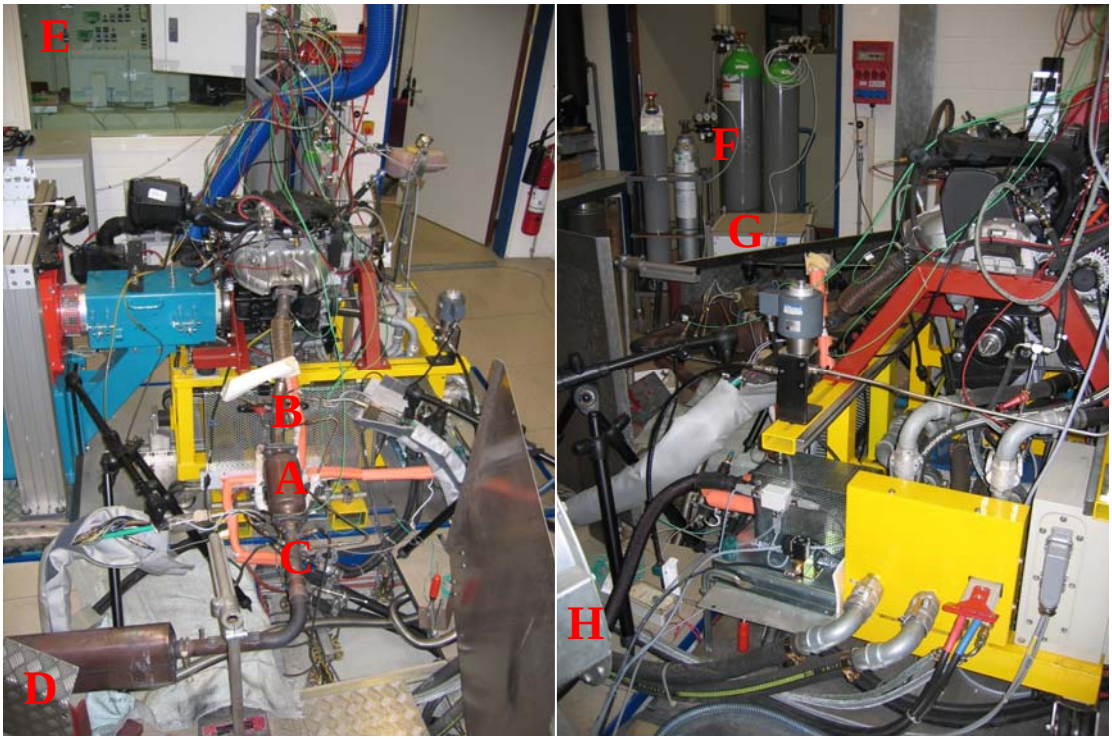

Figure 7. Experimental setup for engine test bench measurements of pre- and post-TWC H_2 measurements of gasoline and CH_4 exhaust gas. A = TWC, B = pre-TWC measurements, C = post-TWC measurements, D = Heat barrier to protect H-Sense, E = Control room, F = Standard and zero air tanks, G = H-Sense MS, H = Ventilator to cool engine.

Table 12. Major settings for each engine operating point (OP).

Operating point	Engine speed (rpm)	Brake mean effective pressure (bar)	Torque (Nm)	Power (kW)
OP1	2000	2	31.6	6.6
OP1 (cooled)[a]	2000	2	31.6	6.6
OP2	2000	4	63.2	13.2
OP3	4000	2	31.6	6.6

[a] The mean exhaust temperature difference after the TWC between OP1 and OP1 (cooled) was 50 °C.

2.2 Quantitative scenarios of global anthropogenic H_2 emissions to the atmosphere throughout the 21st century

The following section details the methodology associated with Task 2 outlined in section 1.6.

2.2.1 Global Multi-regional MARKAL model

The Global Multi-regional MARKAL (MARKet ALlocation) model (GMM) is a bottom-up, least-cost optimisation model that uses perfect foresight [5]. It reflects the entire energy system from the extraction of resources to energy conversion technologies and end-use sectors, with particular focus on power generation, fuel conversion chains, and current and future light-duty vehicle (LDV) technologies. The model is applied to study scenarios of global energy and transport system development, which (among other less stringent scenarios) includes a stringent policy mechanism designed to stabilize atmospheric CO_2 levels at 450 ppm. Results from the GMM are based on the modelling work of T. Gül (see [5]).

In this study, the GMM was applied to model LDV fleets and global H_2 production for direct energy services — in this case, a baseline (business-as-usual) scenario and a scenario consistent with achieving a stable atmospheric CO_2 mixing ratio of 450 ppm. Both scenarios were assessed for the time periods 2010, 2020, 2050, and 2100. Results for 2010 correspond to the baseline scenario, as it was assumed that measures that have been pursued to date are insignificant on a global scale to abate climate change.

In the baseline scenario, CO_2 emissions are left to increase unabated without the intervention of any specific climate policies aimed at addressing global climate change. Under this scenario, H_2 production for energy services increases only very modestly throughout the 21st century and FCVs do not penetrate the market at all. Under the 450 ppm CO_2 climate policy scenario, specific mechanisms are applied that are designed to stabilize atmospheric CO_2 mixing ratios at 450 ppm by the end of the 21st century. Under this scenario, H_2 production for direct energy services increases significantly over the period of study, notably with the penetration of FCVs and

exponential increase in H_2 production for primary energy consumption. Under both scenarios, the changing H_2 emissions from transportation are combined with projected losses from H_2 production, distribution, storage, and other end-uses in order to provide an overview of projected overall anthropogenic H_2 emissions to the atmosphere throughout the 21st century.

2.2.2 Vehicle fleet scenarios

Vehicle fleet scenarios were assessed to account for the inherent variability of H_2 emissions in exhaust gas according to vehicle technology and world region over time. Results were drawn from two separate models: the GMM and the Sustainable Mobility Project transport model (SMP). For details of the SMP, see [34].

The GMM separates global vehicle kilometres into various LDV technologies projected to be relevant over the study period. These are oil products and synfuels (primarily conventional gasoline and diesel) internal combustion engine vehicles (ICEVs), natural gas ICEVs, biofuels ICEVs, oil products and synfuels hybrids (HEVs), natural gas hybrids, biofuels hybrids, H_2 hybrids, plug-in hybrids, and FCVs. The GMM projects fleet results until 2100.

The SMP model results were incorporated to account for additional vehicle technologies and the separation of vehicle kilometres according to world region, which was not included in the GMM. In addition to LDVs, 2-wheelers, medium-sized trucks, large buses, and mini-buses are included. Heavy-duty (long-haul) trucks are not considered, as these are almost solely fuelled by diesel, and H_2 emissions from diesel vehicle have been shown to emit marginal amounts of H_2 (see Table 15).

By considering a more complete range of vehicle technologies, the combination of these 2 models provides a more inclusive overview of global vehicle kilometres, which is necessary for the accurate upscaling of global H_2 emissions from the most significant road-based transportation sources. It should be noted that projections for global LDV kilometres from the SMP were 1% and 0.3% higher than projections from the GMM in 2010 and 2020, respectively, which was deemed acceptable when choosing to apply results from both models.

2.2.3 Key assumptions associated with global H_2 upscaling

The global upscaling of H_2 emissions involved applying emission factors specific to each vehicle technology in conjunction with vehicle kilometres associated with specific time periods and world regions. As vehicle technologies, global kilometres travelled, technologies designed to address vehicle exhaust emissions, and emissions/emission standards for different world regions are different and change with time, a number of assumptions were formulated to develop an accurate account of global H_2 emissions for the subject time periods (2010, 2020, 2050, and 2100). The main assumptions are as follows:

1. The percentage share of each LDV technology for 2010, 2020, 2050, and 2100 is based on results from the GMM (see section 2.2.1 for an overview of the GMM with particular focus on its relevance to this study, and [5] for complete details of the GMM).
2. Projections of global LDV kilometres separated by world region in 2010 and 2020 are based on SMP model results from [34]. World regions are distinguished as follows: Organisation for Economic Co-operation and Development (OECD) North America, OECD Europe, OECD Pacific (Japan, Korea, Australia, New Zealand), former Soviet Union, Eastern Europe, China, other Asia, India, Middle East, Latin America, and Africa. OECD North America, OECD Europe, and OECD Pacific are considered developed regions, while the others are considered developing regions.
3. Beyond 2020 (i.e. for 2050 and 2100 scenarios), projections of global LDV kilometres and emissions are exclusively according to the GMM. The separation by world region (as described in assumption 2) is not applied because all vehicles of similar technology were assumed to have same E_{H2}, irrespective of region.
4. Projections of global kilometres for medium-sized trucks, large buses, and mini-buses for specific regions and time periods are derived from [34], and based on kilometres driven by region for 2010 and 2020, total global kilometres in 2050 and the forecast according to the regression for global kilometre projections to 2100.

5. Projections of global 2-wheeler kilometres for specific regions and time periods are derived from [34], and based on kilometres driven by region in 2000, projected model results based on 2-wheeler ownership by region to 2050, and the forecast according to the regression for kilometre projections to 2100.
6. The percentage share of fuel types for conventional vehicle types (gasoline and diesel) are based on projections by [34]. This percentage share of gasoline- and diesel-based transportation applies to the oil products & synfuels ICEVs. The fractions projected for 2050 are assumed to be the same in 2100.
7. Medium-sized trucks, large buses, and mini-buses are all assumed to be fuelled by either gasoline or diesel over the course of the study period.
8. Technologies other than conventional gasoline (including 2-wheelers) and diesel vehicles (i.e. natural gas, biofuels, and all hybrid vehicles) are assumed to be incorporated only into developed country vehicle fleets for 2010 and 2020.
9. A 10-year time lag for each world region is applied according to predicted emission standards or emission factors for LDVs from [34]. For example, LDV E_{H2} derived for 2010 are based on the emission standards or assumed emissions predicted for each region as of 2000. This is done to account for older (more polluting) vehicles still present within the fleet following the introduction of a new emission standard. This is done only for the years 2010 and 2020 (see assumption 11).
10. For large buses, medium-sized trucks, and mini-buses, E_{H2} are derived based on the assumed average emissions for each vehicle stock from [34]. Alternatively to the LDVs (assumption 9), average emissions are provided for each time period rather than adopted emissions standards for these vehicle technologies. Thus, for these vehicle technologies, a time lag was not applied since an average emission for each vehicle technology and time period was provided. This is done only for the years 2010 and 2020 (see assumption 11).
11. Beyond 2020 (i.e. for 2050 and 2100) similar vehicle technologies are assumed to have the same E_{H2}, irrespective of world region. For example, conventional gasoline LDVs are assumed to have the same E_{H2} in Europe as in China.

12. E_{H2} from technologies other than conventional gasoline and 2-wheeler vehicles are assumed to be constant over time.
13. E_{H2} from diesel vehicles were assumed to be constant with time based on the consistently oxidizing operating point of diesel engines (see section 3.1.3).
14. The calculation of emission factors from vehicles measured on a chassis dynamometer can be found in section 2.1.4. The derivation of other E_{H2} can be found in section 2.2.4.
15. Further to the assumptions made for the global upscaling of emissions from transportation, leakage rates of H_2 to the atmosphere from production, distribution, storage, and end-uses systems other than transportation (section 4.3.1) are deduced based on assumptions and information from personal communication from industrial and commercial sources, along with estimations from the literature [7, 9, 10, 15, 51-56]. H_2 emissions from other fossil fuel-based processes such as industrial and residential heating systems are not accounted for in this study. However, H_2 emissions from such systems have been found to expel only marginal H_2 to the atmosphere (M.K. Vollmer, Empa, pers. comm.), suggesting that H_2 emissions from other industrial processes not related to intentional (e.g. the petroleum refining, NH_3 production, and CH_3OH production industries) H_2 production are also minor (compared to CO), particularly as fossil fuel consumption begins to decline, clean-up technologies improve, and renewable resources gain in market share.

2.2.4 Calculation and derivation of H_2 emissions factors for global upscaling

For vehicles tested directly on the chassis dynamometer, E_{H2} were calculated through direct exhaust gas measurements. These are the same vehicles detailed in section 2.1.1, and the derivation of E_{H2} for these vehicles can be found in section 2.1.4. Where applicable, E_{H2} calculated from chassis dynamometer measurements were applied directly in the upscaling of emissions. The following E_{H2} have been applied directly from chassis dynamometer measurements (see Table 17): gasoline Euro-3 automobiles (59.4 mg km^{-1}) [47], gasoline Euro-4 automobiles (26.5 mg km^{-1}) (Table 15), gasoline Euro-3 2-wheelers (141 mg km^{-1}) (Table 16), diesel Euro-4 automobiles and delivery vehicles (0.12 mg km^{-1}) (Table 15), and Euro-4 natural gas automobiles

(73.5 mg km^{-1}) (Table 15). All vehicles beyond the Euro-4 emission standard for LDVs, medium-sized trucks, large buses, and mini-buses (and beyond the Euro-3 standard for 2-wheelers) were assumed to produce identical emissions to the Euro-4 LDV standards since restrictions on CO emissions are not slated to become more stringent beyond the Euro-4 emission standard. This suggests that H_2 emissions will also remain the same. Thus, a mean E_{H2} of 26.5 mg km^{-1} (E_{H2} for gasoline Euro-4 automobiles) was adopted for all gasoline-based travel beyond the Euro-4 standard (and Euro-3 standard for 2-wheelers). Plans for the Euro-4 and Euro-5 emission standards for motorcycles are tentatively scheduled for 2012 and 2015, respectively, which should result in CO emission limits identical to those of the same standard for automobiles [74]. H_2 emissions are expected to follow suit.

Emission factor data was not available for all vehicle technologies expected to be relevant for this study over the projected time horizon. For vehicle technologies not directly tested on a chassis dynamometer, E_{H2} were derived from other independent measurements and assumptions made about the individual technologies. The derivation of E_{H2} for gasoline-based vehicle technologies not directly measured was based primarily on estimated E_{CO} and the known correlation of H_2 and CO in the exhaust gas of older vehicle technologies. The following equation was used to derive E_{H2} for these vehicles:

$$E_{H_2} = E_{CO} \cdot 0.55/13.87$$

where, E_{CO} is the mean CO emission factor by vehicle technology, world region, and time period [34, 75], 0.55 is the corrected weighted mean H_2/CO ratio observed from a purely gasoline-based real world fleet [33], and 13.87 is the mass ratio (g mol^{-1}) of CO to H_2. This ratio of 0.55 was applied because it represents the composite ratio of slightly older gasoline technologies that are also relevant in this study. Furthermore, the highest absolute emissions of H_2 and CO — which are also the most relevant in an atmospheric context — resulted in similar H_2/CO ratios in this study (see section 3.2.3). This ratio was only applied to gasoline vehicles since diesel vehicles emit only marginal H_2 (see Table 15). The exception to this method was the gasoline Euro-2 vehicles, for which the E_{H2} was derived from ratio of the mean Euro-2 E_{CO} (1373.1 mg km^{-1}) from a study performed at Empa [76] to the mean Euro-3 E_{CO} (753.1 mg km^{-1}) from a separate Empa study [77], then multiplied by the mean E_{H2} for Euro-3

automobiles (59.4 mg km^{-1}) from [47]. The reason for this exception was the assumed analogous H_2 and CO emissions from Euro-2 and Euro-3 vehicles based on the almost identical emission standards for CO (2.2 g km^{-1} for Euro-2 and 2.3 g km^{-1} for Euro-3).

For LDVs in the year 2010, it was assumed that the Euro-3 emission standard (E_{H2} of 59.4 mg km^{-1}) is representative of the aggregate developed world vehicle fleet. The Euro-1 standard (based on mean E_{CO} of 7.125 g km^{-1} from Euro-1 automobiles from [75]) was assumed for most of the developing world, and the pre-Euro-1 standard (based on mean E_{CO} of 28.55 g km^{-1} from non-TWC automobiles from [75]) for the Middle East and Africa. In 2020, the Euro-5 standard (E_{H2} of 26.5 mg km^{-1}) is applied for the developed countries. For most of the developing world, the Euro-3 standard (E_{H2} of 59.4 mg km^{-1}) is applied, and for the Middle East and Africa, the Euro-2 standard (E_{H2} of 108 mg km^{-1}) is applied.

For 2-wheelers in 2010, the E_{CO} from the developed countries was assumed to be an average of 15 g km^{-1} and those from the developing world to be 20 g km^{-1}. Based on the above equation, E_{H2} of 595 mg km^{-1} for the developed countries and 793 mg km^{-1} for the developing countries are calculated. For 2020, mean E_{CO} were assumed to be 6.467 g km^{-1} for OECD North America, 6.575 g km^{-1} for OECD Europe, 4.628 g km^{-1} for OECD Europe, and 7.5 g km^{-1} for the developing world. These E_{CO} correspond to E_{H2} of 256 mg km^{-1}, 261 mg km^{-1}, 184 mg km^{-1}, and 297 mg km^{-1} for OECD North America, OECD, Europe, OECD Pacific, and the developing countries, respectively.

For large buses in 2010, a mean E_{CO} of 10 g km^{-1} in developed countries and 46.7 g km^{-1} in developing countries were assumed. According to the above equation, these emission factors equate to E_{H2} of 397 mg km^{-1} and 1850 mg km^{-1} in developed and developing countries, respectively. In 2020, a mean E_{CO} of 7.5 g km^{-1} in developed countries and 20 g km^{-1} in developing countries were assumed. These E_{CO} correspond to E_{H2} of 297 mg km^{-1} and 793 mg km^{-1} in developed and developing countries, respectively.

For medium-sized trucks and mini-buses, 75% of the E_{CO} of large buses was assumed based on the assumption by [34] that emissions are similar, but somewhat lower. For

medium-sized trucks and mini-buses in 2010, a mean E_{CO} of 7.5 g km^{-1} in developed countries and 35 g km^{-1} in developing countries was assumed. According to the above equation, these E_{CO} equate to E_{H2} of 297 mg km^{-1} and 1390 mg km^{-1} in developed and developing countries, respectively. In 2020, a mean E_{CO} of 5.625 g km^{-1} in developed countries and 15 g km^{-1} in developing countries was assumed. These E_{CO} correspond to E_{H2} of 223 mg km^{-1} and 595 mg km^{-1} in developed and developing countries, respectively.

The mean E_{H2} derived for biofuels vehicles was assumed to be 50% of those from conventional gasoline automobiles, which is based on the relative reduction of CO emissions from [78]. The mean E_{H2} for gasoline HEVs was assumed to be 87.3% of conventional (non-hybridised) gasoline vehicles, which is based on the reduction in fuel consumption from model results from [79]. The mean E_{H2} for natural gas hybrid vehicles was assumed to be 80% of conventional (non-hybridised) natural gas vehicles, which is based on a 20% reduction in fuel consumption (C. Bach, Empa, pers. comm.). The mean E_{H2} for biofuels hybrid vehicles was assumed to be 80% of conventional (non-hybridised) biofuels vehicles, which is based on a 20% reduction in fuel consumption (C. Bach, Empa, pers. comm.). The mean E_{H2} for plug-in hybrid vehicles was assumed to be 56% of conventional (non-hybridised) gasoline vehicles, which is based on the reduction in fuel consumption from model results from [79]. The mean E_{H2} for H_2 hybrids is based on the assumption that emissions are 50% of those from gasoline hybrid electric vehicles [79] plus 50% of those from H_2ICEVs [80]. Scenarios for FCVs were developed based on variable E_{H2}, including assumed low- and high-end E_{H2} of 26.5 mg km^{-1} and 265 mg km^{-1}.

Table 13 details the selection criteria and derivation of E_{H2} for all vehicle technologies considered in this study.

Table 13. Selection criteria and derivation of E_{H2} for all vehicle technologies considered in this study.

Vehicle Type
Gasoline automobiles 1. pre-Euro-1, based on E_{CO} of 28.55 g km^{-1} [75] 2. Euro-1, based on E_{CO} of 7.125 g km^{-1} [75] 3. Euro-2, based on ratio of gasoline Euro-2 E_{CO} (1373.1 mg km^{-1}) [76] to gasoline Euro-3 E_{CO} (753.1 mg km^{-1}) [77], multiplied by mean E_{H2} (59.4 mg km^{-1}) from [47] 4. Euro-3, E_{H2} from [47] 5. Euro-4, E_{H2} (Table 15) 6. post-Euro-4, assumed to be the same as Euro-4 based on identical CO emissions limits for subsequent Euro emission standards
Gasoline 2-wheelers 1. based on E_{CO} of 20 g km^{-1} [34] 2. based on E_{CO} of 15 g km^{-1} [34] 3. based on E_{CO} of 7.5 g km^{-1} [34] 4. based on E_{CO} of 6.575 g km^{-1} [34] 5. based on E_{CO} of 6.467 g km^{-1} [34] 6. based on E_{CO} of 4.628 g km^{-1} [34] 7. Euro-3, E_{H2} (Table 16) 8. post-Euro-3, assumed to be the same as post Euro-4 gasoline automobiles [74]
Diesel vehicles 1. pre-Euro-4, assumed to be same as diesel Euro-4 vehicles based on oxidizing operating principle of diesel engines 2. Euro-4, E_{H2} (Table 15) 3. post-Euro-4, assumed to be same as diesel Euro-4 vehicles based on oxidizing operating principle of diesel engines
Gasoline large buses 1. based on E_{CO} of 46.7 g km^{-1} [34] 2. based on E_{CO} of 20 g km^{-1} [34] 3. based on E_{CO} of 10 g km^{-1} [34] 4. based on E_{CO} of 7.5 g km^{-1} [34] 5. post-Euro-4, assumed to be the same as Euro-4 based on identical CO emissions limits for subsequent Euro emission standards
Gasoline medium-sized trucks/small buses (emissions assumed to be 75 % of those from gasoline large buses) 1. based on E_{CO} of 35 g km^{-1} [34] 2. based on E_{CO} of 15 g km^{-1} [34] 3. based on E_{CO} of 7.5 g km^{-1} [34] 4. based on E_{CO} of 5.625 g km^{-1} [34] 5. post-Euro-4, assumed to be the same as Euro-4 based on identical CO emissions limits for subsequent Euro emission standards
Natural gas automobiles Euro-4, E_{H2} (Table 15)
Biofuels vehicles, based on assumption that emissions are 50% of those from conventional gasoline automobiles [78]
Gasoline hybrid electric vehicles, based on model results from [79] that predict average fuel consumption to be 87.3% of conventional (non-hybridised) gasoline vehicle
Natural gas hybrids, based on assumption of a 20% reduction in fuel consumption compared with conventional (non-hybridised) natural gas vehicles (C. Bach, Empa, pers. comm.)
Biofuels hybrids, based on assumption of a 20% reduction in fuel consumption compared with conventional (non-hybridised) biofuels vehicles (C. Bach, Empa, pers. comm.)
Plug-in hybrids, based on model results from [79] that predict average fuel consumption to be 56% of conventional (non-hybridised) gasoline vehicle
H_2 hybrids, based on assumption that emissions are 50% of those from gasoline hybrid electric vehicles [79] plus 50% of those from H_2 ICEVs [80]
H_2 fuel cell vehicles, scenarios with variable FCV E_{H2}, including 26.5 mg km^{-1} and 265 mg km^{-1}

2.2.5 H_2 production and consumption scenarios

In this study, the distinction is made between the categories of H_2 production for direct energy services and production for industrial processes. Typically, H_2 production and consumption are approximately equal [48]. Table 14 outlines the primary contributors to each of the categories (see also Fig. 2).

Table 14. Primary direct energy end-uses and industrial end-uses considered in this study.

Direct energy	**Industrial**
Transportation	Petroleum refining
Industrial power	Ammonia production
Commercial power	Methanol production
Residential power	Other minor contributors including metallurgical applications, chemical processing, food industry

Results for H_2 production for direct energy end-uses (section 4.2.1) are from the GMM. For these end-uses, the focus is on transportation since H_2 is used primarily as a transportation fuel, while electricity is most prominent for the other major end-uses (see [5] for details).

H_2 production and consumption for industrial end-uses (section 4.2.2) was upscaled starting with 2008 estimations [81]. For the petroleum refining industry, annual growth rates were derived based on global oil supply figures from [5]. In parallel to these projections, a continuous 1% annual increase in H_2 production per unit of refinery throughput is assumed, which accounts for the increase in H_2 production required for continuously decreasing crude oil feedstock quality, coupled with increasingly stringent environmental regulations (see Table 20). This procedure for petroleum refining is applied for all scenarios to 2100. For the other industrial end-uses (primarily the NH_3 and CH_3OH production industries), individual projections to 2020 were first based on fixed annual growth rates derived from the relevant industries (see section 4.2.2.2 for details). It becomes increasingly challenging to predict individual longer-term (e.g. 2050 and 2100) patterns due to the inherent uncertainties surrounding these markets. Thus, beyond 2020 (i.e. for 2050 and 2100 scenarios), these end-uses were grouped and an aggregate growth rate was applied using global economic growth as a guide. Economic growth figures according to the B2 scenario from [82] were applied, which is the same scenario applied for long-term economic growth by [5]. For the period 2020–2050, a 2.8% annual economic growth

figure (i.e. H_2 production for these end-uses is projected to increase at a growth rate of 2.8% from 2020–2050) is applied, which is the growth rate projection according to [82] for the period 1990–2050. For the period 2050–2100, an annual growth rate of 1.5% is applied, which is considered to be the average of the projected growth rate from 1990–2100 from [82] (see Table 21).

2.3 Continuous free tropospheric H_2 observations

The following section details the methodology associated with Task 3 outlined in section 1.6.

2.3.1 Gas chromatographic separation and detection of H_2

At Jungfraujoch, H_2 and CO are measured with a gas chromatograph (GC), using a modified reduction gas analyzer (RGA-3, Trace Analytical), which uses a technique based on chromatographic separation followed by the reduction of mercuric oxide (HgO):

$$X + HgO\ (solid) \rightarrow XO + Hg\ (vapour)$$

where, X represents an appropriate reducing gas. The resultant mercury vapour is quantitatively determined through ultraviolet light absorption detection at 254 nm [83]. The detection limit of the instrument is ~10 ppb. The Hg bed in the RGA-3 at Jungfraujoch was never replaced subsequent to its initial installation; new Hg beds were once tested, however, and found inferior to the originally installed Hg bed. The GC modifications include a gas selector valve, an internal carrier gas pressure regulator, a nafion drier, and a thermally insulated sample loop with a volume of ~1 mL. The detector and column temperatures are set to 270 ^{o}C and 110 ^{o}C, respectively. Figure 8 depicts the RGA-3 instrument in the observatory at Jungfraujoch.

Figure 8. RGA-3 instrument setup at Jungfraujoch. A = RGA-3, B = Device to convert analog signal to digital signal (A/D Box), C = Laptop used to control measurements and instrument, D = Working standard is located behind rack underneath table, E = Ambient air samples are drawn in from outside through sample lines using a standard KNF pump located behind the RGA-3 instrument.

Although more frequent measurements are possible, air samples were taken at 30-minute intervals, bracketed by working standard measurements to calibrate the RGA-3 and to determine and correct for any short-term instrumental drift. As results based

on peak height integration are more precise than those based on peak area (presumably due to the non-Gaussian nature of the peaks), peak heights were used for the determination of atmospheric mixing ratios. Figure 9 depicts a standard chromatogram of H_2 (first peak) and CO (second peak) at Jungfraujoch. The instrument is controlled by Linux-based chromatography software (GCWerks, gcwerks.com). All data was synchronized to a primary data processing computer at Empa.

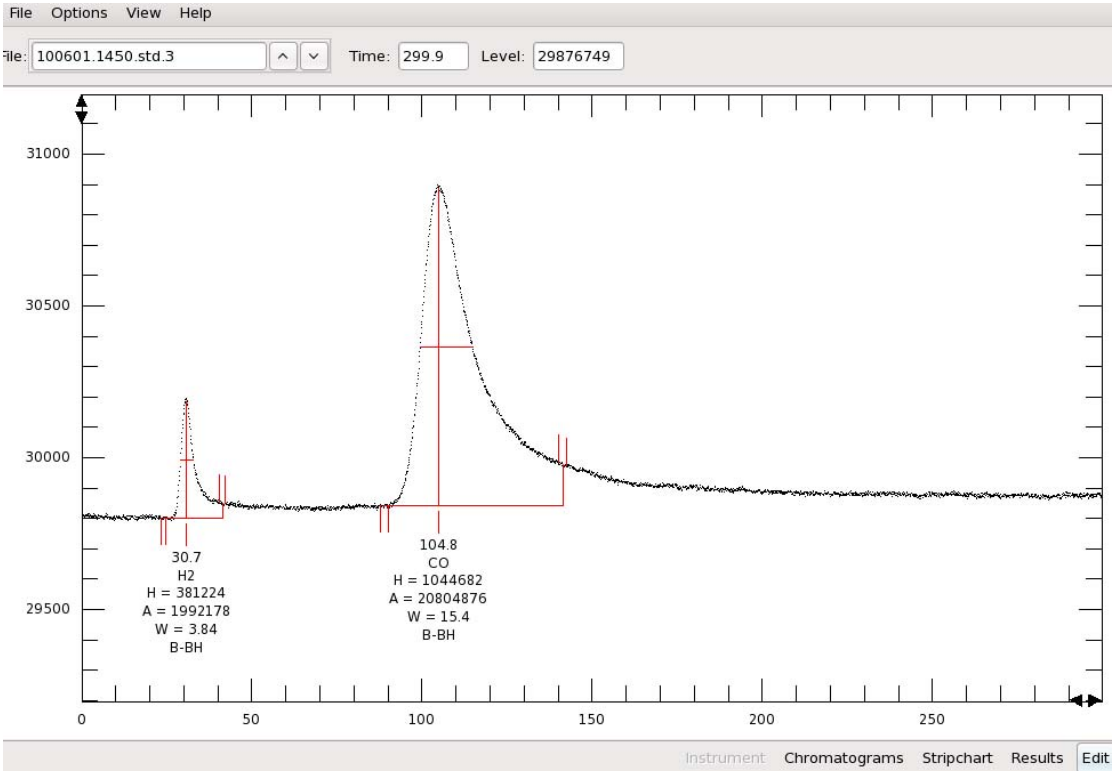

Figure 9. Chromatogram of H_2 (first peak) and CO (second peak) of a standard measurement taken on the RGA-3 at Jungfraujoch, and displayed with GCWerks software.

2.3.2 Quality assurance and quality control

2.3.2.1 Calibration, standards, and scales

The GCWerks software was programmed such that air samples were typically alternated with working standard measurements to track and correct for short-term sensitivity fluctuation. Working standards were referenced to a higher ranking standard known as the “gold standard” (EG-004). The Max Planck Institute Jena (A.

Jordan) has prepared a primary calibration scale. An initial scale termed EuroHydros07 was replaced in 2009 when the scale was revised to the Max Planck Institute (MPI)-2009 primary calibration scale and led to an increase in EG-004 mixing ratios of ~18–20 ppb. All results reported in this study are based on the MPI-2009 calibration scale.

EG-004 has a mixing ratio of 637.1 ppb on the MPI-2009 scale, which is based on the mean of two measurements by the MPI Jena of 636.5±1.6 ppb (in June/July 2007) and 637.7±2.0 ppb (in August 2008).

Working standards were prepared by compressing ambient air into ~35 L stainless steel canisters (Essex Cryogenics and Graeven Metalltechnik) using an oil-free diving compressor (RA-3, RIX Industries). These working standards — in this study ranging from 559.3–822.4 ppb H_2 and 209.5–298.0 ppb CO — were referenced against higher ranking standards and ultimately linked to the MPI-2009 calibration scale for H_2, which has an accuracy of 0.5% (A. Jordan, MPI Jena, pers. comm.), and the World Meteorological Organization (WMO-2000) calibration scale for CO, which has an accuracy of 1% [84]. The Jungfraujoch measurement precision, which was derived from recurrent standard measurements, was 0.9% (1σ) for H_2 and 0.6% (1σ) for CO. Including the uncertainties from the measurements of the higher-ranking and working standards, the accuracies of the field measurements are estimated at 1.2% for H_2 and 1.3% for CO.

The following working standards have to date been utilized at Jungfraujoch:

- E–033: August 8, 2005 – November 16, 2007 (578.8 ppb)
- E–049: November 16, 2007 – December 10, 2008 (822.4 ppb)
- E–053: December 10, 2008 – October 15, 2009 (583.8 ppb)
- E–055: October 15, 2009 – present (559.3 ppb)

The precision of the standard measurements are typically better than 1%, with rare exceptions exceeding 2% relative error with reference to the standard concentration. Figure 10 below depicts the precision of the instrument through plotting of normalized height.

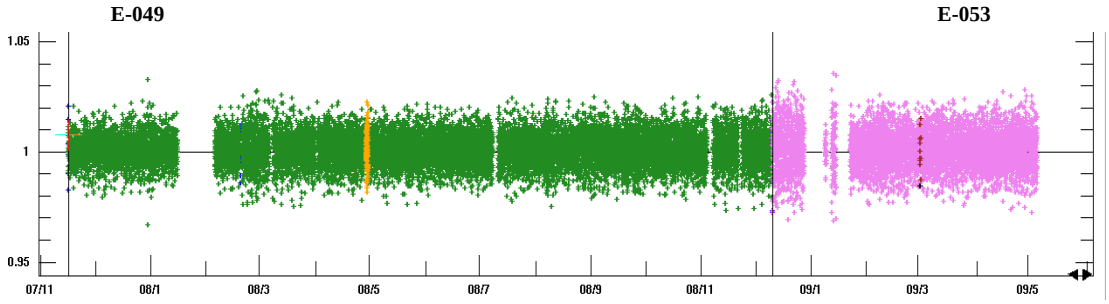

Figure 10. Plot of normalized heights for working standards E-049 and E-053 on the RGA-3 instrument at Jungfraujoch.

2.3.2.2 Target tanks

Target tanks with accurately known H_2 and CO mixing ratios provide an independent measurement validation method to ensure the stability of the instrument and accuracy of the measurements. The following target tank has to date been utilized at Jungfraujoch:

- E-052: September 25, 2008 – present (586.8 ppb)

E-052 is an old-style Essex tank. Starting on September 25, 2008, E-052 was measured at Jungfraujoch 5 times every Sunday and Thursday. As the stability of H_2 and CO mixing ratios in E-052 had been previously confirmed through measurements on the RGA-3 at Jungfraujoch (April 30, 2008) and on an independent RGA-3 in the laboratory at Empa (May 15/16, 2008 and July 23/24, 2008), measurements of E-052 as a target tank were reduced to 5 measurements every Sunday starting on November 9, 2008. Results have shown stability in the target tank within the measurement uncertainty to the present time.

2.3.2.3 Independent external quality assurance and quality control

Quality control was also assured through participation in a round-robin intercomparison as part of the European FP6 EuroHydros project, during which the measurements of the 4 intercomparison canisters (spanning 490 ppb – 650 ppb) were found to be well within the uncertainty limits of those determined at MPI Jena (home of primary scale) for the same canisters. Additionally, a specific time period of the in-situ RGA-3 H_2 measurements was compared with flask measurements (A. Jordan, unpublished data) taken at Jungfraujoch over the same period. The comparison did not

exhibit a significant bias (mean difference between in-situ and flask measurements = 4.7±8.3 ppb (~0.9%), R^2 = 0.67, n = 28), and results were generally in good agreement considering the constraints associated with matching the results of non-simultaneous sampling. CO measurements from this study agree well with ongoing CO measurements conducted with 3 other independent instruments (R^2 ranging from 0.935 to 0.981) at Jungfraujoch [85].

2.3.2.4 Non-linearity corrections of the RGA-3

RGA-3 instruments are known for the non-linear behaviour of their detectors, and this issue must be manually corrected. The non-linearity of the detector was initially characterized in 2005 through the dynamic dilution of a high mixing ratio reference cylinder that contained (among some other compounds) ~3.0 ppm H_2 and ~1.2 ppm CO (in synthetic air). Simultaneous CH_4 measurements were conducted on a linear GC-FID as a cross-check of the dynamic dilution. Synthetic air was used for the dilution, which was further purified to remove potential traces of H_2 and CO using a Sofnocat-magnesium perchlorate ($Mg(ClO_4)_2$) cartridge. Residual CH_4 was removed using an AADCO 737 pure air generator. The purified synthetic air was mixed with the high mixing ratio reference to provide 14 different H_2 and CO mixing ratios ranging from air completely free of H_2 and CO to pure high mixing ratio reference levels. Dilution ratios were set with mass flow controllers to ensure stable flow rates. These flow rates were accurately measured with a DryCal flowmeter (Bios International Corp.). CH_4, which is assumed to be linear on a GC-FID over the whole range of the experiment, was used as an independent check of the dynamic dilutions.

This experiment was repeated in 2008 with slight modifications. As a cross-check during these experiments, simultaneous CO measurements with a vacuum ultraviolet (UV) resonance fluorescence instrument (Aerolaser AL5001) with linear response were used. Aliquots of these dynamic dilution mixtures were sub-sampled into stainless steel flasks and measured on the RGA-3 at Jungfraujoch within a week of collection, serving as a second non-linearity check for this instrument. The aliquots in the stainless steel flasks were found to remain stable for at least 2 weeks following filling. Figure 11 depicts the scheme of the non-linearity experiment and Fig. 12

depicts the setup of the non-linearity experiment conducted in the laboratory at Empa in April, 2008.

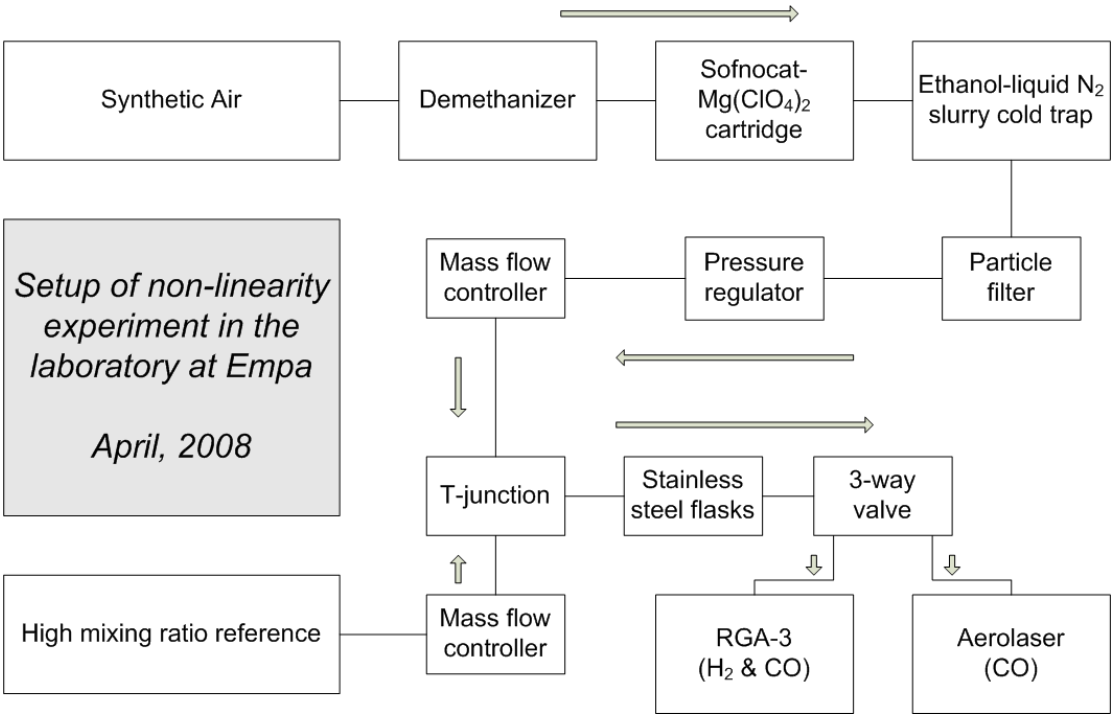

Figure 11. Scheme of non-linearity experiment conducted at Empa in April, 2008.

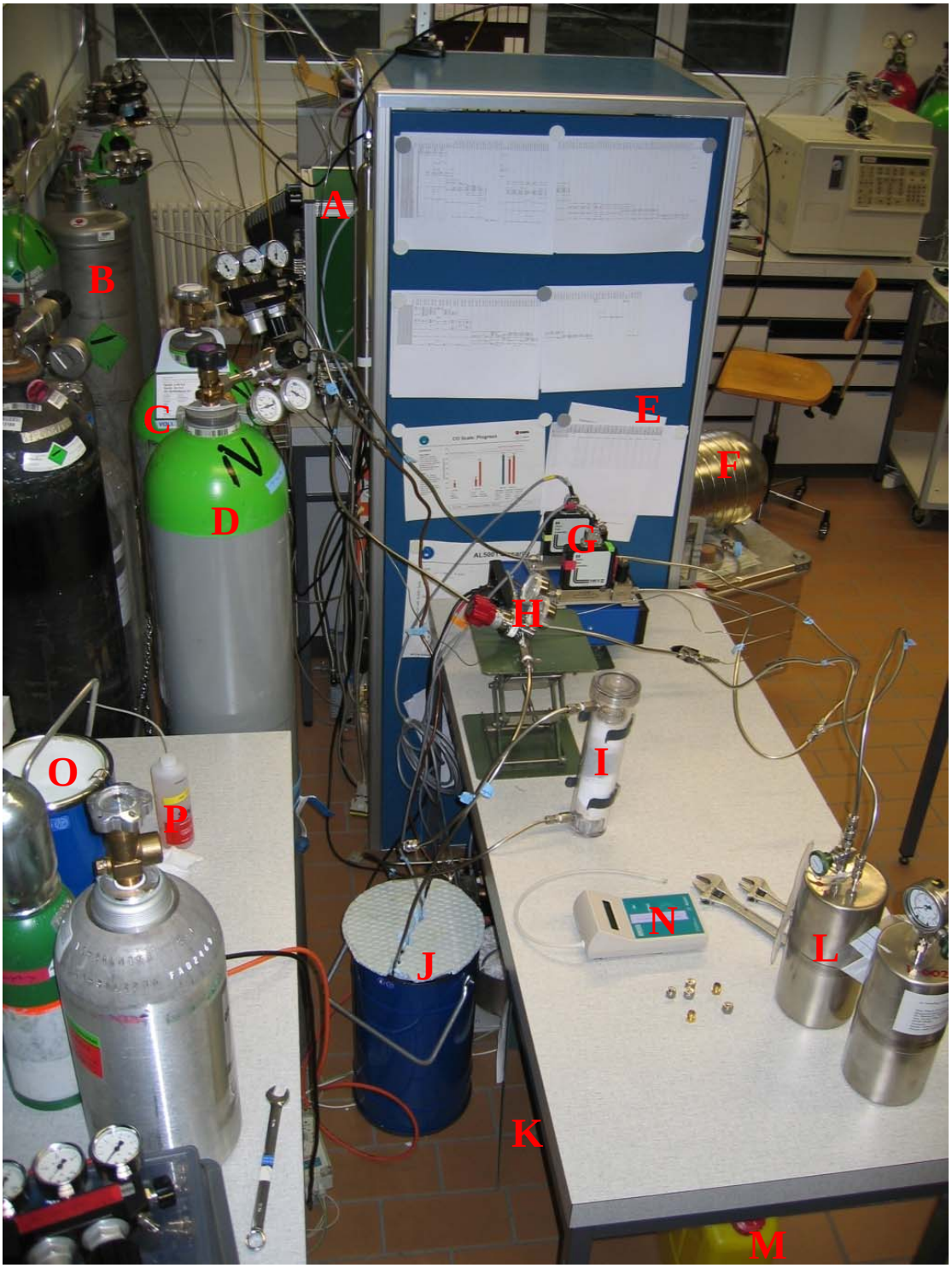

Figure 12. Experimental setup of non-linearity experiment within the laboratory at Empa in April, 2008. A = RGA-3, B = Gold standard (EG-004), C = High mixing ratio reference standard, D = Synthetic air, E = Rack containing Aerolaser AL5001 instrument, F = Old-style Essex tank (target tank E-052), G = Mass flow controllers, H = Pressure regulator to maintain pressure throughout system, I = Sofnocat-magnesium perchlorate ($Mg(ClO_4)_2$) cartridge, J = Ethanol-liquid N_2 slurry, K = AADCO 737 pure air generator (under table), L = Stainless steel flasks, which were measured on the RGA-3 at Jungfraujoch, M = Ethanol container, N = Air flow meter, O = Vessel for transferring liquid N_2 to slurry (J), P = Liquid for detecting system leaks.

The two non-linearity experiments resulted in minor differences, which were well within the measurement precisions. For the sake of simplicity and consistency, only the 2008 non-linearity results have been applied. Figure 13 depicts the variable detector sensitivity used to correct the non-linearity of the RGA-3 at Jungfraujoch as a function of the normalized height. The normalized height equals the ratio of the unknown sample peak height divided by the mean of the bracketing standard's peak height. The experiments showed that the instrument sensitivity increases with increasing mixing ratios. For example, the normalized height sensitivity (height mol^{-1} of a sample divided by height mol^{-1} of the standard) is enhanced by approximately 10% for H_2 and 20% for CO for a sample with a peak height about double the height of a standard with mixing ratios of $H_2 \approx 640$ ppb and CO≈210 ppb.

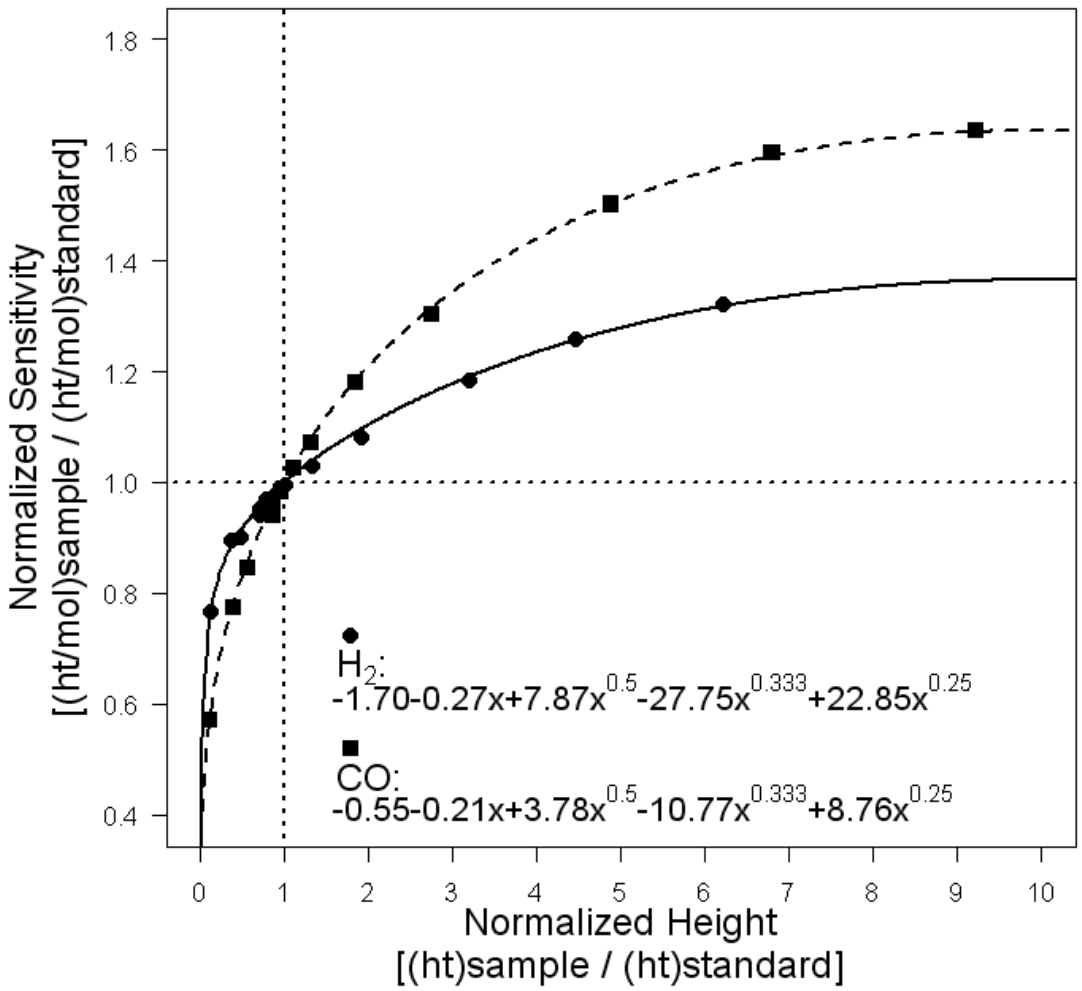

Figure 13. Non-linearity functions for the RGA-3 at Jungfraujoch. The experimental results for H_2 (filled circles) and CO (filled squares) were fitted to the functions shown in the graph using a least-square fitting technique. Fits were forced through (1,1) to approach unity sensitivity at the normalized height of 1.

2.3.3 Baseline estimation

The measurements at Jungfraujoch were filtered to identify pollution events using the statistical 2-dimensional Robust Extraction of Baseline Signal (2D-REBS) filter. The method was not developed in this study, but rather applied to the Jungfraujoch data. This 2-dimensional filter is an extension of the Robust Baseline Estimation (RBE) filter by Ruckstuhl et al. [86] for baseline estimations of spectroscopic measurements. The RBE approach, which is a purely statistical means of estimating the baseline from a time series that is partly influenced by recent source/sink processes (emissions, but also surface depletion), is available as a package for the statistical software program R [87]. With this approach, a local regression is iteratively fit to the data. This regression successively excludes data points for the next iteration that are not within $\pm 3.5\sigma$ around the current fitted curve. σ is the standard deviation of the fit residuals. Individual data points are weighted by their distance to the previous baseline fit using an asymmetric version of Tukey's bisquare robust weight function.

The 2-dimensional REBS was developed for atmospheric constituents that display strong latitudinal gradients due to asymmetric source/sink distributions about the equator (i.e. source/sink strengths that differ hemispherically) (S. Henne, Empa, method in prep.). Separating the background signal from a time series containing pollution events is difficult and can only be solved by the RBE filter if the baseline signal varies slowly in time (primarily dominated by a seasonal cycle in the case of atmospheric trace species). However, for species displaying a strong latitudinal gradient in background mixing ratios (i.e. H_2 and CO in this study), rapid latitudinal transport may carry air masses to a sampling site that are not representative of the site's latitude. Such events create a fast change in background mixing ratios that is not handled well by the original RBE approach.

The 2D-REBS method provides an option to derive the latitudinal distribution of a trace species' background mixing ratio and uses this information to estimate the baseline at a receptor site (Jungfraujoch in this case). Assumptions of neither the latitudinal gradient nor the source/sink distribution need to be made. In addition to the standard RBE approach, a second explanatory variable is added to the local regression: the latitude of origin of a sampled air mass. To achieve this, 10-day back-trajectories were calculated using FLEXTRA [88] and European Centre for Medium-

Range Weather Forecasts (ECMWF) analysis, along with 3-hour forecast (T+3) wind fields with a horizontal resolution of 1° by 1° and a temporal resolution of 3 hours. Trajectories were initialized every 4 hours over the investigation period at the location of Jungfraujoch. The initial altitude was set to the actual Jungfraujoch station altitude (i.e. 3580 metres above sea level (m a.s.l.)). The latitude of origin was then calculated from the back-trajectories. With this approach, it is possible to derive a smoothed surface fit of baseline mixing ratios in time and latitude. While for the original RBE, the main model parameter to be varied is the bandwidth of the local regression, there are several more parameters that have to be adjusted for the 2-dimensional version. These parameters include the means of estimating (a) the air mass origin from the back-trajectories, (b) the bandwidth of the local regression, (c) the degree of the local polynomial, and (d) a scaling factor for the two incomparable dimensions (time and latitude) of the fit. Next to estimating a baseline time series, the 2D-REBS allows the estimation of latitude-time distributions of the baseline.

3 MEASUREMENTS OF H_2 FROM FOSSIL FUEL-BASED INTERNAL COMBUSTION ENGINES

Direct online measurements of H_2 emissions in the exhaust gas of vehicles tested on a chassis dynamometer provide the ability to characterize and quantify emissions specifically related to individual engine dynamics and driving conditions. In this study, the dataset of H_2 (and CO) measurements in the exhaust gas of 27 different fossil fuel-powered vehicles under various driving conditions allows the thorough investigation of vehicular H_2 emissions and the main processes determining the source strength from this important anthropogenic source. Additional H_2 measurements from an engine capable of combusting both gasoline and natural gas allows an investigation into the role of a TWC in the removal (and production) of H_2 from exhaust gas from fossil fuel-powered internal combustion engine vehicles, along with the influence of various engine operating points (OPs) and lambda settings (see section 2.1.6).

In the first section of this chapter (section 3.1), background information is provided regarding qualitative factors influencing H_2 production and removal from fossil fuel-powered internal combustion engine vehicles. This section provides the basis for the factors affecting absolute emissions from these vehicles, which at times involves a qualitative comparison of certain aspects of the studied technologies.

The second section of this chapter (section 3.2) covers the quantitative aspects of the vehicles tested on the chassis dynamometer. This undertaking is approached through the calculation of H_2 emissions factors (E_{H2}) and the molar ratio of H_2/CO in the dry exhaust gas of the tested vehicles, primarily the gasoline-powered vehicles.

3.1 Qualitative overview of H_2 emissions from fossil fuel-powered vehicles

Hydrogen emissions in the exhaust gas of internal combustion engine vehicles are dependent on several interrelated factors, including:

- the presence/absence of a TWC;
- vehicle type;

    - the engine state (engine speed and torque), which is defined by the vehicle state (e.g. speed, acceleration);
    - the quality of lambda control;
- fuel type; and
- engine and catalyst temperature at start-up.

Ambient conditions (e.g. temperature, humidity) are also factors contributing to H_2 in vehicle exhaust. For example, cold-start emissions increase at lower ambient temperatures [23]. However, specific results involving variable ambient conditions were not assessed in detail in this study.

3.1.1 Presence/Absence of TWC

For vehicles that operate under fuel-rich conditions, the presence or absence and the state (fresh or aged) of the TWC dictate to a large extent the timing and magnitude of H_2 emissions in vehicle exhaust. In Fig. 14, pre-TWC exhaust measurements from the engine test bench at Empa (section 2.1.6) are compared with a much earlier study involving no TWC [89]. D'Alleva and Lovell [89], in their early 20th century study of the relationship between the exhaust gas composition and the air-fuel ratio, revealed H_2 mixing ratios in raw exhaust that decreased in a slight non-linear fashion as the air-fuel ratio increased. One aspect of the current study involved pre- and post-TWC measurements of gasoline and CH_4 (the primary component of natural gas) exhaust at various engine operating points (see section 2.1.6 for details of the method and operating point settings of the test bench measurements). A comparison of results from gasoline exhaust in this study with those from [89] confirmed a similar relationship and the predictability of H_2 mixing ratios in raw gasoline exhaust. The relationship of pre-TWC H_2 mixing ratios to the air-fuel ratio (and λ) for both studies is illustrated in Fig. 14. In this study, a much tighter window of air-fuel ratios, corresponding to λ values of approximately 0.9 to 1.05, was applied (coloured points in Fig. 14). The consistency in the results from both studies illustrates the predictability of the combustion principle and the dependency of H_2 emissions on the air-fuel ratio when not subject to the complexities of a TWC.

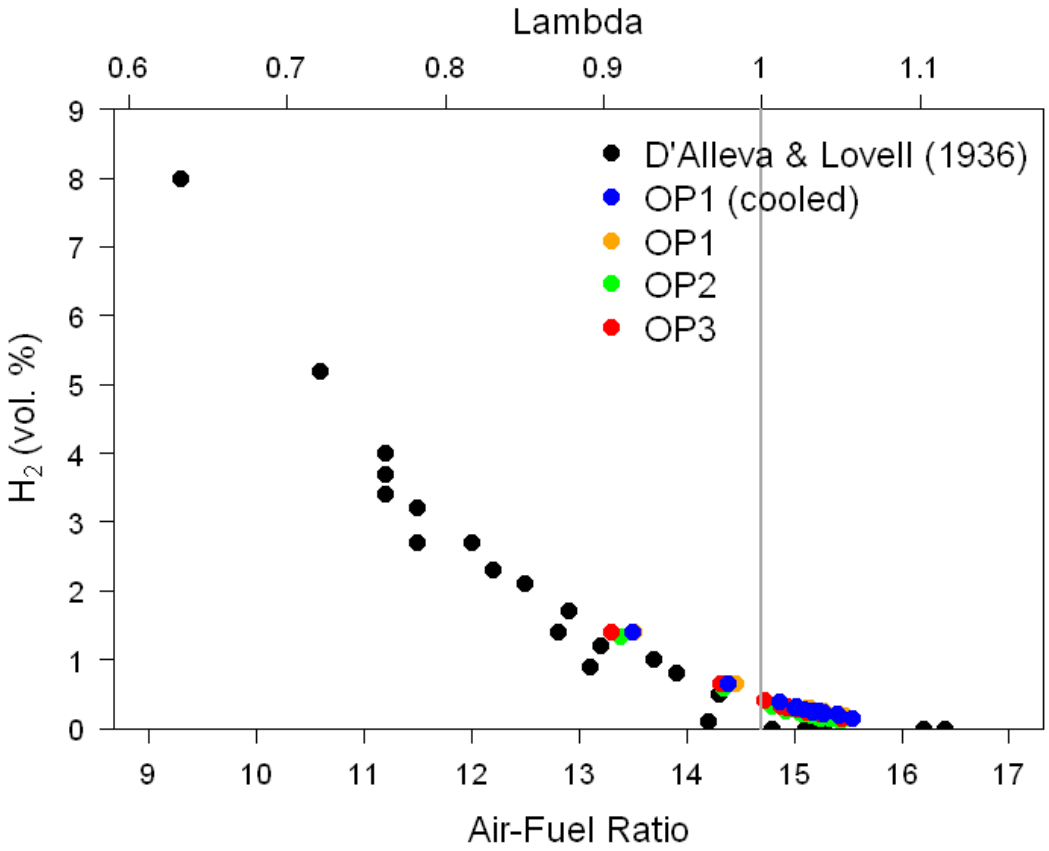

Figure 14. H_2 mixing ratios (% volume) in raw gasoline exhaust gas with an air-fuel ratio ranging from approximately 9–17. The approximate corresponding λ values are shown on the upper x-axis. The black filled circles are from D'Alleva and Lovell [89], the coloured circles from this study. The dark grey vertical line represents stoichiometric (λ=1) conditions.

To further illustrate the role of a TWC, an example using measurements of H_2 emissions in the gasoline exhaust gas from the test bench study were analysed (see section 2.1.6). Results based on various λ settings, both before and after the TWC, are depicted in Fig. 15 through the application of operating points OP3 and OP1 (cooled). H_2 is removed (oxidized) from the vehicle exhaust by the TWC, particularly when λ>1. Pre-TWC measurements (filled circles) result in similar emissions for each of the operating points at each λ setting. However, emissions at OP1 (cooled) decrease more rapidly as the fuel mixture moves from fuel rich (λ<1) towards the stoichiometric point (λ=1). At OP3, much less H_2 is removed by the TWC in the fuel-rich region, a function of the higher engine speed and exhaust throughput (OP3 is the operating point with the highest engine speed setting). This example therefore also illustrates the importance of the engine state (e.g. engine speed) and the fuel injection strategy of the λ control system in the overall emissions of H_2 in vehicle exhaust.

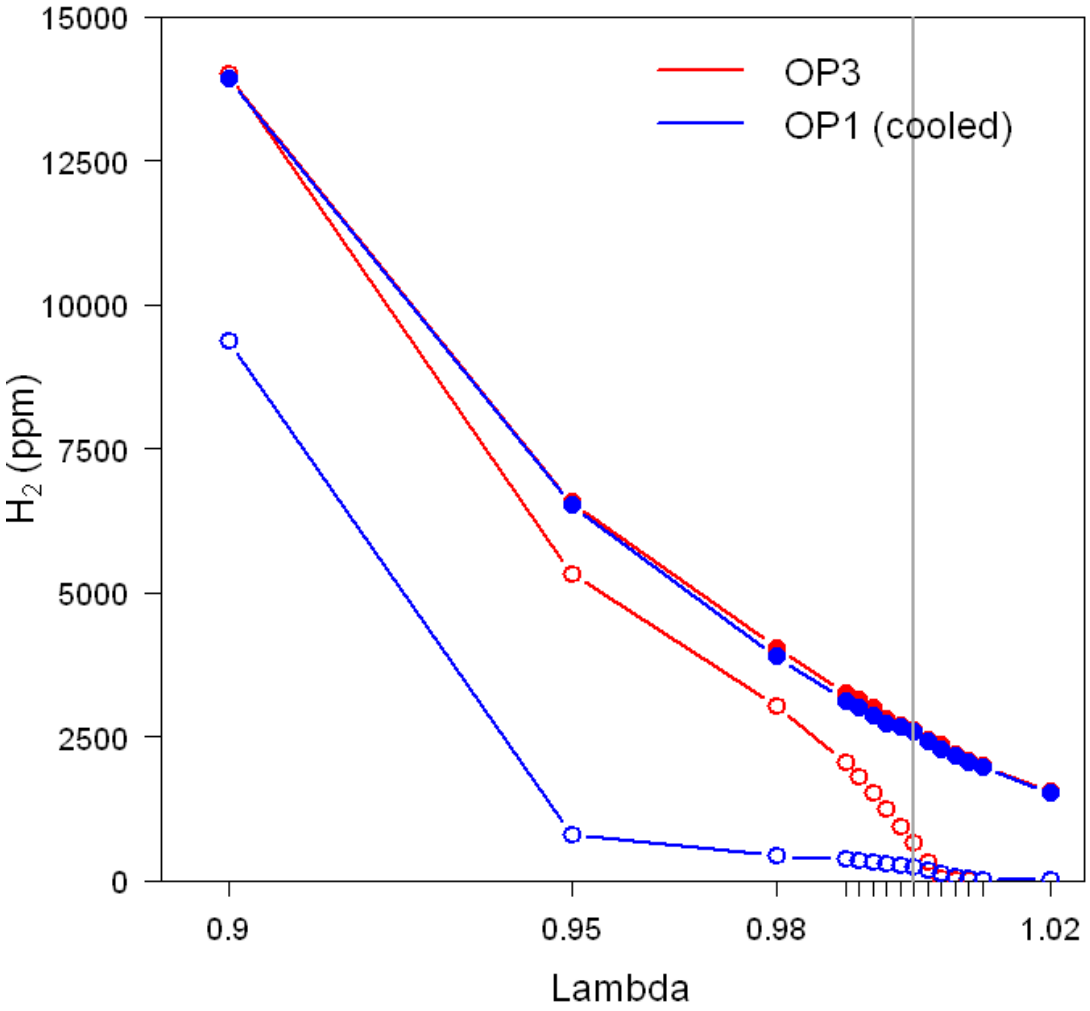

Figure 15. H_2 mixing ratios for pre- (filled circles) and post-catalytic converter (open circles) H_2 measurements as a function of the λ setting for operating points OP3 and OP1 (cooled) from a gasoline-powered engine in a test bench study (section 2.1.6). The dark grey vertical line represents stoichiometric (λ=1) conditions.

3.1.2 Vehicle type

Vehicle type is a further parameter influencing the magnitude of H_2 in current technology vehicle emissions. In this study, 2-wheelers emitted the most H_2 on average, approximately 5 times more than the gasoline automobiles (see section 3.2 for a quantitative assessment of the different vehicle technologies). The greater emissions from 2-wheelers are largely due to less developed ECUs, which are unable to efficiently maintain λ at 1 (stoichiometry) compared to most modern-day automobiles. Alvarez et al. [35] report that although emissions for newer motorcycles have improved substantially through the incremental tightening of regulations to the present European Euro-3 standard, emissions are still significantly greater than those

associated with today's automobiles. The state at which an engine is operated (engine speed (revolutions per minute, rpm) and torque) and the quality of λ control are 2 factors related to H_2 emissions from specific vehicle types. These two topics are covered individually below.

3.1.2.1 Engine state

The state at which the engine is operated is an important factor contributing to H_2 emissions in vehicle exhaust. This observation is depicted in Fig. 16 for a gasoline Euro-4 automobile over the course of the Common Artemis Driving Cycle (CADC). The greatest emissions occur under conditions of high engine speed and torque. These high rpm and load situations occur at high speeds and during periods of acceleration, or when a vehicle requires significant power for climbing a hill, for example. This is a primary reason for the sharp H_2 peak during the acceleration event at the high speed (~150 km h^{-1}) in Fig. 16A. Fuel-rich conditions equate to more power. Although high H_2 emissions are typically most prominent as speeds approach the upper end of the speed range for a highway-based chassis dynamometer sub-cycle, high H_2 emissions would also be observed if slope profiles were incorporated into the driving cycles. Thus on a chassis dynamometer, although greater emissions are often observed at high vehicle speeds, they are the result of high engine speed, and not necessarily the vehicle speed itself. H_2 emissions are elevated in cycles with higher proportions of fuel rich phases. In order to prevent the engine from overheating under such conditions, some ECUs are set to convert to a fuel-rich regime ($\lambda<1$) as the excess evaporated fuel cools the engine and TWC. The state of the engine is therefore related to the ECU and λ-control system of a vehicle.

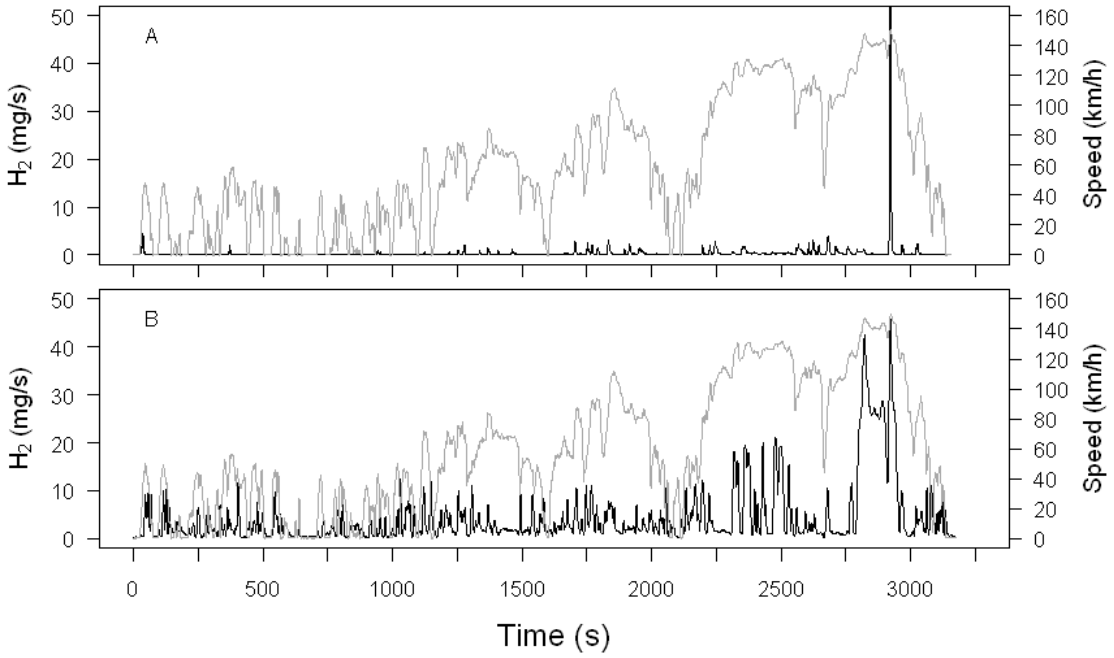

Figure 16. H_2 emissions (black lines, mg s^{-1}) from a gasoline Euro-4 automobile (panel A) and a gasoline Euro-3 motorcycle (panel B). The speed profile of the Common Artemis Driving Cycle is depicted by the grey line. The high emissions for the automobile at the end of the cycle are due to the engine control unit switching to a fuel rich ($\lambda<1$) regime under high engine speed and load conditions. Emissions from the automobile are much lower throughout the cycle due to the more developed lambda control system compared with the motorcycle, which displays consistently higher emissions, irrespective of the engine state.

3.1.2.2 Quality of lambda control

Emissions from current technology vehicles are also a function of how the vehicle's ECU is programmed to respond to the changes in the engine's state. Depending on the vehicle, the ECU is set to convert to fuel-rich conditions at a certain point under high engine speed and load conditions, as the excess fuel acts to cool and protect the catalyst (P. Soltic, Empa, pers. comm.). The quality of λ control by the ECU is therefore a critical parameter dictating absolute H_2 emissions in exhaust gas. H_2 emissions are elevated in cycles with higher proportions of fuel-rich phases and fuel-rich phases are more frequent with less sophisticated λ control systems. This is evident in Fig. 16A, with emissions only markedly elevated as the automobile accelerates at already high vehicle speed. Hydrogen emissions from 2-wheelers tend to be substantially greater than from gasoline-powered automobiles, which is largely due to the less developed ECUs for motorcycles, resulting in less precise λ control and higher emissions, despite identical driving conditions. Figure 16B illustrates this

phenomenon for a Euro-3 motorcycle, as high emissions are observed throughout the cycle, irrespective of the individual sub-cycle driving conditions.

In another example, Fig. 17 (panel A) depicts the cumulative H_2 emissions of 2 separate gasoline automobiles and a diesel delivery vehicle operated under the L2 driving cycle (see section 2.1.3 for details of the individual driving cycles). Also depicted is the λ setting for each vehicle (panel B). For one of the gasoline vehicles (blue line), very high emissions are observed as speeds approach 150 km h^{-1}. For this car, the ECU converts to a fuel-rich setting, which results in very high H_2 emissions. This is apparent from the λ setting, as approximately 60% of the total emissions from the cycle occur at a drop in λ to approximately 0.85 at the end of the cycle. This is not the case for the other gasoline automobile (red line), where emissions are much more evenly distributed over the course of the cycle and are overall much lower. The fuel mixture does not run rich ($\lambda<1$) at the highest speeds, which avoids the high H_2 emissions during the latter part of the cycle. H_2 emissions in the exhaust gas of the diesel delivery vehicle are almost completely absent (green line). As can be seen from the λ profile of this vehicle, fuel-rich conditions were never approached over the course of the driving cycle. Gasoline-powered vehicles sometimes operate under fuel-rich reducing conditions with incomplete fuel combustion in the absence of O_2, thereby limiting NO_x in exchange for H_2 and CO. However, diesel-powered vehicles constantly operate under fuel-lean oxidizing conditions ($\lambda>1$) with an excess of O_2, limiting H_2 and CO in exchange for NO_x [90]. This results in H_2 emissions from diesel vehicles being often undetectable in the exhaust gas over the course of a typical driving cycle.

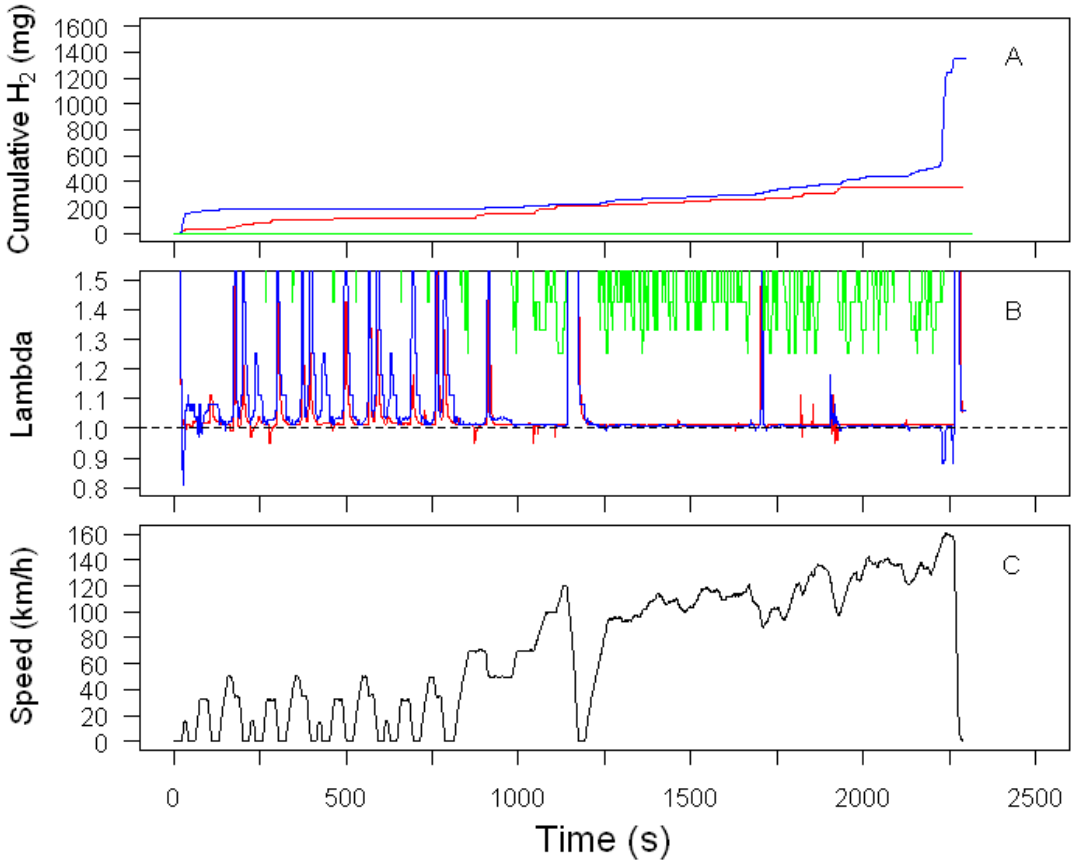

Figure 17. Cumulative H_2 emissions (panel A) and lambda settings (panel B) of 2 gasoline automobiles (red and blue lines) and a diesel delivery vehicle (green line) under the L2 cycle (panel C). The dashed line in panel B represents stoichiometric conditions.

3.1.3 Fuel type

Fuel type is another important factor contributing to H_2 emissions from the technologies studied in this project. Figure 18 depicts cumulative H_2 emissions (in mg) from the diesel automobile and delivery vehicles, gasoline automobiles, natural gas automobiles, and 2-wheelers over the course of the CADC driving cycle.

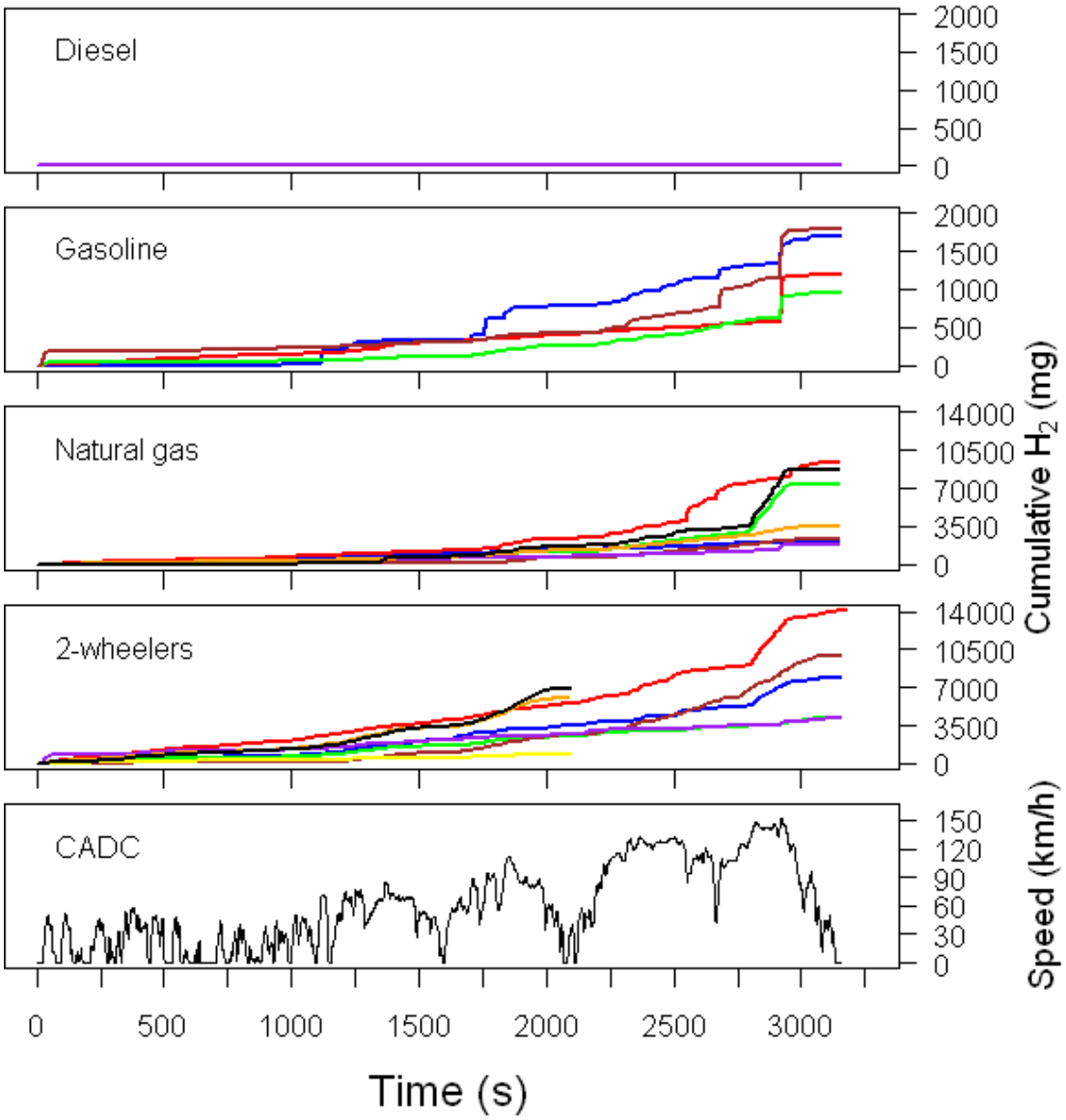

Figure 18. Cumulative H_2 emissions (mg) for diesel vehicles, gasoline automobiles, natural gas automobiles, and 2-wheelers. All vehicles were operated under cycle CADC. Different colours represent different vehicles. Note the difference of scales for H_2 on the y-axis. The 3 shorter curves for the 2-wheelers represent scooters, whose displacements and top speeds prevented them from conducting the highway sub-cycle of the cycle.

Highest H_2 emissions from vehicles tested in this study were produced by 2-wheelers, followed by natural gas vehicles, gasoline automobiles, and diesel vehicles. H_2 emissions from gasoline-powered vehicles are much higher than those from diesel-powered vehicles, and in many instances H_2 was not detectable at all over the course of a typical driving cycle conducted by a diesel vehicle. As discussed above, H_2 emissions (or lack thereof) from diesel vehicles result from the constantly oxidizing operating point of diesel engines. Thus, for diesel vehicles, it is not the diesel fuel in

itself that leads to low H_2 emissions, but rather that the H_2 is almost always completely oxidized prior to emission.

H_2 emissions from natural gas vehicles depend on many of the same factors that produce H_2 in current technology gasoline vehicles. Similarly to gasoline automobiles, natural gas vehicles sometimes operate under fuel-rich reducing conditions. On average, however, H_2 emissions from natural gas vehicles are considerably higher under the same driving conditions. A comparison of post-TWC H_2 emissions in gasoline and methane exhaust from the test bench study (section 2.1.6) is illustrated in Fig. 19. H_2 emissions are plotted as a function of λ for each of the engine operating points (OP1, OP2, OP3, and OP1 (cooled)).

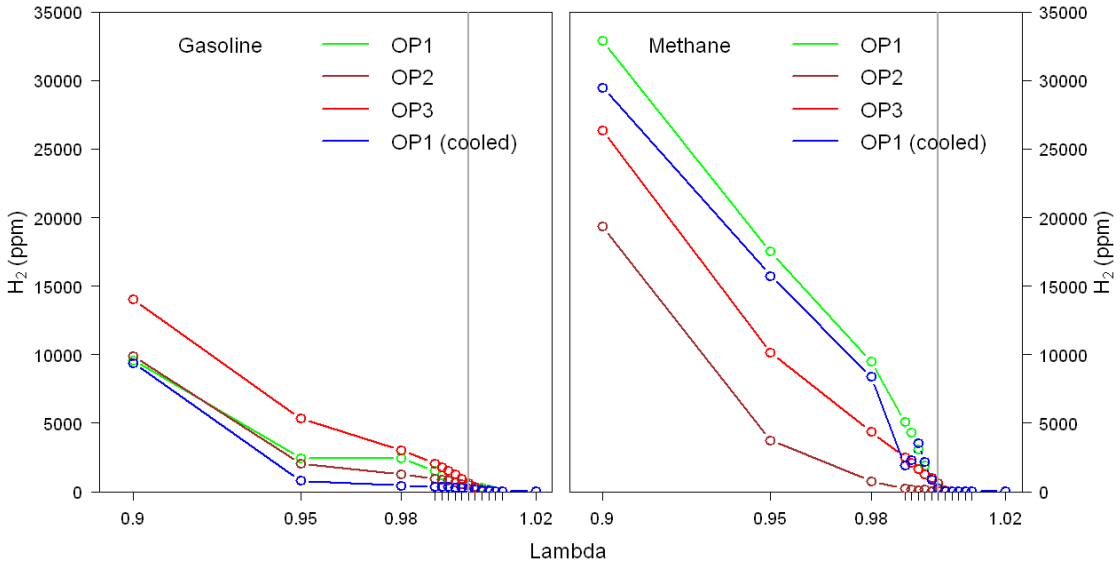

Figure 19. H_2 emissions in gasoline and natural gas exhaust from test stand measurements of a stationary engine. Emissions are plotted as a function of λ for each of the tested operating points (OP1, OP2, OP3, and OP1 (cooled)). The dark grey vertical lines represent stoichiometric conditions.

Higher absolute H_2 emissions almost always result from CH_4 compared with gasoline at all operating points in the most fuel rich region (λ=0.9–0.98). In general terms, H_2 emissions from combusted CH_4 are higher than from gasoline because the hydrogen-carbon ratio in natural gas is approximately double compared to that of gasoline. This also results in greater H_2O production from CH_4 combustion, which is favourable for enhanced water-gas shift activity (i.e. $CO + H_2O \rightarrow H_2 + CO_2$).

3.1.4 Engine and catalyst temperature at start up

The temperature of the engine and TWC is a further important factor dictating emissions of H_2 from an internal combustion engine vehicle. Figure 20 illustrates the importance of cold-start emissions from a gasoline-powered Euro-4 automobile. Approximately 40% of total H_2 emissions occur during the ignition of the cold engine, with an additional 25% of total emissions resulting from the first major acceleration event while the engine and catalyst are still cold. The rate of emissions (mg s^{-1}) and the speed profile are depicted in Fig. 20B by the black and grey lines, respectively.

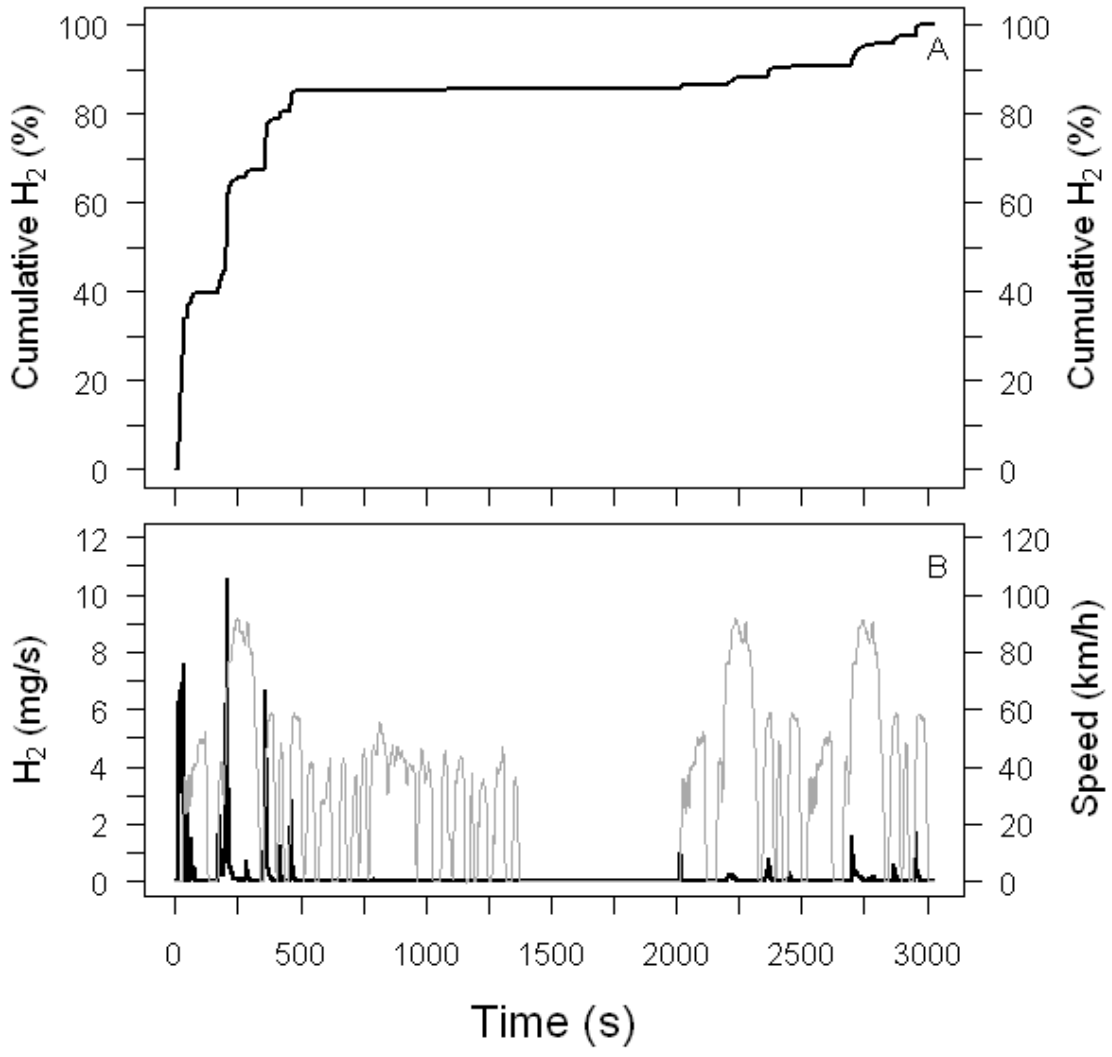

Figure 20. Cumulative H_2 emissions from a cold-start cycle (LA) as a percent of the total emissions (panel A) and absolute H_2 emissions (black) and the speed profile (grey) (panel B). The cold-start phase of the cycle contributes the largest fraction of overall emissions from the cycle.

When prolonged fuel-rich conditions do not dominate the cumulative emissions, cold start emissions generally contribute the greatest cumulative H_2 emissions. An initially cold catalyst needs to attain a minimum temperature before operating and converting optimally. The light-off temperature is often used to describe the temperature at which the catalyst becomes more than 50% effective with respect to CO oxidation [90]. This temperature is above 200 ^{o}C [91]. In addition, most gasoline cars are run with a rich air-fuel ratio at start-up, as this guarantees a smooth running of the cold engine where gasoline condenses on the cold walls (M. Weilenmann, Empa, pers. comm.). The ECU usually then converts to λ=1 at the catalyst light-off temperature. Cold start emissions generally affect all vehicle and fuel types measured in this study, although their relative magnitude in terms of total emissions is different for each vehicle, fuel type, and cycle driven. An advantage of natural gas vehicles over conventional gasoline-powered vehicles is the reduced cold start and low temperature emissions [92].

In a second example, cumulative H_2 emissions from a vehicle conducting a driving cycle (Rb) with a previously warmed-up engine is depicted in Fig. 21. Clearly there is no influence from a cold engine start, as cumulative emissions increase almost linearly across the entire cycle.

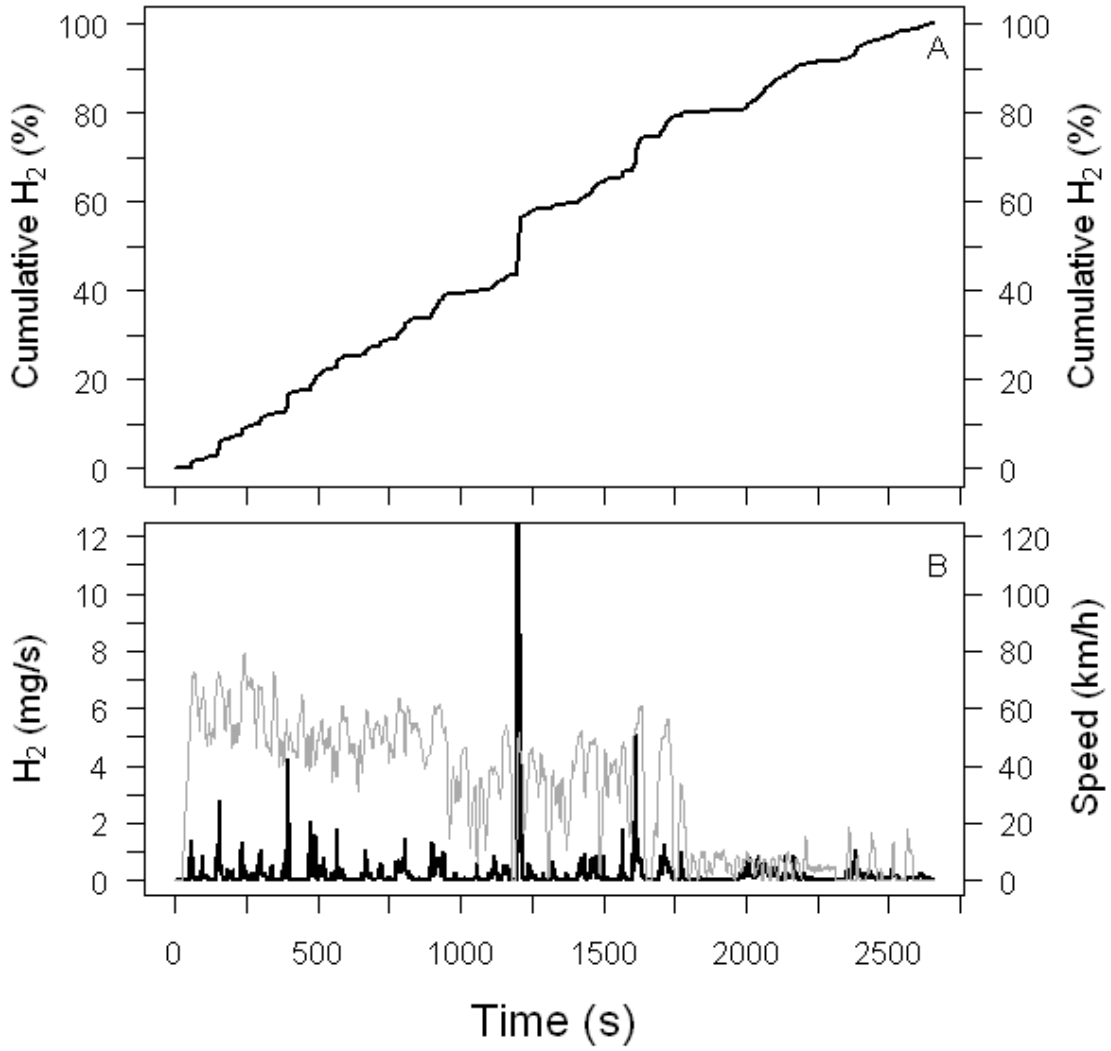

Figure 21. Cumulative H_2 emissions from a warm-start cycle (Rb) as a percent of the total emissions (panel A) and molar H_2 emissions (black) and the speed profile (grey) (panel B). Enhanced emissions at the start of the cycle do not result due to the driving cycle starting with a previously warmed-up engine.

3.2 Quantified H_2 emissions from fossil fuel-powered vehicles

This section of the chapter involves the quantification of H_2 emissions from the fossil fuel-powered internal combustion engine vehicles tested in this study. The first sub-section covers E_{H2}. This first part involves a detailed analysis of E_{H2} from the 4-wheeled vehicles, which includes the gasoline automobiles, diesel automobile and delivery vehicles, and natural gas automobiles. This detailed overview is then followed in the second part by an in-depth survey of H_2 emission factors for the 2-wheelers (motorcycles and scooters) evaluated in this study. In parallel to the E_{H2} in both parts, E_{CO} are covered in some detail for sake of comparison.

In the second sub-section, the relationship between H_2 and CO is examined, both through molar H_2/CO ratios and the relationship of E_{H2} to E_{CO}. This sub-section is also separated into individual discussions for 4-wheeled vehicles and 2-wheeled vehicles.

3.2.1 H_2 emission factors from 4-wheeled vehicles

E_{H2} were calculated to assist in the accurate upscaling of the source term of H_2 from technological processes (section 4.1). Table 15 provides the mean E_{H2} and E_{CO} for each of the 4-wheeled vehicles across the range of driving cycles/sub-cycles, along with individual cycle/sub-cycle characteristics. E_{H2} from the diesel vehicles were marginal and are therefore not covered in depth in the remainder of this discussion.

3.2.1.1 Gasoline-powered vehicles

When considering E_{H2} for the gasoline automobiles for all cycles, highest emissions were found with the 3 cycles subject to a cold start. As an average for all vehicles, E_{H2} were highest for the IUFC15 driving cycle at 39.9±23.0 mg km^{-1}, a reflection of the high emissions from the cold start, along with regular excursions of λ away from stoichiometry into the fuel-rich range. By separating E_{H2} into individual sub-cycles, the highest mean values are found with sub-cycle I for cycles IUFC15 (69.8±38.4 mg km^{-1}) and LA (53.7±19.5 mg km^{-1}), followed by sub-cycle III for cycle L2 (45.4±40.5 mg km^{-1}). The reasons for these observations are in large part due to the

cold start emissions for cycles IUFC15 and LA, along with the subsequent emissions throughout the remainder of sub-cycle I under cooler conditions before the TWC is functioning optimally (see section 3.1.4). The high E_{H2} for sub-cycle III of cycle L2 is almost exclusively due to the emissions at the highest speeds, which reach 160 km h^{-1}, indicating simultaneous high engine speed and torque. At that point, λ drops well below 1 for several seconds, representing fuel-rich conditions.

The lowest overall emission factors for the gasoline automobiles are found with the Rb cycle, likely a result of the warm engine start, coupled with the relatively dynamic speed profile that likely leads to frequent overrun fuel cut-off events (i.e. when the engine is motoring during deceleration events, the ECU turns off fuel injection and ignition) that allow the TWC to regularly replenish and store O_2, leading to consistent H_2 oxidation. However, sub-cycle III of cycle Rb displays a higher mean E_{H2} at 35.3±44.7 mg km^{-1} despite the fact that lambda never drops below 1 at any point during this sub-cycle for any of the vehicles. This would suggest that the stop-and-go driving characteristic of sub-cycle III sometimes produces significant H_2 through other means, such as enhanced water-gas shift activity, which Vollmer et al. [33] also suggested for congested rush hour traffic in a tunnel study. This hypothesis is supported here by the simultaneous lower E_{CO} for sub-cycle III of the Rb cycle and the high H_2/CO ratio for this sub-cycle (see section 3.2.3 on H_2/CO ratios). The forward water-gas shift reaction is favoured under lower temperatures, which is the case for sub-cycle III of Rb compared with other sub-cycles due to lower engine load and exhaust throughput. Despite the relatively high E_{H2} for sub-cycle III of Rb, absolute emissions are relatively low since the distance travelled is only 1.1 km. The lowest overall E_{H2} for individual sub-cycles is from sub-cycle I for cycle Rb at 6.2±7.4 mg km^{-1}, followed by sub-cycle I of cycle Ra at 8.1±4.7 mg km^{-1}.

The overall mean E_{H2} and E_{CO} for gasoline automobiles in this study were 26.5±12.1 mg km^{-1} and 453±325 mg km^{-1}, respectively. This E_{H2} is lower than the overall mean measured by Heeb et al. [47] for gasoline Euro-3 automobiles (59.4 mg km^{-1}). The mean E_{H2} for the 4 highway sub-cycles in this study (Ra – I & II, L2 – III, CADC – III) was 26.0±17.3 mg km^{-1}. This is also lower than that reported for a 2004–2005 Swiss highway tunnel study (E_{H2} of 67 mg km^{-1}) for a strictly gasoline-based fleet [33]. These comparisons suggest that H_2 emissions from gasoline Euro-4 vehicles

have decreased by ~55% compared with gasoline Euro-3 automobiles, and that highway-based H_2 emissions with the Euro-4 technology have decreased by ~61% compared with previous technologies based on a real-world vehicle fleet. A possible explanation is the improved λ control systems with Euro-4 vehicles, which provide more consistent regulation around the stoichiometric air-fuel ratio, and thus fewer fuel-rich excursions and lower resultant emissions. Other technical progress, such as increasing the rate at which the TWC heats up and improving cold start procedures (i.e. less extreme fuel-rich excursions) are likely also responsible for the observed decrease.

3.2.1.2 Natural gas-powered vehicles

For the natural gas automobiles, although the cycles subject to cold starts had high emissions influenced largely by the initial cold start sub-cycle, the highest overall E_{H2} were from the 3 cycles involving highway-based sub-cycles (i.e. CADC, Ra, and L2). The highest overall E_{H2} was from the CADC driving cycle (96.5±65.9 mg km^{-1}), which is due primarily to the emissions during the highway-based sub-cycle. Evaluating mean E_{H2} for individual sub-cycles, the highest values were for sub-cycle III for cycles Rb (160±113 mg km^{-1}), CADC (140±112 mg km^{-1}), and L2 (102±113 mg km^{-1}). Interestingly, the highest sub-cycle E_{H2} was for an urban-based sub-cycle. This would suggest that H_2 production is occurring through some other means, such as enhanced water-gas shift activity, which was also observed for sub-cycle III of the Rb driving cycle for the gasoline automobiles (see next paragraph). Since these stop-and-go conditions would most likely result in a cooler TWC (less exhaust throughput) and the TWC being consistently depleted in O_2 during acceleration events, the H_2O in the exhaust is likely in constant reaction with CO in the TWC, thereby producing H_2 in the process. For the highway-based sub-cycles with high E_{H2}, the high exhaust gas throughput leads to reduced TWC efficiency coupled with fuel-rich conditions and resultant elevated H_2 emissions, similarly to the gasoline automobiles.

As with the gasoline automobiles, the lowest overall E_{H2} for the natural gas automobiles was for the Rb driving cycle. Although the highest mean individual sub-cycle E_{H2} was found for sub-cycle III of the Rb cycle, the fact that such a short total distance is covered with this sub-cycle makes it less influential in terms of its

contribution to overall emissions. Similarly to the gasoline automobiles, the frequent replenishment of O_2 into the TWC through overrun fuel cut-off events for the first two sub-cycles leads to much of the H_2 being oxidized. The lowest individual sub-cycle E_{H2} were sub-cycles I (34.2±19.7 mg km^{-1}) and II (36.6±27.9 mg km^{-1}) for cycle Rb and sub-cycle II for the IUFC15 driving cycle (47.8±41.0 mg km^{-1}).

The overall mean E_{H2} and E_{CO} for the natural gas automobiles in this study were 73.5±21.8 mg km^{-1} and 654±417 mg km^{-1}, respectively. The E_{H2} and E_{CO} for the natural gas automobiles provided in this study are to my knowledge the first documented case reported for individual-vehicle emission factors for natural gas vehicles.

3.2.2 H_2 emission factors from 2-wheeled vehicles

Unlike the automobiles, E_{H2} for the 2-wheelers are not higher overall for the cold start cycles than those with a previously warm engine. Moreover, E_{H2} for the two highway sub-cycles (sub-cycle III for WMTC and CADC) are comparable to other sub-cycles, illustrating the consistently less effective λ control and exhaust after-treatment systems of 2-wheelers, irrespective of driving conditions. Table 16 outlines the E_{H2} and E_{CO} for the 2-wheelers. The overall mean E_{H2} and E_{CO} for 2-wheelers in this study were 141±38.6 mg km^{-1} and 3470±951 mg km^{-1}, respectively. Highest overall E_{H2} were found for the CADC cycle (175±104 mg km^{-1}), simulating urban, rural, and highway conditions, followed by CC (170±76.7 mg km^{-1}), which simulates completely urban driving. For the individual sub-cycles, E_{H2} were highest for sub-cycle I of the CC cycle (197±93.0 mg km^{-1}), sub-cycle I of the WMTC cycle (172±94.5 mg km^{-1}), and sub-cycle II of the CC cycle (172±86.8 mg km^{-1}). Each of these 3 sub-cycles represents urban driving conditions. In their study involving H_2 emissions from Euro-3 automobiles, Heeb et al. [47] found substantially higher E_{H2} for urban stop-and-go traffic compared with other driving conditions. The highest E_{H2} for 2-wheelers conducting urban sub-cycles could therefore be analogous to the observations by [47], in that the integrated systems that ultimately control emissions from the tailpipe were not as developed as they are with current technology vehicles.

The lowest overall E_{H2} are from the LM cycle (93.3±57.5 mg km^{-1}), a legislative cycle covering speeds typically found under urban and rural driving conditions, followed by the WMTC cycle (127±58.5 mg km^{-1}), which simulates urban, rural, and highway driving conditions. The lowest individual sub-cycle E_{H2} was observed for sub-cycle II of the LM cycle (58.7±35.9 mg km^{-1}) and sub-cycle III of the WMTC cycle (91.7±58.9 mg km^{-1}). All other individual sub-cycle E_{H2} were well above 100 mg km^{-1}. The characteristics of LM's sub-cycle II (a legislative cycle) provide a possible explanation for these observations, as they involve generally steady driving conditions with moderate acceleration and deceleration events. This same sub-cycle for the automobiles (sub-cycle II from the L2 cycle) also had comparatively low overall E_{H2} because λ rarely dropped below 1.

3.2.3 H_2 vs. CO

3.2.3.1 4-wheeled vehicles

Due to the positive correlation of H_2 and CO in exhaust gas and the widely quantified CO inventories, H_2/CO ratios from vehicle exhaust have previously been applied in order to upscale emissions of H_2 considered to be representative of the dominant traffic source [18]. Here, molar H_2/CO ratios through the simultaneous direct measurement of H_2 and CO at the exhaust pipe of gasoline-powered vehicles are reported, along with the relationship of E_{H2} to E_{CO}. Ratios are reported as the cumulative relationship of integrated totals for each overall cycle, along with integrated totals for each individual sub-cycle. Molar H_2/CO ratios for Euro-4 gasoline automobiles measured on the chassis dynamometer were typically higher than those that have been reported in past literature for atmospheric mixing ratios characteristic of traffic-based sources without the influence from outside H_2 loss processes [33]. Results from the Euro-4 gasoline-powered automobiles are presented in Table 15. The overall mean molar H_2/CO for the gasoline Euro-4 automobiles in this study was 1.02.

For individual cycles, cumulative H_2/CO ratios were lowest for those involving a cold-start. For individual sub-cycles, the lowest ratios were from sub-cycle I of all three cold-started cycles. These conditions can be considered analogous to pre-TWC

(exhaust upstream of catalytic converter) or no-TWC ratios [20, 39, 89], all of which reported H_2/CO ratios well below 1. During the cold start phase, the mean H_2/CO ratio in this study was ~0.33 before the vehicle even moved; this ratio therefore represents the mean engine ignition H_2/CO ratio. Emissions from the cold start phase often represented a significant fraction of overall emissions, indicating that subsequent emissions often had proportionally less influence on the overall H_2/CO ratios. Following the cold-start phase, H_2/CO ratios increased in proportion to the magnitude of absolute emissions throughout the rest of the cycle, since the ratio during the cold start was the lowest for the entire cycle. Once the engine and catalyst heated up, conversion of CO improved, and H_2/CO ratios increased, due presumably in part to water-gas shift activity, which is promoted by newer-technology TWCs [40]. Figure 22 depicts cumulative mixing ratios of H_2 and CO, along with cumulative H_2/CO ratios for gasoline automobiles under the IUFC15 cycle. Evident are the lowest ratios during the cold-start segment of the cycle, with ratios for each vehicle gradually increasing throughout the remainder of the cycle.

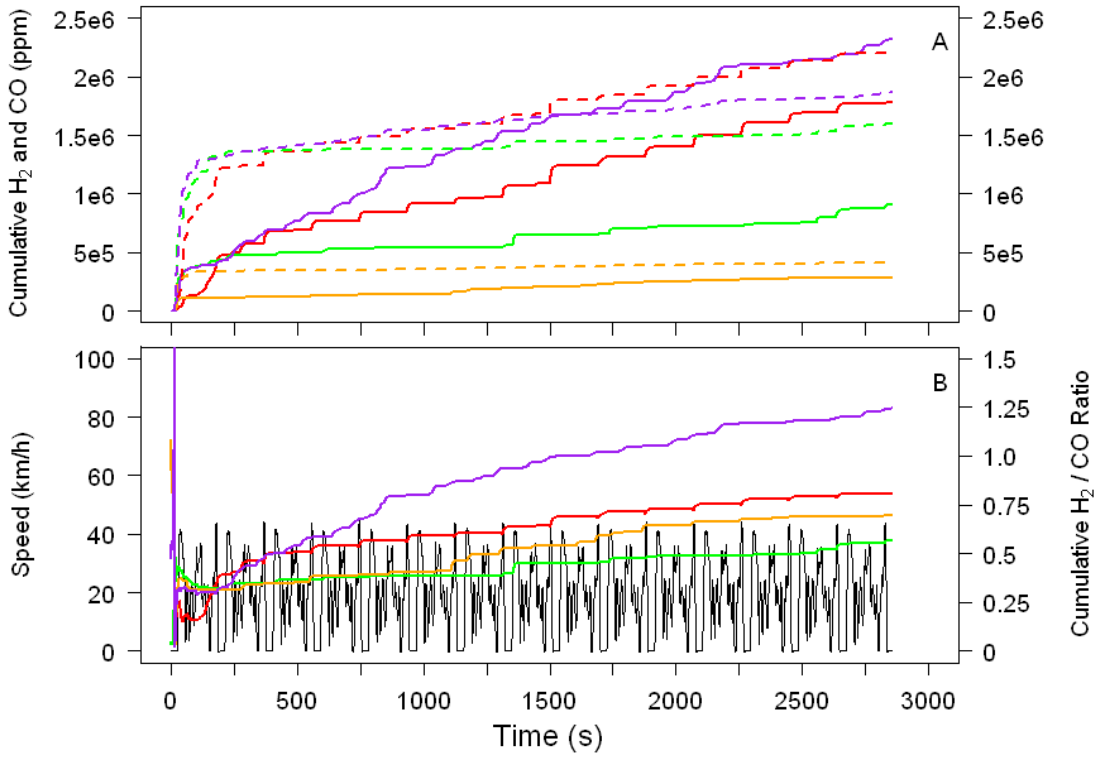

Figure 22. Cumulative cold-start cycle (IUFC15) H_2 (solid lines) and CO (dashed lines) mixing ratios (panel A) and cumulative molar H_2/CO ratios (panel B) for gasoline-powered Euro-4 automobiles. The speed profile is depicted by the black line in panel B. Colours represent different vehicles.

Figure 23 depicts cumulative mixing ratios of H_2 and CO, with cumulative H_2/CO ratios of gasoline automobiles under the CADC cycle. It can be seen that with the warm engine start, H_2 emissions start out higher than those of CO, with ratios gradually decreasing as the cycle progresses. For the vehicle corresponding to the red line in Fig. 23B, virtually no H_2 or CO emissions occurred during the urban (initial) sub-cycle. However, as emissions were produced at the start of the rural sub-cycle, it can be seen that H_2 emissions outweighed those of CO.

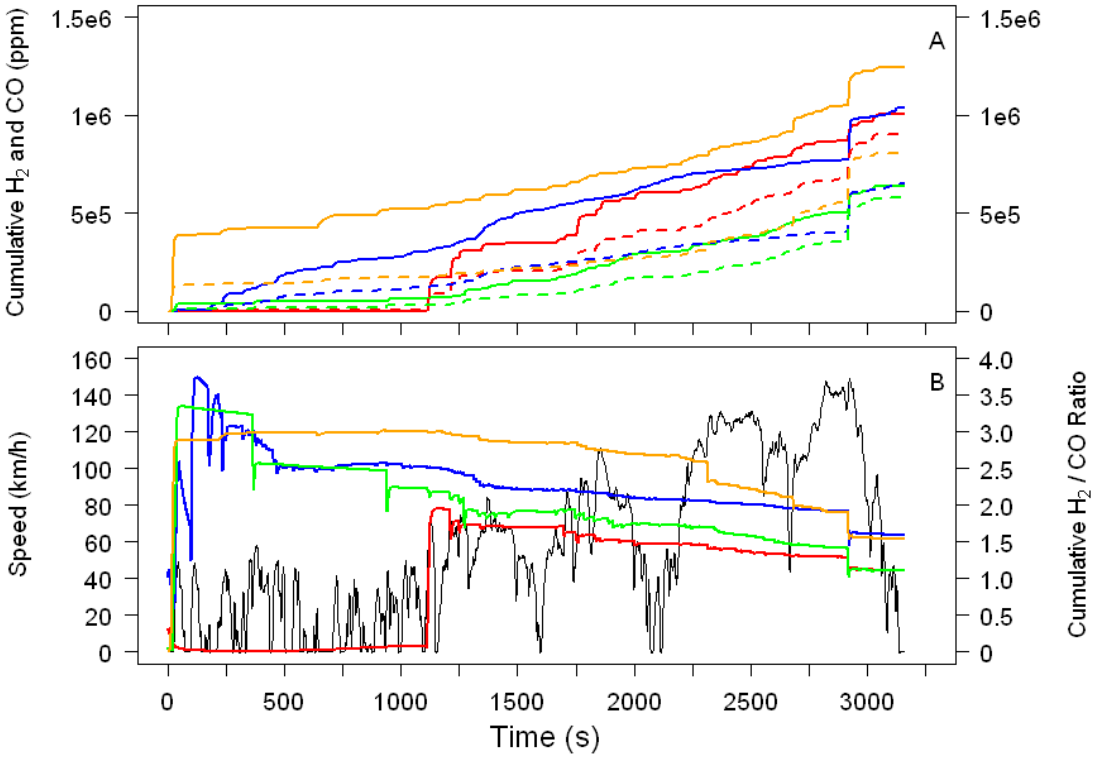

Figure 23. Cumulative warm-start cycle (CADC) H_2 (solid lines) and CO (dashed lines) mixing ratios (panel A) and cumulative molar H_2/CO ratios (panel B) for gasoline-powered Euro-4 automobiles. The speed profile is depicted by the black line in panel B. Colours represent different vehicles.

After cold-start sub-cycles, the lowest H_2/CO ratios were observed for highway-based sub-cycles. These sub-cycles involve high vehicle speeds, corresponding to high engine speed and load conditions, and thus high catalyst temperatures and fuel-rich conditions. The lower H_2/CO ratios for highway-based sub-cycles appear to be due to conditions that hinder proper TWC activity, namely fuel-rich excursions. This is most evident at the highest speeds in Fig. 23B, where H_2/CO ratios decrease significantly at the end of the cycle for each of the vehicles. Since the highest H_2 (and CO) emissions occur under fuel rich conditions, λ control therefore plays an important role in

regulating the H_2/CO ratio in vehicle exhaust. Figure 24 depicts cumulative H_2/CO ratios for a gasoline automobile operating under the CADC cycle. Corresponding H_2 and CO mixing ratios, the speed profile, and the lambda setting have been included for reference. The step decreases in the cumulative H_2/CO ratio display how the initial efficient CO removal with some H_2 production due to a warm, optimally operating TWC, perpetually decreases as proportionally more CO is produced with each fuel-rich excursion.

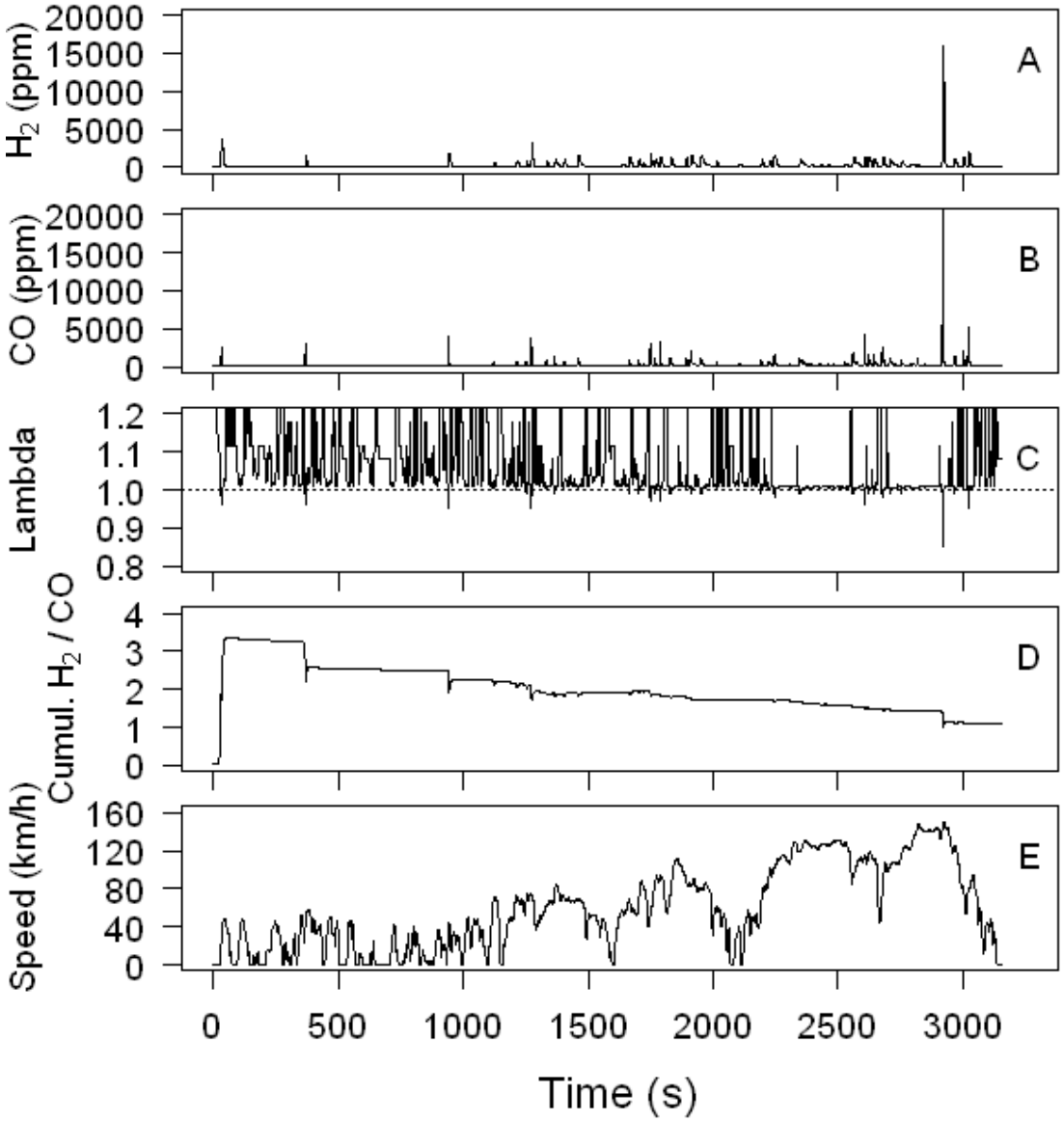

Figure 24. H_2 mixing ratios (panel A), CO mixing ratios (panel B), lambda setting (panel C), cumulative H_2/CO ratio (panel D), and speed profile (panel E) for a gasoline automobile operating under the CADC driving cycle.

H_2/CO ratios were highest for sub-cycles representing urban and rural driving conditions. These ratios correspond to a warmer catalyst and moderate engine speed and load profiles, allowing more efficient TWC conversion. Vollmer et al. [33] also observed higher H_2/CO ratios during rush hour traffic in a tunnel study, and attributed the observation to enhanced water-gas shift activity, which is likely the case in congested situations where the exhaust throughput is much lower than during free flowing highway traffic conditions, and hence exhaust and TWC temperatures are also lower. Haryanto et al. [93] experienced higher conversion of CO through the water-gas shift reaction at lower temperatures, which provides an explanation for these observations in congested rush hour traffic. Although urban and rural driving conditions tend to correspond to higher H_2/CO ratios, lower absolute emissions typically result, making these emissions less influential in a large-scale atmospheric context. Observed atmospheric H_2/CO ratios are therefore primarily a function of cold-start and other fuel-rich-induced emissions. In past studies that cited H_2/CO ratios well below 1, these excursions would have occurred much more frequently. The generally fewer fuel-rich excursions by newer gasoline automobiles, along with the promotion of the water-gas shift reaction, could therefore provide an explanation for the generally higher H_2/CO ratios observed in this study.

It is also important to bear in mind emission standard regulations when considering H_2/CO ratios. Keller and Zbinden [94] projected with model results that the Swiss vehicle mix for gasoline-powered light duty vehicles in 2005 comprised 15% Euro-4, 18% Euro-3, 28% Euro-2, 18% FAV1 (Swiss exhaust regulation for light vehicles, which was a Swiss standard used at time of Euro-1), 4% regulated TWC prior to 1991, and 1% conventional (without catalytic converter) vehicles. Emission standards could also provide an explanation for higher H_2/CO ratios experienced with newer vehicles compared with those cited in past studies involving technologies subject to less stringent CO regulations. The European emission standard Euro-4 entered into force in January 2005, and stipulates a maximum CO emission factor of 1000 mg km^{-1}. CO emission limits for Euro-1, Euro-2, and Euro-3 were 2720 mg km^{-1}, 2200 mg km^{-1}, and 2300 mg km^{-1}, respectively. Today's TWC are much more sophisticated than those in the past, and have been developed to maximize O_2 storage capacity for oxidation of CO and hydrocarbons, while also promoting water-gas shift and steam reforming reactions [40]. According to *EC Regulation No 715/2007*, the Euro-5

emission standard for gasoline and diesel passenger vehicles and most light commercial vehicles became a statute in September 2009, with the Euro-6 standard for the same vehicles slated for September 2014 [95]. The future CO emission allowance for the Euro-5 and Euro-6 standards for passenger cars will be the same as for Euro-4 (1000 mg km^{-1}), suggesting that efforts to control CO for gasoline automobiles may not advance significantly in the future.

The scatterplot of mean E_{H2} vs. E_{CO} for the gasoline automobiles in Fig. 25 shows that as both E_{H2} and E_{CO} increase, the slope of the curve becomes more gradual, indicating that the removal of CO is becoming less efficient under conditions that lead to high CO emissions. This pattern is in contrast to the observations of molar H_2 vs. CO by Steinbacher et al. [21] and Vollmer et al. [33], who observed a slight enhancement of H_2 compared with CO under the most polluted conditions. In their study of the relationship of exhaust gas composition to λ, D'Alleva and Lovell [89] found this same enhanced H_2 characteristic under very fuel-rich conditions ($\lambda<0.8$) without a TWC. Based on past studies of pre-/without-TWC exhaust measurements [39, 89], a lambda range of 0.9–1.02 resulted in a visually linear relationship between H_2 and CO. As the fuel mixture became much richer ($\lambda<0.8$), however, a shift towards H_2 importance over CO was observed [89]. These observations provide a plausible explanation for the H_2 enhancement at the highest mixing ratios in [21] and [33]. As many older technology vehicles with less/un-regulated λ control would have been relevant in each of those studies, frequent acceleration events may have caused λ to drop below 0.8, which would have led to the enhanced H_2 over CO events that were observed in those studies. In contrast to those studies, the λ setting of the gasoline automobiles in this study never dropped below 0.8 at any point. As a result, the concave tendency of E_{H2} vs. E_{CO} in Fig. 25 is likely due to efficient catalytic CO removal and H_2 production through the water-gas shift reaction for E_{H2} and E_{CO} near the origin, which makes the slope of the curve there steeper. For E_{H2} larger than 20 mg km^{-1}, the relationship between E_{H2} and E_{CO} becomes much more linear.

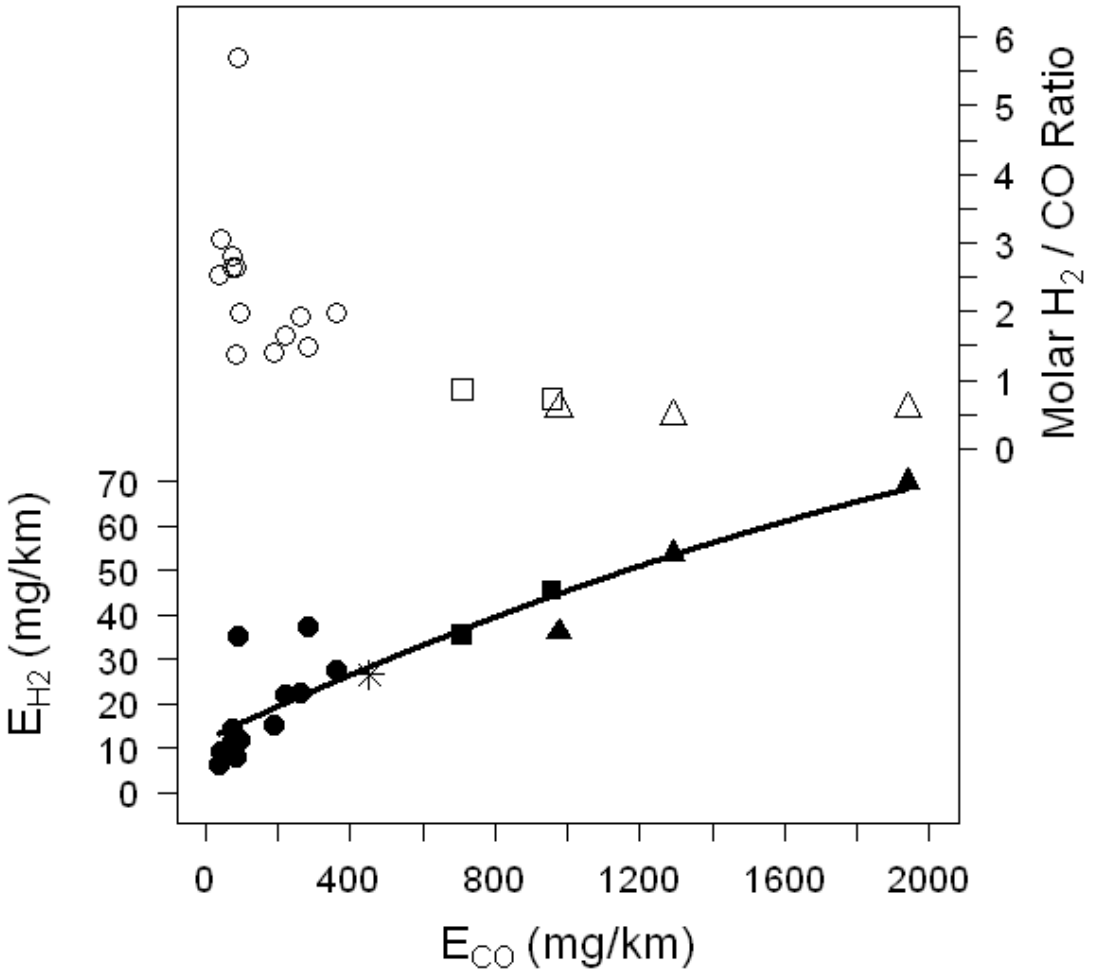

Figure 25. Scatterplot of mean E_{H2} vs. mean E_{CO} (filled points, left y-axis) for each sub-cycle of the gasoline automobiles with a polynomial fit of 2nd order. Open points correspond to mean molar H_2/CO ratios vs. E_{CO} of each sub-cycle (right y-axis). The star represents the mean overall E_{H2} and E_{CO} across all vehicles. Triangles represent sub-cycles subject to a cold-start. Squares represent highway-based sub-cycles (these two sub-cycles reach the highest speeds).

Mean molar sub-cycle values (ppm) of H_2 vs. CO are shown in Fig. 26. A steeper slope (1.45) near the origin is observed, indicating effective CO removal and H_2 production. Considering only CO values above 1000 ppm, however — representative of more frequent fuel-rich conditions — the slope becomes much more gradual (0.37). The slope of the dashed curve in Fig. 26 represents the slope corresponding to CO values above 1000 ppm. This slope is in agreement with that of pre-TWC measurements (0.39) through the experiment outlined in section 2.1.6, which are depicted by the triangles and dot-dashed curve in Fig. 26. Since H_2/CO ratios more representative of past studies based on traffic-influenced measurements occur

primarily with high emissions under fuel-rich conditions with newer technology vehicles, it suggests that past reported H_2/CO ratios from traffic-based measurements are largely the result of older technology vehicles (e.g. vehicles without a TWC), or vehicles with less developed exhaust after-treatment systems (e.g. Euro-1, Euro-2, Euro-3 vehicles). In the current study, molar H_2/CO ratios (Fig. 25) typically decrease as both E_{H2} and E_{CO} increase. Since H_2/CO ratios decrease as both E_{H2} and E_{CO} increase, it becomes apparent that emissions of CO generally dominate those of H_2 for vehicles subject to today's emissions standards and exhaust after-treatment systems, along with driving behaviour simulating real-world conditions. Through all of this, it becomes apparent that under current conditions, H_2/CO ratios for gasoline automobiles representative of those from current literature estimates become approached only under conditions representing the highest emission levels.

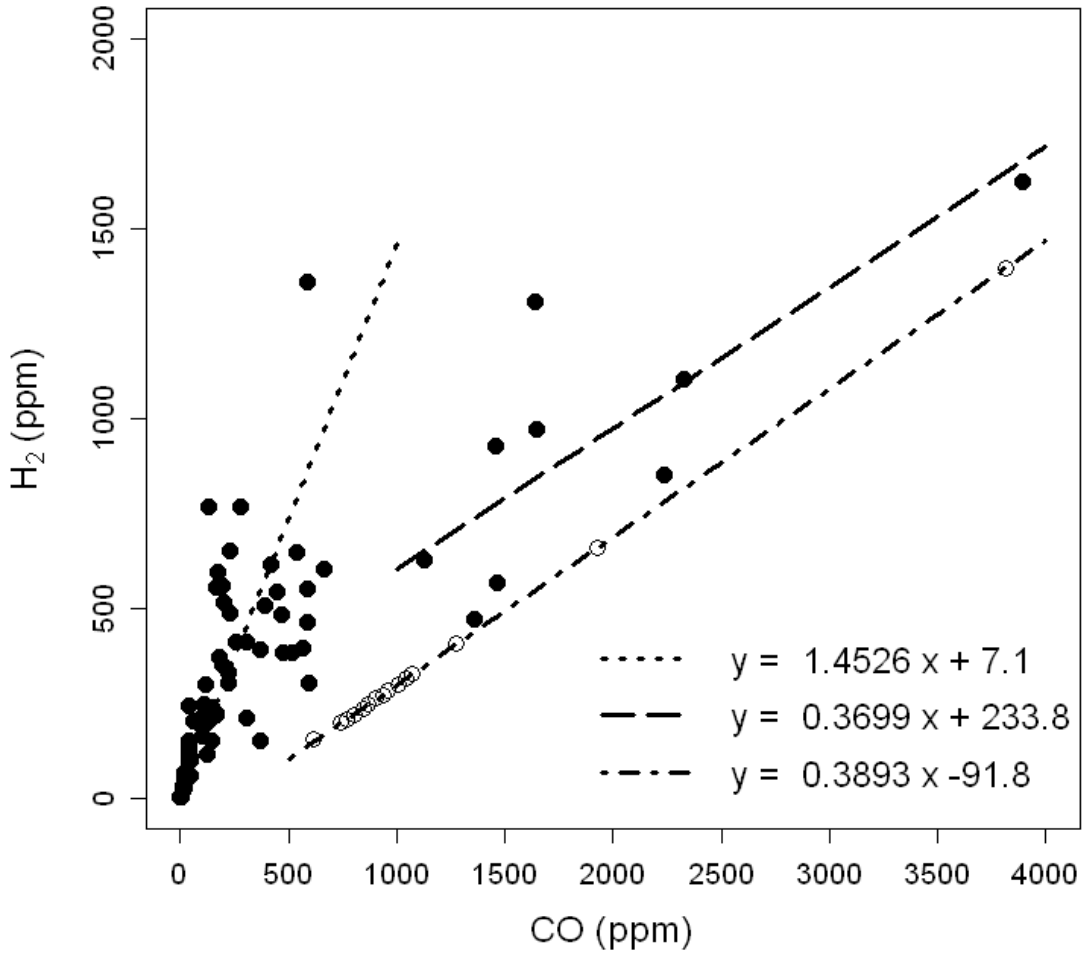

Figure 26. Scatterplot of mean mixing ratios (ppm) of H_2 vs. CO for each sub-cycle of each gasoline automobile (filled circles). The dotted curve represents the linear regression of H_2 vs. CO for CO values < 1000 ppm. The dashed curve represents the linear regression of H_2 vs. CO for CO values > 1000 ppm. The open circles represent H_2 vs. CO of pre-catalytic converter measurements, while the dot-dashed curve represents the slope of these measurements (note that the pre-TWC H_2 and CO mixing ratios have been scaled down by a factor of 10 to fit the points onto the diagram). The linear regressions are based on a function that fits in both the x and y directions.

The relationship of H_2/CO for the natural gas vehicles is not covered in detail in this study for a number of reasons. First, the relationship of H_2/CO has been applied in the past for gasoline-based vehicles in order to quantify emissions from traffic and upscale emissions for purposes of quantifying the source strength. Natural gas vehicles were virtually non-existent to be influential for such past measurements, and are thus irrelevant here for a cycle/sub-cycle comparison in this regard. Second, the relationship of H_2/CO in the exhaust gas of natural gas vehicles will never be applied for such purposes of quantifying and upscaling emissions from road-based transportation because natural gas vehicles will not penetrate the market sufficiently

to make such an analysis useful (see Table 18 for a list of modelled results of vehicle kilometres by technology for different time periods throughout the 21st century). Third, the reason for the applicability of H_2/CO ratios for quantifying emissions from gasoline-based vehicles is due to the much more well known and quantified CO emissions from such vehicles. Thus, CO emissions would have to first be well quantified from natural gas vehicles before this ratio would become relevant. Even then, the ratio would be used to quantify emissions from natural gas vehicles, and as can be seen in Table 18, natural gas vehicles will never become the predominant mode of transportation throughout the 21st century. Nevertheless, it is illustrative to provide an overall mean H_2/CO ratio from the natural gas automobiles to compare to the overall mean H_2/CO ratio of the gasoline automobiles. This ratio is 1.99. One reason for the significantly higher H_2/CO ratio than that of gasoline is in part due to the hydrogen-carbon ratio being approximately double that of gasoline. This result is supported by the overall mean H_2/CO ratio of 1.02 for the similar Euro-standard gasoline automobiles (Euro-4) in this study.

3.2.3.2 2-wheeled vehicles

H_2/CO ratios of the Euro-3 2-wheelers are presented in Table 16. The overall mean H_2/CO ratio for all 2-wheelers in this study was 0.59. The ratios from the 2-wheelers approached those that would be expected from older technology vehicles, particularly for urban-based sub-cycles involving a cold start, and highway-based sub-cycles subject to high engine speed and fuel-rich lambda settings. The mean engine ignition H_2/CO ratio for 2-wheelers in this study was 0.26. The same conditions leading to lower H_2/CO ratios for the automobiles also hold true for the 2-wheelers. However, with the 2-wheelers, mean H_2/CO ratios are even lower under similar conditions. Lambda control systems and TWCs have not yet been designed adequately for many 2-wheelers, as Euro-3 is the first generation with this technology (M. Weilenmann, Empa, pers. comm.). This results in higher emissions more representative of pre-TWC measurements, less efficient CO conversion, presumably less water-gas shift activity, and thus lower H_2/CO ratios. Essentially, conditions for 2-wheelers are closer to emissions without a TWC than are those for automobiles, meaning that H_2/CO ratios also follow suit.

Considering the above, it is therefore possible that in addition to lower future absolute mixing ratios of H_2, higher H_2/CO ratios from transportation may be expected, depending on the efforts invested in cleaning up 2-wheeler CO emissions, improving TWC technology for 2-wheelers, and barring any significant changes to the major atmospheric sink strengths and/or sources of H_2 and CO. It is important to realize that the major loss process of atmospheric H_2 is through oxidation within the upper soil layers. Thus, although higher H_2/CO ratios may result from direct exhaust gas emissions, overall atmospheric ratios will likely depend in large part on how soil oxidation processes react to these changes.

Table 15. H_2 emission factors of 4-wheeled vehicles and H_2/CO ratios of gasoline automobiles. Error ranges represent the standard deviation.

Cycle, Sub-cycle (Driving Conditions)	Duration (s)	Speed (km h^{-1})			E_{H2} (mg km^{-1})				E_{CO} (mg km^{-1})				H_2/CO Ratios[b] (ppm ppm^{-1})
		Min.	Max.	Mean	Gasoline Cars	Diesel Car	Diesel Delivery Vehicles	Natural Gas Cars	Gasoline Cars	Diesel Car	Diesel Delivery Vehicles	Natural Gas Cars	Gasoline Cars
IUFC15 (urban, urban, urban)[a]	**2835**	**0.0**	**44.0**	**19.0**	**39.9±23.0**	**0.4**	**0.31±0.36**	**59.4±38.3**	**855±474**	**26.5**	**82.9±66.2**	**460±369**	**0.87**
IUFC15, I (urban)[a]	945	0.0	44.0	19.0	69.8±38.4	1.1	0.89±1.04	76.9±31.2	1940±902	74.6	216±186	1010±906	0.59
IUFC15, II (urban)	945	0.0	44.0	19.0	27.3±14.8	0.0	0.03±0.04	47.8±41.0	361±437	2.6	20.5±28.4	181±134	1.99
IUFC15, III (urban)	945	0.0	44.0	19.0	22.5±16.3	0.0	0.00±0.01	53.6±50.3	260±229	2.2	12.3±13.2	193±137	1.94
L2 (urban, rural, highway)[a]	**2290**	**0.0**	**160.9**	**70.1**	**38.9±29.4**	–	**0.07±0.04**	**89.4±79.1**	**797±712**	–	**90.5±71.5**	**1320±1110**	**0.75**
L2, I (urban)[a]	780	0.0	50.0	18.7	35.9±8.0	–	0.74±0.45	76.8±76.6	977±543	–	949±769	683±432	0.58
L2, II (rural)	400	0.0	120.0	62.6	14.4±7.7	–	0.03±0.06	48.1±37.5	72.6±39.8	–	10.0±10.9	164±116	2.81
L2, III (highway)	1000	88.4	160.9	117.5	45.4±40.5	–	0.00±0.00	102±113	957±988	–	4.5±2.4	1700±1550	0.73
LA (rural, urban, urban)[a]	**1880**	**0.0**	**91.2**	**34.0**	**27.9±14.3**	**0.3**	**0.13±0.10**	**64.9±39.1**	**419±119**	**40.9**	**89.1±65.9**	**376±188**	**0.77**
LA, I (rural)[a]	505	0.0	91.2	41.2	53.7±19.5	0.9	0.37±0.29	92.9±61.2	1290±704	131.4	255±212	828±455	0.48
LA, II (urban)	870	0.0	55.1	25.7	9.4±11.7	0.2	0.00±0.00	54.4±56.3	45.1±60.1	1.9	4.4±0.8	156±95.7	3.05
LA, III (rural)	505	0.0	91.2	41.2	37.1±47.7	0.0	0.02±0.05	51.5±31.6	281±306	1.2	15.7±26.1	235±169	1.48
CADC (urban, rural, highway)	**3136**	**0.0**	**150.4**	**59.3**	**27.3±7.8**	**0.0**	**0.05±0.11**	**96.5±65.9**	**436±120**	**1.4**	**12.6±13.6**	**892±511**	**1.34**
CADC, I (urban)	920	0.0	57.7	17.5	11.1±12.9	0.0	0.50±1.00	53.6±50.3	72.5±72.5	2.6	69.8±127	195±125	2.65
CADC, II (rural)	980	0.0	111.5	60.4	21.9±17.4	0.0	0.03±0.07	58.8±30.8	219±226	1.2	9.4±11.6	303±73.9	1.65
CADC, III (highway)	735	42.9	150.4	120.4	35.4±12.3	0.0	0.00±0.00	140±112	710±209	1.2	6.3±3.3	1560±1080	0.87
Ra (highway, highway, rural)	**2655**	**0.0**	**131.1**	**93.2**	**14.2±6.7**	**0.0**	**0.00±0.00**	**89.7±93.4**	**146±49.1**	**0.9**	**3.1±1.2**	**727±795**	**1.61**
Ra, I (highway)	800	82.1	127.2	112.4	8.1±4.7	0.0	0.00±0.00	92.1±102	84.3±51.4	1.0	3.4±1.6	891±1050	1.37
Ra, II (highway)	805	66.4	131.1	97.4	15.3±5.0	0.0	0.00±0.00	98.9±103	191±37.4	0.8	2.9±1.2	840±908	1.40
Ra, III (rural)	805	46.3	105.9	73.5	11.5±4.4	0.0	0.00±0.00	65.5±57.0	92.8±23.4	0.7	2.4±0.6	300±251	1.98
Rb (rural, urban, urban)	**2580**	**0.0**	**79.2**	**30.9**	**11.0±10.6**	**0.0**	**0.02±0.01**	**40.9±21.2**	**63.7±58.0**	**1.4**	**8.9±9.4**	**151±83.0**	**3.18**
Rb, I (rural)	800	32.4	79.2	52.7	6.2±7.4	0.0	0.01±0.01	34.2±19.7	35.9±36.1	1.0	3.8±2.4	131±71.4	2.53
Rb, II (urban)	800	0.0	60.9	32.8	10.8±13.7	0.0	0.03±0.04	36.6±27.9	87.1±107	1.2	15.7±24.4	161±112	2.64
Rb, III (urban)	800	0.0	34.5	5.1	35.3±44.7	0.0	0.03±0.07	160±113	89.0±108	4.6	13.9±8.3	339±181	5.69
Overall Mean	**–**	**–**	**–**	**–**	**26.5±12.1**	**0.1**	**0.10±0.11**	**73.5±21.8**	**453±325**	**11.9**	**47.9±43.6**	**654±417**	**1.02**

[a]Subject to cold-start emissions

[b]These are cumulative ratios. For an individual cycle or sub-cycle, they are calculated by dividing the sums of all H_2 measurements by the sum of all CO measurements. The overall mean H_2/CO ratio is calculated analogously by using the sums of all individual H_2 and CO measurements.

Table 16. H_2 emission factors and H_2/CO ratios of 2-wheeled vehicles. Error ranges represent the standard deviation.

Cycle, Sub-cycle (Driving Conditions)	Duration (s)	Speed (km h^{-1}) Min.	Speed (km h^{-1}) Max.	Speed (km h^{-1}) Mean	E_{H2} (mg km^{-1})	E_{CO} (mg km^{-1})	H_2/CO Ratios[b] (ppm ppm^{-1})
LM (urban, rural)[a]	**1575**	**0.0**	**120.0**	**29.8**	**93.3±57.5**	**2900±2230**	**0.48**
LM, I (urban)[a]	1175	0.0	50.0	18.6	114±84.7	3640±2240	0.44
LM, II (rural)	400	0.0	120.0	62.6	58.7±35.9	1160±711	0.76
LM, III[c]	–	–	–	–	–	–	–
WMTC (urban, rural, highway)[a]	**1800**	**0.0**	**125.3**	**57.8**	**127±58.5**	**2580±1220**	**0.69**
WMTC, I (urban)[a]	600	0.0	60.0	24.4	172±94.5	4610±2280	0.52
WMTC, II (rural)	600	0.0	94.9	54.7	156±77.6	2340±1370	0.92
WMTC, III (highway)	600	0.0	125.3	94.4	91.7±58.9	1680±770	0.89
CC (urban, urban, urban)[a]	**1800**	**0.0**	**50.0**	**23.0**	**170±76.7**	**3650±2270**	**0.62**
CC, I (urban)[a]	600	0.0	50.0	23.0	197±93.0	5460±2620	0.49
CC, II (urban)	600	0.0	50.0	23.0	172±86.8	2950±2700	0.74
CC, III (urban)	600	0.0	50.0	23.0	142±77.0	2540±2110	0.73
CADC (urban, rural, highway)	**3136**	**0.0**	**150.4**	**59.3**	**175±104**	**4720±3300**	**0.57**
CADC, I (urban)	920	0.0	57.7	17.5	170±126	3350±2850	0.71
CADC, II (rural)	980	0.0	111.5	60.4	166±101	3840±4120	0.47
CADC, III (highway)[d]	735	42.9	150.4	120.4	153±119	5110±3310	0.45
Overall Mean	**–**	**–**	**–**	**–**	**141±38.6**	**3470±951**	**0.59**

[a]Subject to cold-start emissions

[b]These are cumulative ratios. For an individual cycle or sub-cycle, they are calculated by dividing the sums of all H_2 measurements by the sum of all CO measurements. The overall mean H_2/CO ratio is calculated analogously by using the sums of all individual H_2 and CO measurements.

[c]There is no sub-cycle III for the LM driving cycle

[d]Scooters do not conduct sub-cycle III

3.3 Summary

This part of the study has provided a state-of-the-art insight into the simultaneous characterization of direct H_2 emissions from current technology gasoline, diesel, and natural gas vehicles, along with detailed H_2 (and CO) emission factors and molar H_2/CO ratios based on variable driving conditions representative of real-world driving behaviour. H_2 emissions were found to be dependent on several interrelated factors, including the presence/absence of a TWC, vehicle and fuel type, the state of the engine, the quality of lambda control, and the engine and catalyst temperature at start-up. Measurements from a stationary engine provided specific results related to H_2 emissions from gasoline and natural gas under a variety of operating points and lambda settings, with measurements both pre- and post-catalytic converter. The results confirmed the oxidizing nature of TWCs (with respect to H_2), but also illustrated their limitations under fuel-rich conditions with high engine speed and exhaust throughput. An example with natural gas also illustrated the higher H_2 emissions vis-à-vis gasoline, which is in part due to both the conditions more conducive to water-gas shift activity with natural gas and the higher H:C ratio in the fuel.

Of the vehicles tested on a chassis dynamometer, diesel-powered vehicles consistently emitted very low, often undetectable levels of H_2. Gasoline- and natural gas-powered vehicles emitted significantly more H_2 than the diesel-powered vehicles, but the highest H_2 emissions were from 2-wheelers, approximately 5 times higher than from the gasoline automobiles and approximately twice as high as the natural gas vehicles. Emissions of H_2 and CO from 2-wheelers are not only significant, but have been shown to vastly outweigh those from gasoline-powered automobiles under urban driving conditions — an observation that is supported by the findings in [36]. This is significant because even though 2-wheelers are present in smaller absolute numbers and driven less frequently in many countries, their global numbers continue to increase and their emissions contribute significantly to the source term. This highlights the importance of H_2 emissions from 2-wheelers on a global scale, where such vehicles make up the majority of personal transportation vehicles in some countries. Emissions from 2-wheelers will not only continue to be an important factor for absolute H_2 emissions, but may also contribute significantly to future observed

H_2/CO ratios. The highest absolute emissions of H_2 and CO were attributed to cold-start and fuel-rich conditions, and contributed to the lowest overall H_2/CO ratios due to the proportionately higher CO emissions under such conditions. Thus, H_2/CO ratios of ~0.5 cited in previous studies are likely the result of: 1) cold-start emissions, 2) older vehicle technologies with less developed fuel management and exhaust after-treatment systems, 3) the influence of emissions from 2-wheelers with even currently insufficient exhaust after-treatment systems, and 4) all vehicles having been bound in the past by less stringent CO emissions targets.

4 SCENARIOS FOR CURRENT AND FUTURE GLOBAL ANTHROPOGENIC H_2 EMISSIONS FROM TECHNOLOGICAL PROCESSES

The most significant current anthropogenic sources of H_2 to the atmosphere from technological processes are the exhaust gas from road-based transportation and losses through fossil fuel-based industrial processes (e.g. petroleum refining). Future source strengths will depend on changing vehicle fleet compositions and H_2 production strategies for both industrial processes and direct energy-based end-uses (e.g. H_2-based transportation, industrial, commercial, residential heat and power). Global upscaling applies quantitative information (e.g. results from chassis dynamometer studies) with variable fleet compositions, vehicle emissions/emission standards, leakage and losses from non-transport-based sources, and different world regions. In this study, H_2 emissions are quantified globally for the time periods 2010, 2020, 2050, and 2100.

4.1 Individual vehicle H_2 emission factors and global upscaling of H_2 emissions from road-based transportation

In this section, E_{H2} from the vehicle technologies relevant to this study are applied to project global emission scenarios from road-based transportation. As the ongoing tightening of regulations requires the consistent reduction of emissions, systematic improvements of engines, TWCs, and engine controls have reduced the number and length of fuel-rich events, and hence emissions of CO and hydrocarbons. In parallel, H_2 emissions have also decreased for newer generations of cars (see section 3.2.1.1). Vehicle E_{H2} have been assigned to individual vehicle technology classes based on direct measurements and derived values (see section 2.1.4). Table 17 provides vehicle E_{H2} according to vehicle technology and world region applied in this study. Based on the global variability in vehicle fleet composition, emissions, and emission standards, individual E_{H2} have been assigned to specific world regions and time periods. The letters for each time period in Table 17 correspond to the E_{H2} for the vehicle technology class assumed to be representative of the vehicle fleet for the specified world region and time period. As similar vehicle technologies were assumed to have

the same E_{H2} irrespective of world region in 2050 and 2100, the same E_{H2} for each vehicle technology was applied to all world regions for those time periods.

An E_{H2} of ~43 mg km^{-1} has been reported for a cryogenic liquid H_2ICEV [80], but to my knowledge, published E_{H2} data for FCVs does not exist. Thus in this study, variable FCV E_{H2} are applied in order to establish scenarios for emissions from transportation when FCVs are anticipated to become more widespread (i.e. under the 450 ppm CO_2 climate policy scenario in 2050 and 2100). These scenarios include FCV E_{H2} that are assumed to be at the lower end of the expected range (e.g. no net FCV H_2 emissions and an E_{H2} of 26.5 mg km^{-1}, which is identical to the E_{H2} of conventional gasoline-based Euro-4 automobiles measured in this study) and higher-end estimations (e.g. an FCV E_{H2} that is expected to maintain total road-based H_2 emissions at similar levels to today and an FCV E_{H2} of 265 mg km^{-1}, which is a factor of 10 higher than the mean E_{H2} for the gasoline Euro-4 automobiles measured in this study). Other individual FCV E_{H2} have been applied in specific cases for reference. These FCV E_{H2} have not been entirely arbitrarily chosen; the selected higher E_{H2} (265 mg km^{-1}) is based on what is considered to be a high-end FCV E_{H2}, which is in accordance with my knowledge of emissions from prototype (non-road-ready) FCVs. A reduction in emissions of 50% for road-ready FCVs even by 2020 is conceivable (C. Bach, Empa, pers. comm.).

Table 17. H_2 emission factors for all vehicle technologies and world regions applied in this study. The letters for each time period represent the E_{H2} that was applied for each world region. Where 'all' has been written signifies that all world regions were subject to that particular E_{H2}. All E_{H2} are reported in mg km^{-1}. Letters for each time period refer to: (a) OECD North America, (b) OECD Europe, (c) OECD Pacific (Japan, Korea, Australia, New Zealand), (d) Former Soviet Union, (e) Eastern Europe, (f) China, (g) other Asia, (h) India, (i) Middle East, (j) Latin America, (k) Africa.

Vehicle Technology Class	**E_{H2}**	**2010**	**2020**	**2050**	**2100**
Gasoline automobiles					
1. pre-Euro-1	1130	i,k	–	–	–
2. Euro-1	283	d,e,f,g,h,j	–	–	–
3. Euro-2	108	–	i,k	–	–
4. Euro-3	59.4	a,b,c	d,e,f,g,h,j	–	–
5. Euro-4	26.5	–	–	–	–
6. post-Euro-4	26.5	–	a,b,c	all	all
Gasoline 2-wheelers					
1. based on E_{CO} of 20 g km^{-1}	793	d,e,f,g,h,i,j,k	–	–	–
2. based on E_{CO} of 15 g km^{-1}	595	a,b,c	–	–	–
3. based on E_{CO} of 7.5 g km^{-1}	297	–	d,e,f,g,h,i,j,k	–	–
4. based on E_{CO} of 6.575 g km^{-1}	261	–	b	–	–
5. based on E_{CO} of 6.467 g km^{-1}	256	–	a	–	–
6. based on E_{CO} of 4.628 g km^{-1}	184	–	c	–	–
7. Euro-3	141	–	–	–	–
8. post-Euro-3	26.5	–	–	all	all
Diesel vehicles					
assumed to be same as diesel Euro-4 vehicles (Table 15) based on oxidizing operating principle of diesel engines	0.1	all	all	all	all
Gasoline medium-sized trucks/mini-buses					
1. based on E_{CO} of 35 g km^{-1}	1390	d,e,f,g,h,i,j,k	–	–	–
2. based on E_{CO} of 15 g km^{-1}	595	–	d,e,f,g,h,i,j,k	–	–
3. based on E_{CO} of 7.5 g km^{-1}	297	a,b,c	–	–	–
4. based on E_{CO} of 5.625 g km^{-1}	223	–	a,b,c	–	–
5. post-Euro-4	26.5	–	–	all	all
Gasoline large buses					
1. estimated, based on E_{CO} of 46.7 g km^{-1}	1850	d,e,f,g,h,i,j,k		–	–
2. estimated, based on E_{CO} of 20 g km^{-1}	793	–	d,e,f,g,h,i,j,k	–	–
3. estimated, based on E_{CO} of 10 g km^{-1}	397	a,b,c		–	–
4. estimated, based on E_{CO} of 7.5 g km^{-1}	297	–	a,b,c	–	–
5. post-Euro-4	26.5	–	–	all	all
Natural gas vehicles	73.5	a,b,c	a,b,c	all	all
Biofuels vehicles	13.3	a,b,c	a,b,c	all	all
Gasoline hybrid electric vehicles	23.1	a,b,c	a,b,c	all	all
Natural gas hybrid vehicles	58.8	a,b,c	a,b,c	all	all
Biofuels hybrid vehicles	10.6	a,b,c	a,b,c	all	all
Plug-in hybrid vehicles	14.8	a,b,c	a,b,c	all	all
H_2 hybrid vehicles	33.1	–	a,b,c	all	all
H_2 fuel cell vehicles	vary	–	–	all	all

Results for global vehicle kilometres travelled by technology for both the baseline and 450 ppm CO_2 climate policy scenarios are provided in Table 18. Model results from the GMM are based on the work of T. Gül (see [5]). Figures in Table 18 are not intended to characterize all road-based kilometres travelled, but rather those that are anticipated to influence global emissions of H_2 (e.g. heavy-duty diesel vehicles have been excluded as outlined in section 2.1.4). LDV kilometres travelled are based on results from the GMM; results for the other categories are from the SMP [34]. Note that vehicle kilometres travelled by 2-wheelers, medium-sized trucks, large buses, and mini-buses are assumed to be identical for both the baseline and 450 ppm CO_2 climate policy scenarios within each time period, as unlike the personal transportation options associated with LDVs, alternatives to such technologies are not envisaged, irrespective of climate policy.

In 2010, LDVs comprise ~70% of global road-based kilometres travelled, with conventional gasoline and diesel vehicles accounting for the most significant share of LDV kilometres. 2-wheelers account for ~20% of total kilometres travelled, while medium-sized trucks, large buses, and mini-buses combine for ~10% of the total.

In 2020, the same general breakdown of global kilometres travelled is observed. However, the shift towards emerging technologies such as natural gas ICEVs, biofuels ICEVs, and hybrid technologies within the LDV category becomes more pronounced compared with baseline 2010 conditions, particularly under the 450 ppm CO_2 climate policy scenario. 2-wheelers, medium-sized trucks, large buses, and mini-buses account for 22%, 6%, 2%, and 2% of total kilometres, under both scenarios, respectively.

In 2050 under the baseline scenario, conventional gasoline and diesel vehicles still make up the largest fraction of global kilometres travelled by any single technology (44% of total LDV kilometres). Other ICEV technologies, such as natural gas and biofuels, have become more widespread, accounting for 22% and 16% of LDV kilometres, respectively. HEVs have also become more widespread and account for 13% of total LDV kilometres. Under the 450 ppm CO_2 climate policy scenario, 2-wheelers account for the largest share of global kilometres driven of any single technology. LDV kilometres are very much balanced between conventional gasoline and diesel vehicles, and other technologies such as natural gas ICEVs, biofuels

ICEVs, and many hybrid technologies. H_2 hybrids and plug-in hybrids also begin to account for a larger share of total kilometres. FCVs account for ~8% of total LDV kilometres travelled in 2050. 2-wheelers, medium-sized trucks, large buses, and mini-buses account for 22%, 7%, 1%, and 1% of total kilometres, under both scenarios, respectively.

In 2100 under the baseline scenario, the shift away from conventional gasoline and diesel LDVs is marked, with HEVs (34%) and biofuels hybrids (38%) accounting for the most significant fractions of LDV kilometres travelled. Conventional gasoline and diesel LDVs account for only 10% of global LDV kilometres travelled. The 450 ppm CO_2 climate policy scenario is characterized primarily by a significant increase in FCV kilometres. FCVs account for ~78% of global LDV kilometres travelled in 2100. Global 2-wheeler kilometres comprise ~26% of total kilometres travelled, primarily from vehicles in Asia, India, and Latin America. 2-wheelers, medium-sized trucks, large buses, and mini-buses account for 26%, 11%, 1%, and 1% of total kilometres, under both scenarios, respectively.

Table 18. Global vehicle kilometres travelled (in 10^9 km) according to vehicle technology based on model results from the GMM [5] and SMP [34].

Vehicle technology	**2010**	**2020**		**2050**		**2100**	
	Baseline	Baseline	450 ppm	Baseline	450 ppm	Baseline	450 ppm
LDVs							
Oil products and synfuels ICEV	*10060*	*11350*	*10790*	*11300*	*3980*	*3450*	*520*
Natural gas ICEV	*720*	*1870*	*1870*	*5620*	*3690*	*1350*	*840*
Biofuels ICEV	*190*	*450*	*550*	*4080*	*3280*	*3860*	*750*
Oil products and synfuels hybrids	*90*	*260*	*400*	*3400*	*3750*	*11870*	*1230*
Natural gas hybrids	*0*	*100*	*150*	*500*	*3900*	*1210*	*2270*
Biofuels hybrids	*0*	*20*	*150*	*580*	*3540*	*13350*	*1670*
H_2 hybrids	*0*	*0*	*20*	*20*	*370*	*0*	*80*
Plug-in hybrids	*0*	*0*	*70*	*20*	*870*	*0*	*200*
H_2 fuel cell	*0*	*0*	*60*	*0*	*2120*	*0*	*27530*
Total LDVs	**11060**	**14050**	**14060**	**25520**	**25500**	**35090**	**35090**
2-wheelers	**3053.2**	**4396.5**	**4396.5**	**8167.7**	**8167.7**	**14779**	**14779**
Medium-sized trucks	**968.4**	**1311.0**	**1311.0**	**2672.5**	**2672.5**	**6210.8**	**6210.8**
Large buses	**307.7**	**317.2**	**317.2**	**347.9**	**347.9**	**406.0**	**406.0**
Mini-buses	**302.9**	**320.3**	**320.3**	**379.1**	**379.1**	**498.7**	**498.7**
TOTAL	**15692**	**20395**	**20405**	**37087**	**37067**	**56985**	**56985**

Table 19 provides the results of global projections of H_2 emissions (in Tg a^{-1}) from road-based transportation. Results are based on the E_{H2} from Table 17 and global kilometres travelled from Table 18 (for vehicle kilometres travelled according to individual world regions, please refer to [34]). Current (2010) conditions represent H_2 emissions based on global kilometres travelled and vehicle fleet composition according to the baseline scenario (i.e. no effective climate policy implementation) since it is assumed that measures that have been pursued to date are insignificant on a global scale to abate climate change. For 2020, 2050, and 2100, results have been applied for both the baseline scenario and the 450 ppm CO_2 climate policy scenario. However, for these time periods, the focus of the discussion is based on the results from the 450 ppm CO_2 climate policy scenario. Given their marginal contribution to global kilometres in 2020, specific scenarios for H_2 emissions from FCVs in 2020 are not applied (e.g. an FCV E_{H2} of 265 mg km^{-1} in 2020 would add an additional 0.01 Tg H_2 to the total). In 2050 and 2100, the cells for FCV emissions, and hence also the cells for total LDV and total emissions, have been split. The left-hand cell corresponds to H_2 emissions based on an FCV E_{H2} of 26.5 mg km^{-1}, whereas the right-hand cell corresponds to H_2 emissions based on an FCV E_{H2} of 265 mg km^{-1}.

Table 19. Globally projected H_2 emissions (in Tg a^{-1}) from road-based transportation. The split cells for FCVs under the 450 ppm CO_2 climate policy scenario in 2050 and 2100 corresponds to FCV E_{H2} of 26.5 mg km^{-1} (left) and 265 mg km^{-1} (right).

Vehicle Technology	**2010**	**2020**		**2050**		**2100**	
	Baseline	Baseline	450 ppm	Baseline	450 ppm	Baseline	450 ppm
LDVs							
Oil products & synfuels ICEV	*1.242*	*0.419*	*0.411*	*0.240*	*0.084*	*0.073*	*0.011*
Natural gas ICEV	*0.042*	*0.098*	*0.098*	*0.413*	*0.271*	*0.099*	*0.062*
Biofuels ICEV	*0.002*	*0.004*	*0.005*	*0.043*	*0.044*	*0.041*	*0.010*
Oil products & synfuels hybrids	*0.002*	*0.004*	*0.007*	*0.079*	*0.087*	*0.275*	*0.028*
Natural gas hybrids	*0*	*0.004*	*0.006*	*0.029*	*0.229*	*0.071*	*0.134*
Biofuels hybrids	*0*	*0.0002*	*0.001*	*0.006*	*0.038*	*0.142*	*0.018*
H_2 hybrids	*0*	*0*	*0.0005*	*0.0007*	*0.012*	*0*	*0.003*
Plug-in hybrids	*0*	*0*	*0.0007*	*0.0003*	*0.013*	*0*	*0.003*
H_2 fuel cell	*0*	*0*	*0*[a]	*0*	*0.056*[b] *0.562*[c]	*0*	*0.730*[b] *7.295*[c]
Total LDVs	**1.288**	**0.529**	**0.529**	**0.811**	**0.834**[b] **1.340**[c]	**0.701**	**0.998**[b] **7.564**[c]
2-wheelers	**2.383**	**1.297**	**1.297**	**0.216**	**0.216**	**0.392**	**0.392**
Medium-sized trucks	**0.476**	**0.333**	**0.333**	**0.043**	**0.043**	**0.099**	**0.099**
Large buses	**0.082**	**0.040**	**0.040**	**0.002**	**0.002**	**0.003**	**0.003**
Mini-buses	**0.277**	**0.127**	**0.127**	**0.006**	**0.006**	**0.008**	**0.008**
TOTAL	**4.506**	**2.326**	**2.326**	**1.078**	**1.102**[b] **1.607**[c]	**1.203**	**1.499**[b] **8.065**[c]

[a] Scenarios for FCV emissions not applied in 2020
[b] FCV E_{H2} of 26.5 mg km^{-1}
[c] FCV E_{H2} of 265 mg km^{-1}

In 2010, global H_2 emissions from transportation are estimated at 4.5 Tg, which is at the lower end of the estimated range of 5–20 Tg a^{-1} from [18] and 9±3 Tg a^{-1} from [16], but in line with global 2004 emissions based on travel distance (5.4±3.2 Tg) and the molar relationship of H_2 to CO (8.1±4.9 Tg) by [33]. This lower estimation is attributed primarily to systematically improving exhaust after-treatment systems, despite annually increasing global vehicle kilometres travelled. Emissions are currently dominated by LDVs (~28.6%) and 2-wheelers (~52.9%), with medium-sized trucks, large buses, and mini-buses combining for ~18.5% of global emissions. Gasoline ICEVs account for ~27.5% of global H_2 emissions. Of the total LDV emissions, conventional gasoline vehicles account for ~96.4%, natural gas ICEVs ~3.3%, biofuels ~0.2%, and HEVs ~0.1% of emissions. Diesel ICEVs account for ~0.02% of LDV emissions. Figure 27 depicts the H_2 emissions from each of the contributing vehicle technologies in 2010.

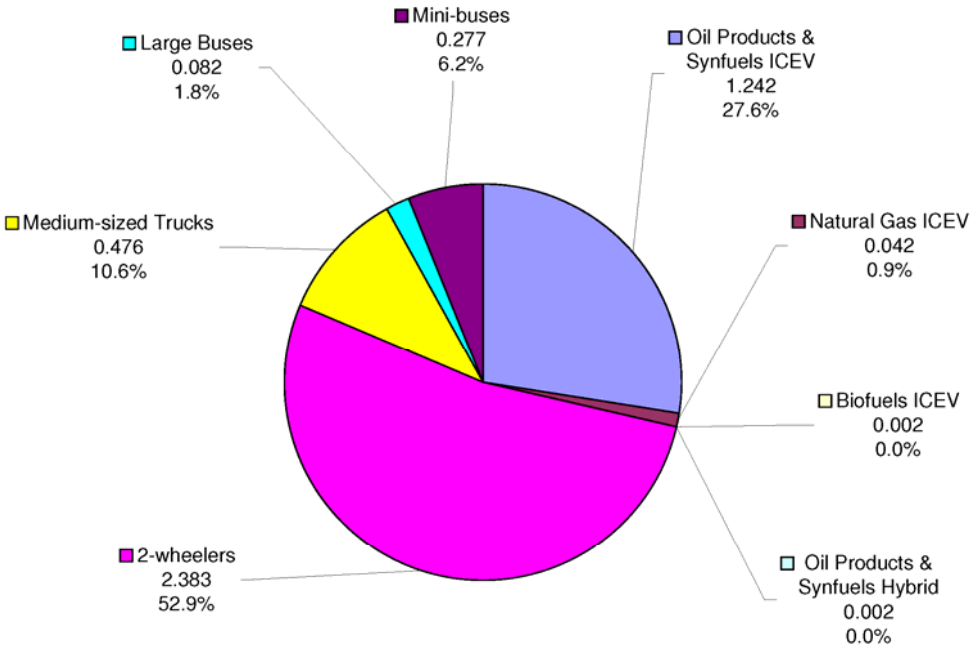

Figure 27. H_2 emissions from each vehicle technology in 2010 separated by absolute emissions (in Tg) and percentage of total emissions.

Figure 28 separates the vehicle technologies further into emissions by world region for each technology in 2010. 2-wheeler emissions are most prominent in China, other parts of Asia, and India. In fact, 2-wheeler emissions in China and other parts of Asia alone exceed global H_2 emissions from gasoline-powered light-duty ICEVs. Emissions from gasoline-powered light-duty ICEVs are more evenly distributed by world region than are those from 2-wheelers. North America is responsible for the largest share of emissions due to the sheer number of vehicle kilometres driven in that region. Emissions in Africa make up the second largest fraction, despite global kilometres travelled in that region being almost 25 times less than in North America.

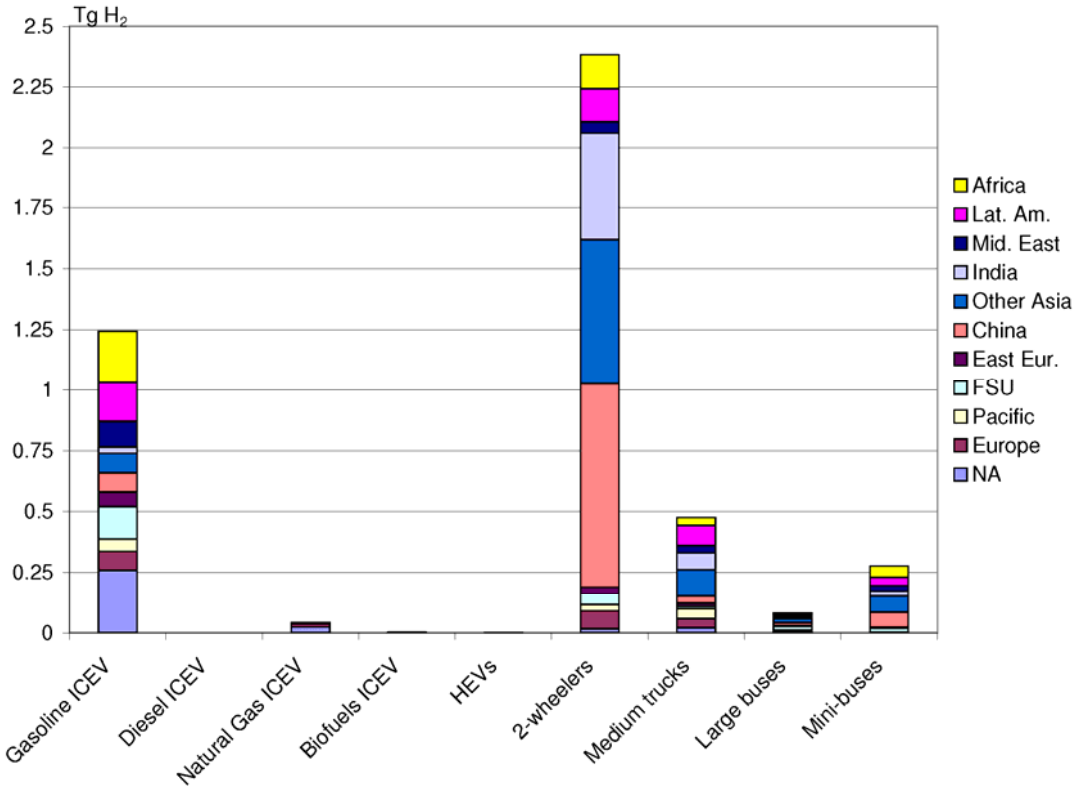

Figure 28. H_2 emissions from each vehicle technology in 2010 separated by the absolute contribution (in Tg) from each world region.

Global emissions projections for 2020 result in 2.3 Tg of H_2 from road-based transportation under both scenarios due to very similar vehicle fleet compositions. These projections are approximately half (51%) of that projected for 2010 (4.5 Tg), primarily due to tightening emission standards and corresponding improvements in exhaust after-treatment systems, despite the greater number of global vehicle kilometres travelled. The rate of decrease from 2010–2020 for global H_2 emissions from road-based transportation (~6.5% a^{-1}) is broadly in line with that projected by

Vollmer et al. [33] for the period 2004–2015 based on the measured H_2/CO ratio (7.3% a^{-1}). The 2-wheeler share increases slightly to approximately 56% of this total. Although H_2 emissions from 2-wheelers are expected to decrease by 2020 (~5.9% a^{-1}), the rate at which emissions actually decrease is less than that for conventional gasoline LDVs (~10.5% a^{-1}), presumably because the development of exhaust after-treatment systems and fuel management systems has failed to maintain pace with that of conventional automobiles. Two-wheelers aside, LDVs account for ~23% of total emissions, while medium-sized trucks, large buses, and mini-buses combine for ~22% of total H_2 emissions. Conventional gasoline ICEVs account for ~18% of total emissions, while natural gas ICEVs account for ~4% of total emissions. Of the LDV emissions, conventional gasoline ICEVs account for ~80% and natural gas ICEVs account for ~18% of emissions. All other technologies contribute marginally to both LDV and total H_2 emissions. Figure 29 depicts the H_2 emissions from each of the contributing vehicle technologies in 2020.

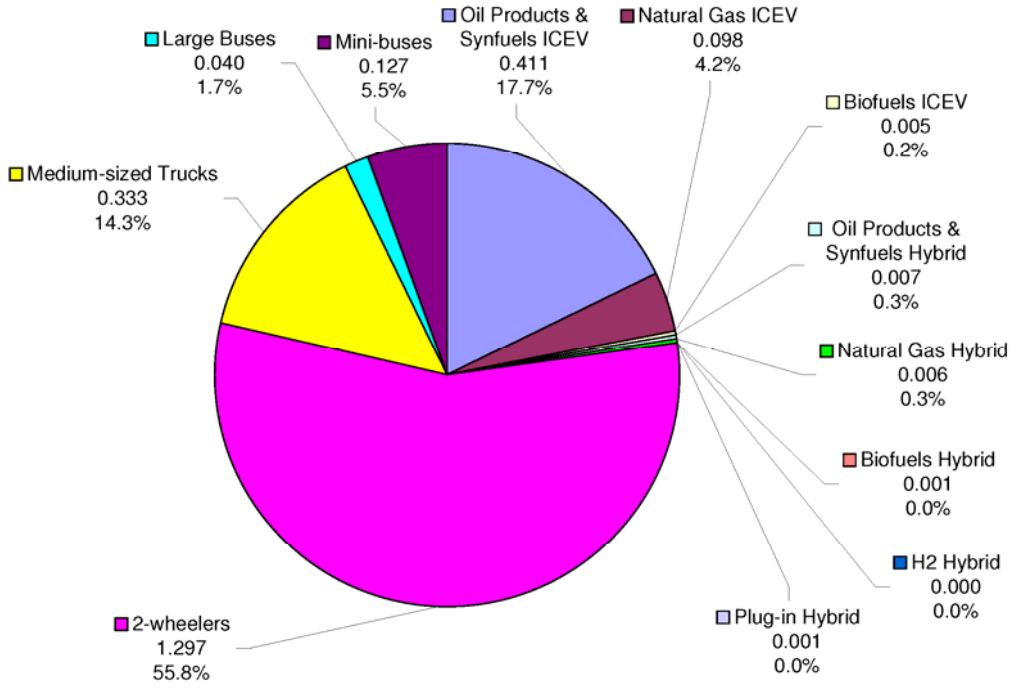

Figure 29. H_2 emissions from each vehicle technology in 2020 separated by absolute emissions (in Tg) and percentage of total emissions under the 450 ppm CO_2 climate policy scenario.

Figure 30 depicts the fraction of emissions attributed to each vehicle technology according to world region for the 450 ppm CO_2 climate policy scenario (note the difference in scale compared with 2010 (Fig. 28)). In 2020, emissions from 2-wheelers are still dominant in the Asian region of the world, particularly again in China where the largest rate of increase in 2-wheeler kilometres has been observed. Similarly, in other parts of Asia and India, large increases in the number of 2-wheeler kilometres has led to comparatively high total emissions in those regions, despite improvements in exhaust after-treatment technologies. Although global H_2 emissions from gasoline-powered light-duty ICEVs have decreased significantly, emissions are still highest in North America, as the large number of vehicle kilometres travelled — coupled with the improvements in exhaust after-treatment systems in other parts of the world — have more than offset the low mean E_{H2} for this gasoline light-duty ICEVs in North America.

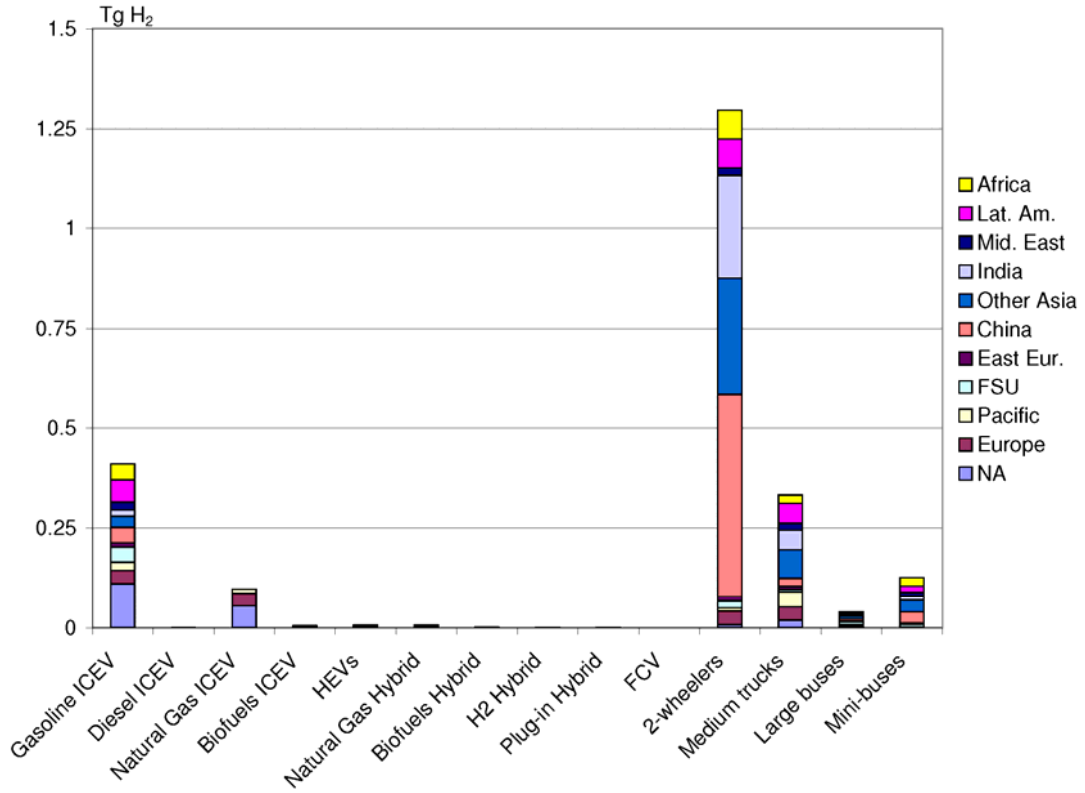

Figure 30. H_2 emissions from each vehicle technology in 2020 under the 450 ppm CO_2 climate policy scenario, separated by the absolute contribution (in Tg) from each world region.

In 2050, a number of quantitative scenarios are applied using various FCV E_{H2}, which enables a range of H_2 emissions from transportation to be evaluated. FCVs account for 8.3% of the global LDV vehicle kilometres under the 450 ppm climate policy scenario; FCVs do not penetrate the global vehicle fleet at all under the baseline scenario. In a first example, two criteria for FCV emissions were selected when assessing emissions from transportation in 2050: (1) no net H_2 emissions from FCVs and (2) FCV E_{H2} that would maintain overall H_2 emissions from transportation within the realm of current and near-term (2020) estimates. The reason for the selection of these FCV E_{H2} is: (1) to illustrate overall road-based transport emissions based on optimal fuel cell efficiency and complete recycling of purged H_2, for example through the development of catalytic burners within the fuel cell systems, and (2) to illustrate upper-end boundaries using current emissions as an acceptable guide, as it is currently unknown to what extent an increasing anthropogenic H_2 source would be balanced by increasing removal of atmospheric H_2 through soil oxidation, for example.

Assuming no net H_2 emissions from FCVs, baseline conditions result in 1.08 Tg H_2 emitted from transportation in 2050, while 450 ppm CO_2 climate policy scenario conditions result in 1.05 Tg H_2. Reasons for the perpetual decrease in H_2 emissions to the mid-point of the century are again emissions regulations stringency and improvements in exhaust after-treatment systems, particularly also now in the world's less developed regions, where a previous vehicle technology time lag existed, and where the highest emissions are typically found in the near-term. By 2050, the shift from conventional gasoline vehicles to emerging technologies such as biofuels and hybrid vehicles is marked, and this development plays an important role in the decrease in global H_2 emissions. The introduction of the Euro-4 and Euro-5 emission standards for 2-wheelers in the coming decade should reduce 2-wheeler emissions significantly, conceivably to levels of current technology automobiles [74]. This is a primary reason why H_2 emissions are expected to decrease considerably throughout the 21st century, particularly considering the perpetual increase in global 2-wheeler kilometres travelled. Also, depending on the extent of the future electrification of 2-wheelers, H_2 emissions from this group of vehicles could be reduced even further.

Although FCVs contribute less than 10% of global vehicle kilometres in 2050, it is illustrative to consider how emissions from FCVs may relate to current and near-term

emissions scenarios. Based on global vehicle kilometres under the 450 ppm CO_2 climate policy scenario and vehicle E_{H2} projected for 2050, it was estimated that a range of E_{H2} for FCVs of 600–1625 mg km^{-1} would result in similar global H_2 emissions from transportation to conditions for 2010–2020 (2.3–4.5 Tg). In other words, barring a major breakdown in the development of fuel cell efficiency during the first half of the century, emissions from transportation in 2050 are expected to remain well below those currently observed. To put this last statement into a quantitative perspective, an FCV E_{H2} of ~16 mg km^{-1} under the 450 ppm CO_2 climate policy scenario in 2050 would result in similar levels of H_2 from transportation that is estimated under the baseline scenario (~1.08 Tg).

In a second scenario, a range of FCV E_{H2} (26.5 mg km^{-1} and 265 mg km^{-1}) based on a low- and high-end FCV E_{H2} is evaluated for the 450 ppm CO_2 climate policy scenario in 2050. When an FCV E_{H2} of 26.5 mg km^{-1} is applied, H_2 emissions from transportation are estimated at 1.1 Tg, a factor of 4 lower than current H_2 emissions (4.5 Tg). Two-wheelers account for ~20% of emissions, but are only 9% of 2-wheeler emissions in 2010 on an absolute basis. This reduction in 2-wheeler emissions is due to the implementation of more stringent emission standards for 2-wheelers, which will lead to their development and resultant emissions conceivably as low as today's gasoline-powered automobiles [74]. The group of medium-sized trucks, large buses, and mini-buses comprise ~5% of total emissions. In this scenario, LDVs make up ~76% of global H_2 emissions from transportation. The natural gas ICEVs and natural gas hybrids account for ~45% of the total, while conventional ICEVs (primarily gasoline) account for ~8%, biofuels ICEVs ~4%, HEVs ~8%, and biofuels hybrids ~3%. FCVs would account for ~5% of global H_2 emissions from transportation with an FCV E_{H2} of 26.5 mg km^{-1}. Considering a second scenario with a mean FCV E_{H2} an order of magnitude higher at 265 mg km^{-1}, H_2 emissions from transportation would be ~1.6 Tg. This value is ~0.5 Tg higher than expected emissions with an FCV E_{H2} of 26.5 mg km^{-1}, but still a factor of ~2.8 lower than 2010 levels. Under this scenario, FCVs would account for ~42% of LDV emissions and ~35% of total emissions from road-based transportation. Figure 31 depicts H_2 emissions from each of the contributing vehicle technologies in 2050 under the 450 ppm CO_2 climate policy scenario with an FCV E_{H2} of 26.5 mg km^{-1} (panel A) and 265 mg km^{-1} (panel B), respectively.

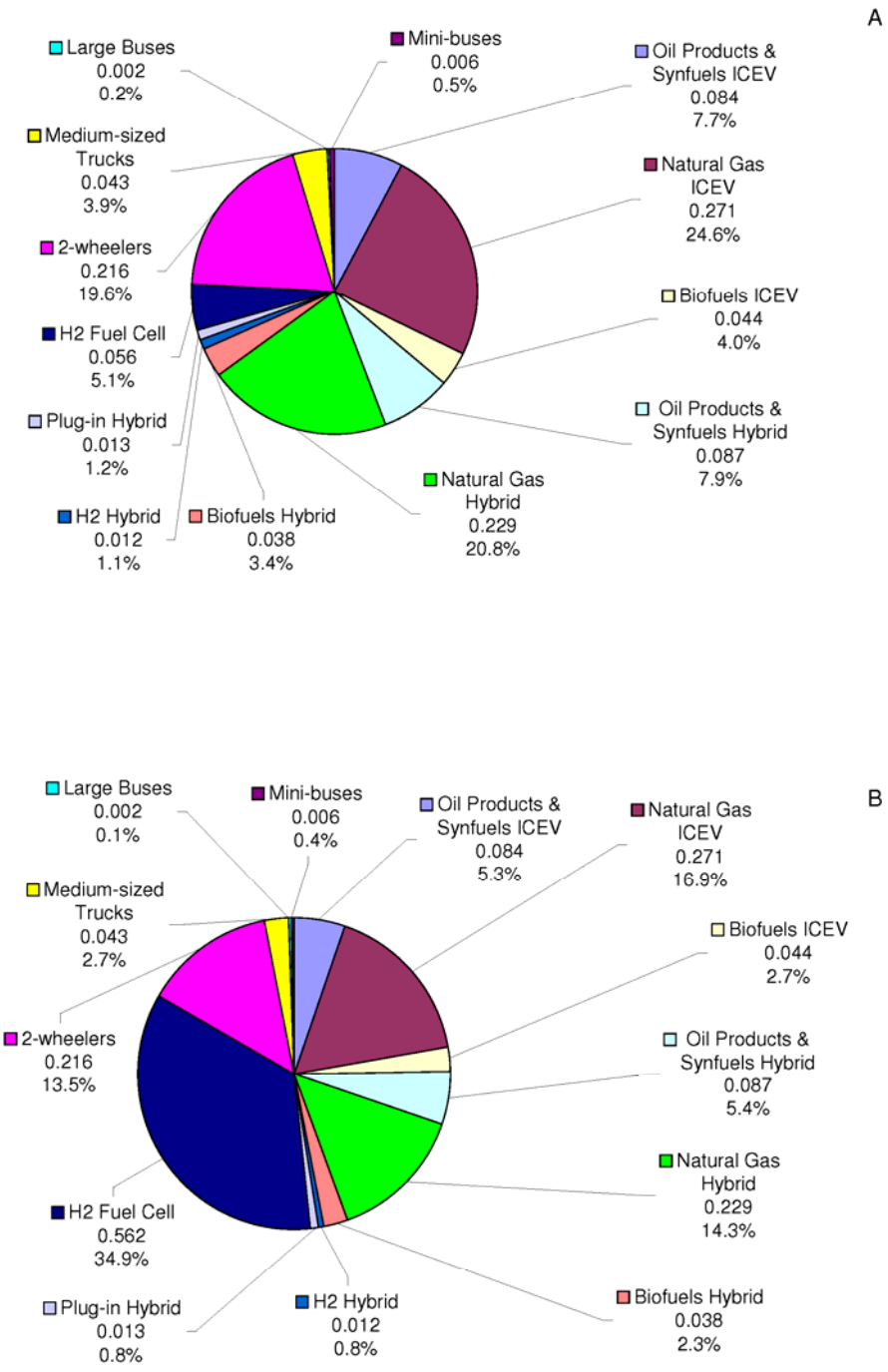

Figure 31. H_2 emissions from each vehicle technology in 2050 separated by absolute emissions (in Tg) and percentage of total emissions under the 450 ppm CO_2 climate policy scenario. Emissions scenarios are based on an FCV E_{H2} of 26.5 mg km^{-1} (panel A) and an FCV E_{H2} of 265 mg km^{-1} (panel B).

By 2100, FCVs are expected to make up ~80% of global LDV vehicle kilometres travelled under the 450 ppm CO_2 climate policy scenario; FCVs are again not expected to penetrate the global vehicle fleet under the baseline scenario. Similarly to 2050, a number of quantitative scenarios using various FCV E_{H2} are applied in 2100 under the 450 ppm CO_2 climate policy scenario. In the first instance (similarly to 2050), FCV E_{H2} were selected such that: (1) no net H_2 emissions from FCVs result, and (2) overall H_2 emissions from transportation within the realm of current (2010) and near-term (2020) estimates.

Discounting emissions from FCVs again for now, H_2 emissions from transportation under the baseline scenario are estimated at ~1.20 Tg and those under the 450 ppm CO_2 climate policy scenario at ~0.77 Tg. Two-wheelers still represent approximately 33% of total emissions in 2100 under baseline conditions, but only ~16% of 2-wheeler emissions from 2010 in absolute terms. An E_{H2} range of 55–135 mg km^{-1} from FCVs is estimated to result in H_2 emissions from transportation remaining within the realm of current (2010) and near-term (2020) global H_2 emissions from transportation (2.3–4.5 Tg). It is clear that the E_{H2} for FCVs would have to be significantly lower in 2100 than in 2050 due to the sheer number of vehicle kilometres driven by FCVs. In 2050 (under the 450 ppm CO_2 climate policy scenario), FCVs will travel approximately 2.1 trillion kilometres globally, while in 2100, FCVs will travel approximately 27.5 trillion kilometres.

In a second scenario under the 450 ppm CO_2 climate policy scenario, FCV E_{H2} of 26.5 mg km^{-1} and 265 mg km^{-1} are applied. With an E_{H2} of 26.5 mg km^{-1} in 2100, H_2 emissions to the atmosphere would be on the order of 1.5 Tg. FCVs would account for ~50% of H_2 emissions from all road-based transportation combined. In the second scenario with a mean FCV E_{H2} of 265 mg km^{-1}, H_2 emissions from transportation would be ~8.1 Tg, a factor of ~5.4 higher than emissions in 2100 with an FCV E_{H2} of 26.5 mg km^{-1} (1.5 Tg). FCVs would account for ~90% of H_2 emissions from all transportation combined. Figure 32 depicts H_2 emissions from each of the contributing vehicle technologies in 2100 under the 450 ppm CO_2 climate policy scenario with an FCV E_{H2} of 26.5 mg km^{-1} (panel A) and 265 mg km^{-1} (panel B), respectively.

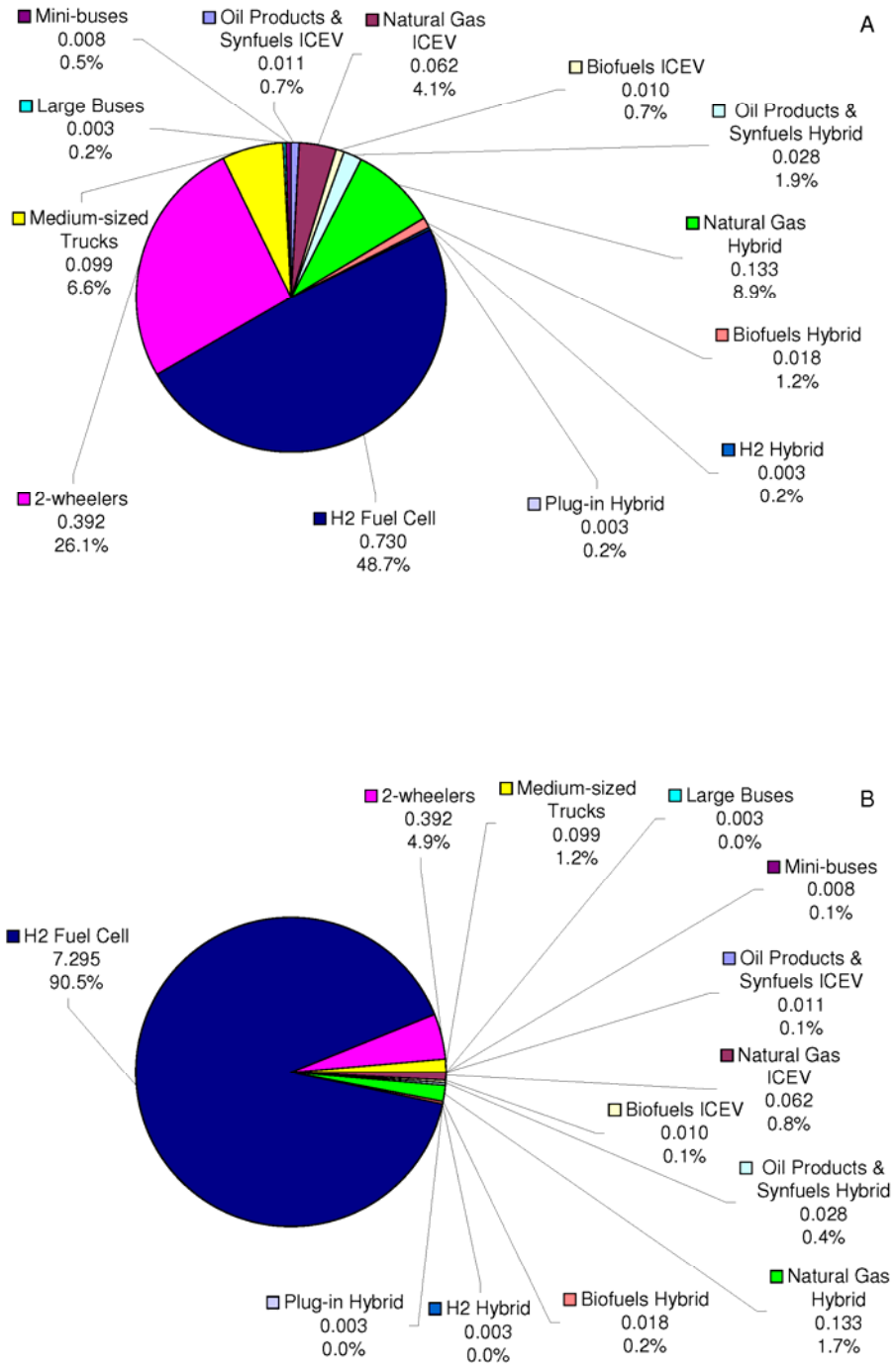

Figure 32. H_2 emissions from each vehicle technology in 2100 separated by absolute emissions (in Tg) and percentage of total emissions under the 450 ppm CO_2 climate policy scenario. Emissions scenarios are based on an FCV E_{H2} of 26.5 mg km^{-1} (panel A) and an FCV E_{H2} of 265 mg km^{-1} (panel B).

As a third independent criterion in 2100, a small set of FCV E_{H2} was selected to provide a quantitative picture of overall transport-based H_2 emissions based on various mean FCV E_{H2}. Hypothetical FCV E_{H2} of 200 mg km^{-1} and 70 mg km^{-1} would result in total H_2 emissions from road-based transportation of approximately 6.3 and 2.7 Tg, respectively — values 1.4 and 0.6 times 2010 levels, respectively.

Figure 33 displays road-based H_2 emissions for various scenarios throughout the 21st century. In the first column, current (2010) baseline conditions are portrayed and in the second column, 2020 conditions under the 450 ppm CO_2 climate policy scenario are depicted. The remaining columns for 2050 and 2100 conditions are based on the 450 ppm CO_2 climate policy scenario. In the columns depicting 2050 conditions, the first column (a) represents overall H_2 emissions based on an FCV E_{H2} of 265 mg km^{-1}, while the second column (b) represents total road-based emissions based on an FCV E_{H2} of 26.5 mg km^{-1}. Total emissions in 2050 would remain well below 2010 and 2020 conditions with both the low and high FCV E_{H2}. The final 6 columns (2100a–f) represent total road-based H_2 emissions based on a series of sequentially decreasing FCV E_{H2} (FCV E_{H2} of 265 mg km^{-1} (a), 200 mg km^{-1} (b), 135 mg km^{-1} (c), 70 mg km^{-1} (d), 26.5 mg km^{-1} (e), and 0 mg km^{-1} (f)). In 2100 with an FCV E_{H2} of 265 mg km^{-1}, road-based emissions would be higher than in 2010 and 2020 by factors of ~1.8 and 3.5, respectively. As can be seen through a comparison with emissions in 2010, an FCV E_{H2} of ~135 mg km^{-1} in 2100 is predicted to maintain total transportation-based H_2 emissions similar to current levels. With an FCV E_{H2} of 26.5 mg km^{-1}, H_2 emissions would be approximately one third and two thirds of those in 2010 and 2020, respectively.

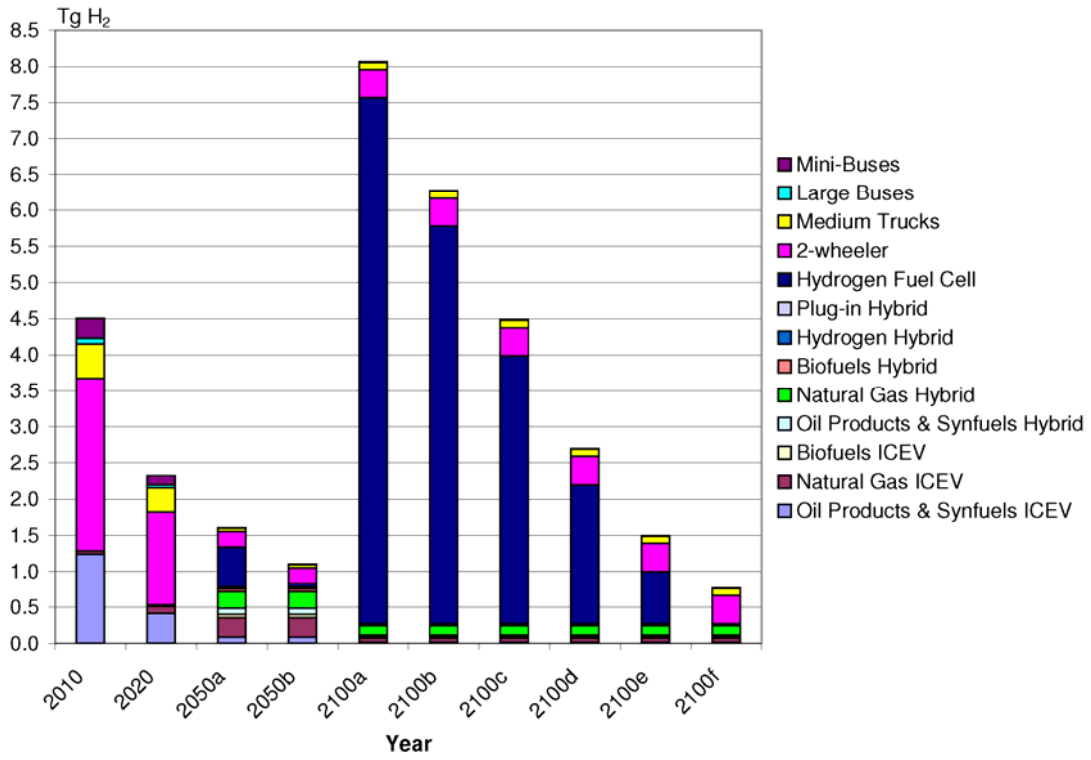

Figure 33. Global road-based H_2 emissions for 2010 (baseline) and 2020 (450 ppm CO_2 climate policy scenario), along with scenarios for 2050 and 2100 based on various FCV E_{H2}. In 2050, overall H_2 emissions correspond to FCV E_{H2} of 265 mg km^{-1} (a) and 26.5 mg km^{-1} (b). In 2100, overall H_2 emissions correspond to FCV E_{H2} of 265 mg km^{-1} (a), 200 mg km^{-1} (b), 135 mg km^{-1} (c), 70 mg km^{-1} (d), 26.5 mg km^{-1} (e), and 0 mg km^{-1} (f).

In summary, H_2 emissions from road-based transportation in 2010 and 2020 are dominated primarily by 2-wheelers, gasoline-powered ICE LDVs, and a group of gasoline-powered vehicles consisting of medium-sized trucks, large buses, and mini-buses. The primary reason for the drastic decrease in emissions between 2010 and 2050 is the clean-up of emissions from 2-wheelers, and to a lesser extent those from gasoline-powered ICEVs, medium-sized trucks, large buses, and mini-buses. Thus, transport-based H_2 emissions in 2050 are expected to be significantly lower than in both 2010 and 2020. As an example, the FCV E_{H2} of 265 mg km^{-1} applied as an upper-end figure in 2100 would result in total H_2 emissions from transportation of 1.6 Tg in 2050, approximately one-third of 2010 transport-based emissions estimates. In 2100, FCVs will have far more influence on transport-based H_2 emissions than in 2050 due to the 13-fold increase in global FCV kilometres. Thus, smaller ranges of FCV E_{H2} will have greater effects on total emissions.

It has been demonstrated that fuel cells have a variable purge requirement in order to prevent the accumulation of inert gases, water, and impurities such as CO and CO_2 in the anode channels [96, 97]. Purging at regular intervals occurs in order to maintain efficiency and stable cell performance [98], and since H_2 is delivered via the anode channel, H_2 is simultaneously purged during these events. An important consideration might therefore be how much effort will be invested in optimizing the trade-off between fuel cell efficiency and loss of H_2 to the atmosphere due to the purge requirement of fuel cells. Such an optimum has been demonstrated by Ahluwalia and Wang [99], which could well ensure that future H_2 losses to the atmosphere from marketed FCVs are minimized. As noted by Owejan et al. [100], water management is one of the key engineering challenges facing the commercialization of proton exchange membrane fuel cells, suggesting that such areas are already being contemplated.

4.2 Global projections of H_2 production and consumption

In contrast to the previous section that covered the global upscaling of H_2 emissions from road-based transportation, this section covers global H_2 production and consumption scenarios. The end-uses covered in this section include industrial processes (e.g. petroleum refining and ammonia fertilizer production) and direct energy-based end-uses (e.g. H_2-based transportation, industrial, commercial, and residential heating and power). This section does involve emissions scenarios. Rather, the quantitative scenarios developed in this section will be coupled with the leakage and loss rate ranges estimated in the first part of the next section (section 4.3), which together will form the basis of H_2 emissions from leakage and losses from non-transport-based emissions in section 4.3.2.

Approximately 44.5 million metric tons (44.5 Tg) of H_2 were produced globally for all end-uses in 2008 [81].

4.2.1 Direct energy-based end-uses

H_2 production for direct energy-based end-uses has been projected with the GMM to 2100 (see Table 22); production is expected to increase considerably throughout the 21st century under the 450 ppm CO_2 climate policy scenario — an annual growth rate of 14.5% from 2010–2100. Climate policy efforts dictate H_2 production for direct energy-based end-uses throughout the 21st century, and the more stringent the policy with respect to atmospheric CO_2 mixing ratios, the more H_2 is produced. H_2 production increases exponentially throughout the 21st century, with the strongest increases occurring for the 450 ppm CO_2 climate policy scenario [5]. Hydrogen production prior to 2050 is largely based on natural gas reforming, supplying aggregate single load centres (i.e. pilot projects) by pipeline systems or combined pipeline and truck delivery systems. After 2050, with more significant uptake of hydrogen demand, H_2 is increasingly produced using coal gasification with CCS as well as nuclear energy and wind farms dedicated to hydrogen production via electrolysis. By 2100 and with widespread deployment of FCVs under a 450 ppm CO_2 climate policy regime, H_2 would largely be distributed by pipelines [5].

In 2010, ~0.0073 Tg of H_2 is estimated to be produced for direct energy, the mass equivalent that would provide ~0.0009 exajoules (EJ) of direct energy services. In 2020, already ~3.1 Tg H_2 is estimated to be produced, a mass that would provide ~0.4 EJ of direct energy. In 2050, an estimated 92.6 Tg would be produced, which would provide roughly 11 EJ of direct energy service. In 2100, an estimated 1440 Tg H_2 will be produced, a mass that would provide ~10% of primary energy consumption in 2100 (~170 EJ). As a comparison, only ~5 Tg H_2 (~0.5 EJ) would be produced in 2100 under a business-as-usual scenario that would lead to atmospheric CO_2 mixing ratios increasing to ~770 ppm by 2100 [5].

4.2.2 Industrial end-uses

In 2010, H_2 production for industrial end-uses vastly outweighs that for direct energy-based end-uses. In the United States for example, ~99% of H_2 production is used in the chemical and petrochemical industries, primarily the petroleum refining and NH_3 fertilizer production industries [101]. Although H_2 production in these areas is projected to increase in the coming decades, due largely to increasing gasoline and diesel consumption, the rates at which H_2 production increase are expected to slow as global oil supply declines and more advanced alternative energy technologies continue to gain market share (see [1] and [5]). H_2 production and consumption for industrial end-uses was upscaled based on 2008 estimations from [81].

4.2.2.1 Petroleum refining

Peak oil production is likely to occur in the first half of the 21st century [102]. However, global H_2 production per unit of refinery throughput in the petroleum industry will continue to increase throughout the 21st century even after the peak in oil supply, due to the decreasing quality petroleum feedstocks (e.g. oil sands), coupled with stricter environmental regulations (S. Schlag, SRI Consulting, pers. comm.). In 2008, the petroleum refining industry was responsible for ~18.2 Tg (41%) of global H_2 consumption. Table 20 outlines the results of H_2 production in the oil refining industry.

Table 20. H_2 production based on global oil supply and mass of H_2 required per petajoule (PJ) of oil refined. Global oil supply figures are from [5]. The mass of H_2 required per unit (PJ) of oil refined is based on a continuous 1% annual growth rate per unit of refinery throughput. The H_2 consumption for oil refining from 2008 is from [81].

Climate policy	Global oil supply (PJ)[a]	Tg H_2 PJ^{-1} oil	H_2 for oil refining (Tg)
	2000		
–	155873.5	–	–
	2008		
–	156285.4	0.000116	18.2[b]
	2010		
Baseline	156388.5	0.000119	18.6
	2020		
Baseline	184978.7	0.000131	24.3
450 ppm	188775.3		24.8
	2050		
Baseline	192906.0	0.000177	34.1
450 ppm	163476.2		28.9
	2100		
Baseline	158009.8	0.000291	46.0
450 ppm	128372.3		37.3

[a] from [5]
[b] from [81]

Based on global H_2 production in the petroleum refining industry of 18.2 Tg in 2008, global oil supply figures from [5] were considered as a guide for projections of global H_2 production throughout the 21st century. In parallel, a continuous 1% annual growth rate in H_2 production in the refining industry was applied to account for the growing requirements of H_2 per unit of refinery throughput. This results in H_2 production of 18.6 Tg in 2010 (baseline), 24.3 Tg and 24.8 Tg in 2020 under the baseline and 450 ppm CO_2 climate policy scenarios, respectively, 34.1 Tg and 28.9 Tg in 2050 under the baseline and 450 ppm CO_2 climate policy scenarios, respectively, and 46.0 Tg and 37.3 Tg in 2100 under the baseline and 450 ppm CO_2 climate policy scenarios, respectively.

4.2.2.2 Other industrial end-uses

Ammonia (NH_3) production was responsible for ~18.6 Tg of global H_2 consumption in 2008, which corresponds to 42% of the global H_2 production aggregate. According to the International Fertilizer Industry Association [103], world NH_3 production has increased from 105 Tg in 1999 to 125 Tg in 2008, an average increase of ~1.9% a^{-1}. Schmid [104] has shown that the global NH_3 trade has remained approximately constant since 1970, and according to the United Nations Population Division [105],

world population has increased approximately linearly from 1970, and is expected to do so until at least 2020. The primary driver for NH_3 production considered here is population growth, which accounts for the increasing food production requirements for a growing global population. As such, this growth rate of ~1.9% is expected to perpetuate to 2020, which would result in global H_2 production for the NH_3 industry of 19.3 Tg and 23.3 Tg in 2010 and 2020, respectively.

Approximately 10% (4.2 Tg) of global H_2 consumption in 2008 was attributed to the methanol (CH_3OH) industry. Global production of CH_3OH increased from 29.1 Tg in 1999 to 41.1 Tg in 2007, corresponding to a growth rate of ~4.4%; more than half of this production is for CH_3OH consumption in China [106]. Annual growth of ~10% has been projected until 2014 [107]. It was assumed here that this 10% growth rate continues until 2020, particularly due to strong demand in China. Thus, a 10% growth rate corresponds to an increase in H_2 production from 4.2 Tg in 2008 to 5.1 Tg in 2010 and 13.1 Tg in 2020.

In 2008, a category of other captive uses including metallurgical applications, chemical processing, and the hydrogenation of fats and oils in the food industry accounted for 1.2 Tg of global H_2 consumption, corresponding to ~3% of the global H_2 production total. Its fraction is not expected to largely influence global H_2 production throughout the 21st century. Nevertheless, a modest 2% growth rate for this category to 2020 was assumed, which is an estimation based on the growth rate of this category for both European and Japanese H_2 consumption from 2006–2011 [48]. As such, the global 2008 consumption level of 1.2 Tg H_2 results in consumption levels of 1.3 Tg and 1.6 Tg for 2010 and 2020, respectively.

Merchant H_2 (sold primarily by industrial gas companies; non-captive H_2) accounted for only ~5.1% (2.3 Tg) of global H_2 consumption in 2008 [48]. Merchant H_2 is being used in increasing volumes in the petroleum refining industry to supplement captive H_2 production for hydroprocessing activities, largely because the systematic tightening of regulations on the levels of impurities in refined oil products, along with the decreasing quality of the feedstock arriving at refineries [108]. Merchant H_2 consumption in the chemical and refining industries is expected to increase at a growth rate of 10% until 2020, which is supported by the projection that merchant H_2 consumption in the U.S. and Western Europe is expected to increase from 2006–2011

at annual rates of 10% and 8%, respectively [48], in addition to the trend of increasing on-site H_2 production facilities by gas companies. At a growth rate of 10%, merchant H_2 consumption is expected to grow from 2.3 Tg in 2008 to 2.8 Tg and 7.2 Tg in 2010 and 2020, respectively.

Beyond 2020 (i.e. for 2050 and 2100 scenarios), all of the other industrial end-use categories were grouped, and individual growth rates were applied to the aggregate total H_2 production for these categories for the two relevant time periods (i.e. 2020–2050 and 2050–2100). Global economic growth rates were considered as a guide for H_2 demand in these industries. These growth rates are based on the B2 scenario of the Intergovernmental Panel on Climate Change (IPCC) Special Report on Emissions Scenarios [82], which is the same report from which long-term economic growth in [1] and [5] is derived. For the period 2020–2050, an annual growth rate of 2.8% was applied, which is the same average growth rate projected for the period 1990–2050. For 2050–2100, an annual growth rate of 1.5% was applied, which is considered an average value for the global economic growth projected for the period 1990–2100. This results in aggregate H_2 production from the other significant industrial end-uses (i.e. industrial end-uses other than petroleum refining) of 103.4 and 217.6 Tg in 2050 and 2100, respectively. It was assumed that production for these end-uses did not differ between climate policies. Table 21 outlines the results of industrial H_2 production and consumption (excluding refining processes).

Table 21. H_2 production and consumption for the major industrial processes (excluding oil refining). Figures for 2008 are from [81]. Figures for 2010 and 2020 are based on derived growth rates for those time periods (see text above for details). Total H_2 production in 2050 is based on the total from 2020 and an annual growth rate of 2.8% from 2020–2050. Total H_2 production for 2100 is based on the total from 2050 and an annual growth rate of 1.5% from 2050–2100. Units are in Tg.

	2008[a]	**2010**	**2020**	**2050**	**2100**
Ammonia	18.6	19.3	23.3		
Methanol	4.2	5.1	13.1		
Other captive	1.2	1.3	1.6	**103.4**	**217.6**
Merchant	2.3	2.8	7.2		
TOTAL	**26.3**	**28.5**	**45.2**		

[a] from [81]

Based on the projections from Tables 20 and 21 above, total H_2 production for industrial end-uses is estimated at 47.0 Tg for 2010. In 2020, H_2 production and consumption of 69.4 Tg (baseline) and 69.9 Tg (450 ppm) are projected. Total industrial H_2 production is projected at 137.5 and 263.5 Tg under the baseline

scenario in 2050 and 2100, respectively, while production is projected at 132.3 and 254.9 Tg under the 450 ppm CO_2 climate policy scenario in 2050 and 2100, respectively. Table 22 provides results of upscaled industrial and direct energy-based H_2 production for both the baseline and 450 ppm CO_2 climate policy scenario.

Table 22. H_2 production scenarios for industrial and direct energy-based end-uses. Figures have been provided for both the baseline and 450 ppm CO_2 climate policy scenarios. Units are in Tg.

Year	Baseline scenario		450 ppm CO_2 climate policy scenario	
	Industrial[b]	Direct energy	Industrial[b]	Direct energy
2010	47.0	<0.1[a]	–	–
2020	69.4	0.1	69.9	3.1
2050	137.5	0.8	132.3	92.6
2100	263.5	5.1	254.9	1436.6

[a] based on the baseline climate policy (from GMM)
[b] based on sum of totals from Tables 20 and 21 for corresponding year

From Table 22 it is apparent that direct energy-based H_2 production remains only a small fraction of total H_2 production through 2100 under the baseline scenario. Under the 450 ppm CO_2 climate policy scenario, direct energy-based H_2 production in 2020 also makes up only a small fraction of total H_2 production (~4%). However by 2050, the fraction of H_2 produced for direct energy-based applications has increased considerably to ~41% of the total, while in 2100, this figure reaches 85% of total H_2 production. Direct energy-based H_2 production would be more than 5 times higher than industrial H_2 production in 2100 under the 450 ppm CO_2 climate policy scenario.

4.3 Current and future H_2 emissions from hydrogen production, distribution, storage, and non-transportation-based end-uses

An important category of anthropogenic H_2 emissions is that of leakage or other fugitive emissions from production, distribution, storage, and non-transport-based end-uses. This category includes all direct energy and industrial non-transport-based end-use sectors. In this section, results from global production and consumption scenarios (section 4.2) are combined with established leakage and loss rate ranges (section 4.3.1) to develop scenarios of total leakage and losses of H_2 to the atmosphere from non-transport-based anthropogenic emissions from technological sources (section 4.3.2).

4.3.1 State-of-the-art knowledge of non-transport-based well-to-use leakage rates of H_2

Leakage and losses of H_2 to the atmosphere inevitably occur at various points along the H_2 life cycle. Such emissions are independent from road-based transportation tailpipe emissions. Currently, the majority of these losses occur during the industrial production of H_2 for captive end-uses, as virtually all currently produced H_2 is generated for on-site consumption, such as in petroleum refineries or during the production of NH_3 fertilizer. However, it has been shown that inefficiencies and losses of H_2 in refineries can be extremely costly [109], suggesting that losses of H_2 in other industries involving large volumes of H_2, such as the NH_3 and CH_3OH industries are also expensive, and that measures will therefore be implemented to minimize such losses. As production for direct energy services increases throughout the 21st century, losses can be expected at various points along the production, distribution, storage, and non-transportation-based end-use chain.

In the context of large-scale H_2 production and distribution, Zittel and Altmann [56] report that losses of gaseous H_2 are significantly less than 1% (citing losses of 0.1% from the existing German H_2 distribution grid), while those of liquid H_2 are on the order of 1–10%. A leakage rate of 0.1% for the same H_2 pipeline in Germany was confirmed in a fiscal context by an engineer at Air Liquide (formerly Hüls AG), where the largest hydrogen filling centre in Europe is located. Although the goal for

H_2 production, delivery, and storage is to achieve zero losses, a 0.1% loss rate to the atmosphere is more realistic, since a loss rate of 1% would result in massive financial losses (F. Balzer, Air Liquide, pers. comm.) — a seemingly robust incentive for large industrial gas companies to prevent losses of H_2 to the atmosphere. Loss rates lower than 0.1% for an H_2-intensive economy have even been envisaged [15].

A leakage and loss rate range of 1–4% is adopted here for 2010 for the entire production, distribution, and utilization chain, which reflects a current low loss projection (1%) due to the more widely applied gaseous state and predominantly captive uses (involving direct consumption) of H_2, but also considers what is estimated to be a "worst-case" loss rate (4%) due to some venting and other fugitive losses in refineries, for example. The potentially over-ambitious loss rates of less than 1% as a guide for current representative conditions has been avoided. In 2020, potentially lower loss rates are anticipated, which is due to increasing volumes of H_2 being captured and recycled in petroleum refineries (the primary consumers of H_2 in 2020). Thus in 2020, loss rates as low as 0.5% over the entire H_2 life cycle are expected, but a high end loss rate of 4% is also applied, due to the use of existing natural gas pipelines for the delivery of H_2 [7], for example. In 2050, as H_2 production for direct energy services begins to contribute more significantly to overall H_2 production figures, a leakage rate range of 0.1–2% is envisaged to cover the losses of H_2 to the atmosphere from mostly mature H_2 systems. Refineries will also likely dedicate significant effort to minimizing H_2 losses as their requirements continue to intensify. This range for 2050 is therefore based on assumptions that these systems will perpetually develop and improve their efficiency, primarily due to safety, ecological, and monetary concerns as production and requirements increase. In 2100, a leakage rate range of 0.01–0.5% is predicted based on fully mature and developed H_2 production, distribution, storage, and end-use systems.

4.3.2 Scenarios for non-transportation-based H_2 emissions to the atmosphere

Table 23 outlines the global production of H_2 in 2010, 2020, 2050, and 2100 (section 4.2), along with a range of loss rates of H_2 to the atmosphere from production, delivery, storage, and end-use systems established in section 4.3.1.

Table 23. Global projections of non-transport-based H_2 losses (Tg) to the atmosphere from production, distribution, storage, and end-use systems under a range of loss rates (%). Total production and losses comprise H_2 production for both industrial and energy-based end-uses. See Table 22 for the breakdown of total production between industrial and energy-based end-uses.

Year	Baseline scenario			450 ppm CO_2 climate policy scenario		
	Total production (Tg)	Loss rate (%)	Total losses (Tg)	Total production (Tg)	Loss rate (%)	Total losses (Tg)
2010	47.0	1	0.47	–	–	–
		2	0.94		–	–
		3	1.41		–	–
		4	1.88		–	–
2020	69.5	0.5	0.35	73.0	0.5	0.37
		1	0.70		1	0.73
		2	1.39		2	1.46
		4	2.78		4	2.92
2050	138.3	0.1	0.14	224.9	0.1	0.22
		0.2	0.28		0.2	0.45
		0.5	0.69		0.5	1.12
		2.0	2.77		2.0	4.50
2100	268.6	0.01	0.03	1691.5	0.01	0.17
		0.05	0.13		0.05	0.85
		0.1	0.27		0.1	1.69
		0.5	1.34		0.5	8.46

If a current loss rate range of 1–4% over the entire production, distribution, storage, and end-use chain (with 4% considered to be an upper-end figure) is considered, between 0.5–1.9 Tg H_2 will be emitted to the atmosphere in 2010 under the baseline scenario. However, Zittel and Altmann [56] and Schultz et al. [7] have reported that losses of GH_2 from the existing H_2 distribution grid in Germany are on the order of 0.1%, suggesting that future systems should attain lower loss rates. This argument is driven primarily by financial, safety, and environmental concerns. By 2050 under the 450 ppm CO_2 climate policy scenario, as the fraction of global H_2 production for direct energy services begins to gain a foothold, a loss rate range of 0.1–2% is assumed to be representative over the entire production, distribution, storage, and end-uses phases (excluding transportation) of the H_2 life cycle. Under such conditions, losses of H_2 to the atmosphere would be on the order of 0.2–4.5 Tg. Direct energy-based H_2 applications would be responsible for ~41% of these losses.

By 2100, approximately 1400 Tg H_2 will be produced for direct energy services, equivalent to ~170 EJ and 10% of primary energy consumption (total primary energy consumption of ~1690 EJ) under the 450 ppm CO_2 climate policy scenario. With H_2 providing such a significant fraction of primary energy, production, storage, and delivery systems should be advanced enough to attain a maximum 0.5% loss rate of

H_2 due to safety, monetary, and ecological concerns. Leakage rates of 0.5% over the entire chain would result in emissions to the atmosphere on the order of approximately 8.5 Tg a^{-1}, with direct energy applications accounting for 7.2 Tg. Most H_2 applications are fuelled by GH_2, however, from which losses to the atmosphere are significantly less than those from LH_2. If a loss rate of 0.1% over the entire production and end-use chain with the annual H_2 production of 1690 Tg a^{-1} for all end-uses is considered, an annual leakage of 1.7 Tg H_2 would result, with direct energy-based applications accounting for 1.4 Tg. In other words, by 2100 with a well-to-use H_2 loss rate of 0.1%, an economy reliant on H_2 for approximately 10% of primary energy consumption would release a comparable amount of H_2 into the atmosphere as estimations of today's anthropogenic non-motor vehicle source of 0.5–2.0 Tg (Table 23). By 2100, lower loss rates are conceivable for fully mature H_2 production, distribution, and utilization systems, and loss rates of 0.01% and 0.05% have been considered for illustrative purposes. Should such leakage rates be achieved by 2100, well-to-use losses (i.e. excluding emissions from transportation) would be on the order of 0.17 Tg and 0.85 Tg, respectively, at the lower end of current H_2 emissions from the non-motor vehicle source.

It is apparent in Table 23 that in the majority of cases, total losses remain within the realm of H_2 emissions from the current non-motor vehicle source. Exceptions are the 4% loss rate in 2020 for both the baseline and 450 ppm CO_2 climate policy scenarios, the 2% loss rate in 2050 for both scenarios and the 0.5% loss rate for the 450 ppm CO_2 climate policy scenario in 2100. It should be noted, however, that these are all considered worst-case loss rates for these time periods, and that industrial end-uses are also responsible for large fractions of the losses — 95.7–99.9% in 2020, 58.8–99.4% in 2050, and 15.1% of losses under the 450 ppm CO_2 climate policy scenario in 2100.

4.4 Global upscaling scenarios for overall anthropogenic H_2 emissions to the atmosphere between 2010 and 2100

In this section, H_2 emissions (from sections 4.1 and 4.3) are combined to provide an overall (transportation + non-transport-based well-to-use losses) estimate of direct H_2 emissions from the most significant technological anthropogenic sources for 2010, 2020, 2050, and 2100. Table 24 provides global H_2 production, a range of estimated average leakage rates (section 4.3.1), total leakage, global emissions from transportation, and overall technological anthropogenic H_2 emissions for both the baseline and 450 ppm CO_2 climate policy scenarios. Since overall anthropogenic H_2 emissions throughout the 21st century are projected to remain below current H_2 emissions levels under the baseline scenario, the bulk of this discussion focuses on the 450 ppm CO_2 climate policy scenario.

In 2010, based on a loss rate range of 1–4% and a total contribution of 4.5 Tg H_2 from transportation, overall baseline anthropogenic H_2 emissions are estimated at 5.0–6.4 Tg from the most significant technological anthropogenic H_2 sources. This range is lower or at the lower end of overall fossil fuel-based anthropogenic H_2 emissions from other studies [13, 18, 29, 31, 32]. The results here provide an update of previous estimates based on older and less developed vehicle technologies. Given the close positive correlation of H_2 and CO in the exhaust gas of motor vehicles (the most significant source of atmospheric H_2 from fossil fuels), many studies have based their estimates primarily by scaling H_2 estimations against the much more well-known CO inventories. However, since some of the known fossil fuel combustion processes appear to emit greater quantities of CO compared to H_2, these or analogous conditions could have led to overestimations of the H_2 source term for fossil fuel combustion in previous studies, which would provide an explanation for the lower estimations in this study. In support of this presumption, it has been shown that some fossil fuel combustion processes emit much smaller amounts of H_2 relative to CO compared with the exhaust gas of motor vehicles. For example, H_2 emissions in the flue gas of industrial and residential heating systems have been shown to emit much smaller ratios of H_2 to CO compared with the direct exhaust of motor vehicles (M.K. Vollmer, Empa, pers. comm.).

In 2020, overall emissions are projected to remain either below or within the range of those estimated for 2010. A range of overall direct anthropogenic H_2 emissions to the atmosphere is estimated at 2.7–5.2 Tg H_2 based on an H_2 leakage rate range of 0.5–4%. Transportation would account for 44–88% of the total, although non-transport leakage and losses (predominantly from industrial end-uses) would account for more than half (~53%) of overall emissions with a leakage rate of 4%. With a loss rate of 0.5–2%, emissions would be lower than those estimated for current overall anthropogenic emissions. However, based on an assumed high-end loss rate of 4% under both the baseline and 450 ppm CO_2 climate policy scenario in 2020, overall anthropogenic emissions would be within the range estimated for 2010.

The combined anthropogenic emissions column for both 2050 and 2100 has been split. The first column represents combined emissions based on an FCV E_{H2} of 26.5 mg km^{-1}. The second column represents combined emissions based on an FCV E_{H2} of 265 mg km^{-1}. Based on these scenarios with FCV E_{H2} of 26.5 mg km^{-1} and 265 mg km^{-1} and a leakage and loss rate range of 0.1–0.5% in 2050, overall anthropogenic H_2 emissions would remain well below overall 2010 emissions levels. Should an average leakage rate of 2% be the norm in 2050, overall H_2 emissions would be ~5.6 Tg and 6.1 Tg for FCV E_{H2} of 26.5 mg km^{-1} and 265 mg km^{-1}, respectively, and overall H_2 emissions would be similar to current conditions. However, with a loss rate of 2% in 2050, transportation would only be responsible for 20% (26.5 mg km^{-1}) and 26% (265 mg km^{-1}) of overall emissions. Again, industrial end-uses would be responsible for 47% and 43% of overall emissions for FCV E_{H2} of 26.5 mg km^{-1} and 265 mg km^{-1}, respectively.

In a second example, a scenario has been formulated based on a mean FCV E_{H2} that would result in total transport-based emissions remaining similar to the 2010 estimate of 4.5 Tg (section 4.1). As detailed in section 4.1, this E_{H2} for FCVs corresponds to ~1625 mg km^{-1} for 2050. Considering only the 450 ppm CO_2 climate policy scenario in 2050 (under the baseline scenario virtually all H_2 production is destined for industrial end-uses), loss rates of 0.1% and 0.2% would result in overall anthropogenic H_2 emissions to the atmosphere of approximately 4.7 and 5.0 Tg, respectively, if emissions from FCVs are limited to ~1625 mg km^{-1}. Both of these estimations would be at the lower end of the range of current baseline H_2 emissions

estimations. A 0.5% and worst-case 2% loss rate at such a production (224.9 Tg) would lead to H_2 emissions of ~5.6 Tg and ~9.0 Tg, respectively, should FCV emissions be held to a level that would lead to H_2 emissions from transportation comparable to today. Under these conditions, overall emissions based on the 2% loss rate would exceed current overall technological anthropogenic H_2 emissions estimations, whereas the 0.5% loss rate would result in similar overall emissions compared with today. Of course H_2 emissions from FCVs will almost certainly be substantially lower than 1625 mg km^{-1} for reasons detailed in section 4.1, suggesting that overall emissions from anthropogenic processes in 2050 will be largely dictated by leakage and losses and not transportation, and remain significantly lower than current estimates.

In 2100, with an average FCV E_{H2} of 26.5 mg km^{-1}, overall H_2 emissions would be 1.7–10.0 Tg based on a leakage rate range of 0.01–0.5%. Losses to the atmosphere from production, distribution, storage, and end-use systems other than transportation would be dominated by direct energy-based services. These account for 72% of overall H_2 emissions with a leakage rate of 0.5%. With a leakage rate of 0.01–0.3%, overall emissions would be well below current levels. A leakage rate of 0.5% would result in emissions 1.6–2 times higher than current projections. With an FCV E_{H2} of 265 mg km^{-1} in 2100, emissions from transportation would be ~8.1 Tg, with FCVs accounting for ~94% of this total. With a 0.5% leakage rate, overall anthropogenic H_2 emissions would be higher than current conditions even if FCVs emitted no H_2 at all. At the same time, with an FCV E_{H2} of 265 mg km^{-1}, overall anthropogenic H_2 emissions would be higher than current conditions even if there were no net leakage and losses. In order to achieve the range of emissions projected for 2010 (i.e. 5.0–6.4 Tg) based on a leakage rate of 0.1%, FCV E_{H2} would need to be on the order of 120–170 mg km^{-1}.

In a second example, a scenario has been formulated based on a mean FCV E_{H2} that would result in total road-based emissions remaining similar to the 2010 estimate of 4.5 Tg (section 4.1). As detailed in section 4.1, this FCV E_{H2} corresponds to ~135 mg km^{-1} for 2100. In 2100 under the 450 ppm CO_2 climate policy scenario and based on a loss rate range of 0.01–0.1% and an FCV E_{H2} of 135 mg km^{-1}, overall anthropogenic H_2 emissions to the atmosphere are projected to be within the range of 2010 estimates.

In other words, under the 450 ppm CO_2 climate policy scenario, and based on a well-to-use (i.e. excluding transportation) leakage range of 0.01–0.1% in 2100, overall anthropogenic H_2 emissions to the atmosphere should be at worst comparable with today's anthropogenic source of H_2 should E_{H2} for FCVs not exceed ~135 mg km^{-1}. However, should an average leakage rate of 0.5% be the norm in 2100, overall anthropogenic H_2 emissions from technological processes would be roughly a factor of 2–2.5 higher than current emissions.

Table 24. Projections of overall global anthropogenic H_2 emissions to the atmosphere from technological processes in 2010, 2020, 2050, and 2100 under the baseline and 450 ppm CO_2 climate policy scenarios.

Baseline scenario					450 ppm CO_2 climate policy scenario				
Production (Tg)	**Leakage rate (%)**	**Total leakage (Tg)**	**H_2 emissions transportation (Tg)**	**Overall anthropogenic H_2 emissions (Tg)**	**Production (Tg)**	**Leakage rate (%)**	**Total leakage (Tg)**	**H_2 emissions transportation (Tg)**	**Overall anthropogenic H_2 emissions (Tg)**
2010									
47.0	1	0.5	4.5	5.0	–	–	–	–	–
	2	0.9		5.4		–	–		–
	3	1.4		5.9		–	–		–
	4	1.9		6.4		–	–		–
2020									
69.5	0.5	0.4	2.3	2.7	73.0	0.5	0.4	2.3	2.7
	1	0.7		3.0		1	0.7		3.0
	2	1.4		3.7		2	1.5		3.8
	4	2.8		5.1		4	2.9		5.2
2050									
138.3	0.1	0.1	1.1	1.2	224.9	0.1	0.2	1.1[a]	1.3
						0.2	0.5		1.6
	0.2	0.3		1.4		0.5	1.1		2.2
						2.0	4.5		5.6
	0.5	0.7		1.8		0.1	0.2	1.6[b]	1.8
						0.2	0.5		2.1
	2.0	2.8		3.9		0.5	1.1		2.7
						2.0	4.5		6.1
2100									
268.6	0.01	<0.1	1.2	1.2	1691.5	0.01	0.2	1.5[a]	1.7
						0.1	0.9		2.4
	0.1	0.1		1.3		0.3	1.7		3.2
						0.5	8.5		10.0
	0.3	0.3		1.5		0.01	0.2	8.1[b]	8.3
						0.1	0.9		9.0
	0.5	1.3		2.5		0.3	1.7		9.8
						0.5	8.5		16.6

[a] FCV E_{H2} of 26.5 mg km^{-1}
[b] FCV E_{H2} of 265 mg km^{-1}

4.5 Summary

In 2010, anthropogenic H_2 emissions from fossil fuel-based sources are dominated by emissions in the exhaust gas of road-based transportation. These emissions currently contribute the largest fraction of the overall anthropogenic source term of the global H_2 budget from technological processes. The second important anthropogenic source, and one that has the potential to become increasingly influential throughout the 21st century, is leakage and losses from H_2 production, storage, distribution, and other non-transport-based end-use systems. Leakage and losses of H_2 to the atmosphere inevitably occur at various points along the H_2 life cycle. Currently, the majority of these losses occur during industrial production through captive end-uses, as almost all currently produced H_2 is allocated for on-site consumption, such as in petroleum refineries. However, inefficiencies and losses of H_2 in refineries can be extremely expensive [109], suggesting that H_2 losses for other industries such as the NH_3 and CH_3OH industries are also costly, and that measures will therefore be applied to minimize such losses. In the future as production for direct energy services increases, losses can be expected at various points along the production, distribution, storage, and end-use chain. Leakage and losses of H_2 to the atmosphere from production, storage, distribution, and end-use systems other than transportation should be driven throughout the coming century primarily by safety, ecological, and monetary concerns. Particularly as H_2 production for direct energy-based end-uses begins to increase, efforts invested in controlling such losses should intensify, meaning lower future leakage and loss rates as such systems mature.

H_2 emissions from road-based transportation in 2010 (~4.5 Tg) are at the lower end of the figures provided in previous literature (~5–20 Tg). Emissions from road-based transportation are expected to perpetually decrease throughout the 21st century as emission standards tighten, exhaust after-treatment systems develop and improve, and alternative vehicle technologies increase their market share in relation to conventional gasoline vehicles. Throughout the first half of the century, 2-wheeler emissions are expected to dominate emissions from transportation, contributing ~53% in 2010 and ~56% in 2020 to total H_2 emissions. Other primarily gasoline-based technologies account for the bulk of the remaining fractions. Non-conventional vehicles such as natural gas ICEVs, biofuels, and hybrid vehicles contribute to overall H_2 emissions

only very marginally in the first half of the century, and although their relative fraction and absolute number of global kilometres travelled increases, emissions from non-conventional vehicles remain small and never approach those of the most significant current technologies.

Overall H_2 emissions (transportation + non-transport-based leakage and losses) in 2010 range from 5.0–6.4 Tg, which is based on a leakage rate range of 1–4% and global emissions from road-based transportation. These emissions to the atmosphere are at the lower end of those projected from earlier sources citing anthropogenic fossil fuel-based H_2 emissions, likely due in part to improving exhaust after-treatment systems and to scaling overestimations for non-transport-based sources. More research into fossil fuel-derived H_2 from sources other than motorized transportation would be beneficial. In 2020, projections of H_2 emissions to the atmosphere range from 2.7–5.2 Tg based on a leakage rate range of 0.5–4%. This range is lower than that estimated for 2010 because the ~50% decrease in emissions from exhaust gas has more than offset the increase in H_2 production for industrial processes and energy services. Through to 2020, combined anthropogenic H_2 emissions from transportation and well-to-use leakage based on a 0.5–4% leakage rate should remain within the realm of current overall emissions. Virtually all non-transport-based emissions would originate from industrial end-uses (primarily petroleum refining and ammonia production).

After 2050, emissions from the vehicle technologies important throughout the first half of the century are expected to decrease considerably. In 2050, as FCVs account for ~8% of global vehicle kilometres under the 450 ppm CO_2 climate policy scenario, a seemingly immense FCV E_{H2} of ~1625 mg km^{-1} is estimated to maintain total H_2 emissions from transportation at similar levels to today. Although H_2 emissions from transportation will have perpetually decreased throughout the first half of the century, the increase in H_2 production for energy services and industrial activities makes leakage and losses more influential. Although a mean loss rate range of 0.1–0.5% in 2050 would result in overall emissions well below current estimates, a loss rate of 2% would result in overall H_2 emissions within the range of 2010 estimates. Based on a leakage rate range of 0.1–2% in 2050, overall H_2 emissions should remain either lower or within the range projected for 2010 conditions. This is even the case for all

loss rates where an FCV E_{H2} of 1625 mg km^{-1} has been applied. An exception is a 2% loss rate under the 450 ppm CO_2 climate policy scenario at this high FCV E_{H2}. In this case, overall anthropogenic emissions would be a factor of 1.4–1.8 higher than current overall emissions. However, considering the fact that average FCV emissions will almost certainly be substantially lower than 1625 mg km^{-1}, overall emissions in 2050 should remain lower or within the realm of 2010 estimates. Irrespective of transport-based emissions, emissions from direct energy-based applications would only be responsible for ~41% of non-transport-based emissions in 2050, as the bulk of H_2 is still allocated to industrial processes.

In 2100, an FCV E_{H2} of ~135 mg km^{-1} is estimated to result in total emissions from transportation comparable to today's road-based transport emissions. This lower E_{H2} of more than an order of magnitude compared with 2050 (1625 mg km^{-1}) is largely due to the 13-fold increase in global FCV kilometres driven between 2050 and 2100. Considering a leakage rate range of 0.01–0.1% and an FCV E_{H2} of 135 mg km^{-1} in 2100 under the 450 ppm CO_2 climate policy scenario, overall emissions would remain within the range of current estimates. With a leakage rate of 0.5% in 2100, overall H_2 emissions to the atmosphere would be a factor of 1.4–1.9 higher even if FCVs were to emit no H_2. In 2100, direct energy-based end-uses would account for ~85% of non-transport-related emissions. Minimizing systems leakage and controlling emissions from FCVs should be priorities in 2100. Alternatively, FCV E_{H2} of 265, 200, and 70, and 26.5 mg km^{-1} in 2100 are estimated to result in H_2 emissions approximately 1.8, 1.4, 0.6, and 0.3 times 2010 emissions from transportation, respectively. Should H_2 emissions from FCVs remain below 135 mg km^{-1} throughout the century, total emissions from transportation are projected to remain lower or comparable to today's estimated road-based transport H_2 emissions. Further research into the direct H_2 emissions from FCVs — and particularly into optimizing the trade-off of fuel cell efficiency and purge losses of H_2 — would be beneficial.

In 2100, FCVs have the potential to dominate overall technological anthropogenic H_2 emissions to the atmosphere due to their widespread use. In order to ensure that H_2 emissions from FCVs will not be responsible for upsetting the global H_2 budget, efforts should be invested in evaluating and quantifying H_2 emissions from FCVs. Particular attention should be paid to develop the technology to address the purge

requirements of fuel cells. One option could be optimizing the trade-off between fuel cell efficiency and loss of H_2 to the atmosphere due to purging. It has been shown that the build-up of inert gases such as N_2 and pollutants such as CO and CO_2 in the anode channels of a fuel cell will lead to an increasing purge requirement to maintain fuel cell efficiency [96, 99]. This purging of impurities simultaneously ejects H_2. By utilizing a pure H_2 feedstock, the optimum purge level is lower than with a greater amount of impurities [99]. This provides an argument for nuclear H_2 production [110, 111], or the renewable production of H_2 for feedstock purposes, such as wind and solar power generation with electrolysis [112], as opposed to the use of hydrocarbon reformation, which leads to greater impurities in the H_2 feedstock [96]. Thus, it would appear that an important task in the future development of fuel cells for transportation is achieving a balance between fuel cell efficiency and the intensity and frequency of purge events under a variety of common driving conditions. Further, it can be expected that catalytic converters will be deployed that eliminate H_2 from the FCV exhaust stream, using a comparatively straight-forward catalytic process.

In 2020 and 2050, climate impacts resulting from technological anthropogenic H_2 emissions to a greater extent than 2010 conditions are not envisaged, as overall emissions to the atmosphere are projected to remain either at similar or lower levels compared with current conditions. In a worst-case scenario, an additional ~10 Tg of H_2 would be emitted to the atmosphere in 2100 compared with 2010 conditions. This is the scenario that considers a 0.5% leakage and loss rate, coupled with an FCV E_{H2} of 265 mg km^{-1}. Based on the indirect global warming potential of 5.8 for H_2 [11], these additional 10 Tg of H_2 would lead to an additional climate impact of ~0.2% of the current fossil fuel-based system (which emitted approximately 29 381 Tg CO_2 a^{-1} in 2008 [113]). The overall climatic effect could actually be higher than this (0.2%) by 2100, however, because atmospheric CO_2 would strongly decrease under the 450 ppm CO_2 climate policy scenario. Since part of the CO_2 reduction would be due to a shift towards H_2-based applications, there would be a trade-off between the reduced climate effect from decreasing CO_2 and increasing H_2 in the atmosphere. Thus, although the climatic effect of atmospheric H_2 is minor compared with that of CO_2 (given the much greater abundance of CO_2 in the atmosphere), the effect of H_2 is not completely negligible. To minimize environmental impacts of H_2 emissions to the atmosphere during the potential transition to an increasing H_2-intensive economy,

efforts should be invested in not only limiting anthropogenic emissions of H_2 to the atmosphere, but also in pursuing H_2 production options aimed at mitigating climatic impacts, such as coal gasification and natural gas reforming with CCS, and electrolysis powered by nuclear and wind electricity.

Climate objectives and vehicle fleet composition do not dictate to a large extent the overall emissions of H_2 to the atmosphere in the first half of the 21st century. Rather, global levels of anthropogenic H_2 in the atmosphere appear to be primarily governed by 2-wheelers (at least until 2020), along with the variable loss rates from production, distribution, storage, and non-transport-based end-uses. After 2050, and particularly towards the end of the century, along with efforts invested in controlling leakage and other fugitive well-to-use emissions to the atmosphere, the mean E_{H2} for FCVs will largely influence overall anthropogenic H_2 emissions. In a large-scale context, H_2 measurements at remote sites will contribute meaningfully to the monitoring of any fluctuations in the levels of atmospheric H_2. This, among others, is the focus of the next chapter.

5 CONTINUOUS H_2 OBSERVATIONS IN THE ATMOSPHERE

The primary goal of this chapter is to develop a more thorough understanding of the behaviour of molecular H_2 in the atmosphere prior to a potential large-scale transition to a more H_2-intensive economy. Continuous measurements of H_2 at remote high-altitude sites provide the unique ability to evaluate temporal variations in background mixing ratios and to identify important source regions of the trace gas. Furthermore, through such measurements, trend analysis can be applied to assess changing background levels of free tropospheric H_2. Such ongoing atmospheric measurements at the high-Alpine site Jungfraujoch, Switzerland, have been evaluated. Current measurements represent baseline conditions. As the dataset lengthens, trend analysis could function as a tool to assess the contribution of H_2 applications to the atmosphere as the fraction of H_2-based mobile and stationary applications increases. Measurements at Jungfraujoch, along with other global stations (e.g. the National Oceanic and Atmospheric Administration's Earth System Research Laboratory – Global Monitoring Division (NOAA/ESRL-GMD) cooperative air sampling network (http://esrl.noaa.gov) and the Advanced Global Atmospheric Gases Experiment (AGAGE, http://agage.eas.gatech.edu)) can be used as independent checks to evaluate the influence of a future potentially H_2-intensive economy on atmospheric chemistry.

The Jungfraujoch observatory (46° 32' N, 7° 59' E, 3,580 m a.s.l.) is a high-altitude research station in the Swiss Alps, located between the peaks of Mönch (4,099 m a.s.l.) to the east and Jungfrau (4,158 m a.s.l.) to the west. It is part of the Global Atmospheric Watch (GAW) program of the WMO, and is also part of the Swiss National Air Pollution Monitoring Network (NABEL). With its isolated and elevated position, Jungfraujoch is only periodically influenced by anthropogenic source regions. Pollution events occur primarily during frontal transport, thermally driven vertical transport [114], and southerly foehn events [115, 116]. Jungfraujoch is characterized by typically free tropospheric conditions.

In the first section of this chapter, an evaluation of the entire (slightly more that 4-year) dataset, seasonal cycles, and a brief look at any short-term trend behaviour is performed. These areas provide insight into the temporal behaviour of H_2 in the free

troposphere, along with pollution and depletion events, which are temporally influenced by local and regional sources and sinks. Although the current dataset at Jungfraujoch is too short to draw any concrete conclusions about recent trend developments, it will be shown that the trend observed at Jungfraujoch is broadly in line with other recent trend analyses.

The focus of the chapter will then shift to an analysis of specific case studies, which provide detailed examples of the influence of local and regional sources and sinks on H_2 levels observed at Jungfraujoch. It is shown that H_2 mixing ratios are influenced by a number of factors including advection of air masses with latitudinally variable background H_2 mixing ratios, the influence of H_2 emissions in the atmospheric boundary layer (ABL), and H_2 depletion by soil uptake during transport to the sampling site.

Following the case studies, an assessment of H_2 pollution events is performed, including an analysis of H_2/CO ratios. In an interesting finding, it will be shown that unlike the highly positive correlation between H_2 and CO directly at the exhaust gas source (the most significant anthropogenic source of H_2 from technological processes), the two gases become increasingly less correlated moving further from the source. This phenomenon is largely due to the dominant soil H_2 sink.

The role of the soil sink in the removal of H_2 during the ascent of air masses to the Jungfraujoch observatory is then assessed in the final section. This assessment illustrates the importance of soil oxidation of H_2 during the ascent of air masses to the measurement site, which can be used to partially explain the decreasing correlation of H_2 and CO as the distance from the source to the measurement site increases.

5.1 Time series, seasonal cycles, trends

Ongoing continuous measurements of H_2 and CO have been performed at Jungfraujoch since August, 2005. The H_2 and CO datasets from August, 2005 – November, 2009 are depicted in Fig. 34, and monthly-averaged H_2 mixing ratios are listed in Table 25.

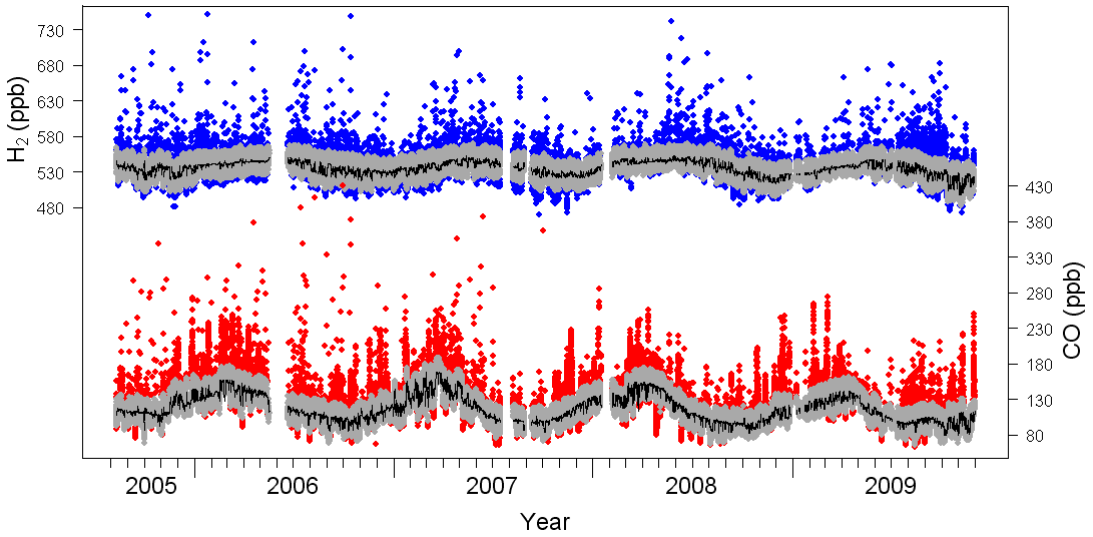

Figure 34. H_2 (top) and CO (bottom) datasets for the period August 2005 – November, 2009 at Jungfraujoch. The calculated baseline fits are depicted by the black lines through the background data. Background mixing ratios (baseline fit ± 2σ of the fit residuals) are depicted by grey shaded areas, while pollution and depletion events border either side of the background measurements.

Table 25. Mean monthly H_2 mixing ratios at Jungfraujoch for the period August, 2005 – November, 2009. All mixing ratios are reported in ppb as dry-air mole fraction on the MPI-2009 calibration scale. 'All' represents mean observations from all measurements; 'BG' represents mean observations from background measurements.

Month	2005		2006		2007		2008		2009	
	All	BG	All	BG	All	BG	All	BG	All	BG
Jan	–	–	545.4	539.6	530.5	530.5	533.9	532.8	529.0	526.7
Feb	–	–	540.1	539.4	535.6	534.5	546.7	546.0	531.0	530.8
Mar	–	–	545.0	543.6	538.4	536.5	544.8	544.2	536.8	536.2
Apr	–	–	545.8	544.5	547.1	544.3	544.9	544.4	538.0	536.9
May	–	–	546.0	544.5	547.3	545.7	549.2	547.5	545.7	544.5
Jun	–	–	548.6	546.6	546.0	543.8	550.2	547.7	540.2	539.1
Jul	–	–	548.2	545.5	543.5	542.5	545.7	543.6	536.8	535.2
Aug	539.2	537.1	531.5	531.0	538.2	536.3	540.6	539.1	537.3	534.6
Sep	536.4	534.4	538.9	535.5	526.6	528.0	533.1	532.9	529.0	525.6
Oct	533.1	529.3	531.9	530.2	529.3	529.8	526.0	525.8	520.5	520.1
Nov	530.8	528.2	529.0	528.7	526.7	526.6	520.8	520.1	515.8	515.3
Dec	534.0	531.9	530.9	529.3	524.9	525.3	523.5	522.8	–	–

"Baseline" mixing ratios have been defined as the fitted curve resulting from the 2D-REBS filter (black lines through grey background band in Fig. 34). "Background" mixing ratios (grey band in Fig. 34) have been defined as the range of mixing ratios within 2σ from the baseline (estimated from the fit residuals, see section 2.3.3). "Pollution" and "depletion" have been defined as the mixing ratios above and below background values, respectively. Baseline mixing ratios oscillate rapidly due to the latitudinal influence of the air mass origin (see Section 2.3.3). The standard deviation

of half-hourly baseline estimates for individual months ranged from 1 to 7 ppb. Neither seasonal cycles nor systematic changes of this oscillation were observed over the observation period. For example, baseline data for H_2 will be higher for air with its origin in the more southerly latitudes than it would be for northerly advection from the Arctic. Depletion events are uncommon for both H_2 and CO. These points represent events in which measurements were outside conditions designated for background conditions (2σ), likely the result of significant soil uptake during the ascent of air masses to the measurement station. Mean baseline mixing ratios for H_2 and CO were 536 ppb and 118 ppb, respectively.

Figure 35 depicts the distinct seasonal cycle of mean baseline H_2 and CO mixing ratios. An average peak-to-trough amplitude (amplitude) of 21 ppb was observed for H_2, with a maximum in spring (May), and a minimum in autumn (November). The seasonal cycle of mean baseline CO mixing ratios is characterized by an amplitude of 45 ppb, a maximum in spring (March), and a minimum in autumn (October).

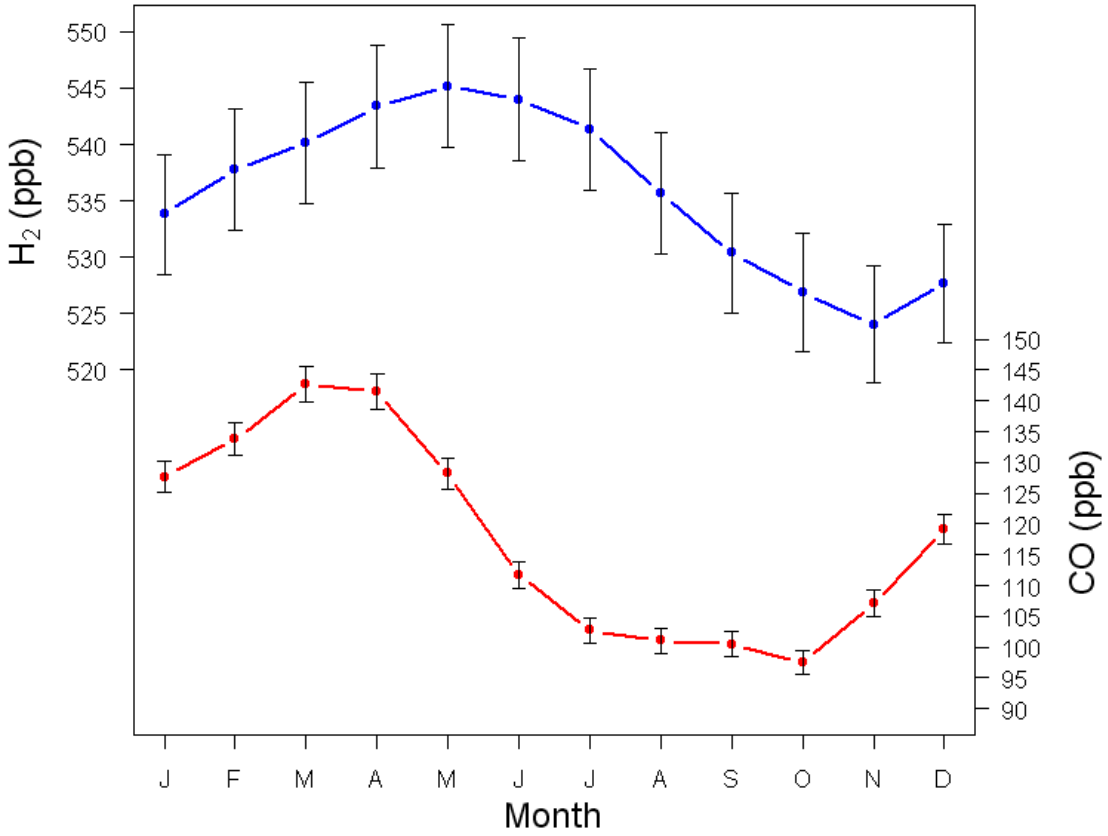

Figure 35. Seasonal monthly mean baseline H_2 (left y-axis, blue) and CO (right y-axis, red) mixing ratios at Jungfraujoch. Error bars represent expanded uncertainty at the 95% confidence level.

A phase shift of 1–2 months was observed in the seasonal cycle of H_2 compared to that of CO. The H_2 minimum is delayed compared to that of CO, which is attributed to optimal soil sink activity expected to occur in the latter part of the year as a result of moderately warm and dry soils in autumn [117]. The H_2 minimum in November at Jungfraujoch is also delayed by ~1 month compared to most other sites situated at similar latitudes [18, 26], but has been similarly observed at the high-altitude Northern Hemisphere sites of Niwot Ridge (3,523 m a.s.l., 40^o 3' N) and Mauna Loa (3,397 m a.s.l., 19^o 32' N). This delay is attributed to the travel time of surface signals to higher altitudes in the free troposphere, particularly during the cooler months due to reduced vertical transport. As a result, air masses that have been transported to the free troposphere during the summer months (that are less depleted in H_2 due to weaker soil uptake and faster vertical transport) will have a prolonged influence on average mixing ratios.

The mean seasonal H_2 amplitude at Jungfraujoch is considerably smaller compared to other stations at similar latitudes. For stations within a latitude band of $\pm 7^o$ of Jungfraujoch, a general decrease in seasonal amplitude with increasing altitude was found. This finding is illustrated in Fig. 36, where Jungfraujoch measurements are compared with data from the NOAA flask sampling network (http://esrl.noaa.gov) and continuous AGAGE observations from Mace Head [26]. The amplitudes for the flask (NOAA) and continuous data (AGAGE) from Mace Head are identical, from which it is concluded that there is no major potential bias due to differing sampling techniques, observational periods, or scales. This altitude effect is attributed to the dislocation of the major H_2 sources and sinks. With increasing altitude, the influence of the soil sink decreases and the tropospheric sources (CH_4 and NMHC oxidation) and the OH sink become more influential. Both of these major atmospheric sources (CH_4 and NMHC), along with the atmospheric H_2 sink (OH), are driven by hydroxyl radical chemistry, but the source strength is approximately double that of the sink (see Fig. 1), assuming that the ratio of the global sources and sinks also hold true for Jungfraujoch. This creates a net tropospheric source with a maximum in summer, thereby counteracting the soil sink at that time, which in turn dominates the free tropospheric fluxes only a few months later. Such a weakening of the seasonal signal with increasing altitude has also been modelled for H_2 [29], and this phenomenon has

also been observed for other atmospheric trace gases, for which the seasonal cycle is influenced by sources and sinks located primarily at the surface (e.g. CO_2) [118, 119].

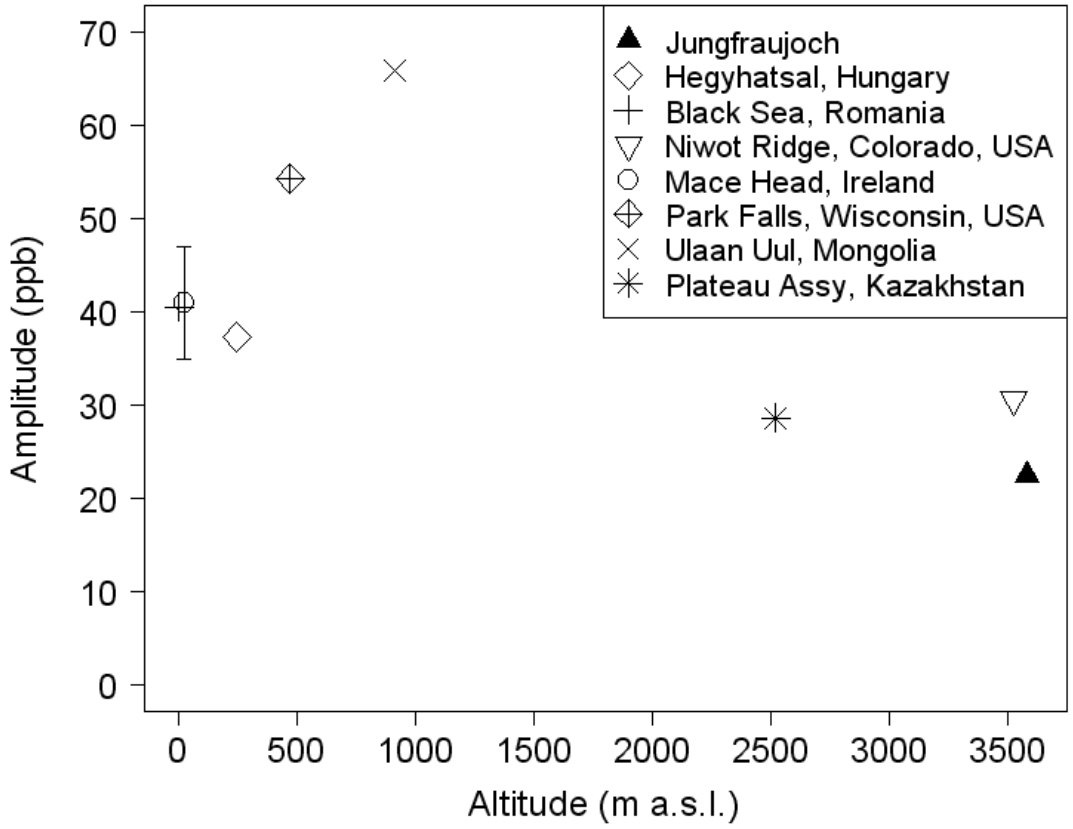

Figure 36. H_2 seasonal amplitudes vs. altitude for sites from flask measurements (http://esrl.noaa.gov) with latitudes similar to that of Jungfraujoch (46.55 ^{o}N ± 7 ^{o}N). Note that the Mace Head data point corresponds to both flask and continuous measurements, which both displayed an amplitude of 41 ppb (continuous Mace Head measurements from [26]). The error bar corresponds to the uncertainty of continuous Mace Head measurements.

Similarly to the work on trend measurements at Jungfraujoch by Zellweger et al. [85], a linear trend model including the first 4 annual harmonics to remove any annual cycle from the data was applied. This method results in a linear trend (± standard error) of –2.04±0.02 ppb a^{-1} for baseline H_2 and –3.77±0.02 ppb a^{-1} for baseline CO results over the entire study period. These short-term trends observed at Jungfraujoch must be approached with caution, however, since inter-annual variation could play a role in trends derived from shorter datasets. Although the time period is too short to evaluate this H_2 trend statistically, its comparability to trends from other datasets [18, 25, 26] complements previous estimates, suggesting that atmospheric H_2 mixing ratios have remained relatively stable over the past couple of decades at least.

5.2 Case studies

H_2 mixing ratios at Jungfraujoch result from a multitude of interactions, including (a) advection of air masses with latitudinally variable background H_2 mixing ratios, (b) the influence of the ABL, (c) photochemical H_2 production in the free troposphere, (d) photochemical H_2 degradation in the free troposphere, and (e) H_2 depletion by soil oxidation during ascent to the measurement station.

These conditions explain why — in contrast to surface measurement sites where H_2 and CO time series generally show a strong positive correlation [21, 45, 46] — that simultaneous pollution events for both H_2 and CO could be detected at Jungfraujoch in only a small number of cases. Figure 37 illustrates such an event, where fast advection of pollution from the nearby Po Basin (Italy) has not allowed adequate time for significant deposition of H_2 to the soil during transport to Jungfraujoch. The backward trajectory analysis (panel C) confirms that the H_2 and CO pollution event on January 12, 2008 corresponds to a stagnant meteorological event where the air masses sampled at Jungfraujoch have spent several days within the European ABL prior to sweeping through the Po Valley and ascending to the measurement station. As pollution events from the Po Valley are observed frequently for other anthropogenic trace gases [116, 120, 121], the relative irregularity and magnitude of such events with H_2 are presumably due to the strong soil sink.

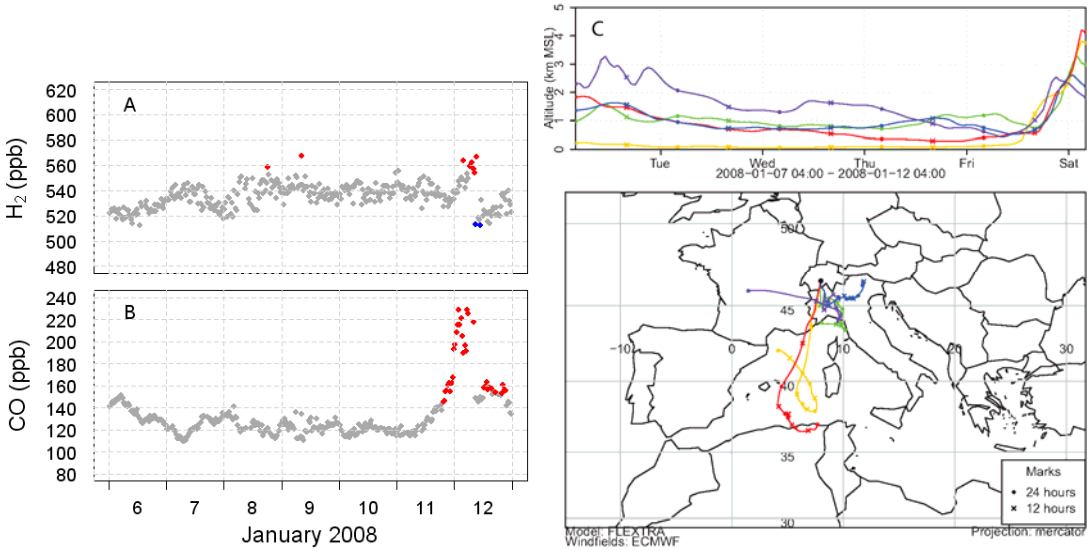

Figure 37. Seven-day time series of H_2 (panel A) and CO (panel B) mixing ratios illustrating a pollution event on January 12, 2008. The grey filled circles correspond to background measurements, the red filled circles to pollution, and the blue filled circles to depletion measurements — all based on the 2D-REBS filter algorithm. The corresponding 5-day backward trajectories arriving at Jungfraujoch at 0400 on January 12, 2008 are depicted in panel C. Different colors represent different arrival altitudes between 2 and 4 km a.s.l.

When the situation at Jungfraujoch is more strongly influenced by larger-scale advection of air masses that have spent a relatively long period of time within the ABL above major land mass regions (with less distinct H_2 emissions), soil deposition becomes increasingly influential. Under these circumstances, events involving CO pollution can be observed in the absence of H_2 pollution, or even depleted H_2 mixing ratios (Fig. 38). Such situations are observed more frequently than the conditions described above, pointing to the dominance of soil uptake during the transport of air masses to the measurement site.

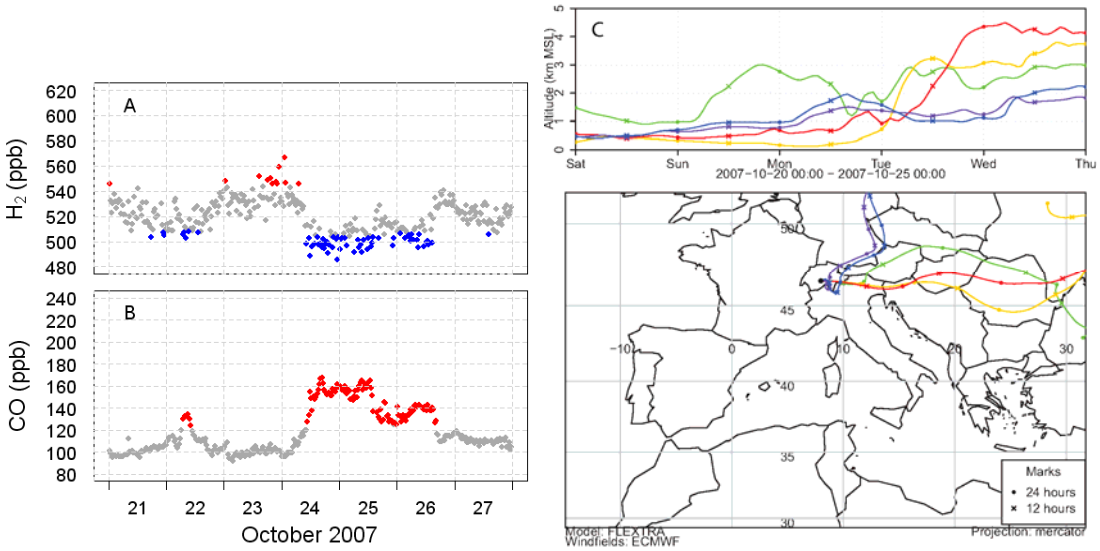

Figure 38. Seven-day time series of H_2 (panel A) and CO (panel B) mixing ratios illustrating a CO pollution event on October 24–26, 2007 with corresponding decrease in background H_2 mixing ratios. The corresponding 5-day backward trajectories (panel C) arriving at Jungfraujoch at 0000 on October 25, 2007. See also caption of Fig. 37 for details.

A few times per year, enhanced H_2 mixing ratios with simultaneous drops in other trace gas mixing ratios are observed when air masses originating from southerly latitudes arrive at Jungfraujoch. This feature is due to the unusual interhemispheric distribution of H_2 (Southern Hemisphere mixing ratios are greater than in the Northern Hemisphere). The most prominent example occurred on October 1, 2005, when clean maritime air masses from the southern North Atlantic reached Jungfraujoch without major land contact over Europe or Africa (Fig. 39). This pattern of reduced mixing ratios in many anthropogenic trace gases and simultaneous enhancement of H_2 is unique to southerly advection. Stratospheric air mass descents to Jungfraujoch would produce depleted mixing ratios for most anthropogenic compounds. However, since H_2 varies negligibly with altitude throughout the upper troposphere and stratosphere [122], enhanced H_2 mixing ratios can serve as an effective tracer for southerly advection.

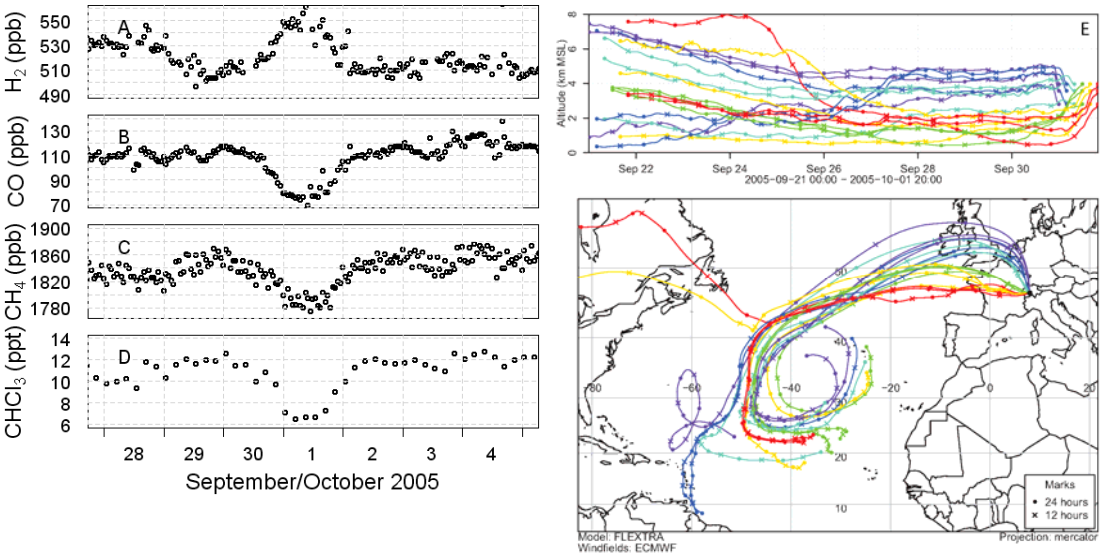

Figure 39. Seven-day time series of H_2 (panel A), CO (panel B), CH_4 (panel C), and $CHCl_3$ (panel D) mixing ratios illustrating a depletion event for the latter gases on October 1, 2005 with simultaneous enhancement in ambient H_2. Panel E illustrates the corresponding 10-day backward trajectories arriving at Jungfraujoch on 01.10.2005. Different colors represent different arrival altitudes and times.

5.3 H_2 pollution events and ratios of excess H_2 to excess CO

Periodically, air masses polluted by anthropogenic sources reach Jungfraujoch. A strong seasonality effect in the mean ABL residence time of air masses attaining Jungfraujoch exists (Fig. 40). ABL residence times over the continent for the period 2005–2008 were calculated from 10-day air mass back-trajectories arriving at Jungfraujoch (FLEXTRA/ECMWF trajectories, see section 2.3.3). An air mass was considered to reside in the ABL when the trajectory altitude above the surface was below the climatological average ABL depth. Summer months displayed more frequent ABL contact with mean monthly residence times of up to 15 hours. This ABL contact time is three to four times as long as during the winter months when ABL contact was infrequent (less than 20%). Additionally, vertical transport of ABL air in thermally-induced circulations that are not fully captured by the trajectory calculations are more common in summer [123, 124], further increasing the seasonal distinction between ABL influenced observations in summer and free tropospheric conditions in winter. With longer residence times close to the surface allowing an enhanced loading of H_2 and CO pollution, these processes alone would suggest that the summer months should display the most frequent and also the strongest pollution events at Jungfraujoch. For H_2, the highest frequency of pollution events in the

summer months was indeed observed (with the exception of January due to an exceptionally high number of pollution events during that month in 2006). However, a pronounced seasonality effect in the magnitude of the H_2 pollution events was not observed. It is speculated that the strong soil sink may be responsible for the absence of large-magnitude pollution events and that there is a resulting compensatory source-sink effect in the ABL (i.e. strong soil sink during warmer months is offset by concurrent surface loading of pollution in the ABL). Following a more quantitative assessment of the H_2 and CO pollution characteristics at Jungfraujoch in the next paragraphs, a rough calculation regarding the effect of soil uptake is then provided in Section 5.4 to support this speculation.

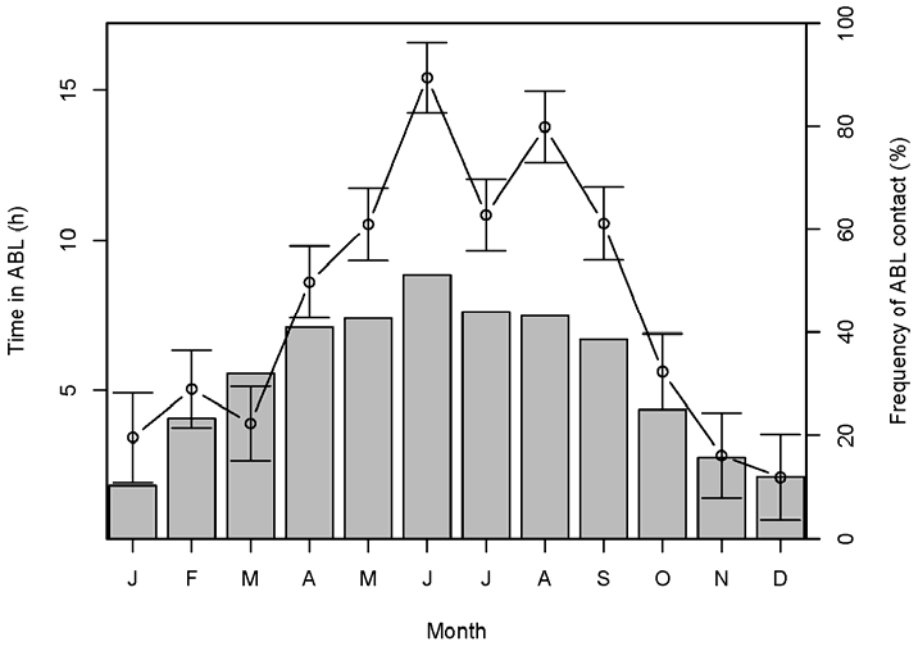

Figure 40. Monthly mean atmospheric boundary layer residence times (curve referring to left y-axis) and its 95 % confidence levels (error-bars; log-normal statistics) calculated from 10-day back trajectories arriving at Jungfraujoch. Bars (right y-axis) give the frequency of ABL influenced trajectories.

Combined investigation of H_2 and CO pollution assists in the understanding of their common sources (e.g. gasoline-powered road-based transportation), along with the upscaling of H_2 emissions against the much more widely known CO emission inventories. For the discussion of pollution, excess H_2 (ΔH_2) has been defined as the H_2 mixing ratio minus the corresponding baseline value. Excess CO (ΔCO) is defined analogously. For measurements in urban and suburban locations, the $\Delta H_2/\Delta$CO is dominated by that of gasoline engine exhaust (see section 3.2.3). These ratios have typically displayed a range of ~0.3–0.5 [21, 33, 44-46]. For more remote stations,

such as Mace Head, the $\Delta H_2/\Delta CO$ is much lower at 0.15–0.18 [25, 26], and the extraction of the anthropogenic $\Delta H_2/\Delta CO$ source signature is more complicated. For Jungfraujoch, the $\Delta H_2/\Delta CO$ relationship was also investigated since it might allow retrieving representative numbers for an aggregate of sources over large parts of Central Europe due to the massive footprint observed at Jungfraujoch. The results must be treated with caution, however, because they depend significantly on the data selections and the type of fitting routine. A least-squares fitting technique was ultimately selected, fitexy [125], which takes the uncertainties of both H_2 and CO data into account. Had a standard linear regression been applied, too much weight would have been put on the high-end extreme values, which would have had too much influence on the slope of the curve, and thus led to less representative results.

$\Delta H_2/\Delta CO$ was found to be 0.324±0.005 (R^2=0.142) when selecting above-background data (red filled circles in Fig. 41). For this calculation, only data when both H_2 and CO were above the grey band in Fig. 34 (baseline plus 2σ) were selected, but the Δ-values used are the differences of the measured values from the baseline fit. This data selection is dependent on the width of the background dataset and also excludes data for which one of the two compounds in not elevated (e.g. elevated CO and depleted H_2). This $\Delta H_2/\Delta CO$ (~1140 data points) is similar to urban measurements, presumably because the data selection process limits the dataset to pollution events that are likely derived from air masses rapidly transported to Jungfraujoch without significant H_2 soil removal or mixing with background air. The poor correlation between ΔH_2 and ΔCO (R^2=0.142) and the relatively high y-axis intercept (~26 ppb) illustrate that this $\Delta H_2/\Delta CO$ ratio must be interpreted with caution.

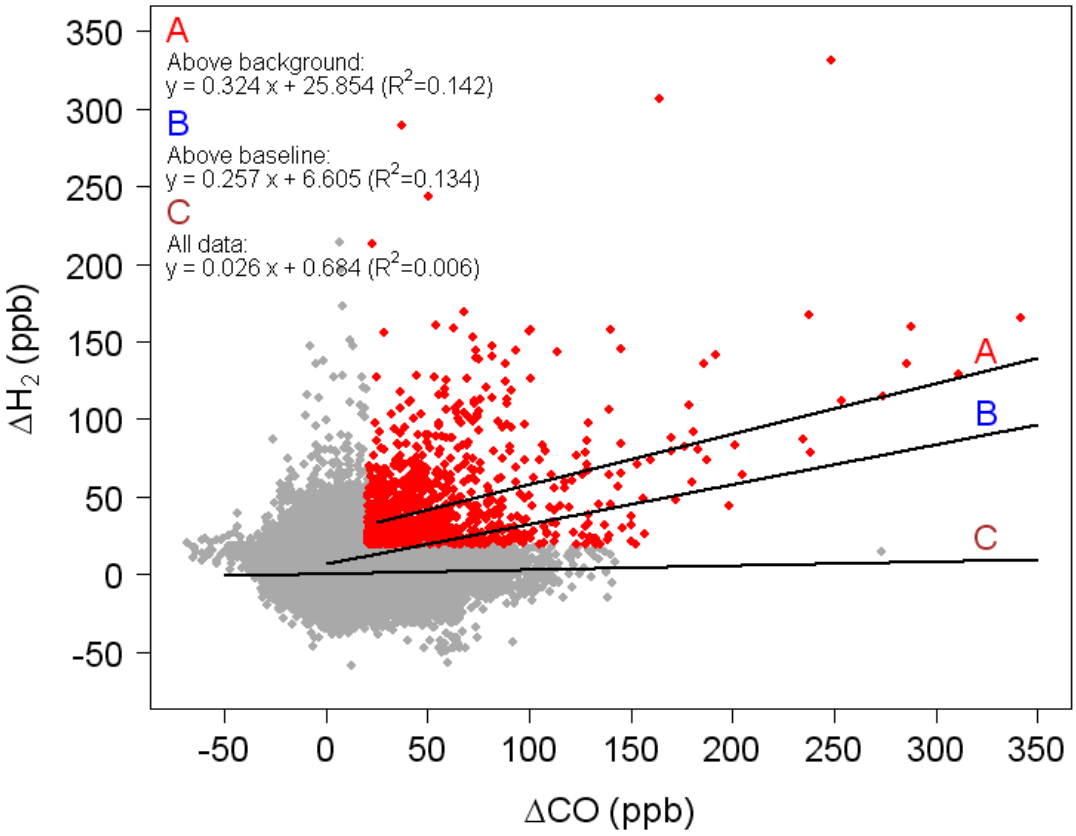

Figure 41. Excess (mixing ratio minus corresponding baseline value) H_2 (ΔH_2) and CO (ΔCO) at Jungfraujoch. The red filled circles correspond to the above-background (pollution) data. Linear regressions are shown as solid lines. The colour-coded regressions refer to the separate datasets.

If all above-baseline data is selected, the $\Delta H_2/\Delta CO$ is 0.257±0.002 (R^2=0.134). This relationship not only captures the pollution (above background) events, but also includes the enhanced events of both H_2 and CO within the upper half of the grey background band. If the entire dataset is then chosen, a $\Delta H_2/\Delta CO$ of 0.026±0.001 with essentially no correlation between the two trace gases (R^2=0.006) results. Nevertheless, these results qualitatively confirm the decreasing $\Delta H_2/\Delta CO$ ratio with increasing distance from the anthropogenic source, but also illustrate the difficulties and dependencies on the data selection for such ratios (Fig. 41). The lack of a correlation between ΔH_2 and ΔCO is attributed to variable H_2 removal by soil. A rough estimate for this removal process is provided in the following sub-section.

5.4 Soil uptake assessment

A method involving 222-radon measurements has recently been proposed to remove the influence of the soil sink from the $\Delta H_2/\Delta CO$ ratio in urban/sub-urban environments [45]. This method can not be applied to the Jungfraujoch data due to the lack of a correlation in the observed $\Delta H_2/\Delta CO$ ratio. To evaluate the possible influence of H_2 soil deposition on the H_2 mixing ratios during air mass ascent to Jungfraujoch, an approximative calculation was made that focuses on assessing the magnitude of the H_2 removal by soil during the warmer and drier months of the year. An initial air mass with a characteristic molar $\Delta H_2/\Delta CO$ ratio of 0.45–0.48 in polluted environments [45] is first considered. Typical transport times to Jungfraujoch of 8 hours, an up-valley wind layer height of 100 m [114], negligible CO deposition, a H_2 deposition velocity of 1×10^{-4} m s^{-1}, and background conditions of 520 ppb and 90 ppb for H_2 and CO, respectively, were assumed. Based on these assumptions a $\Delta H_2/\Delta CO$ of 0.35–0.38 upon arrival at Jungfraujoch is found. This ratio is only slightly higher than the observed $\Delta H_2/\Delta CO$ of 0.324±0.005 (see Section 5.3) for polluted air masses. However, given the uncertainties in the assumptions, it suggests that soil deposition can at least partially explain the observed ratios at Jungfraujoch. Other processes such as photochemistry during transport or entrainment of air masses could also influence the $\Delta H_2/\Delta CO$ at Jungfraujoch.

The key role of soil deposition also becomes apparent when considering the residence times in the boundary layer for the different sub-sets of the H_2 data (i.e. pollution, background, and depletion). Whereas the median residence time in the boundary layer within the last 96 hours prior to arrival at Jungfraujoch for the whole data set is 12.8 hours, the residence times of the sub-sets for pollution, background, and depletion are 10.3 hours, 12.7 hours and 35.3 hours, respectively. This indicates that a strong boundary layer influence favours low H_2 mixing ratios in contrast to most of the other trace gases observed at the high-altitude site.

5.5 Summary

The work associated with the Jungfraujoch aspect of this study has provided a first insight into the characterization of atmospheric molecular H_2 at a site primarily characteristic of the free troposphere, along with the key processes that lead to the observed free tropospheric mixing ratios. Highest background H_2 mixing ratios were observed in May, while the lowest were observed a few months later in November. The seasonal minimum in November was comparatively delayed with other stations at similar latitudes, and the peak-trough amplitude of 21 ppb was less pronounced compared to that of lower elevation sites. These differences suggest that a dampening and delay of the surface soil sink signal occur during its vertical propagation to the free troposphere, and that the delay and decreasing peak-trough amplitude with altitude become more distinct through a combination of increasing distance from the source and greater vertical transport time. Further research in these areas at both high and low altitude stations would help to further develop this hypothesis.

The specific case studies have revealed that H_2 mixing ratios at Jungfraujoch are influenced by a number of factors including advection of air masses with latitudinally variable background H_2 mixing ratios, the influence of the ABL on H_2 emissions, and H_2 depletion by soil uptake during the ascent of air masses the observatory. Measurements of $\Delta H_2/\Delta CO$ at Jungfraujoch often display lower ratios compared to the ~0.5 from past traffic combustion studies, a discrepancy most likely caused by a compensatory effect between pollution loading and the strong H_2 soil sink. The largest of these compensatory effects occurs in summer when air masses have the longest contact time with the ABL before reaching Jungfraujoch. At that time, pollution loading is strongest, but the soil sink activity is also optimal. A simple box model calculation revealed that soil uptake can at least partially explain the lower $\Delta H_2/\Delta CO$ ratios at Jungfraujoch compared to ratios observed at less remote sites.

Jungfraujoch is situated in a favourable location (central Europe) for studying H_2 in the free troposphere. The suitability of the site enables the investigation of transport processes from the ABL to the free troposphere, free tropospheric transport, and their effects on H_2 mixing ratios. Some of the advantages of continuous measurements have been elucidated. Whereas flask sampling is an appropriate course for evaluating

trends and the influence of increasing H_2-based applications on baseline mixing ratios, continuous measurements provide an extended benefit when features such as specific sources, sinks, and transport phenomena are of interest. The lengthening of the time series into the future would allow more reliable trend estimates and enable the investigation of the effects of a more H_2-intensive economy, including the amount of time for the atmospheric system to respond to disturbances (e.g. increased emissions) of the current source-sink equilibrium. Future trend analysis at Jungfraujoch should therefore serve as a robust indicator for assessing the behaviour of H_2 as the fraction of mobile- and stationary-based H_2 applications increases.

6 GENERAL CONCLUSIONS AND OUTLOOK

The work covered throughout this project has provided new knowledge and insights into several aspects of molecular H_2, particularly as it relates to the major anthropogenic sources from technological processes (i.e. road-based transportation, leakage and losses from production, distribution, storage, and other non-transport-based end-uses, and important source regions of tropospheric H_2). Direct measurements of H_2 taken directly at the individual-vehicle source have provided the information necessary to characterize — for the first time — specific characteristics of single vehicles that lead to the emission of H_2 in exhaust gas. The quantitative aspect of such measurements has enabled the comparison of absolute emissions between the different vehicle and fuel types, and their subsequent application in the upscaling of H_2 emissions from road-based transportation based on individual-vehicle emission factors. These results, coupled with leakage and losses of non-transport-based H_2 emissions, has facilitated the development of quantitative scenarios based on a number of different pathways between 2010 and 2100. These pathways were developed using different climate policy options, changing vehicle fleet compositions, vehicle emissions, and H_2 production strategies for both industrial and direct energy-based end-uses. Further to the aspects of individual-vehicle emissions and large-scale upscaling of H_2 emissions, it was found that atmospheric measurements at remote high-altitude sites are valuable for analysing the behaviour of H_2 in the free troposphere, in addition to determining the contribution from important source regions. One of the major advantages of measurements at such sites is the ability to identify and monitor trends in background H_2 mixing ratios, which will become increasingly relevant as the dataset lengthens, particularly as the fraction of H_2-based applications potentially increases.

Chassis dynamometer measurements provide detailed emissions information for individual vehicles based on a variety of common driving conditions. The dynamometer component of this study focused on specific qualitative and quantitative aspects of the production and emission of H_2 from fossil fuel-powered vehicles, which provided an initial basis and understanding of the processes involved with H_2 emissions evolving directly at the source. It was found that H_2 emissions in the exhaust gas of individual fossil fuel-powered vehicles arise from several interrelated

factors, including the presence/absence of a catalytic converter, the vehicle type and fuel used to power the vehicle, the state at which the engine is operated, the quality of lambda control, and the temperature of the engine and catalyst at vehicle start up. These characteristics form the basis, and ultimately dictate the magnitude, of quantifying H_2 emissions.

Emissions from the fossil fuel-powered vehicles measured on a chassis dynamometer were then quantified, both through the calculation of H_2 emission factors and cumulative H_2/CO ratios. It was found that, of the vehicles measured in this study, emissions from 2-wheelers (motorcycles and scooters) far exceeded those of any other single technology — approximately 5 times more in absolute terms than gasoline-powered automobiles and approximately twice the emissions of natural gas-powered automobiles under the same driving conditions. Diesel vehicles consistently emitted marginal, often undetectable levels of H_2 due to the constantly oxidizing operating point at which diesel engines function. Given their significance in both an atmospheric context and the strong positive correlation in the exhaust gas of gasoline-based road-transportation, the cumulative H_2/CO ratios from the gasoline-powered vehicles were also evaluated in detail. H_2/CO ratios from vehicles measured in this study were typically higher than those reported in previous studies, from which the results were typically characteristic of entire vehicle fleets consisting of older vehicles and less developed technologies. The higher ratios in this study had to do with the generally fewer fuel-rich episodes with the newer vehicles tested in this study, as fuel-rich excursions occur much more frequently with older vehicle technologies, and typically result in a higher proportion of CO emissions compared to H_2. The newer technology vehicles characteristic of this study were also equipped with newer generation TWCs, which promote water-gas shift activity, meaning that residual H_2 is produced, while some additional CO is simultaneously destroyed. H_2/CO ratios, coupled with H_2 emission factors from the exhaust gas of gasoline-powered vehicles, played an important role in this study in the global upscaling of H_2 emissions from road-based transportation.

The global upscaling of H_2 emissions from anthropogenic sources in this study involved developing quantitative scenarios — based on a baseline (business-as-usual) climate strategy and a stringent strategy aimed at stabilizing atmospheric CO_2 mixing

ratios at 450 ppm — for different time periods throughout the 21st century. Quantitative scenarios were based on emissions from road-based transportation and leakage and losses of H_2 from production, distribution, storage, and other non-transport-based end-uses. Leakage and loss rates of H_2 to the atmosphere from anthropogenic processes vary according to the state of the H_2 (LH_2 or GH_2), the methods of production, storage, and delivery, end-use, and according to the assumptions made or facts known about the loss rates. Although a more H_2-intensive economy would involve a significantly larger volume of hydrogen as an energy carrier, loss rates of H_2 to the atmosphere are not unanimously expected to increase considerably. On the contrary, it could be anticipated that leakage and losses actually decline as the maturity of the hydrogen chain develops, and some of the quantitative scenarios in this work have shown this.

According to this study, overall H_2 emissions from vehicle exhaust and other non-transport-based leakage and losses should remain either below or within the range of overall anthropogenic H_2 emissions estimated for 2010. Should exceptions occur, they would most likely occur towards the end of the century. Throughout the first half of the 21st century, neither policy mechanisms aimed at addressing climate objectives, nor the variable makeup of global vehicle fleets largely govern overall H_2 emissions to the atmosphere. Instead, emissions from 2-wheelers (at least until 2020) and high-end well-to-use losses from non-transport-based end-uses are primary factors influencing the global atmospheric abundance of anthropogenic H_2 from technological processes. Towards the end of the 21st century, overall technological anthropogenic H_2 emissions will depend largely on the extent to which leakage and other well-to-use losses are controlled, along with H_2 emissions from FCVs.

One of the important findings of this study is that H_2 emissions from FCVs alone are unlikely to lead to levels of atmospheric H_2 that exceed current conditions, and hence potentially upset the balance of the global H_2 budget. Under a potentially worst-case scenario of a mean FCV E_{H2} of 265 mg km^{-1} in 2100, FCVs would be responsible for a significant increase in H_2 emissions compared with current estimations. With a much lower, and likely more realistic FCV E_{H2} of 26.5 mg km^{-1} for FCVs in 2100, overall anthropogenic H_2 emissions would only exceed current levels under estimated worst-case leakage and loss rate levels. With a mean FCV E_{H2} of 26.5 mg km^{-1} in

2100, a corresponding average leakage and loss rate of 0.5% would result in overall H_2 emissions to the atmosphere approximately double those of 2010. On the other hand, should the mean FCV E_{H2} be an order of magnitude higher in 2100 at 265 mg km^{-1}, overall anthropogenic H_2 emissions would be roughly 1.5–3 times higher that 2010 conditions with the range of leakage and loss rates estimated to be representative of 2100 conditions. Under the 450 ppm CO_2 climate policy scenario, and based on a non-transport-based leakage rate range of 0.01–0.1% in 2100, overall anthropogenic (as the sum of transportation and non-transport-based end-uses) H_2 emissions to the atmosphere should be at worst comparable with today's anthropogenic source of H_2 should the mean FCV E_{H2} not exceed ~135 mg km^{-1}.

Continuous H_2 observations at Jungfraujoch have greatly expanded the knowledge base of the behaviour of H_2 in the unpolluted free troposphere above a continental region. The temporal variability has been analysed through the determination of seasonal cycles of background H_2 mixing ratios. These findings revealed that the seasonal minimum is delayed by ~1 month compared to other sites at similar latitude and that the amplitude (difference between the mean maximum mixing ratio in spring and the mean minimum mixing ratio in autumn) was considerably less than at other sites of similar latitude. These findings are attributed to the dominant soil sink influencing the continental background site. The identification of major source regions was another aspect of this study that revealed new information about not only the source regions themselves, but also of the processes involved during transport to the high Alpine region. These processes included advection of air masses with latitudinally variable background H_2 mixing ratios, the influence of H_2 emissions in the atmospheric boundary layer, and H_2 depletion by soil uptake during transport to the sampling site.

In the context of a transition to a future economy more reliant on H_2-based mobile and stationary applications (e.g. fuel cell vehicles, industrial, commercial, and residential heat and power), the identification of important source regions should provide useful information into the extent to which such a transition is influencing atmospheric H_2 mixing ratios. As many of the general characteristics and behaviours of H_2 in the free troposphere have already been evaluated in this study, perhaps the most beneficial aspect of such measurements in the future will be the identification of long-

term trends in background H_2 measurements. Currently, the dataset at Jungfraujoch is too short to draw any concrete conclusions about recent trend developments. However, the lack of a distinct trend over the past 4–5 years observed in this study is broadly in line with many other studies that have performed trend analysis around the globe. This would suggest that the current measurements at Jungfraujoch will act as a baseline starting point for current conditions, to which future measurements can be compared.

To further the work in this field, a number of specific areas could be addressed. First, direct exhaust measurements of H_2 from vehicles not directly measured in this study, such as various hybrid vehicles, biofuels vehicles, and a series of road-ready H_2 fuel cell vehicles, would be beneficial. Such measurements would facilitate the assessment of H_2 emissions from these vehicle types under a variety of common driving conditions. In addition, such measurements would provide the ability to apply direct H_2 emission factors in the local, regional, or global upscaling of H_2 emissions. Although the application of H_2/CO ratios in this study is a robust means of determining H_2 emission factors for the gasoline-powered vehicles, direct measurements and the subsequent application of emission factors from gasoline-powered vehicles would provide a more precise method of approaching this problem. Moreover, for emerging technologies, such as hybrid electric vehicles, biofuels vehicles, and additional H_2 fuel cell vehicles, chassis dynamometer measurements would provide further information into the processes involved in their direct emissions of H_2, in addition to the information required for the calculation of emission factors from such vehicles. These additional measurements would eliminate the requirement of assumptions, such as reductions in fuel consumption, for the calculation of H_2 emission factors for such vehicles.

Second, scenarios for specific environmental and climatic impacts could be developed based on the H_2 emissions scenarios presented in this study, or other independently developed detailed scenarios, through the application of a global chemistry transport model. Such a project would provide an update to past modelling studies and would benefit from a quantitative evaluation of changing tropospheric (and stratospheric) H_2 mixing ratios on levels of tropospheric greenhouse gases (e.g. CO_2, CH_4, and O_3), along with the influence on stratospheric H_2O mixing ratios and O_3 levels. From this

information, scenarios could be developed that would detail the specific environmental and ecological impacts associated with the fluctuation of these climate gases, or the impact on stratospheric ozone based on changing stratospheric H_2O content.

Third, soil sink studies that deal specifically with fluctuations in atmospheric H_2 mixing ratios, and particularly with potentially large-scale increases, would be an area worth pursuing. An important question still eluding this field of study is how the soil oxidation processes would respond to changing, and potentially increasing levels of tropospheric H_2 as hydrogen potentially begins fuelling increasing numbers of vehicles and other H_2-based systems. Soil oxidation represents the most significant H_2 sink, and is the single most influential term in the global H_2 budget. Such a study would benefit from a large number of experiments, which would include a quantitative analysis of e.g. many different soil types, variable ambient temperatures, soil moisture content, elevations, etc., under a variety of atmospheric H_2 mixing ratios. Then, using global soil distribution maps, global soil uptake could be approximated based on known global climate zones and the H_2 production scenarios developed in this study (i.e. for global road-based transportation and global H_2 production). This topic could become an entire project of its own.

Fourth, as was shown in this study, measurements at remote high-altitude sites provide a wealth of information regarding the behaviour of H_2 at locations far removed from sites influenced by local sources and sinks. The dataset at the high-altitude site Jungfraujoch in this study provides observations for the slightly more than 4-year period from August, 2005 – November, 2009. These measurements have provided detailed information regarding the temporal behaviour of H_2 at a site primarily characteristic of the free troposphere, while illustrating the contribution of H_2 from important source regions. Although the dataset offered in this study precludes the concrete interpretation of any trends in background H_2 mixing ratios, the measurements will become increasingly adapted to such trend analyses as the dataset lengthens. It is therefore recommended to monitor H_2 at remote sites and apply the results to identify any trends in background measurements as H_2-based mobile and stationary applications become more abundant. In addition to trend analyses, periodic updates of the measurements and analyses performed in this study would help further

investigate the (potentially changing) roles of the local and regional sources and sinks during the transition to a potentially more H_2-intensive economy.

REFERENCES

[1] Gül T, Turton H, Kypreos S, Barreto L. Long-term scenarios of the global energy and transport system. In: Wilhelm E, Wokaun A, editors. Transition to Hydrogen: Pathways Toward Clean Transportation, Cambridge University Press; submitted.

[2] Pant KK, Gupta RB. Fundamentals and use of hydrogen as a fuel. In: Gupta RB, editors. Hydrogen Fuel: Production, Transport, and Storage, Boca Raton: CRC Press, Taylor & Francis Group; 2009.

[3] Hočevar S, Summers W. Hydrogen production. In: Léon A, editors. Hydrogen Technology Mobile and Portable Applications, Berlin: Springer-Verlag; 2008.

[4] Turner J, G. S, Mann MK, Maness P-C, Kroposki B, Ghirardi M, Evans RJ, Blake D. Renewable hydrogen production. International Journal of Energy Research 2008; 32: 379-407.

[5] Gül T. An Energy-Economic Scenario Analysis of Alternative Fuels for Transport. Unpublished Ph.D. Thesis: Swiss Federal Institute of Technology, Zurich (Available at: http://e-collection.ethbib.ethz.ch), 2008.

[6] Derwent RG, Collins WJ, Johnson CE, Stevenson DS. Transient behaviour of tropospheric ozone precursors in a global 3-D CTM and their indirect greenhouse effects. Climatic Change 2001; 49: 463-87.

[7] Schultz MG, Diehl T, Brasseur GP, Zittel W. Air pollution and climate-forcing impacts of a global hydrogen economy. Science 2003; 302: 624-7.

[8] Stephens-Romero S, Carreras-Sospedra M, Brouwer J, Dabdub D, Samuelsen S. Determining air quality and greenhouse gas impacts of hydrogen infrastructure and fuel cell vehicles. Environmental Science & Technology 2009; 43: 9022-9.

[9] Tromp T, Shia R, Allen M, Eiler JM, Yung YL. Potential environmental impact of a hydrogen economy on the stratosphere. Science 2003; 300: 1740-2.

[10] Warwick NJ, Bekki S, Nisbet EG, Pyle JA. Impact of a hydrogen economy on the stratosphere and troposphere studied in a 2-D model. Geophysical Research Letters 2004; 31: doi:10.1029/2003GL019224.

[11] Derwent RG, Simmonds P, O'Doherty S, Manning A, Collins W, Stevenson D. Global environmental impacts of the hydrogen economy. International Journal of Nuclear Hydrogen Production and Application 2006; 1: 57-67.

[12] Prather MJ. An environmental experiment with H_2? Science 2003; 302: 581-2.

[13] Hauglustaine DA, Ehhalt DH. A three-dimensional model of molecular hydrogen in the troposphere. Journal of Geophysical Research 2002; 107: 4330, doi:10.1029/2001JD001156.

[14] Forster P, Ramaswamy V, Artaxo P, Berntsen T, Betts R, Fahey DW, Haywood J, Lean J, Lowe DC, Myhre G, Nganga J, Prinn R, Raga G, Schulz M, Van Dorland R. Changes in Atmospheric Constituents and in Radiative Forcing. Cambridge, United Kingdom and New York, NY, USA: Cambridge University Press; 2007.

[15] Lovins AB. Letters: Assessing the future hydrogen economy. Science 2003; 302: 226-9.

[16] Ehhalt DH, Rohrer F. The tropospheric cycle of H_2: A critical review. Tellus B 2009; 61: 500-35.

[17] Rohs S, Schiller C, Riese M, Engel A, Schmidt U, Wetter T, Levin I, Nakazawa T, Aoki S. Long-term changes of methane and hydrogen in the stratosphere in the period 1978-2003 and their impact on the abundance of stratospheric water vapor. Journal of Geophysical Research 2006; 111: doi:10.1029/2005JD006877.

[18] Novelli PC, Lang PM, Masarie KA, Hurst DF, Myers R, Elkins JW. Molecular hydrogen in the troposphere: Global distribution and budget. Journal of Geophysical Research 1999; 104: 30427-44.

[19] Paneth FA. The chemical composition of the atmosphere. Quarterly Journal of the Royal Meteorological Society 1937; 63: 433-43.

[20] Schmidt U. Molecular hydrogen in the atmosphere. Tellus 1974; 26: 78-90.

[21] Steinbacher M, Fischer A, Vollmer MK, Buchmann B, Reimann S, Hueglin C. Perennial observations of molecular hydrogen (H_2) at a suburban site in Switzerland. Atmospheric Environment 2007; 41: 2111-24.

[22] Warneck P. Chemistry of the natural atmosphere. San Diego: Academic Press, Inc.; 1988.

[23] Weilenmann M, Favez J-Y, Alvarez R. Cold-start emissions of modern passenger cars at different low ambient temperatures and their evolution over vehicle legislation categories. Atmospheric Environment 2009; 43: 2419-29.

[24] Barnes DH, Wofsy SC, Fehlau BP, Gottlieb EW, Elkins JW, Dutton S, Novelli PC. Hydrogen in the atmosphere: Observations above a forest canopy in a polluted environment. Journal of Geophysical Research 2003; 108: 4197, doi:10.1029/2001JD001199.

[25] Simmonds PG, Derwent RG, O'Doherty S, Ryall DB, Steele LP, Langenfelds RL, Salameh P, Wang HJ, Dimmer CH, Hudson LE. Continuous high-frequency observations of hydrogen at the Mace Head baseline atmospheric monitoring station over the 1994-1998 period. Journal of Geophysical Research 2000; 105: 12105-21.

[26] Grant A, Witham CS, Simmonds PG, Manning AJ, O'Doherty S. A 15 year record of high-frequency, in situ measurements of hydrogen at Mace Head, Ireland. Atmospheric Chemistry and Physics 2010; 10: 1203-14.

[27] Langenfelds RL, Francey RJ, Pak BC, Steele LP, Lloyd J, Trudinger CM, Allison CE. Interannual growth rate variations of atmospheric CO_2 and its $\delta^{13}C$, H_2, CH_4, and CO between 1992 and 1999 linked to biomass burning. Global Biogeochemical Cycles 2002; 16: 1048, doi:10.29/2001GB001466.

[28] Khalil MAK, Rasmussen RA. Global increase in atmospheric molecular hydrogen. Nature 1990; 347: 743-5.

[29] Price H, Jaeglé L, Rice A, Quay P, Novelli PC, Gammon R. Global budget of molecular hydrogen and its deuterium content: Constraints from ground station, cruise, and aircraft observations. Journal of Geophysical Research 2007; 112: doi:10.1029/2006JD008152.

[30] Rhee TS, Brenninkmeijer CAM, Röckmann T. The overwhelming role of soils in the global atmospheric hydrogen cycle. Atmospheric Chemistry and Physics 2006; 6: 1611-25.

[31] Sanderson MG, Collins WJ, Derwent RG, Johnson CE. Simulation of global hydrogen levels using a Lagrangian three-dimensional model. Journal of Atmospheric Chemistry 2003; 46: 15-28.

[32] Xiao X, Prinn RG, Simmonds PG, Steele LP, Novelli PC, Huang J, Langenfelds RL, O'Doherty S, Krummel PB, Fraser PJ, Porter LW, Weiss RF, Salameh P, Wang RHJ. Optimal estimation of the soil uptake rate of molecular hydrogen from the Advanced Global Atmospheric Gases Experiment and other measurements. Journal of Geophysical Research 2007; 112: doi:10.1029/2006JD007241.

[33] Vollmer MK, Juergens N, Steinbacher M, Reimann S, Weilenmann M, Buchmann B. Road vehicle emissions of molecular hydrogen (H_2) from a tunnel study. Atmospheric Environment 2007; 41: 8355-69.

[34] Fulton L, Eads G. IEA/SMP Model Documentation and Reference Case Projection. Auxilliary material to: Mobility 2030: Meeting the challenges to sustainability; The Sustainable Mobility Project. IEA/CRA (Available at: www.wbcsd.org/web/publications/mobility/smp-model-document.pdf); 2004.

[35] Alvarez R, Weilenmann M, Favez J-Y. Assessing the real-world performance of modern pollutant abatement systems on motorcycles. Atmospheric Environment 2009; 43: 1503-9.

[36] Vasic A-M, Weilenmann M. Comparison of real-world emissions from two-wheelers and passenger cars. Environmental Science & Technology 2006; 40: 149-54.

[37] Beijing Traffic Management Bureau. The Statistics of China's Motor Vehicles and Drivers in 2008. 2009 [cited August 12, 2009]; Available from: http://www.bjjtgl.gov.cn/publish/portal1/tab165/info9910.htm.

[38] MOTC. An Introduction to the Transportation and Communications in the Republic of China. Ministry of Transportation and Communications; 2008.

[39] Vollmer MK, Walter S, Bond SW, Soltic P, Röckmann T. Molecular hydrogen (H_2) emissions and their isotopic signatures (H/D) from a motor vehicle: implications on atmospheric H_2. Atmospheric Chemistry and Physics 2010; 10: 5707-18.

[40] Auckenthaler TS. Modelling and Control of Three-Way Catalytic Converters. Unpublished Ph.D. Thesis. Swiss Federal Institute of Technology (ETHZ), Zürich: Swiss Federal Institute of Technology, Zurich (Available at: http://e-collection.ethbib.ethz.ch), 2005.

[41] Poulopoulos SG, Philippopoulos CJ. MTBE, methane, ethylene and regulated exhaust emissions from vehicles with deactivated catalytic converters. Atmospheric Environment 2004; 38: 4495-500.

[42] Shamim T. The effect of oxygen storage capacity on the dynamic characteristics of an automotive catalytic converter. Energy Conversion and Management 2008; 49: 3292-300.

[43] Taylor KC. Automobile catalytic converters. In: Anderson JR, Boudart M, editors. Catalysis - Science and Technology, Berlin: Springer-Verlag; 1984.

[44] Aalto T, Lallo M, Hatakka J, Laurila T. Atmospheric hydrogen variations and traffic emissions at an urban site in Finland. Atmospheric Chemistry and Physics 2009; 9: 7387-96.

[45] Hammer S, Vogel F, Kaul M, Levin I. The H_2/CO ratio of emissions from combustion sources: comparison of top-down with bottom-up measurements in southwest Germany. Tellus 2009; 61B: 547-55.

[46] Yver C, Schmidt M, Bousquet P, Zahorowski W, Ramonet M. Estimation of the molecular hydrogen soil uptake and traffic emissions at a suburban site near Paris through hydrogen, carbon monoxide and radon-222 semi-continuous measurements. Journal of Geophysical Research 2009; 114: doi:10.1029/2009JD012122.

[47] Heeb NV, Saxer CJ, Forss A, Brühlmann S. Correlation of hydrogen, ammonia and nitrogen monoxide (nitric oxide) emissions of gasoline-fueled Euro-3 passenger cars at transient driving. Atmospheric Environment 2006; 40: 3750-63.

[48] CEH. Marketing Research Report - Hydrogen. Menlo Park, CA: Chemical Economics Handbook (CEH) - SRI Consulting; 2007.

[49] Ogden JM. Hydrogen as an energy carrier: Outlook for 2010, 2030 and 2050. The 10-50 Solution: Technologies and Policies for a Low-Carbon Future, 2004.

[50] Lovins AB. Twenty hydrogen myths. Boulder, Colorado: Rocky Mountain Institute; 2005.

[51] Burns LD, McCormick JB, Borroni-Bird CE. Vehicle of Change. Scientific American 2002; 40-9.

[52] de Wit MP, Faaig APC. Impact of hydrogen onboard storage technologies on the performance of hydrogen vehicles: A techno-economic well-to-wheel assessment. International Journal of Hydrogen Energy 2007; 32: 4859-70.

[53] Kammen DM, Lipman TE. Letters: Assessing the future hydrogen economy. Science 2003; 302: 226-9.

[54] Schlapbach L, Züttel A. Hydrogen-storage materials for mobile applications. Nature 2001; 414: 353-8.

[55] Sherif SA, Zeytotinoglu N, Veziroglu TN. Liquid hydrogen: Potential, problems, and a proposed research program. International Journal of Hydrogen Energy 2007; 22: 683-8.

[56] Zittel W, Altmann MA. Molecular hydrogen and water vapour emissions in a global hydrogen energy economy. 11th World Hydrogen Energy Conference; Stuttgart, Germany, 1996.

[57] Seinfeld JH, Pandis SN. Atmospheric chemistry and physics - from air pollution to climate change. 2nd ed. Hoboken: John Wiley & Sons, Inc.; 2006.

[58] Zimmerman PR, Chatfield RB, Fishman J, Crutzen PJ, Hanst PL. Estimates on the production of CO and H_2 from the oxidation of hydrocarbon emissions from vegetation. Geophysical Research Letters 1978; 5: 679-82.

[59] Reimann S, Calanca P, Hofer P. The anthropogenic contribution to isoprene concentrations in a rural atmosphere. Atmospheric Environment 2000; 34: 109-15.

[60] Conrad R, Seiler W. Influence of temperature, moisture, and organic carbon on the flux of H_2 and CO between soil and atmosphere: Field studies in subtropical regions. Journal of Geophysical Research 1985; 90: 5699-709.

[61] Conrad R, Weber M, Seiler W. Kinetics and electron transport of soil hydrogenases catalyzing the oxidation of atmospheric hydrogen. Soil Biology & Biochemistry 1983; 15: 167-73.

[62] Smith-Downey NV, Randerson JT, Eiler JM. Temperature and moisture dependence of soil H_2 uptake measured in the laboratory. Geophysical Research Letters 2006; 33: doi:10.1029/2006GL026749.

[63] Yonemura S, Yokozawa M, Kawashima S, Tsuruta H. Model analysis of the influence of gas diffusivity in soil on CO and H_2 uptake. Tellus 2000; 52B: 919-33.

[64] Hammer S, Levin I. Seasonal variation of the molecular hydrogen uptake by soils inferred from continuous atmospheric observations in Heidelberg, southwest Germany. Tellus 2009; 61B: 556-65.

[65] Conrad R, Seiler W. Decomposition of atmospheric hydrogen by soil microorganisms and soil enzymes. Soil Biology & Biochemistry 1981; 13: 43-9.

[66] Tamagnini P, Axelsson R, Lindberg P, Oxelfelt F, Wünschiers R, Lindblad P. Hydrogenases and hydrogen metabolism of cyanobacteria. Microbiology and Molecular Biology Reviews 2002; 66: 1-20.

[67] Friedrich B, Schwartz E. Molecular biology of hydrogen utilization in aerobic chemolithotrophs. Annual Review of Microbiology 1993; 47: 351-83.

[68] Stephenson M, Stickland LH. XXVII. Hydrogenase: A bacterial enzyme activating molecular hydrogen. I. The properties of the enzyme. Biochemical Journal 1931; 25: 205-14.

[69] Yonemura S, Kawashima S, Tsuruta H. Continuous measurements of CO and H_2 deposition velocities onto an andisol: uptake control by soil moisture. Tellus 1999; 51B: 688-700.

[70] Häring V, Klüber HD, Conrad R. Localization of atmospheric H_2 oxidizing soil hydrogenases in different particle fractions of soil. Biology and Fertility of Soils 1994; 18: 109-14.

[71] Liebl KH, Seiler W. CO and H_2 destruction at the soil surface. In: Schlegel HG, Gottschalk G, Pfennig N, editors. Microbial Production and Utilization of Gases, Göttingen: Goltze; 1976.

[72] Schuler S, Conrad R. Hydrogen oxidation activities in soil as influenced by pH, temperature, moisture, and season. Biology and Fertility of Soils 1991; 12: 127-30.

[73] Brühlmann S. Empa Internal Report - Validierung H-Sense. Duebendorf: Empa; 2004.

[74] ACEM. The Motorcycle Industry in Europe. Brussels: Association des Constructeurs Européens de Motocycles; 2010.

[75] Lenaers G, De Vlieger I. On-board emission measurements on petrol-driven cars and diesel city buses. International Journal of Vehicle Design 1997; 18: 368-78.

[76] Soltic P. Nachführung der Emissionsgrundlagen Strassenverkehr Ergänzung der Messdaten auf das Bezugsjahr 2000 Benzin: Personen- und Lieferwagen Standardprogramm, Nr. 201209. Dübendorf: Empa - Swiss Federal Laboratories for Materials Testing and Research; 2001.

[77] Stettler P, Weilenmann M, Forss A-M, Mohr M, Mattrel P, Saxer C, Heeb N. Nachführung der Emissionsgrundlagen Strassenverkehr Messungen 01-02 Benzinpersonenwagen Euro-0 und Euro-3 sowie Dieselpersonenwagen Euro-2, Nr. 202114. Dübendorf: Empa - Swiss Federal Laboratories for Materials Testing and Research; 2004.

[78] Stilli J, Bach C. Vergleich von Ethanol- (E85) und Benzinbetrieb an einen Ford Focus Flexifuel, Nr. 445'114(B). Dübendorf: Empa - Swiss Federal Laboratories for Materials Testing and Research; 2007.

[79] Wilhelm E. Technical Characterisation and Multi-Criteria Analysis of Light-Duty Vehicles. In: Wilhelm E, Wokaun A, editors. Transition to Hydrogen: Pathways Toward Clean Transportation, Cambridge University Press; submitted.

[80] Wallner T, Lohse-Busch H, Gurski S, Duoba M, Thiel W, Martin D, Korn T. Fuel economy and emissions evaluation of BMW Hydrogen 7 Mono-Fuel demonstration vehicles. International Journal of Hydrogen Energy 2008; 33: 7607-18.

[81] CEH. Chemical Economics Handbook (CEH) - SRI Consulting (2008 data); 2010.

[82] IPCC. Special Report on Emissions Scenarios. Cambridge, United Kingdom: Cambridge University Press; 2000.

[83] Schmidt U, Seiler W. A new method for recording molecular hydrogen in atmospheric air. Journal of Geophysical Research 1970; 75: 1713-6.

[84] Novelli PC, Masarie KA, Lang PM, Hall BD, Myers RC, Elkins JW. Reanalysis of tropospheric CO trends: Effects of the 1997-1998 wildfires. Journal of Geophysical Research 2003; 108: doi:1029/2002JD003031.

[85] Zellweger C, Hüglin C, Klausen J, Steinbacher M, Vollmer MK, Buchmann B. Inter-comparison of four different carbon monoxide measurements techniques and evaluation of the long-term carbon monoxide time series of Jungfraujoch. Atmospheric Chemistry and Physics 2009; 9: 3491-503.

[86] Ruckstuhl AF, Jacobson MP, Field RW, Dodd JA. Baseline substraction using robust local regression estimation. Journal of Quantitative Spectroscopy & Radiative Transfer 2001; 68: 179-93.

[87] Ruckstuhl A, Unternaehrer T, Locher R. R: IDPmisc: Utilities of Institute of Data Analyses and Process Design (www.idp.zhaw.ch), http://CRAN.R-project.org/package=IDPmisc, R package version 1.1.06, 2009.

[88] Stohl A, Wotawa G, Seibert P, Kromp-Kolb H. Interpolation errors in wind fields as a function of spatial and temporal resolution and their impact on different types of kinematic trajectories. Journal of Applied Meteorology 1995; 34: 2149-65.

[89] D'Alleva BA, Lovell WG. Relation of exhaust gas composition to air-fuel ratio. SAE Journal (Transactions) 1936; 38: 90-8.

[90] Heywood JB. Internal combustion engine fundamentals. New York: McGraw-Hill Publishing Company; 1988.

[91] Favez J-Y, Weilenmann M, Stilli J. Cold start extra emissions as a function of engine stop time: Evolution over the last 10 years. Atmospheric Environment 2009; 43: 996-1007.

[92] Thurnheer T, Soltic P, Dimopoulos Eggenschwiler P. S.I. engine fuelled with gasoline, methane, and methane/hydrogen blends: Heat release and loss analysis. International Journal of Hydrogen Energy 2009; 34: 2494-503.

[93] Haryanto A, Fernando SD, To SDF, Steele PH, Pordesimo L, Adhikari S. Hydrogen production through the water-gas shift reaction: Thermodynamic equilibrium versus experimental results over supported Ni catalysts. Energy & Fuels 2009; 23: 3097-102.

[94] Keller M, Zbinden R. Luftschadstoff-Emissionen des Strassenverkehrs 1980-2030. Bundesamt für Umwelt, Wald und Landschaft (BUWAL); 2004.

[95] European Commission. Regulation (EC) No 715/2007 of the European Parliament and of the Council of 20 June 2007 on type approval of motor vehicles with respect to emissions from light passenger and commercial vehicles (Euro 5 and Euro 6) and on access to vehicle repair and maintenance information. Strasbourg 2007.

[96] Ahluwalia RK, Wang X. Effect of CO and CO_2 impurities on performance of direct hydrogen polymer-electrolyte fuel cells. Journal of Power Sources 2008; 180: 122-31.

[97] Owejan JP, Gagliardo JJ, Falta SR, Trabold TA. Accumulation and removal of liquid water in proton exchange membrane fuel cells. Journal of The Electrochemical Society 2009; 156: B1475-B1483.

[98] Yu X, Pingwen M, Ming H, Baolian Y, Shao Z-G. The critical pressure drop for the purge process in the anode of a fuel cell. Journal of Power Sources 2009; 188: 163-9.

[99] Ahluwalia RK, Wang X. Buildup of nitrogen in direct hydrogen polymer-electrolyte fuel cell stacks. Journal of Power Sources 2007; 171: 63-71.

[100] Owejan JP, Gagliardo JJ, Sergi JM, Kandlikar SG, Trabold TA. Water management studies in PEM fuel cells, part I: Fuel cell design and in situ water distributions. International Journal of Hydrogen Energy 2009; 34: 3436-44.

[101] EIA. The impact of increased use of hydrogen on petroleum consumption and carbon dioxide emissions. Washington, DC: Energy Information Administration; 2008.

[102] Aleklett K, Höök M, Jakobsson K, Lardelli M, Snowden S, Söderbergh B. The Peak of the Oil Age – Analyzing the world oil production Reference Scenario in World Energy Outlook 2008. Energy Policy 2010; 38: 1398-414.

[103] International Fertilizer Industry Association. Online production and international trade statistics covering nitrogen, potash and sulphur products: production, exports, imports by region from 1999 to 2008 (calendar year). 2010 [cited March 31, 2010]; Available from: http://www.fertilizer.org/ifa/Home-Page/STATISTICS/Fertilizer-supply-statistics.

[104] Schmid P. Outlook for Ammonia Supply and Trade. IFA Production and International Trade Conference; 17-19 October 2000; Shanghai, China: International Fertilizer Association, 2000.

[105] UN. The world at six billion. New York: United Nations Population Division; 1999.

[106] Ockerbloom & Company I. Methanol & Derivatives Global Outlook 2000-2012. Kittery, Maine: PCI Consulting Group; 2008.

[107] CMAI. 2010 World Methanol Analysis. Houston: Chemical Market Associates, Inc.; 2009.

[108] Pastowski A, Grube T. Scope and perspectives of industrial hydrogen production and infrastructure for fuel cell vehicles in North Rhine-Westphalia. Energy Policy 2009; doi:10.1016/j.enpol.2009.11.058.

[109] Hallale N, Moore I, Vauk D. Hydrogen optimisation at minimal investment. 2003 [cited 2010 May 13]; Available from: www.eptq.com (the refining, gas and petrochemicals processing website).

[110] Khamis I, Malshe UD. HEEP: A new tool for the economic evaluation of hydrogen economy. International Journal of Hydrogen Energy 2010; 35: 8398-406.

[111] Lattin WC, Utgikar VP. Transition to hydrogen economy in the United States: A 2006 status report. International Journal of Hydrogen Energy 2007; 32: 3230-7.

[112] Granovskii M, Dincer I, Rosen MA. Life cycle assessment of hydrogen fuel cell and gasoline vehicles. International Journal of Hydrogen Energy 2006; 31: 337-52.

[113] International Energy Agency. Key world energy statistics. Paris: IEA Head of Communication and Information Office; 2010.

[114] Henne S, Furger M, Nyeki S, Steinbacher M, Neininger B, de Wekker SFJ, Dommen J, Spichtinger N, Stohl A, Prévôt ASH. Quantification of topographic venting of boundary layer air to the free troposphere. Atmospheric Chemistry and Physics 2004; 4: 497-509.

[115] Forrer J, Rüttimann R, Schneiter D, Fischer A, Buchmann B, Hofer P. Variability of trace gases at the high-Alpine site Jungfraujoch caused by meteorological transport processes. Journal of Geophysical Research 2000; 105: 12241-51.

[116] Reimann S, Schaub D, Stemmler K, Folini D, Hill M, Hofer P, Buchmann B. Halogenated greenhouse gases at the Swiss High Alpine Site of Jungfraujoch (3580 m asl): Continuous measurements and their use for regional European source allocation. Journal of Geophysical Research 2004; 109: doi:10.1029/2003JD003923.

[117] Lallo M, Aalto T, Laurila T, Hatakka J. Seasonal variations in hydrogen deposition to boreal forest soil in southern Finland. Geophysical Research Letters 2008; 35: doi:10.1029/2007GL032357.

[118] Stephens BB, Gurney KR, Tans PP, Sweeney C, Peters W, Bruhwiler L, Ciais P, Ramonet M, Bousquet P, Nakazawa T, Aoki S, Machida T, Inoue G, Vinnichenko N, Lloyd J, Jordan A, Heimann M, Shibistova O, Langenfelds RL, Steele LP, Francey RJ, Denning AS. Weak northern and strong tropical land carbon uptake from vertical profiles of atmospheric CO_2. Science 2007; 316: 1732-5.

[119] Tanaka M, Nakazawa T, Aoki S. Concentration of atmospheric carbon dioxide over Japan. Journal of Geophysical Research 1983; 88: 1339-44.

[120] Reimann S, Vollmer MK, Folini D, Steinbacher M, Hill M, Buchmann B, Zander R, Mahieu E. Observations of long-lived anthropogenic halocarbons at the high-Alpine site of Jungfraujoch (Switzerland) for assessment of trends and European sources. Science of The Total Environment 2008; 391: 224-31.

[121] Seibert P, Kromp-Kolb H, Kasper A, Kalina M, Puxbaum H, Jost DT, Schwikowski M, Baltensperger U. Transport of polluted boundary layer air from the Po Valley to high-alpine sites. Atmospheric Environment 1998; 32: 3953-65.

[122] Rahn T, Eiler JM, Boering KA, Wennberg PO, McCarthy MC, Tyler S, Schauffler S, Donnelly S, Atlas E. Extreme deuterium enrichment in stratospheric hydrogen and the global atmospheric budget of H_2. Nature 2003; 424: 918-21.

[123] Henne S, Furger M, Prévôt ASH. Climatology of mountain venting-induced elevated moisture layers in the lee of the Alps. Journal of Applied Meteorology 2005; 44: 620-33.

[124] Zellweger C, Forrer J, Hofer P, Nyeki S, Schwarzenbach B, Weingartner E, Ammann M, Baltensperger U. Partitioning of reactive nitrogen (NO_y) and dependence on meteorological conditions in the lower free troposphere. Atmospheric Chemistry and Physics 2003; 3: 779-96.

[125] Press WH, Vetterling WT, Flannery BP. Numerical recipes in C, The art of scientific computing. Cambridge, U.K.: Cambridge University Press; 1992.

CURRICULUM VITAE

Personal Information

Name:	Steven Wallace Bond
Date of Birth:	November 30th, 1975
Place of Birth:	Vernon, British Columbia, Canada
Nationality:	Canadian

Academic History

09/2007 – 10/2010	**ETH Zurich (Swiss Federal Institute of Technology Zurich)** Zurich, Switzerland **Doctoral Studies (Dr. sc. ETH Zurich)** Department of Chemistry and Applied Biosciences (D-CHAB) PhD Thesis: *Atmospheric abundance and anthropogenic sources of molecular hydrogen: Status and outlook towards a H_2-intensive economy*
11/2006	**MSc Degree** (*with distinction*) **– Sustainable Development** Awarded the James Curran Prize from the Scottish Environmental Protection Agency (SEPA) for "best MSc post-graduate dissertation on the theme of climate change and sustainable development" MSc Dissertation: *Good ecological status and sustainability – trend and forecasting analysis to assess Scottish agricultural practices with respect to the Water Framework Directive goal (1984–2015)*
09/2005 – 09/2006	**The University of Stirling** Stirling, Scotland, United Kingdom **Master of Science Program** in **Sustainable Development**
06/1999	**BSc Degree – Freshwater Science Major**
09/1995 – 05/1999	**The University of British Columbia – Okanagan** Kelowna, British Columbia, Canada **Bachelor of Science Program** in **Freshwater Science**

Professional History

05/2007 – 11/2010	**Swiss Federal Laboratories for Materials Science and Technology (Empa)** Dübendorf, Switzerland **Researcher** Laboratory for Air Pollution/Environmental Technology (Climate Gases group)
07/2004 – 11/2004	**Swiss Federal Institute of Aquatic Science and Technology (Eawag)** Kastanienbaum, Switzerland **Project Technician** Surface Waters Department
05/1999 – 11/2003 & 05/1998 – 08/1998	**ECL Envirowest Consultants Limited** Burnaby (Vancouver), British Columbia, Canada **Freshwater Scientist**

Languages

- **English** – native language
- **German** – very good verbal and written knowledge
  Language certificate: Zertifikat Deutsch
  TELC (The European Language Certificates), Frankfurt/Main, Germany
  Exam succeeded with German grade 1
- **French** – very good verbal and written knowledge
  Language certificate: Diplôme d'Études en Langue Française (DELF) Niveau B1
  Le Ministère Français de l'Éducation Nationale
  Exam succeeded with final grade of 92%
- **Swiss-German** – reasonable knowledge and comprehension

Publications

- Bond, S.W., Alvarez, R., Vollmer, M.K., Steinbacher, M., Weilenmann, M., and Reimann, S. 2010. Molecular hydrogen (H_2) emissions from gasoline and diesel vehicles. *Science of the Total Environment* 408, 3596-3606.
- Vollmer, M.K., Walter, S., Bond, S.W., Soltic, P., and Röckmann, T. 2010. Molecular hydrogen (H_2) emissions and their isotopic signatures (H/D) from a motor vehicle: implications on atmospheric H_2. *Atmospheric Chemistry and Physics* 10, 5707-5718.
- Bond, S.W., Vollmer, M.K., Steinbacher, M., Henne, S., and Reimann, S. in press. Atmospheric molecular hydrogen (H_2): observations at the high-altitude site Jungfraujoch, Switzerland. *Tellus Series B*, doi:10.1111/j.1600-0889.2010.00509.x.
- Bond, S.W., Gül, T., Reimann, S., Buchmann, B., and Wokaun, A. in press. Emissions of anthropogenic hydrogen to the atmosphere during the potential transition to an increasingly H_2-intensive economy. *International Journal of Hydrogen Energy*, doi:10.1016/j.ijhydene.2010.10.016.
- Bond, S.W., Alvarez, R., Reimann, S., Weilenmann, M., and Buchmann, B. submitted. Hydrogen emissions to the atmosphere from industry and transportation. In: *Transition to hydrogen: Pathways toward clean transportation* (Eds. E. Wilhelm and A. Wokaun). Cambridge University Press.
- Bond, S.W., Vollmer, M.K., Steinbacher, M., Henne, S., Reimann, S., and Buchmann, B. 2007. Hydrogen observations at Jungfraujoch, Switzerland. International Foundation High Altitude Research Stations Jungfraujoch and Gornergrat (HFSJG) Activity Report 2007.

Selected Presentations

- Bond, S.W. Sources of anthropogenic H_2 emissions to the atmosphere during the transition to H_2-based transportation, Department 134 Vollversammlung, Swiss Federal Laboratories for Materials Science and Technology (Empa), July 5, 2010, Dübendorf, Switzerland.
- Bond, S.W. Sources of anthropogenic H_2 emissions to the atmosphere during the transition to H_2-based transportation, General Energy Research Department Bereichsseminar, Paul Scherrer Institute (PSI), June 24, 2010, Villigen, Switzerland.
- Bond, S.W. Anthropogenic H_2 emissions to the atmosphere, MIT-PSI Consortium Meeting, Massachusetts Institute of Technology (MIT), October 22–23, 2009, Cambridge, Massachusetts, USA.
- Bond, S.W., Vollmer, M.K., Steinbacher, M., and Reimann S. Direct and remote H_2 measurements – recent results from Empa, 3rd Annual EuroHydros Meeting, Finnish Meteorological Institute, June 3–4, 2009, Helsinki, Finland.
- Bond, S.W., Vollmer, M.K., Steinbacher, M., and Reimann S. H_2 in the atmosphere – an integration from the exhaust pipe to a remote alpine site, European Geosciences Union (EGU) General Assembly, Austria Center Vienna, April 20, 2009, Vienna, Austria.
- Bond, S.W., Vollmer, M.K., Reimann, S., Buchmann, B., and Steinbacher, M. Hydrogen concentrations – test stand and ambient atmosphere measurements, MIT-PSI Consortium Meeting, Empa, December 3–4, 2008, Dübendorf, Switzerland.
- Bond, S.W. Hydrogen in the atmosphere – recent results from Empa and Jungfraujoch, 2nd Annual EuroHydros Meeting, ISAC-CNR, September 15–17, 2008, Bologna, Italy.
- Bond, S.W. Hydrogen in the atmosphere – recent results from emission measurements at Empa, MIT-PSI Consortium Meeting, Ford Motor Company, May 8–9, 2008, Dearborn, Michigan, USA.
- Bond, S.W. and Vollmer, M.K. Sources and sinks of atmospheric H_2 during the transition to hydrogen-based transportation, MIT-PSI Consortium Meeting, CONCAWE, November 5–6, 2007, Brussels, Belgium.
- Bond, S.W., Vollmer, M.K., Steinbacher, M., Henne, S., and Reimann, S. Atmospheric molecular hydrogen (H_2) mixing ratios in the free troposphere derived from continuous observations at the high-Alpine site Jungfraujoch, Empa PhD Symposium, Empa, October 7, 2010, Dübendorf, Switzerland (Poster presentation).
- Bond, S.W., Vollmer, M.K., Steinbacher, M., Reimann, S., and Buchmann, B. Sources of atmospheric H_2 during the transition to hydrogen-based transportation, Empa PhD Symposium, Empa, November 19, 2009, Dübendorf, Switzerland (Poster presentation).

PUBLICATIONS

1. Bond, S.W., Alvarez, R., Vollmer, M.K., Steinbacher, M., Weilenmann, M., and Reimann, S. 2010. Molecular hydrogen (H_2) emissions from gasoline and diesel vehicles. *Science of the Total Environment* 408, 3596-3606.

2. Vollmer, M.K., Walter, S., Bond, S.W., Soltic, P., and Röckmann, T. 2010. Molecular hydrogen (H_2) emissions and their isotopic signatures (H/D) from a motor vehicle: implications on atmospheric H_2. *Atmospheric Chemistry and Physics* 10, 5707-5718.

3. Bond, S.W., Vollmer, M.K., Steinbacher, M., Henne, S., and Reimann, S. in press. Atmospheric molecular hydrogen (H_2): observations at the high-altitude site Jungfraujoch, Switzerland. *Tellus Series B*, doi:10.1111/j.1600-0889.2010.00509.x.

4. Bond, S.W., Gül, T., Reimann, S., Buchmann, B., and Wokaun, A. in press. Emissions of anthropogenic hydrogen to the atmosphere during the potential transition to an increasingly H_2-intensive economy. *International Journal of Hydrogen Energy*, doi:10.1016/j.ijhydene.2010.10.016.

5. Bond, S.W., Alvarez, R., Reimann, S., Weilenmann, M., and Buchmann, B. submitted. Hydrogen emissions to the atmosphere from industry and transportation. In: *Transition to hydrogen: Pathways toward clean transportation* (Eds. E. Wilhelm and A. Wokaun). Cambridge University Press.

6. Bond, S.W., Vollmer, M.K., Steinbacher, M., Henne, S., Reimann, S., and Buchmann, B. 2007. Hydrogen observations at Jungfraujoch, Switzerland. International Foundation High Altitude Research Stations Jungfraujoch and Gornergrat (HFSJG) Activity Report 2007.